MICROENVIRONMENTAL CONTROL IN MICROFLUIDIC BIOREACTORS FOR LONG TERM CULTURE OF BONE MARROW CELLS

by

Geeta Mehta

A dissertation submitted in partial fulfillment
of the requirements for the degree of
Doctor of Philosophy
(Biomedical Engineering)
in The University of Michigan
2008

Doctoral Committee:

Professor Jennifer J. Linderman, Co-Chair
Associate Professor Shuichi Takayama, Co-Chair
Professor Russell Taichman
Associate Professor Nikolas Kotov

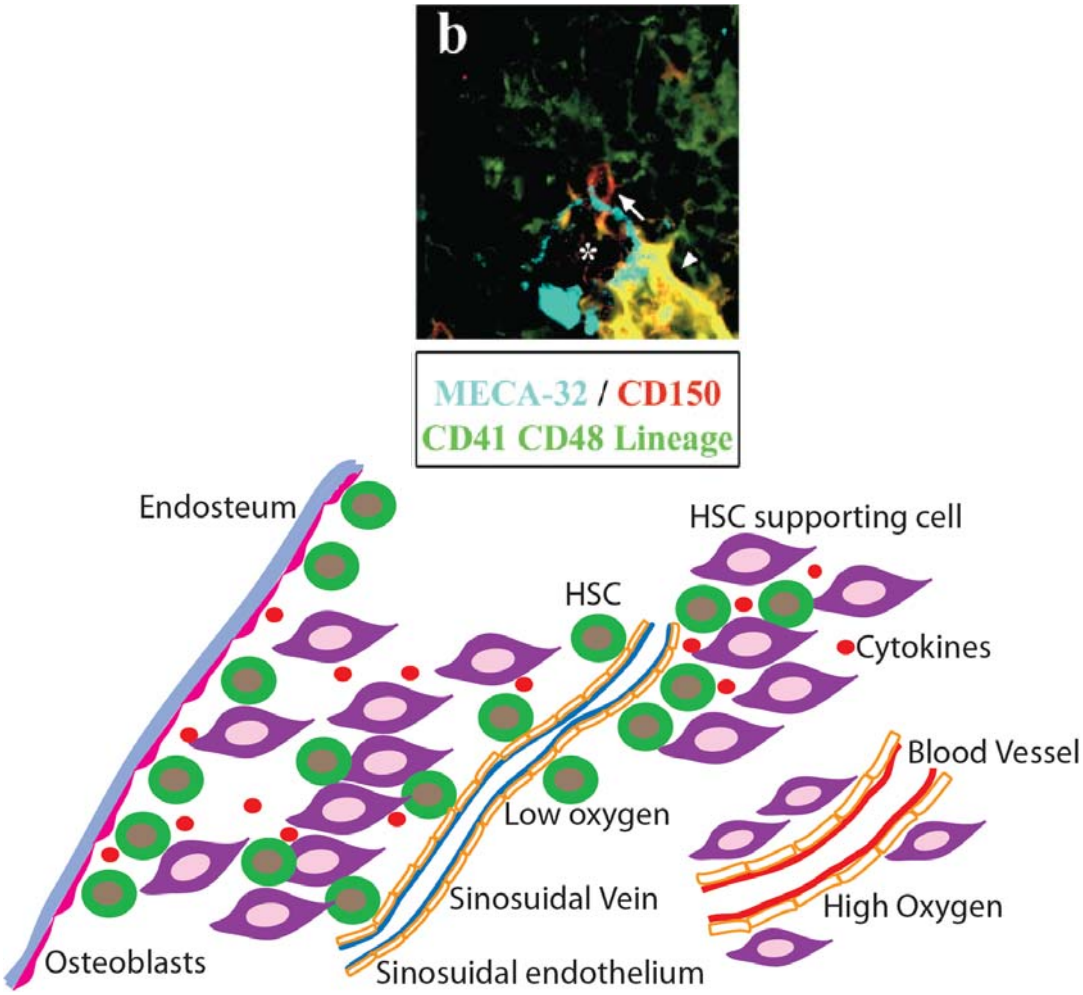

HSCs Microfluidic Niche

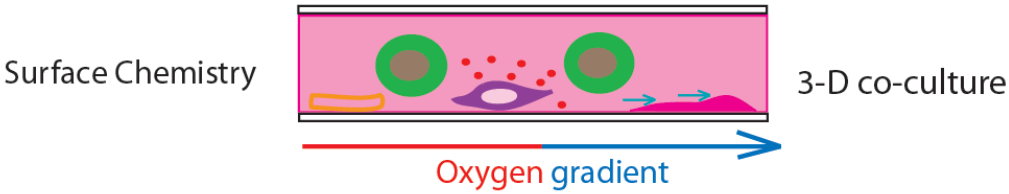

Find a tool.
Find a way.

I don't know
what is stuck:
I don't know
what is jammed.
The night does not close,
The day does not open.

Find a tool.
Find a way.

- Stuck by *Gulzar*

"Far away there in the sunshine are my highest aspirations. I may not reach them, but I can look up and see their beauty, believe in them, and try to follow where they lead."
- *Louisa May Alcott*

"Kitni Shidatt Se Maiyne Tujhe Paane Ki Koshish Ki Hai,
Kii Har Zarre Ne Mujhe Tujh Se Milane Ki Koshish Ki Hai."
- *Javed Akhtar*

This work is dedicated to my family, friends and everyone, who has given me the wings to fly, strength to persist, inspiration to move forward, faith to be brave in desperate situations, and above all love to conquer it all. You all have been my best friend, philosopher and guide; have *stuck* with me through all thick and thin. I thank all of you, I'm so lucky to have you all. Words can not express the warmth of love that I feel all around me because of you all.

To seven years of higher education, to my life, to all the voices who didn't let me quit, to faint rays of light after long dark nights, to birds who livened up the silence with their sweet sounds, to feminists and radical feminists, to all women and girls all around the world, to the lonely trees, to poets, to dark gloomy days, to felines, to memory, to screeching sounds of despair, to deathly gaze of failure, to misery, to sorrow, to melancholy, to abyss, to pain, to journey, to colors, to rainbows, to rain, to valleys, to mighty mountains, to dewdrops, to expectations, to responsibilities, to Andrea Dworkin, to J K Rowling, to the hungry heart, to poverty, to education, to middle class, to numbness, to tears, to smiles, to Twisty Faster, to equality, to freedom, to justice, to dreams, to wonders of nature, to peace, to persistent creature called hope, to you and to me…….

Acknowledgements

The existence of this work owes many thanks to a lot of people. I would like to thank them all individually.

My research advisors: Professor Shuichi Takayama and Professor Jennifer Linderman. It was a unique opportunity to have two research advisors. I would recommend it to all future graduate students. Professor Shuichi Takayama and Professor Jennifer Linderman, both have different working styles, but they share the same passionate and steady commitment to science.

Jennifer is always encouraging; she fills everyone she meets with lively optimism. Every time I saw her, she gave me a morale boost and I always left inspired and happy, no matter how bad the experiments were going. She is also the most organized professor I have seen. I cannot wrap my head around how she manages teaching, research and her family, all simultaneously. If I ever become a faculty, I want to follow her example. I am amazed at the amount of knowledge and insight she has not only about the modeling but also the experiments. I am thankful to her for giving me this opportunity to be a part of her research group. I have enjoyed each conversation that I have had with her. I will never forget our discussions on feminist issues, women in academia, and her help in pushing me through the difficult late writing stages.

To say that Shu is an overachiever would be an understatement. He directs the lab research, teaches undergrad and grad courses, travels everywhere around the world, has his own microfluidics based company, multitasks, and is always on top of everything. His mind never stops, he never rests, and he has been known to regale new research ideas over dinner conversations. He is a sincerely nice professor who always looks out for the interests of the lab members. I have learnt a lot about not only microfluidics and biology, but also about human relationships, the complexity of a medium sized lab, and conducting research in his group.

Dr. Shuichi Takayama and Dr. Jennifer Linderman have been the best advisors I have ever had and I offer my heartfelt thanks to them both. They have provided me with opportunities to travel, network, and present my own work in all settings, showing their dedication to my academic and professional growth. My experience of working with them has made me realize exactly how to handle my future graduate students or employees. They were both instrumental in writing this dissertation, and I am thankful for their guidance. I am also indebted to them for all their guidance, encouragement, and support throughout my graduate study.

Dr. Russell Taichman has been an important part of my graduate education. He has served on my PhD qualifying exam committee, and is a member of my dissertation committee. He has advised me on various aspects of hematopoeitic stem cell biology at various points along her Ph.D. research. Reading the papers from his research group and talking to him about bone marrow biology actually shaped my research interests. I will always remember him as a person who introduced me to the fascinating concept of inductive role of HSCs. He has been very accommodating with his busy schedule and helped me in all the tight spots. I wish him all luck in future research endeavors.

Dr. Sean J. Morrison at Life Sciences Institute has been a prominent influence in my research. He has always offered advice, feedback and shared his vast expertise in the field of HSC and bone marrow biology.

Special thanks and recognition also go to Dr. Nicholas Kotov, who has always been extremely generous with his time, whenever I needed technical or professional advice. I am grateful to him for serving on my committee, for helpful discussions, and for reviewing my research program. I am grateful to him for his help with the surface modification via polyelectrolyte multilayers project to facilitate culture of primary bone marrow stromal cells in PDMS microbioreactors.

I am very grateful to Dr. Omolola Eniola-Adefeso for stepping in the last minute and helping me with my dissertation committee.

Many people have contributed and collaborated to make this research possible. I am thankful to every one of them. Khamir Mehta from Linderman lab has been involved in this work, right from the beginning. He gave me the orientation to the project as well as the Linderman research group.

Morrison lab at Life Sciences Institute has happily provided supplies, expertise, HSCs, mice and many other things whenever I asked. Mark J. Kiel has been an important contributor and critic since the beginning. I have learnt to follow his advice since he is always right! He also knows everything there is know about the bone marrow biology and beyond. Christopher Mountford, also from Morrison lab helped me with mice. Dr. Injune Kim, a postdoc from Morrison lab was always friendly, and gave insightful ideas about murine liver endothelial cells and bone marrow endothelial cells. Dr. Mike Perron, another postdoc at Morrison Lab was very generous with his time and help with FACS.

My undergraduate friends and helpers made many experiments and analyses possible. I am thankful to Jay Lee, Jane Xiao, Ji Sun Sunny Choi, and Amy Oberlin for helping me in spite of their busy undergrad schedules. I wish all of them good luck for medical school, graduate school and other career paths.

Jung Woo Lee in the lab of Dr. Nicholas Kotov helped me with protocols for creating multilayer nanocomposite films of PDDA and clay.

Long time ago, a poet told me that common sufferance binds living beings together. I have a deep connection with the people that I worked and shared ideas with, and with whom I shared the experience of grad school. I express my gratitude to past and present members of Takayama Group and Linderman Group for their camaraderie, support, friendship, love and care. I wish them all best in all arenas of life. From Takayama group I would like to especially thank the following people: Terry Xiaoyue Zhu, Dan Dongeon Huh, Albert Bor Han Chueh, Mai Lam, Yoko Kamotani, Angela Dixon, Andre Yao Kuang Chung, Jason W Guo, Wei Gu, Bobby Bobak Mosadegh, Nobuyuki Futai, Yi-Chung Tung, Tommaso Bersano-Begey, Yusuke Torisawa, Wansik Cha, Amy Hsiao, Nick Douville, Andreja Jovic, Hossein Tavana, Jonathan Song, Ying Zheng, Yun Seok Heo. It was fun, exciting and productive to collaborate with so many of you. Thank you all! In the Linderman group, the following people were exceptionally helpful: Wendy Comisar, Tamara Ursem, Christopher Brinkerhoff, Prasanna Thwar, Khamir Mehta, and Stewart Chang. My colleagues provided not only scientific, but also moral support made coming into the lab fun and interesting and were always ready to lend a helping hand.

I am thankful to the friendship of Mai Lam, Angela Dixon, Yoko Kamotani, Shelley Brown, Danese Joiner, Shani Ross, Sylva Kryzan, and Mayte Brown for all the love, support and care they have showered on me. I have always turned to them for comfort, understanding, and motivation and will continue to do so.

I wouldn't be here without the people who kept me in good health. I am thankful to: Cindy, Donna, David, Vanessa, Erica, Roseanne, Andy, Maria, Tamra and Christine.

I am exceedingly appreciative of the Department of Biomedical Engineering, College of Engineering, and Rackham Graduate School of the University of Michigan Ann Arbor for providing me with graduate assistantship, research assistantships and fellowship. I am thankful to Rackham for providing me various avenues of financial support through Rackham pre-doctoral fellowship, Rackham travel grants and Rackham summer research grant.

Drs. David Mooney, Paul Krebsbach, Chun Yu Wang, Sean Morrison, Jennifer Linderman and Shuichi Takayama wrote the original grant for the US Army MURI project which facilitated this research. The regular annual quarterly MURI meetings were very helpful in learning about ongoing work in different labs and for collaborating across all the labs involved in the project.

Mayte Brown, Tonya Brown, Maria Steele, Jane Mackie, Sandy Staneff, Alayna Roper, Kevin Saari, Susan Bitzer, Kristin Romelhardt, Ruth Halsey, Dana Jackson, Deb Lyons Vera Williams, and Chuck Nicholas, who kept things running in the BME whether this calls for ordering materials, handling crisis, career advice, always providing help gladly, or remembering somebody on a special day. The work they do is invaluable, and without them, students, staff and faculty alike would be lost.

Special thanks are given to many faculty and staff members in the Department of Biomedical Engineering, College of Engineering, and the Rackham Graduate School, University of Michigan for their assistance during my graduate study.

Finally, I would like to acknowledge the financial support provided by Dr. Takayama and Dr. Linderman through grants from the U.S. Army Research Office (DAAD19-03-1-0168), National Science Foundation (BES-0238625) and The Whitaker Foundation.

My utmost appreciation and thanks are given to my partner Anish, Mom, Dad, sisters Rajni and Pooja, and niece Jiya for all the love and support throughout my graduate career. My family has been my rock to whom I could always turn for comfort, understanding, and motivation. They made me see the silver lining in the clouds when all I could see was an abysmal black hole. My family has always stood by me, through all the ups and downs, and has been very patient and encouraging in everything I have ventured to do. Mom and Dad sacrificed their lives for their children. And I wouldn't be myself without my lovely sisters Rajni and Pooja. My niece Jiya has filled our lives with joy. I could not have made it this far without them. Special thanks to cats Leo I, Leo II, Chloe, Cleo, and Ceasar who have provided me constant companionship, unconditional love and high drama to color my world.

In the end I would like to thank all grad students, post docs, undergrads, scientists and researchers who came before me and shaped the destiny of knowledge.

PREFACE

This dissertation contains the following published articles and manuscripts in preparation:

1. G. Mehta, Y. Torisawa, S. Takayama, "Engineering Cellular Microenvironments with Microfluidics", in *Biological Applications of Microfluidics*, F. A. Gomez (Editor), John Wiley and Sons, (2008), 87-114.
2. G. Mehta, M. J. Kiel, J. W. Lee, N. Kotov, J. J. Linderman, S. Takayama, "Automated Formation of Polyelectrolyte Layer Films on PDMS Bioreactor Surfaces for Primary Murine Bone Marrow Culture", *Advanced Functional Materials*. (2007), 17, 2701-09. [Epub 28 Aug 2007]
3. G. Mehta, K. Mehta, D. Sud, J. Song, T. Bersano-Begey, N. Futai, M.-A. Mycek, J. J. Linderman, S. Takayama, "Quantitative Measurements and Analysis of Cellular Oxygen Uptake in Microfluidic Poly(dimethylsiloxane) Bioreactors" *Biomedical Microdevices.* (2007), 9(2), 123-34. [Epub 12Dec 2006]
4. D. Sud, G. Mehta, K. Mehta, J. J. Linderman, S. Takayama, M.-A. Mycek, "Optical Imaging in Microfluidic Bioreactors Enable Oxygen Monitoring for Continuous Cell Culture" J*ournal of Biomedical Optics.* (2006), 11(5), 050504/1-050504/3.
5. G. Mehta, C. Mountford, M. J. Kiel, J. J. Linderman, S. Takayama, "Capture and Expansion of Small Numbers of Non-Adherent Precursor Cells To Generate Erythrocytes in Microniches with Embedded Semi-Porous Membranes", to be submitted to Lab on a Chip
6. G. Mehta, K. Mehta, J. Lee, A. Oberlin, J. J. Linderman, S. Takayama, "*In Vitro* Drug Screening in Microbioreactors with Axial Oxygen Gradients" in preparation.
7. G. Mehta, J. Lee, W. Cha, Y.-C. Tung, J. J. Linderman, S. Takayama, "Hot Embossed Microfluidic Devices from Hybrid Bonded Materials for Cell Culture and Chemical Analysis", in preparation.
8. G. Mehta, M. J. Kiel, J. Xiao, C. Mountford, N. Futai, S. J. Morrison, J. J. Linderman, S. Takayama, "Three Dimensional Cultures of Primary Murine Hematopoeitic Cells in Microfluidic Bioreactors for Improving HSC *In Vitro* Self Renewal", in preparation.
9. K. Mehta, G. Mehta, J. Lee, J. J. Linderman, S. Takayama, "Parameter Estimation of Cellular Oxygen Uptake Rates in Mammalian Microbioreactor Cultures", in preparation.

TABLE OF CONTENTS

LIST OF FIGURES

LIST OF TABLES

LIST OF APPENDICES

LIST OF ABBREVIATIONS

PDMS:	Poly(dimethylsiloxane)
PETG:	Poly(ethylene terephthalate glycol)
PS:	Poly(styrene)
COC:	Cyclic olefin copolymer
PU:	Thermoplastic polyurethane
PMMA:	Poly(methylmethacrylate)
RTDP:	Ruthenium tris(2,2'-dipyridyl) dichloride hexahydrate
HSC:	Hematopoeitic stem cells
HPC:	Hematopoeitic progenitor cells
BMSC:	Bone marrow stromal cells
BMMNC:	Bone marrow mono nuclear cells

ABSTRACT

The goal of this research is to create *in vitro* microenvironments for long term culture of hematopoeitic stem cell (HSC) in microfluidic bioreactors. *In vivo*, HSCs reside in the bone marrow osteoblastic and vascular niches in adult mammals. Defining features of their *in vivo* niche include: small number of HSCs, heterogeneous population of bone marrow cells that support HSCs, and low oxygen tension. We engineer niche elements in microfluidic bioreactors by modulating oxygen tension, optimizing attachment and growth of HSC-supporting bone marrow stromal cells, and culturing small numbers of HSCs in their physiologically relevant ratios between HSCs and supporting cells.

By using a combination of a mathematical model and quantitative experiments, we have created a design tool to manipulate and control oxygen tension for cell culture inside the poly(dimethyl siloxane) (PDMS) microbioreactors. Dissolved oxygen concentrations in the microbioreactor are quantified in real time using fluorescence lifetime imaging of an oxygen sensitive dye. Experimental results are consistent with the mathematical model and give insight into operating conditions required for a desired oxygen tension in cell culture regions of the microbioreactor.

We used microfluidic perfusion systems to develop nanocoatings made from electrostatic self assembly of PDDA (poly(diallyldimethyl ammonium chloride)), clay, type IV

collagen and fibronectin to optimize attachment of primary murine bone marrow cells (support cells for HSCs) onto PDMS bioreactors. PDDA-topped coatings were found to be cytotoxic, while coatings with two or more bilayers of proteins collagen and fibronectin were found to optimize spreading, proliferation, and viability as compared to other surfaces.

On-chip erythropoiesis was achieved with a 3-D co-culture of HSCs with supporting cells in PDMS bioreactors. In addition, an optimal ratio of support cells to HSCs was found to maximize self renewal potential of HSCs *in vitro*. By the combination of hypoxia (which simulates *in vivo* bone marrow oxygen tension), biofunctional surfaces, and 3-D co-cultures, we are moving towards a 'microfluidic HSC niche', in which hypothesis-driven studies about crosstalk between HSCs and stromal cells can be carried out.

CHAPTER 1

INTRODUCTION

The Journey

Often in our darkness
we forget to see the light:
The sun is constant,
even behind the clouds,
The river's current
washes away the debris.
Let the wind on your cheeks
help you remember
there is more -
There is more for you.

-Ruth Gilmore Langs, Ann Arbor Artist, 2006

1.1 Specific Aims

In this thesis, we aim to understand and develop various tools to engineer hematopoiesis-on-a-chip. Efforts to understand and control hematopoietic stem cell (HSC) proliferation and differentiation would benefit from development of artificial stem cell niches where a single or a few hematopoietic stem cells and primary bone marrow cells can be cultured in nanoliter volumes of fluids under investigator defined microenvironments. This thesis describes efforts to accomplish this goal using microfluidic poly(dimethylsiloxane) (PDMS) bioreactors. The nanoliter scale microfluidic bioreactors have an advantage over conventional bioreactors or other macroscopic culture systems in that the small volume allows even one or a few HSCs to condition the culture environment significantly. Additionally microfluidic PDMS bioreactors have the potential to utilize computerized

flow control to prepare engineered substrates for cell attachment prior to cell seeding as well as to optimize oxygen environments. This thesis is partly a design-directed engineering project to design, fabricate, and characterize microfluidic bioreactors, and partly a biological project to study the *in vitro* self renewal of HSCs in the niche using the optimized bioreactor.

The central hypothesis of the research undertaken is that *in vitro* niches can be created to manipulate HSC microenvironments in microfluidic bioreactors to optimize the seld-renewal of HSCs. Such *in vitro* models can provide a tool for studying the autocrine, paracrine and mitogenic factors regulated by HSCs to exercise control over the niche constituent cells. Specifically, with the combined effect of oxygen tension, physical attachments between HSC, supporting cells and niche substrate; three dimensional co-cultures of HSCs and niche constituent cells, the *in vitro* self renewal of HSCs can be improved resulting in undifferentiated multipotent primitive state of HSCs. The labs of Drs. Takayama and Linderman were perfectly suited for this thesis as they synergize the advantages of microfluidics with those of mathematical models to pre-screen amongst the plethora of complex interactions in HSC niche to study important and non-redundant crosstalk between HSCs and stromal cells in the bone marrow HSC niche. The research outlined here can ultimately be applied for creation of engineered bony organs, novel biosensors and new treatment strategies for hematological diseases such as myeloproliferative disorders.

The specific aims for this thesis are as follows:

1) **Quantitatively measure and control the oxygen tension inside microbioreactors (Chapters 3, 4 and 5)**

Oxygen tension in the niche has been directly correlated with fate of stem and tumor cells (Csete 2005). Additionally, the most primitive HSCs in the *in vivo* bone marrow are found near low oxygen tensions, while more differentiated progenitors are found near comparatively higher oxygen tension (Parmar et al. 2007). Moreover, oxidative stress is a

metabolic element which can lead to accumulation of reactive oxygen species (ROS) in HSCs and lead to changes in cellular functions (Ito et al. 2004). For the first part of this thesis, we develop an optics-based oxygen detection system in PDMS microfluidic devices. We also use a nutrient-based quantitative mathematical model (Mehta et al. 2006) to explain how key parameters control the spatial distribution of oxygen. By combining the model and the experiments we create a design tool to enable control of oxygen tensions in microfluidic devices for different cell types, including HSCs.

To further lower oxygen tensions in microdevices so that they are suitable for culture of primary HSCs and other cells desiring lower oxygen, we fabricate microdevices from polymeric materials with lower oxygen and water vapor permeabilities compared to PDMS. Such low oxygen tensions are realized in 'hard top – soft bottom' microbioreactors made from two hybrid bonded materials which are perfused using peristaltic Braille pumps and valves.

Another application of the 'design tool' that we develop using experimental and modeling methods, is in the determination of the intrinsic cell parameters for microfluidic cell culture. We use oxygen tension profiles of three different cell types, and evaluate Michaelis-Menten rate parameters, V_{max} and k_m, (V_{max} is the maximum consumption rate (at normoxic conditions) and k_m is the oxygen concentration at which the oxygen consumption rate is half of its maximum rate), for each cell type by utilizing the mathematical model.

2) Modify the surface of the microbioreactor to create physiological microenvironment for culture of primary bone marrow cells (Chapter 6)

Primary cells from the bone marrow are not amenable to culture on PDMS surface (Lee et al. 2004; Mehta et al. 2007). We aim to make PDMS surface biofunctional by growing polyelectrolyte multilayers (PEMs) nanocoatings by layer-by-layer (LbL) self assembly. We use microfluidic peristaltic pumps (Braille operated) to make custom nanocoatings of polymers and proteins for 2-3 week culture of bone marrow stromal cells (unsorted

primary murine whole bone marrow). Such coatings can also be customized for primary endothelial cells and other primary cells which are hard to grow for long times on PDMS surfaces.

3) Three dimensional co-culture of hematopoeitic and support cells to create an *in vitro* model of HSC niche (Chapters 7 and 8)

One of the important features of the HSC niche is three dimensional hierarchy and arrangement of various cell types in the marrow space. In fact, three dimensional cultures of HSCs have been reported to increase the expansion of HSCs *in vitro* (Banu et al. 2001; Kim et al. 2003; Li et al. 2001; Takagi 2005; Tun et al. 2000; Wang et al. 1995). *In vivo* HSCs are surrounded by a heterogeneous population of supporting cells, which provide soluble and adhesive signals to HSCs to support the proliferation, survival and self-renewing capacity of HSCs. In the third part of this research, three dimensional co-cultures of hematopoeitic stem and progenitor cells is performed with different support cells to test our *in vitro* microfluidic niches for HSCs. Using 3-D cultures, we create an erythropoiesis-on-a-chip model for generating erythrocytes from bone marrow cells for up to two weeks. We also use 3-D co-cultures to figure out the physiological ratio of HSCs to support cells needed to keep HSCs in a self-renewing state for an extended time *in vitro*. These results will help establish *in vitro* conditions ideal for long term HSC self-renewal.

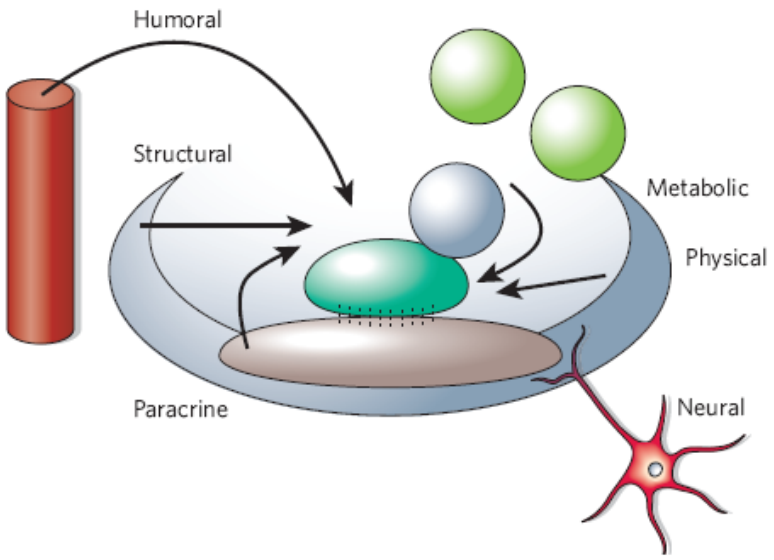

Figure 1.1: Stem cell niche is regulated by many elements including: constraints of the architectural space (structural), physical engagement of the cell membrane with tethering molecules on neighboring cells or surfaces, signaling interactions at the interface of stem cells and niche or descendent cells, paracrine and endocrine (humoral) signals from local or distant sources, input from central nervous system (neural), and metabolic products of tissue activity (Scadden 2006).

Our engineered '*in vitro* HSC niche' will provide a new tool to biologists, a system in which they can perform screening assays to find *the autocrine and paracrine factors secreted by a small number of HSCs* and metabolic elements in the niche. Researchers working on cell biology have assays to identify the secreted factors (Majka et al. 2001) and they also have tools to figure out the signaling regulated by those secreted molecules. Our engineered niche would provide them a system in which they can look at miniscule amounts of molecules secreted by HSCs. We also propose to work with pure HSCs and well-defined microenvironments in order to elucidate the biological processes involved, which the current *in vivo* and *in vitro* systems are lacking. Thus, with this microbioreactor system it will be possible to introduce a new *in vitro* model of HSC bone marrow niche which enables study of key biological behavior as a function of different oxygen tensions, flow rates, and surface chemistry. Figure 1.1 summarizes a typical stem cell niche. With the tools developed in this thesis, we are creating this functional HSC niche to study how HSCs exercise their regulation on the niche.

The long term goal of our work is to create biosensors with multiple bone cell types in order to engineer a bone marrow. The proposed physiologic biosensor could be used for precision sensing of the presence of cytotoxic environmental agents including myeloablative radiations or chemicals. Such agents cause tremendous toxic effects to the bone marrow, making it more prone than any other organ to cytotoxic environmental agents. We also aim to engineer a functional bone marrow, producing different blood cells types in the microbioreactor. In this thesis, we describe the crucial first steps in this process by recreating physiologically relevant microenvironments in the bioreactor. The combination of computerized microfluidics, in situ oxygen sensing, and mathematical models opens new windows for microphysiologic studies utilizing different surface chemistries, oxygen gradients and low oxygen tension. These results will be significant for the development, design, and optimization of novel, more physiological, *in vitro* systems for cellular studies.

1.2 Outline of the Thesis

The thesis is arranged as follows: chapter two scrutinizes the literature in the areas of microfluidics, microfluidic cell culture, bone marrow biology, *in vitro* culture of HSCs, and *in vivo* bone marrow niche. The first part of chapter two, which is about biological microenvironmental in microfluidic devices, was written as a chapter (*Engineering Cellular Microenvironments with Microfluidics*) for a book titled, "*Biological Applications of Microfluidics*". The second part of this chapter focuses on the bone marrow biology and HSC background.

Chapter three describes an experimental and modeling method to control dissolved oxygen tensions in PDMS microbioreactors, as a part of Aim 1. This work was published as an original research article in *Biomedical Microdevices*.

Chapter four shows how lower oxygen concentrations (hypoxic) can be achieved in microbioreactors by making devices from low oxygen permeability materials. This chapter is also an extension of Aim 1.

Chapter five looks at estimation of cellular characteristic parameters, (Michelis-Menton uptake parameters, km and Vmax) in microbioreactors from oxygen measurements for three cell lines. The experiments for this chapter were conducted by me; however, the modeling part as well the actual estimation of parameters was done by Khamir Mehta. This chapter is a part of the Aim 1 and shows an important application of our experimental technique.

Chapter six deals with surface modification in PDMS microbioreactors, and demonstrates creation of polyelectrolyte multilayers with different compositions made inside the same microbioreactors. Primary bone marrow stromal adherent cells are cultures on PEMs of 30 different compositions for 15 days, and assays for cell spreading, proliferation and viability are performed and results compared. This chapter encompasses Aim 2 and was published as an article for *Advanced Functional Materials*.

As a part of Aim 3, chapter seven shows three dimensional *in vitro* HSC co-culture with different support cells. Seven day long *in vitro* co-cultures are followed by two week long colony formation unit (CFU) assays.

Chapter eight demonstrates generation of red blood cells from primary bone marrow progenitors for 15 days in microbioreactors, creating a model for 'erythropoiesis-on-a-chip'. This chapter is also a part of Aim 3.

In chapter nine conclusions of the thesis and remaining future challenges are discussed.

References

Banu N, Rosenzweig M, Kim H et al. Cytokine-augmented culture of haematopoietic progenitor cells in a novel three-dimensional cell growth matrix. Cytokine 2001; 13 (6):349-58.

Csete M. Oxygen in the cultivation of stem cells. Ann N Y Acad Sci 2005; 1049:1-8.

Ito K, Hirao A, Arai F et al. Regulation of oxidative stress by ATM is required for self-renewal of haematopoietic stem cells. Nature 2004; 431 (7011):997-1002.

Kim HS, Lim JB, Min YH et al. Ex vivo expansion of human umbilical cord blood CD34+ cells in a collagen bead-containing 3-dimensional culture system. Int J Hematol 2003; 78 (2):126-32.

Lee JN, Jiang X, Ryan D et al. Compatibility of mammalian cells on surfaces of poly(dimethylsiloxane). Langmuir 2004; 20 (26):11684-91.

Li Y, Ma T, Kniss DA et al. Human cord cell hematopoiesis in three-dimensional nonwoven fibrous matrices: in vitro simulation of the marrow microenvironment. J Hematother Stem Cell Res 2001; 10 (3):355-68.

Majka M, Janowska-Wieczorek A, Ratajczak J et al. Numerous growth factors, cytokines, and chemokines are secreted by human CD34(+) cells, myeloblasts, erythroblasts, and megakaryoblasts and regulate normal hematopoiesis in an autocrine/paracrine manner. Blood 2001; 97 (10):3075-85.

Mehta G, Kiel MJ, Lee JW et al. Automated Formation of Polyelectrolyte Layer Films on PDMS Bioreactor Surfaces for Primary Murine Bone Marrow Culture. Advanced Functional Materials 2007; 17:2701-09.

Mehta K, Linderman JJ. Model-based analysis and design of a microchannel reactor for tissue engineering. Biotechnol Bioeng 2006; 94 (3):596-609.

Parmar K, Mauch P, Vergilio JA et al. Distribution of hematopoietic stem cells in the bone marrow according to regional hypoxia. Proc Natl Acad Sci U S A 2007; 104 (13):5431-6.

Scadden DT. The stem-cell niche as an entity of action. Nature 2006; 441 (7097):1075-9.

Takagi M. Cell processing engineering for ex-vivo expansion of hematopoietic cells. J Biosci Bioeng 2005; 99 (3):189-96.

Tun T, Miyoshi H, Ema H et al. New type of matrix support for bone marrow cell cultures: in vitro culture and in vivo transplantation experiments. Asaio J 2000; 46 (5):522-6.

Wang TY, Brennan JK, Wu JH. Multilineal hematopoiesis in a three-dimensional murine long-term bone marrow culture. Exp Hematol 1995; 23 (1):26-32.

CHAPTER 2

BACKGROUND AND LITERATURE REVIEW

2.1 Introduction

In order to create *in vitro* niche for hematopoietic stem cells, and ultimately, functional bony organs on a chip, a comprehensive study of microfluidic microenvironments and background of bone marrow stem cell biology is required. In this chapter, the current understanding of both these areas is presented. In the first part of this chapter, the microenvironments in microfluidic bioreactors are discussed. In the second part, the bone marrow biology as well as current knowledge about HSC self-renewal are communicated.

2.1.1 The microenvironment gap

There are many biomedical applications where it is necessary to manipulate mammalian cells outside of the body. The most common of such applications are: 1.Basic cell biological research; 2. Drug testing; 3. Cell-based therapies. A frequent problem in these types of *in vitro* cell manipulations, which typically occur in culture dishes, is that one can study, test, or use the exact same cells, but get very different responses from them because the microenvironment they are subjected to *in vitro* is very different from what the cells experience physiologically *in vivo*. This "microenvironment gap" may cause the

cell biologist to make scientific conclusions about cells that are contrary to their physiological behavior, or the drug developer to identify false positives and false negatives in drug testing, or the clinician to have to settle for a suboptimal therapeutic outcome. Biologists have identified and made available many bimolecular components that comprise the physiologic microenvironment for *in vitro* culture. And the list of available components continues to increase. However, the typical culture process of adding excessive volumes of culture media that contain a variety of these biomolecules together in a dish with a thin layer of cells attached often only goes so far in closing the microenvironment gap to elicit physiological cellular responses. Why is this? What comprises the physiological microenvironment and what are ways in which the microenvironment gap between *in vivo* and *in vitro* can be narrowed? This chapter will address these questions with a particular focus resolving the microfluidic aspects of this problem.

2.1.2 Cellular Microenvironment

For discussions in this chapter, we define "microenvironment" as a specific set of physical, chemical, and biological conditions in the vicinity of cells within a distance where those conditions can have an effect on or be sensed by the cells. The microenvironment provides cells with physical architecture, fluid and solid mechanical stimulation, adhesive signals, growth factors and cytokines, nutrients, inhibitor chemicals, and cell-cell interactions. The *in vivo* cellular microenvironment is composed of an intricate blend of extracellular matrix proteins, immobilized protein factors, proteoglycans, mineralized tissue, soluble protein factors, small molecule signals, and

various adjacent cell types, which vary in space and time due to material deformation, fluid flow, chemical reactions, or cell proliferation, differentiation, death, or migration (Adams et al. 2006; Jang et al. 2006; Shim et al. 2003). Cells continually sense these inputs, process the information through signal transduction and genetic regulation, and execute a cell behavior or determine a cell fate. Therefore, to study cell biology under well-controlled and versatile yet physiologically relevant conditions *in vitro* or to manipulate cells for clinical applications to elicit their maximum therapeutic potential, it is important to not only have the correct mixture of biomolecules but to also recreate the physical characteristics of the tissue.

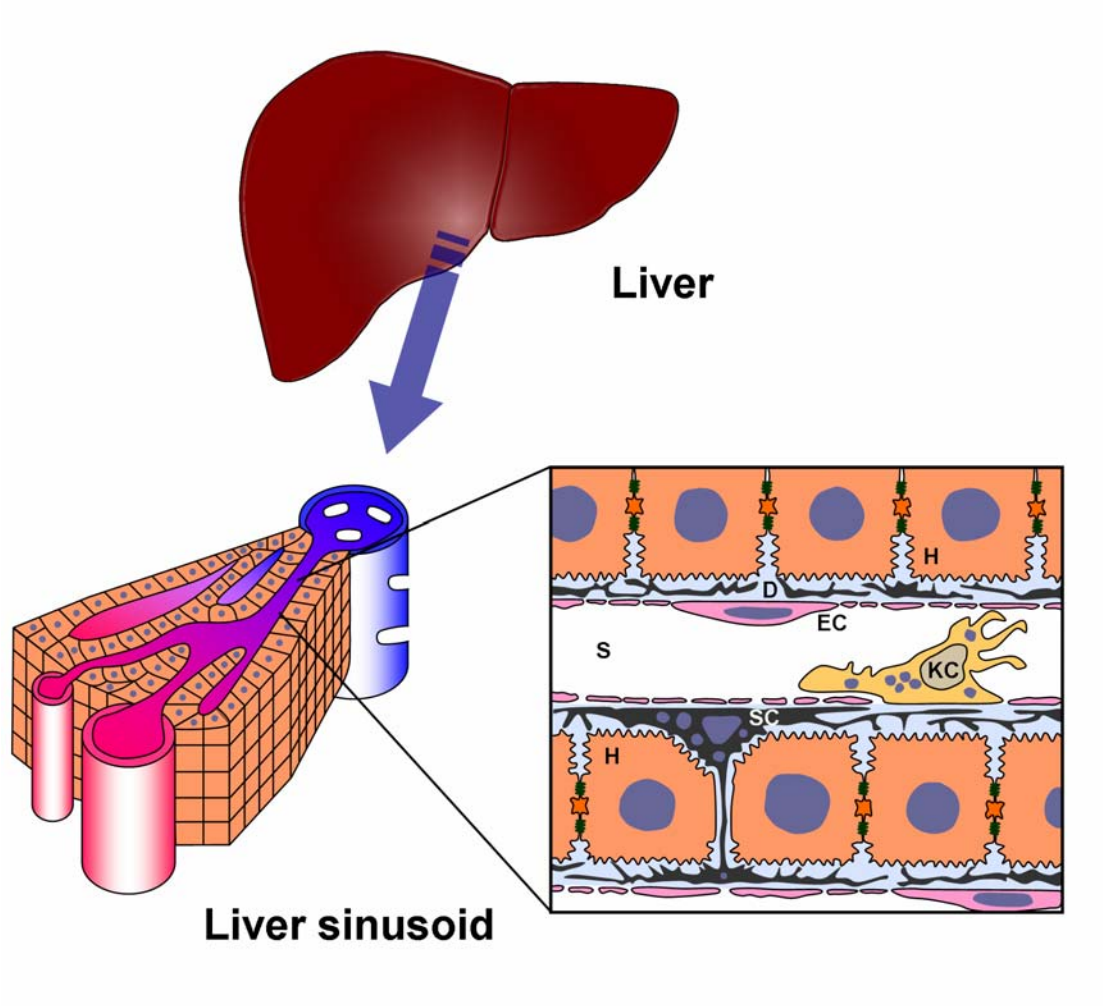

Figure 2.1: Physiology is microfluidic. An example of a microfluidic environment presented in human liver. The liver is composed of parenchymal cells, hepatocytes (H) (epithelial cells), and at least four major types of nonparenchymal cells (mesenchymal cells), Kupffer cells (KC) (resident macrophages), perisinusoidal or stellate cells (SC), sinusoidal epithelial cells and large granular lymphocytes (natural killer cells). Blood flows through the sinusoids (S) formed by fenestrated endothelial cells (EC). Kupffer cells and large granular lymphocytes bulge into the sinusoidal lumen from the endothelial cells. The space between the endothelial cell lining and the hepatocyte plates is the space of Disse (D) in which perisinusoidal or stellate cells and the extracellular matrix are located. Adjacent hepatocytes form bile canaliculi with their apical membranes.

2.1.3 Opportunities for microenvironment engineering using microfluidics

Use of microfluidics makes intuitive sense for cell microenvironment engineering. The physiological microenvironments in living systems are largely microfluidic in nature. Just a glance at the vascular network, pulmonary system, liver sinusoids, reproductive tracts, other tissues and organs of animals and humans reveals a wealth of physiologic microfluidic structures. The structure is very different from the architecture of the typical cell culture dish. An example of the physiologic microenvironment in the human liver is presented in Figure 2.1.

More substantially there are differences in the chemical and mechanical environment cells will experience in a microfluidic environment, even if one cultures the exact same cells in the exact same medium. Some of the major microenvironment differences are discussed conceptually in the next few paragraphs and examples of how microfluidics can be used to engineer more physiologic conditions described in the subsequent section.

2.1.3.1 The fluid volume to cell volume ratios leads to chemical changes

In a typical culture dish, the volume of culture media is vastly greater compared to the volume of cells adhered to the bottom of the dish. In contrast, physiologically, a majority

of the volume within tissues are taken up by cells rather than the fluid surrounding them. This difference in fluid volume to cell volume ratio can lead to differences in the chemical microenvironment of cells. Nanoliter scale microfluidic bioreactors have an advantage over conventional bioreactors or other macroscopic culture systems in that the small volumes allow even one or a few cells to condition the culture environment significantly. By having physiological ratios of cells to liquid volumes, better *in vitro* model systems can be developed in microfluidic devices, in terms of autocrine and paracrine signaling, for example, and pave way for biological studies that may otherwise not be possible. The small volumes also facilitate formation of significant cell-generated chemical gradients because cells can consume and secrete at appreciable levels where compounds are depleted or accumulate along the channel length.

2.1.3.2 Flow effects on chemical environment

Another difference between *in vitro* and *in vivo* cellular environments is fluid flow. The dish is static whereas the physiologic environment is dynamic. In the last 40 years, many studies have made it clear that the fluid flow and biology are inextricably intertwined. On a macroscopic scale, endocrine effects are exerted through transport by blood flow. On a smaller scale, convection can affect chemical gradients, and how cells sense chemical secreted by themselves (autocrine effects) as well as other cells (paracrine effects). The static nature of conventional cell culture also poses limitations for studying the effects of steady-state and intermittent stimulation with chemical and mitogenic factors.

In conventional cell cultures, spontaneously occurring spatial variability in temperature, solute concentration, or dissolved gas concentration can lead to surface tension differences at the gas–solution interface. These fluctuations cause variable convection and mass transfer making precise control of mitogens difficult. On the other hand, there is no defined fluid flow as is present in the blood stream, lymph, liver or other physiologic conditions. Convection is an important aspect of the *in vivo* microenvironment, particularly with respect to autocrine or paracrine signaling, which can be recreated to an extent in microfluidic bioreactors with controlled flow. Generation of gradients during perfusion is relevant to a variety of physiological cellular microenvironments in developing tissues where morphogenetic gradients are important in specifying cell fate, as well as in mature tissue to regulate and maintain function.

2.1.3.3 Flow effects on mechanical stimuli

Fluid flow also exerts mechanical effects. Cells *in vivo* exist in a dynamic environment where mechanical forces such as shear stress, tension and compression are important. In fact, cells respond to fluid shear stress through a complex process involving several transduction elements and multiple signaling pathways. For example, fluid shear forces acting on endothelial cells produce marked, time-dependent changes in their morphology (Dewey et al. 1981, Flaherty et al. 1972). Fluid-dynamic stresses have been observed to influence the adhesion of leukocytes to the endothelium and the tendency of the blood to clot. Cellular level fluid mechanics are complicated by the three-dimensional nature of the flow, the compliance of the interacting surfaces, and receptor-ligand dynamics.

Mechanical forces are also involved in cell-cell interactions. L-selectin, an adhesion molecule, mediates lymphocyte binding to, and rolling on, high endothelial venules. Puri et al manipulated the bond between selectin and mucin-like ligand by selective and reversible chemical modification of the ligand to show the effect of mechanical properties on the bond strength of interaction between adhesion molecules on two different cells (Puri et al. 1998). Additionally, to promote and maintain rolling interactions between leukocytes and vascular vessel wall through L-selectin, shear above a critical threshold is required but not through E-selectin, P-selectin or VCAM-1. The shear threshold requirement for L-selectin may be physiologically important in low shear to prevent inappropriate aggregation of leukocytes and interaction with the vessel wall (Finger et al. 1996, Alon et al. 1995).

It is important to not only have applied forces in cell culture, but also temporal variations in the forces applied. The endothelium has a completely different response to turbulent shear stress than to a laminar shear stress of the same time-mean magnitude (Davies et al. 1984, 1986). Temporal shear also produces a sustained response in intracellular calcium, whereas steady shear leads to an unrepeated single impulse. Endothelial cells also respond to vascular region-specific flow patterns by changing phenotypes as evidenced from their differential patterns of gene expression. They have distinct phenotypic modulation in response to the wall shear stresses present in prototypic human arterial waveforms (atherosclerosis-susceptible vs. atherosclerosis-resistant) (Dai et al. 2004).

Comparison of biological responses of human umbilical vein ECs to arterial pulsatile flow for 24 hours, at equivalent time-average steady laminar shear stress, and at no flow (static) culture conditions showed changes in cell shape and alignment in case of flow stimuli. However, different patterns of flow stimuli gave rise to distinct patterns of responses in the distribution of actin stress fibers and vinculin-associated adhesion complexes, intrinsic migratory characteristics, and the expression of eNOS mRNA and protein (Blackman et al. 2002). Human endothelial cells exposed to two well defined biomechanical stimuli --a steady laminar shear stress and a turbulent shear stress of equivalent spatial and temporal average intensity-- have the capacity to discriminate among these specific biomechanical forces. They even translate these input stimuli into distinctive phenotypes, and also change gene expression as a result (Garcia-Cardena et al. 2001).

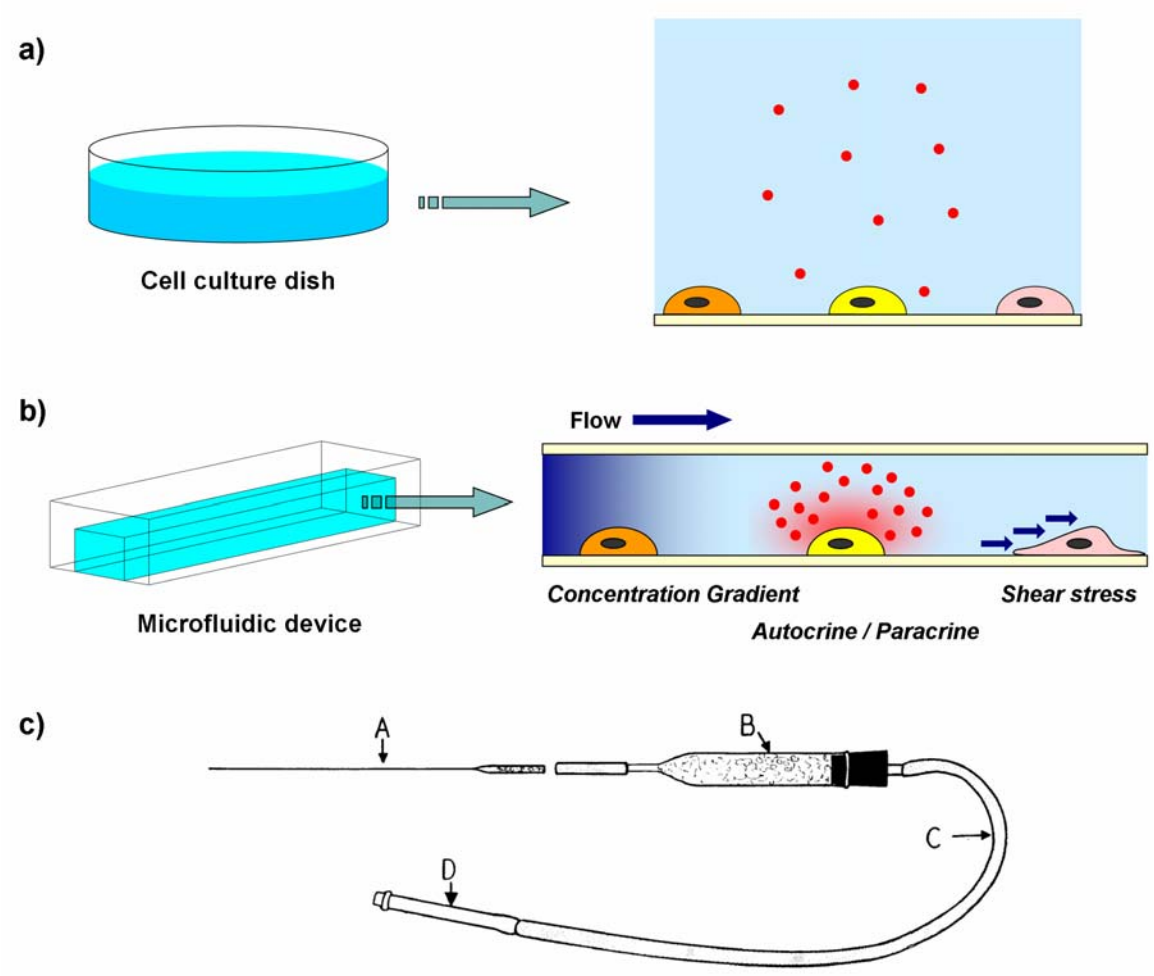

Figure 2.2: Cellular microenvironment in a microfluidic culture compared to a conventional 2D culture. a) Cells cultured in a dish grow in a large volume of medium under static condition. Biomolecules secreted from cells are dissipated in bulk medium by diffusion and some uncontrolled convection. b) Cells cultured in a microfluidic device grow in small volumes of media under static or dynamic conditions. Under static conditions, biomolecules secreted from cells distribute around cells (autocrine/paracrine) and into the surrounding medium by diffusion but in a limited way compared to in a dish. Cell consumption and secretion as well as fluid flow can create concentration gradients and fluid flow can generate shear stress. **c)** Cell culture in a micropipette from a report in 1948. A = micropipette, B = tube filled with cotton which acts as a bacterial air filter, C = rubber tube, D = mouthpiece.

2.1.3.4 Opportunities for microfluidics

Because of the microenvironmental requirements described above, efforts to understand and control cellular signaling, proliferation and differentiation would benefit from development of artificial cell microenvironment where cells can be cultured in nanoliter volumes of fluids under investigator defined conditions. A summary of the difference between conventional 2D cultures and static or dynamic microfluidic cultures are depicted in Figure 2.2.

In the first part of this chapter, we give specific examples of how microfluidic cell culture aids in each of the three above-mentioned categories. In the first subsection of examples of microfluidic cultures, we take a look at the reports of static microfluidic cell culture and the knowledge gained from them. In the second subsection, we follow the progress made by engineering chemical environments with active fluid flow. In the third subsection, we discuss the fluid mechanical effects of microfluidic cell culture. After discussing these three topics of how microfluidics can contribute to cellular microenvironment engineering, we describe additional useful capabilities that microfluidic devices offer including culture of precious cells, integrated biochemical analyses and 3-D culture. We end the microfluidic section with future prospects of microfluidic cell biological studies.

2.2 Microfluidic Cultures can Simulate *In Vivo* Microenvironments

The following are specific examples of how microfluidic cultures can be used to simulate *in vivo* conditions.

2.2.1 Use of substantially static microfluidic devices to engineer the chemical microenvironment

Simply culturing cells in small volumes of fluids can be beneficial and more physiological. An early account of "microfluidic" mammalian cell culture is from 1948 when Sanford et al. described successful growth of isolated cells in a glass pipette that did not grow well in the typical culture dish (Sanford et al. 1948). Small number of cells grew in the capillary (but not in a dish) due to their ability to self-conditioning the small volumes of media surrounding them. The cells, however, eventually died because of nutrient depletion and waste buildup that eventually prevailed, also caused by the small volumes of media. Microfluidics has come a long ways since then, thanks to the semiconductor industry, and now 60 years later, many sophisticated microfluidic tools are being developed with enhanced structures, materials, and flow manipulation to manipulate mammalian cells. There are still many beneficial uses, however, of static microfluidic cell cultures.

PDMS microfluidic devices, for example, have been used for static culture of mammalian and fruit-fly embryos (Walker et al. 2004, Raty et al. 2004, Walters et al. 2004, Clark et al. 2005, Glasgow et al. 2001, Lucchetta et al. 2005). The diffusion dominant microchannel environment has also been characterized by static culture of fall armyworm ovarian cells (Sf9) in different sized microchannels (height, width, length) at different seeding densities. The cell proliferation was found to be dependent on seeding density and channel height (Yu et al. 2005).

An alternative to the conventional macroscopic passive gradient generation systems, such as the Boyden chamber and Zigmond chamber, has been developed in a microfluidic format. Chemotaxis of neutrophils to gradients of formyl-Met-Leu-Phe (fMLP) was shown to cause polarization and migration in six hours in this passive flow microfluidic device (Abhyankar et al. 2006).

Substantially static microfluidic devices can be useful for formation of microscale tissue-like constructs such as spheroids. Multicellular tumor spheroids, for example, have been widely used in 3-D culture methods for solid tumor model. Tumor spheroids exhibit a characteristic *in vivo*-like morphology and cellular microenvironment that can be used to determine gene expression and biological behavior of cells. A tumor spheroid is composed of proliferating, quiescent, and necrotic cells. Cells located at the periphery of the spheroid are actively proliferating, whereas those located in the center are necrotic. These characteristics make tumor spheroids a useful tool for a variety of experimental studies on radiotherapy, chemotherapy, and photodynamic therapy. A microchip has been used to perform long-term culture (2 weeks) of HepG2 and MCF-7 spheroids and to evaluate viability and response to different concentrations of the cytotoxic agent sodium azide (Torisawa et al. 2007a).

A straightforward method to control the formation of embryoid bodies (EBs) using microfluidic techniques has also been recently developed using static culture conditions. The device consists of two microchannels separated by a semi-porous membrane treated to be resistant to cell adhesion. Mouse embryonic stem (ES) cells were introduced into

the upper channel where they self-aggregate to form uniformly-sized EBs. The size of EBs is regulated by adjusting the cross-sectional size of the microchannels. The semi-porous membrane allows subsequent treatment of the non-attached EBs with different reagents without the need for EB wash out. This method is compatible with on-chip EB culture, differentiation, and manipulation opening the way for more comprehensive ES cell processing on a chip (Torisawa et al. 2007b).

2.2.2 Use of microfluidic devices with active fluid flow to engineer the chemical microenvironment

Active fluid flow and recirculation gives rise to many physiologic chemical phenomena, including but not limited to generation of longer range biochemical gradients, formation of spatial and temporal heterogeneity, autocrine/paracrine/endocrine effects and metabolic interactions between different cells and tissues. Fluid flow also enables use of microfluidic phenomena such as patterned laminar flows not possible in static systems. Examples of studies made possible by microfluidic devices with active fluid flow are showcased in Figure 2.3.

2.2.2.1 Cell culture with flow

Cell types vary in their need or tolerance for static or dynamic flow environments. For example, Hickman *et al.* demonstrated that static culture of embryos developing from the two-cell to the blastocyst stage produced higher numbers of blastocysts and morulas compared to a dynamic flow culture condition at two different flow rates (0.1 and 0.5 microl/h) (Hickman et al. 2002). Static culture conditions also had lower number of

abnormal and eight cell embryos compared to constant flow. Thus, in this case, static culture was better for embryo development compared to dynamic flow conditions. Allen *et al.* were able to create an *in vitro* model of liver zonation with three sinusoidal zones by forming oxygen gradients along the length of the bioreactor by perfusion (Allan *et al.* 2003, 2005). Here, the oxygen concentration decreased along the length of the channel because the oxygen uptake by hepatocytes depleted oxygen in the downstream regions. Primary rat hepatocytes and their co-cultures with non-parenchymal fibroblasts showed regionally heterogeneous expression of CYP2B and CYP3A proteins in a manner that mimics their distribution in the zonated liver *in vivo*, thus demonstrating the importance of perfusion in creating *in vitro* models of liver physiology. In another study using HFF11 HeLa cells, the signal transduction resulting in the expression of the reporter protein *Photinus* luciferase was shown in microfluidic channels to have no unspecific activation which is caused by stress to cells, common in microtiter plate assays (Davidson et al. 2004).

For some applications, a delicate balance of substantially static and dynamic environment needs to co-exist. Taylor *et al.* created microdevices with two larger microfluidic compartments that are separated by a physical barrier of very small micron-sized grooves. Neurites, but not the cell body can extend from one microfluidic compartment across the small grooves into the adjacent microfluidic compartment. The authors plated primary rat E18 cortical neurons into the somal (cell body) compartment, and after 3-4 days, neurites had extended into the neuritic compartment. When combined with surface micropatterning, neuronal attachment and orientation of neurite outgrowth could be

further regulated. The system opens many opportunities for engineering the neuronal microenvironments (Taylor *et al.* 2003). For example, the same authors demonstrated the ability to perform localized physical or chemical treatment of just the axons or soma independently (Taylor et al. 2005).

Whereas many dynamic microfluidic cell culture systems are flow through devices, some physiological applications require fluid recirculation. The Shuler group has developed a cell culture analogue reactor (CCA) for culture of mammalian cells together with a corresponding physiologic pharmacokinetic model (PBPK) to study drug toxicology. The devices have a liver compartment (containing rat H4IIE hepatoma cells), a lung compartment (with rat lung L2 cells), and other tissue compartments interconnected to each other with fluid recirculating among the compartments with physiologic residence times. The systems have been used, for example, to test the toxicity of naphthalene (Ghanem and Shuler 2000a, 2000b) and the bioaccumulation of naphthalene in adipocytes (Viravaidya et al. 2002). They have also used a four chamber CCA device (with compartments for lung, liver, fat and other tissue) to screen drugs for colon cancer (Viravaidya et al. 2004, Sung et al. 2006).

A challenge for microfluidic recirculation systems where sub-microliter volumes of fluid are used is evaporation. This problem is particularly problematic when using permeable polymeric microdevices such as PDMS. Heo *et al.* characterized the evaporation-mediated osmolality shifts of cell culture media through thin PDMS membranes in microfluidic devices (Heo et al. 2007). They also demonstrated that a PDMS-parylene-

PDMS hybrid membrane can slow down evaporation and osmolality shifts for static culture of single-cell mouse embryos into blastocysts as well as dynamic culture of human endothelial cells with recirculation of submicroliter volumes of media.

Microfluidic architecture can be used to enhance mass transport. The Fujii lab fabricated microfluidic bioreactors by stacking 10 PDMS layers to create four cell culture chambers and one chamber for oxygen supply, then used the system to grow large number of HepG2 cells at high cell densities (Leclerc et al. 2004a). Glucose consumption and albumin production measures showed that cellular activity gradual increased and eventually became saturated. The authors also cultured rat liver cells within the microfluidic bioreactors for 15 day and demonstrated that albumin secretion and ammonia removal by these cells was increased by seven times compared to static culture (Ostrovidov et al. 2004). In a more simple device, hepatocytes and 3T3-J2 fibroblasts were co-cultured in a microgrooved substrate (Park et al. 2005) where perfusion provided oxygen for stable liver-specific function and the grooves protected cells from shear stress due to the perfusion.

Recently, a microfluidic device for stem-cell culture with both logarithmically varying perfusion rates and concentration gradients has been developed, making it possible to explore a wide range of biological perfusion conditions (including effect of shear) simultaneously for mouse embryonic stem cells (Kim et al. 2006). Human Embryonic Stem (ES) cells have been co-cultured with a feeder layer of human foreskin fibroblasts in microfluidic channels and culture conditions have been established as a function of

flow rate (Korin et al. 2007).

In other examples, cell arrays of multiple phenotypes (hepatocytes, fibroblasts, and embryonic stem cells,) have been fabricated by sequential delivery of fluids or cells into microwells on substrate using reversibly sealable PDMS molds (Khademhosseini et al. 2005). Astrocyte and glioblastoma cells have been cultured in PDMS microdevices modified with silane coupling agents to study cell adhesion and growth (Cox et al. 2002). An integrated microfluidic bioreactor with integrated indium-tin-oxide heater and miniature temperature probe and uniform media perfusion system has been developed to culture HeLa cells for up to two weeks (Petronis et al. 2006).

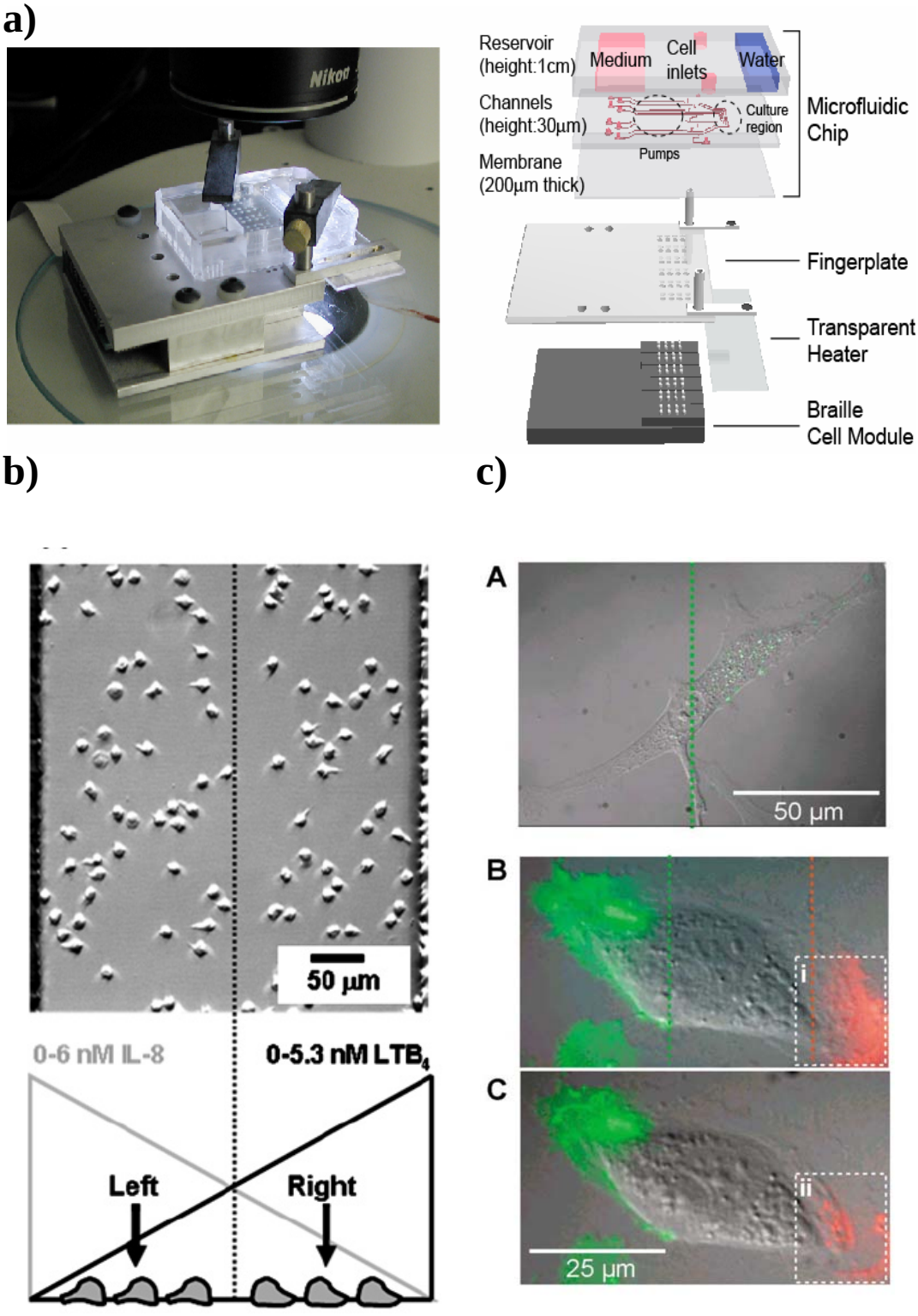

Figure 2.3: a) A Braille display-based microfluidic cell culture system. (Futai et al. 2006b) **b) Chemotaxis of neutrophils** in opposing gradients of IL-8 (0–6 nM) and LTB4 (0–5.3 nM). A selected frame from the time-lapse images of a representative experiment where most of the cells of the "left" population polarized to the right and most of cells of

the "right" population polarized to the left (Lin et al. 2005). **c) PARTCELL on bovine endothelial cells. A)** Area-selective delivery of fluorescently labeled, acetylated, low-density lipoprotein (DiI Ac-LDL) to a portion of the cell surface. The green dotted line indicates the position of the interface between the flows, with and without DiI Ac-LDL. **B)** Intracellular transport of cell-surface glycoproteins labeled with wheat germ agglutinin (WGA) conjugated to green (Alexa 488-WGA) and red (TRITC-WGA) fluorescent markers. **C)** Cell after one hour of WGA treatment. (Takayama et al, 2003)

2.2.2.2 Patterned microfluidic flows for spatio-temporal patterning of biochemicals

The signal transduction in cells occurs through cytoskeleton and various scaffolding proteins and other subcellular components. Such structural elements are not distributed randomly in cells, but are present heterogeneously throughout the cell with micron scale spatial variations. The structural order of these components is necessary for the propagation and processing of cellular signals. Taking inspiration from *in vivo* microenvironments where molecular and spatial discrimination can be at the micrometer scale, patterned microfluidic flows have been used to perform localized cell and tissue stimulation with spatial precision that allows even subcellular biochemical delivery. 'Partial treatment of cells using laminar flows', or PARTCELL uses multiple laminar streams in a microfluidic channels to deliver molecules to selected subcellular microdomains on the surface or inside single mammalian cells in the case of cell permeable molecules. The low Reynolds number flows in these microfluidic channels ensure that there is no turbulent mixing of chemicals between the adjacent laminar streams, although diffusive mixing still occurs.

Using this technique, rapidly diffusing, membrane-permeable molecules are directed to subcellular regions of a single cell. Two subcellular processes of mitochondrial movement and changes in cytoskeletal structure of bovine capillary endothelial cells were

studied by using PARTCELL. Localization of molecules is achieved by a combination of rapid influx and efflux of molecules in distinct regions of the cell, created by using multiple laminar streams, and the process is simple and requires no special equipment (Takayama et al. 1999, 2001a, 2003).

Using the PARTCELL approach, the Miyawaki lab took a closer look at the epidermal growth factor receptor (EGFR) signaling in single live COS cells (a monkey cell line) to find if the activation of signaling is localized or propagated over the entire cell. The EGFR signaling pathway is one of the most important pathways that regulate growth, survival, proliferation, and differentiation in mammalian cells. The receptor is often upregulated in tumor cells and the difference in EGF signaling between normal and malignant cells is of great biological and medical interest. Through the combined use of microfluidic subcellular EGF delivery and real-time visualization of intracellular signaling based of fluorescent protein reporters, cells were shown to exhibit localized activation of receptor phosphorylation and Ras activation or ligand-independent lateral propagation of signals depending on the cell surface receptor density and receptor internalization. The results provide unique insights on intracellular events in ways that would be very difficult to obtain without use of microfluidics (Sawano et al. 2002).

Using a similar microfluidic approach, embryonic patterning of Drosophila with warm (27 ^{o}C) and cool (17 ^{o}C) media under time specific conditions, showed that anterior and posterior halves of the embryo which are exposed to different temperatures, develop at different rates (Lucchetta et al. 2005). In another related use of microfluidics,

Tourovskaia et al. performed localized delivery of agrin to myotubes formed inside microchannels (Tourovskaia et al. 2005) to induce localized acetylcholine receptor clustering in the stimulated portions of the myotubes (Tourovskaia et al. 2006a, 2006b).

Using a different microfluidic approach, Piston's group developed a microfluidic bioreactor capable of partially stimulating islet beta cells to create glucose gradients across the islet and observed cellular NAD(P)H and $[Ca^{2+}]_i$ responses (Rocheleau et al. 2004). They demonstrated that extent of Ca^{2+} propagation across the islet depends on a delicate interaction between the degree of metabolic coupling and the extent of ATP-sensitive K^+-channel activation.

2.2.2.3 Biochemical gradients

The two common methods for using perfused microfluidic systems to create chemical gradients are: i) use of patterned laminar flows, where adjacent streams contain different concentrations of the chemical of interest, to create chemical gradient in a direction lateral to the direction of fluid flow; and ii) use of the ability of cells to secrete and consume biochemicals in their vicinity combined with slow perfusion to create gradients in a direction parallel to the direction of fluid flow.

A useful category of devices to create lateral gradients of biochemicals is the branched network microchannels (Jeon et al. 2002; Lin et al 2004). Homogenous and heterogeneous (hill gradient, cliff gradient) linear gradient, have been generated and used to study chemotaxis of human neutrophils towards IL-8 (Jeon et al. 2002). The

chemotaxis behavior of these cells was quantified and important observations regarding migration of neutrophils with respect to different profile IL-8 gradients were made.

A microfluidic stem-cell culture platform with a concentration gradient has been used to study the effect of growth-factor concentration on human neuronal-stem-cell behavior. The observed proliferation rate in the device was proportional to growth-factor concentration, whereas differentiation (to astrocytes) was inversely proportional. In these studies, flow in the device minimized autocrine and paracrine signaling (Chung et al. 2005). The same group also quantified migration of the MDA-MB-231 human metastatic breast cancer cells in various conditions by simultaneously generating multiple growth factor (EGF and anti-EGFR) gradients in the microfluidic chemotaxis chamber (Saadi et al. 2006). Microfluidic gradient generator was also utilized to differentiate between neutrophil chemotactic response to equal host-derived conflicting gradients of chemotactic factors IL-8 and LTB4 (Lin et al., 2005). Chemotaxis of human T cells in response to single and competing gradients (spatial and temporal) of chemokine CCL19 and CXCL12 was studied in 'Y' shaped microfluidic bioreactor (Lin and Butcher 2006). Concentration gradients over few hundred microns were generated by combination of controlled fluid distribution at each intersection of a microfluidic network (due to liquid pressure) and subsequent diffusion between streams in the microchannel (Yang et al. 2002).

Chemical gradients have been created in microfluidic devices by using arrays of externally connected, horizontally oriented tubes compatible with commercialized

multichannel pipettors. This Horizontally-Oriented Mini-Reservoirs pumping scheme or HOMR pump provides a steady pulse-free flow by keeping a constant hydraulic pressure drop across a microchannel; thus the pump overcomes the problem of decreasing flow rate typical for gravity driven pumps. The HOMR pump does not require any external power connection, is compact in size, and was compatible with generation of multiple laminar streams (up to 8 in this example) of alternating liquids, smooth gradients of various concentration profiles, as well as a step gradient of biochemicals which can be used for microfluidic drug assays (Zhu et al. 2004).

Apart from generation of lateral chemical gradients, microfluidic systems with slow perfusion can take advantage of cellular consumption or production of biochemicals to generate gradients along the length of a channel. For example, changes in oxygen concentration have been detected in a continuously perfused PDMS microfluidic bioreactor for cell culture (Park et al. 2006, Szita et al. 2005, Zanzotto et al. 2004). Steep oxygen gradients caused by uptake by cells have been observed along the length of a mammalian cell culture channel in continuously perfused microfluidic bioreactors (Allen and Bhatia 2003, Allen et al. 2005, Mehta et al. 2007).

The area of microfluidic gradient generation is a very active and fruitful area. Considering that *in vivo* microenvironments have more complex gradients such as pulsed gradients, exponential gradients or other non-linear gradients (Katz and Lasek, 1980) of multiple factors simultaneously, one can expect many more enhancements and innovations in this area.

2.2.2.4 Paracrine effects

Active perfusion allows control of directionality in terms of intracellular chemical communications. For example, interactions between macrophages and osteoblasts were studied while the cells remained physically separated in different parts of a microfluidic bioreactor. The cytokines released upstream by macrophages (IL-1□ and TNF-□), flowed through the device in linear gradients and induce downstream osteoblasts to secrete prostaglandin E2 (PGE2) (Wei et al. 2006).

2.2.2.5 Perfusion culture of three-dimensional cell aggregates

Spherical cell aggregates of hepatocyte spheroids retain the 3-D architecture and cell-cell contacts required for maintenance of many liver-specific functions (N Koide et al. 1990). Spheroids are generated when their cellular adhesion sites to a substrate are blocked, thereby forcing the cells to adhere to each other. Recently, microscale technologies have been applied to spheroid culture for development of alternative tools for cellular biology. Co-culture spheroid arrays have been developed using micropatterning techniques (H Otsuka et al. 2004, Fukuda et al. 2006). Hepatocytes spheroids co-cultured with endothelial cells or fibroblasts maintain their liver-specific functions for at least one month. Such 3-D cell cultures have been combined with microfluidic systems. 3-D culture inside PDMS microfluidic bioreactors (with uniform and non-uniform flow) was achieved by stacking two pieces of PDMS containing 3-D features. The culture of HepG2 cells was demonstrated in this bioreactor and metrics of cell functionality (albumin production, glucose consumption) were evaluated (Leclerc et al. 2003). Kojima et al. created agar microstructures with cell-culture holes to culture primary neonatal rat

cardiac myocytes and observed synchronized beating in them 90 min after they had made physical contact (Kojima et al. 2003).

2.2.2.6 Microarrayed bioreactors

A number of interesting microfluidic array systems have been developed, some of which are outlined below:

A 10 x 10 microfluidic cell culture array for long term monitoring of HeLa cells was developed by Hung et al (Hung et al. 2005a, 2005b). By continuous perfusion, it was possible to passage confluent cells within the microfluidic chambers, thereby creating a stable culture environment.

A bioreactor array (8 x 8) with culture regions disjoint from flow channels to create low shear spaces for cells and convective flow for transport of fluids was made for continuous flow in multiplexed environment (Lee et al. 2006). The device enabled uniform cell loading, low shear for cell culture units, and low pressure stresses on cultured cells for culture of HeLa, NIH 3T3 fibroblasts, primary bovine endothelial cells, HepG2 hepatocytes, human SY5Y neuroblastoma cells.

A 64 (8 x 8) array of microfluidic wells connected with two microfluidic perfusion networks for culture medium and oxygen was fabricated to support micropatterned coculture of primary rat hepatocytes and 3T3-J2 fibroblasts (Kane et al. 2006). The

hepatocytes cultures in the array were able to continuously generate albumin synthesis and urea production in a steady-state.

Chueh et al. have recently reported fabrication of 8 x 12 criss-crossing microfluidic channel array by overlaying polyester and polycarbonate membranes over PDMS structures (Chueh et al. 2007).

2.2.2.7 Use of microfluidic flow for creating layered structures

Defined 3-D microsctructural multilayered arrangements of live cells have been created by photopatterning of 3-D hydrogel (Liu and Bhatia 2002) to culture different cell types. 3-D layers of extracellular matrix biopolymers (collagen, chitosan, fibronectin) have been micropatterned on PDMS substrates for culture of human umbilical vascular endothelial cells (HUVECs) and fibroblasts (Tan and Desai 2003). Microfluidic layer-by-layer 3-D biomimetic structures were also created using collagen, chitosan, matrigel, and fibrin to culture human lung fibroblasts (IMR-90), human umbilical vein smooth muscle cells (HUVSMC), human umbilical vein endothelial cells (HUVECs) for 5 days (Tan and Desai 2004).

Microfluidic channels were utilized to create polyelectrolyte multilayers of poly(allylamine hydrochloride) (PAH) and poly(styrene sulfonic acid) (PSS) on PDMS substrate in order to culture neuron-like cells (NLCs) derived from pluripotent embryonal carcinoma P19cells (Forry et al. 2006). Additionally, primary murine bone marrow stromal cells were grown on nanocomposite coatings deposited onto PDMS using layer-by-layer assembly in microfluidic bioreactors (Mehta et al. in revision). The cells

attached, spread, and proliferated well on the nanocomposite coatings whereas the cells detached, rounded, and died on native PDMS even when coated with cell adhesive proteins.

2.2.2.8 Long term culture

Using microfluidic bioreactors, long term culture of cells can be easily carried out in controlled environments for many physiological functional assays which take place over time in range of few weeks. For example, differentiation of alveolar epithelial cells takes two weeks to complete (Huh et al. 2004; Huh et al. in revision) and finding the frequency of long term culture initiating hematopoeitic cells takes over 3 weeks to complete (Bock 1997). Long-term culture combined with imaging of cells has always been one of the important goals of microfluidic cell culture labs. Although still somewhat low resolution in terms of cell imaging, a recently developed microfluidic recirculation system with built-in transparent heater when used with customized media allowed time lapse imaging of proliferation of C2C12 myoblasts and MC3T3-E1 osteoblasts for over 2 weeks in ambient atmosphere without medium exchange (Futai et al. 2006a).

2.2.3 Use of microfluidic devices with active fluid flow to engineer the fluid mechanical microenvironment

The most well known and important example of the influence of fluid mechanical forces in physiology is that of endothelial cells. Vascular endothelial cells are located at the innermost layer of the blood vessel wall and are always exposed to three different mechanical forces: shear stress due to blood flow, hydrostatic pressure due to blood pressure and cyclic stretch due to vessel deformation. It is well known that endothelial

cells respond to these mechanical forces and change their shapes, cytoskeletal structures and functions. After applying fluid shear stress, cultured endothelial cells show marked elongation and orientation in the flow direction. In addition, thick stress fibers of actin filaments appear and align along the cell long axis. Thus, endothelial cell morphology is closely related to the cytoskeletal structure. (Sato and Ohashi 2005)

When endothelial cells are exposed to hydrostatic pressure, they exhibited a marked elongation and orientation in a random direction, together with development of centrally located, thick stress fibers. Pressured endothelial cells also exhibited a multilayered structure with less expression of VE-cadherin unlike under control conditions. Simultaneous loading of hydrostatic pressure and shear stress inhibited endothelial cell multilayering and induced elongation and orientation of endothelial cells with well-developed VE-cadherin in a monolayer.

Wall shear stress also regulates adaptive vessel growth and angiogenesis, and might be a local risk factor in the pathogenesis of atherosclerosis. Shear stress also modulates the production of vasoactive substances such as endothelium-derived relaxing factor, prostacyclin, histamine and endothelin, and regulates macromolecule permeability and endocytosis. More recent studies have shown that shear stress exerts an influence on the expression of mRNA such as tissue plasminogen activator mRNA. (Ando and Kamiya 1993)

Additionally, different flow patterns elicit distinct responses of Kruppel-like factor-2 (KLF2) in endothelial cells (ECs) in vitro and in vivo. The pulsatile flow with a significant forward direction induces sustained expression of KLF2 in cultured ECs, but oscillatory flow with little forward direction causes prolonged suppression after a transient induction. The KLF2 protein levels ECs at arterial branch points are related to local hemodynamics (Wang et al. 2006).

2.2.3.1 Two phase flows

Gas-liquid two-phase flow configurations have been used to study alveolar epithelial cells and also for microfluidic flow cytometer (Huh et al. 2003). To expose pulmonary epithelial cells to various fluid flows, Huh et al. developed a compartmentalized microfluidic bioreactor that mimics *in vivo* microenvironment with different flows under normal and pathological pulmonary conditions (Huh et al. 2004; Huh et al. in revision).

2.2.3.2 Shear stress in microfluidic bioreactors

Exposure of cultured endothelial cells to controlled levels of shear stress is possible in microfluidic culture systems using computer controlled pulsatile fluid flows, as represented in Figure 2.4. The high-velocity flows created by these microfluidic bioreactors generated shear stress levels capable of fluid mechanical regulation of vascular endothelial cells (Song et al. 2005).

A variable height flow cell has been developed to create an increasing stronger laminar shear stress along a flow path. Flow rates of 5-105 ml/min created a wide range of shear

stress to study adhesion characteristics of neuroblastoma X glioma cells, NG108-15, on different self assembled monolayers of organosilicates (Schneider et al. 2001).

By culture of endothelial cells in microfluidic channels of different widths and subjecting them to steady state shear stress levels, shape and function effects were quantified (Gray et al. 2002). Narrow channels had more elongated bovine aortic endothelial cells, however if channel width was 200 μm or larger, the elongation was similar to that in plastic dishes.

Culture of osteoblasts requires shear stress for enhanced differentiation and expression of alkaline phosphatase and osteocalcin. The ALP expression has been shown to increase three times (even with no flow, due to a 3D environment) and 7.5 times (with low flow, due to simulating shear stress and 3D environment) in a bioreactor made of 3D network of microstructures, compared to a conventional dish culture (Leclerc et al. 2006).

Shear stress has also been shown to induce embryonic stem cell differentiation. F1k-1-positive mouse ES cells subjected to shear stress selectively differentiated into vascular endothelial cell. The shear stressed F1k-1-positive ES cells formed tube-like structures and developed an extensive tubular networks significantly faster than the static controls (2005 Yamamoto et al. 2005).

By creating a microfluidic bioreactor with channels whose width narrows uniformly, just as *in vivo* microcirculation, release of ATP from erythrocytes was found to be

proportional to channel cross sectional area (Price et al. 2006). While Weinberg et al. developed three-dimensional microfluidic constructs for tissue engineering which have uniform wall shear stress throughout the network (Weinberg et al. 2004).

Hang et al. used microfluidic devices to quantify cell adhesion as a function of shear stress by manipulating the geometry and surface chemistry (Lu et al. 2004). The adhesion of fibroblasts to fibronectin-coated substrates was evaluated as a function of shear stress or fibronectin concentration in channels. They also confirmed that the fibroblasts cultured in the perfusion-shear device reduced their adhesion strength to the substrate in response to epidermal growth factor stimulation.

Griffith's group has presented a bioreactor that enables morphogenesis of 3-D tissue structures under continuous perfusion (Power et al. 2002a). Three-dimensional scaffolds were created by deep reactive ion etching of silicon wafers to create an array of channels (through hole) with cell-adhesive walls. Scaffolds were combined with a cell-retaining filter and support across the top of the array and through the 3D tissue mass in each channel. Reactor dimensions were constructed so that media flow rates meet estimated value of cellular oxygen demands while providing fluid shear stress at or below a physiological range (<2 dyne cm^2). Primary rat hepatocytes seeded in the bioreactor rearranged to form tissue like structures reminiscent of liver cords. The aggregates formed bile canaliculi and tight junctions and maintained viability at least 2 weeks (Power et al. 2002b).

The embryonic flow-structure interactions influence whether development will proceed normally or become pathogenic. Genetic, pharmacological, or surgical manipulations that alter the flow environment can thus profoundly influence morphologic and functional cardiovascular phenotypes (Hove 2006).

To get a better understanding of fluid dynamics in microchannels, a three-dimensional numerical flow-model incorporating mass transport has been recently developed to compute substrate concentrations and shear stresses in the fluid environment of the microfluidic bioreactors (Zeng et al. 2006).

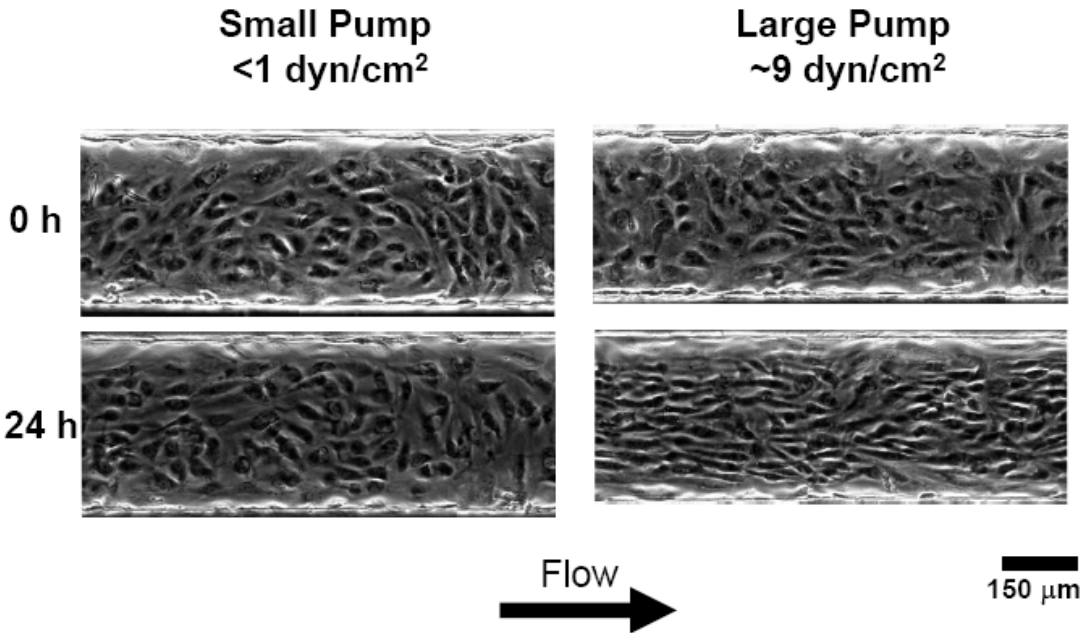

Figure 2.4: Study of effects of shear stress on microvascular endothelial cells inside a continuously perfused microfluidic bioreactor (Song et al. 2005). Time lapse images of ECs comparing changes in their elongation and alignment in response to varying levels of shear stress.

2.2.3.3 Squeezing cells through microchannels

Microchannels have also been used to observe healthy and malaria (Plasmodium falciparum) infected red blood cells (Shelby et al. 2003). The normal erythrocytes were very elastic and passed through channels of varying widths (2-8 □m) and squeezed through blockages readily, while the infected cells in different stages of the disease could not do so.

2.2.3.4 Osmotic Loading

Chao et al. developed a microfluidic device to apply hydrostatic pressure-driven dynamic osmotic loading to observe dynamic changes in cell sizes of cultured bovine articular chondrocytes (Chao et al. 2005). The cells showed a trend of increasing changes in cell size with decreasing loading frequency (for a given osmotic loading magnitude), with significant differences from isotonic control at 0.0125 Hz.

2.3 Other Useful Capabilities of Microfluidic Cell Culture Devices

2.3.1 Efficient manipulation of precious cells or cells available in only small numbers

Some of cell types are so precious and rare or hard to isolate --for example, primary cells like neurons, hematopoeitic stem cells, and human embryos for clinical treatment-- that any study or handling involving them has to be done with great care. Moreover, the biochemical responses of such a small population of cells in culture are difficult to observe because of the dilution effects in the large pool of media surrounding them. Biological studies with such small number of precious cells would greatly benefit from the use of microfluidic culture systems integrated with microanalysis capabilities where

even miniscule quantities of secreted and soluble products can be assayed with accuracy. One example of rare cell culture is shown in Figure 2.5, where murine embryos are grown in a microfluidic device for *in vitro* fertilization.

Stem cell biology in microfluidic bioreactors has focused on two key aspects of differentiation and self renewal of the cells. Recently, attempt has been made to expose primary human neural precursor cells in a parallel manner to various ECM signals and perform a quantitative, multi-parameter analysis of cellular responses. The ECM arrays of signals provided to cells were composed of mixtures of extracellular matrix components, morphogens, and other signaling proteins. The signals affecting developmental decisions on the differentiation of these precursor cells were quantified. Wnt and Notch co-stimulation maintained the cells in an undifferentiated-like, proliferative state, whereas bone morphogenetic protein 4 induced an 'indeterminate' differentiation phenotype characterized by simultaneous expression of glial and neuronal markers (Soen et al. 2006).

ES cell differentiation is often initiated by generation of embryoid bodies (EBs), which are three-dimensional cell aggregate formed by culturing ES cells on a non-adherent substrate (Desbaillets et al. 2000). EB differentiation has been shown to recapitulate many aspects of early embryogenesis, resulting in the generation of a wide variety of cell type within EBs (Choi et al. 2005). Regulating the size of EBs is crucial for controlling the differentiation of ES cells. Recently, several approaches, including microtechnological approaches, have developed to control EB size. There have been

reports of regulating EB size by using microwells to produce ES colonies of defined size and then forming EBs from those colonies (Khademhosseini et al. 2006, Mohr et al. 2006). Uniformly-sized EBs were formed in microfluidic device with semi-porous membrane between two microchannels. This method is compatible with on-chip EB culture and differentiation, opening the way for more comprehensive ES cell processing on a chip (Torisawa et al. 2007b).

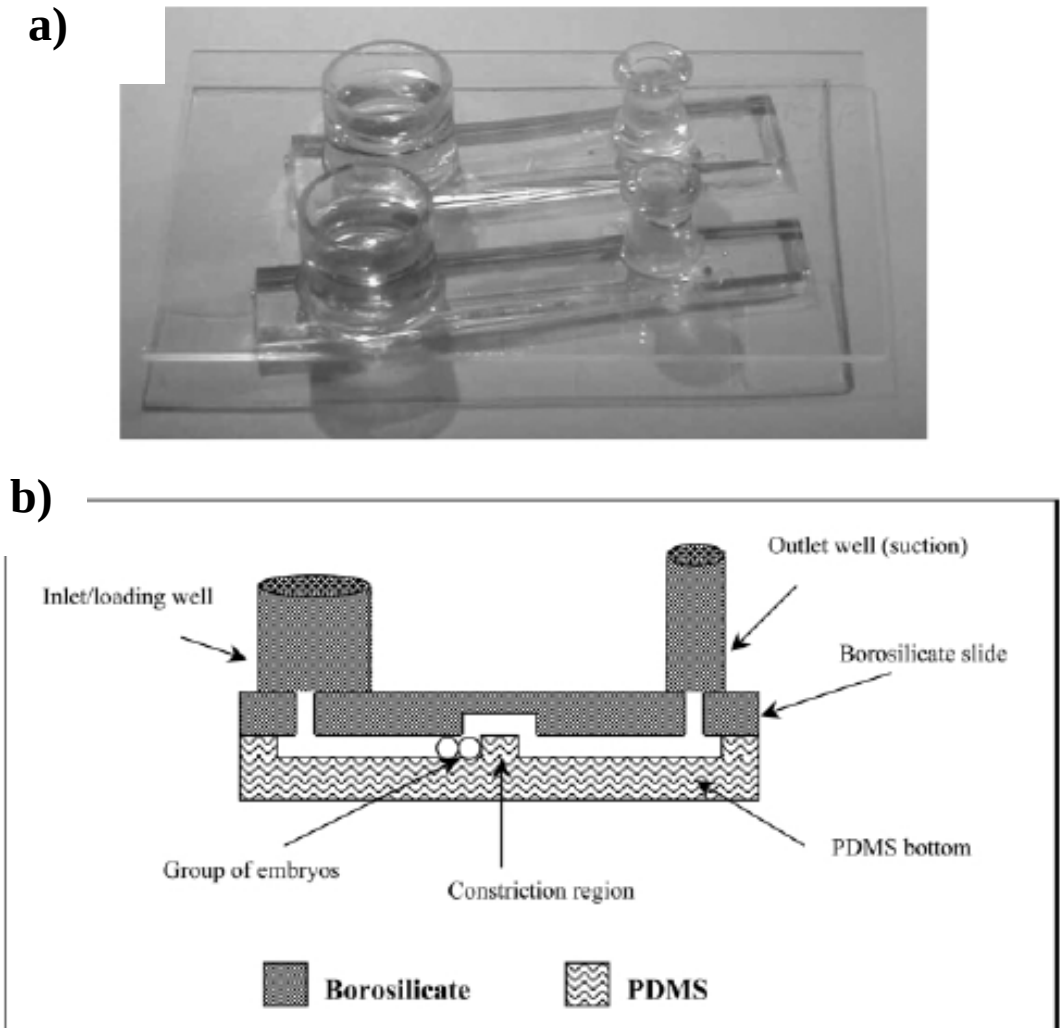

Figure 2.5: **A PDMS/borosilicate device for embryo culture**: a) side view, and b) schematic cross-section of the PDMS/borosilicate device. The basic structure of the device is a PDMS bottom covered with a borosilicate slide that forms the top of the microchannels (Raty et al. 2004).

2.3.2 Integrated assays

Rather than monitoring only simple phenotypic changes, integrated microfluidic bioreactors can gather precise biochemical and mechanistic data from cells and tissues, as in shown in Figure 2.6, in which secretion of a soluble factor by living cells is continuously monitored over time. The rationales for integration of sensing and analysis in the microdevice include greater accuracy and reproducibility, smaller sample sizes, and higher throughput (Park et al. 2003).

Controlled perturbations followed by monitoring cellular responses can provide insight into cellular pathways that govern phenotype and behavior. Thus, a fundamental study of biochemical pathways, cell-fate decisions and tissue morphogenesis is underway in microfluidic bioreactors. These "integrated microfluidic bioreactors" are capable of fast and reproducible measurements with as little as femtomolar sample concentrations and nanoliter volumes. Combining these aspects with the integration of sample preparation and separation steps on the same microfluidic bioreactor has resulted in these systems finding considerable commercial applications in the fields of genomics and proteomics (Clayton 2005).

Immunoassays can be readily analyzed by absorption techniques and fluorescent markers. Quantitative protein analysis and detection can be performed with antibody capture in microdevices as they have high selectivity and affinity of antibody–antigen binding to achieve specificity in analysis. Enzyme-linked immunosorbent assays (ELISA) that amplify the signal from each labeled molecule are now routinely used to detect analytes

with high sensitivity in microfluidic bioreactors (Weigl and Bardell 2004, Rossier and Girault 2001, Roberts and Durst 1995, Diamandis 1996, Hatch et al. 2001, Bernard et al. 2001, Schweitzer et al. 2000, 2002, Carroll et al. 2003, Hayes et al. 2001, Roos and Skinner 2003, von Heeren et al. 1996, Koutny et al. 1996, German and Kennedy 2000, Chiem and Harrison 1997, Jiang et al. 2003).

Microfluidic bioreactors that can continuously monitor insulin secretion from islets of Langerhans with four integrated electrophoresis-based immunoassay channels have been recently developed. The detection limit of the bioassay was 10 nM insulin and insulin release was evaluated every 6.25 s from four islets. (Dishinger and Kennedy 2007). A microfluidic bioreactor with an on-line electrophoresis immunoassay and continuous perfusion was developed by same group to monitor insulin levels in live islet culture. The detection limit of the assay was 0.8 nM and it allowed quantitative monitoring of classical biphasic and oscillatory insulin secretion with 6 s sampling frequency following step changes in glucose from 3 to 11 mM (Shackman et al. 2005). Electrophoretic separation of anti-insulin antibody (Ab), fluorescein isothiocyanate-labeled insulin (FITC-insulin), and insulin from different reservoirs was also carried out in a microfluidic bioreactor. The detection limits for insulin were 3 nM and assays could be collected at 15-s intervals with continuous sampling (Roper et al. 2003).

In a glass microdevice with integrated cell culture, chemical and enzymatic reactions, and detection capabilities, nitric oxide released from macrophage-like cells stimulated by lipopolysaccharide was successfully monitored. The micro-immunoassay was much

faster (assay time 4 h compared to 24 h), detection limit of NO was improved (from 1x10-6 to 7x10-8 M) and the system was also able to monitor a time course of the release (Goto et al. 2005). Moreover, microfluidic bioreactors with an integrated assay modality was able to test potency of different concentrations of 5-Fluorouracil (in gradients) as a cancer drug against live stomach cancer cells (Fujii et al. 2006).

Real-time characterization of gene expression in living hepatocytes in a device has been carried out by King et al. (King et al. 2007). High density matrixes of stimulus-response experiments were performed with help of microvalve arrays (control row-seeding and column-stimulation) in 256 nanoliter-scale bioreactors to obtain quantitative live cell imaging of fluorescent protein transcriptional reporters. Weider et al. fabricated a microfluidic device to monitor GFP-based gene expression in a high-throughput manner, and found that transcription factor NF-kappa B response of live reporter cells on stimulation TNF-alpha shows the same fluorescence kinetics as observed in standard tissue culture (Weider et al. 2005). In another report of on-chip immunoassay, Matsubara et al. fabricated a microfluidic device for on-chip detection of allergic response of rat basophilic leukemia cell line RBL-2H3 to antigen stimulus by fluorescence (Matsubara et al. 2004).

Impedance sensors which monitor morphological changes and motility of adherent cells (Giaever and Keese 1993) and pH sensors which evaluate functional responses of cells upon receptor stimulation by measuring the extracellular H+ have also been developed in microfluidic bioreactors (Park and Shuler 2003). There are also various reports of

measuring oxygen concentrations inside microfluidic devices using optical as well as polarographic measurements (Benninger et al. 2005; Chang-Yen et al. 2003; Mitrovski et al. 2005; Park et al. 2006; Sin et al. 2004; Szita et al. 2005; Vollmer et al. 2005). A PDMS bioreactor coupled with pH and glucose sensors has also been developed to characterize culture of fibroblast cell line, CHO cells, hepatocytes and hybridoma cell lines (Prokop et al. 2004).

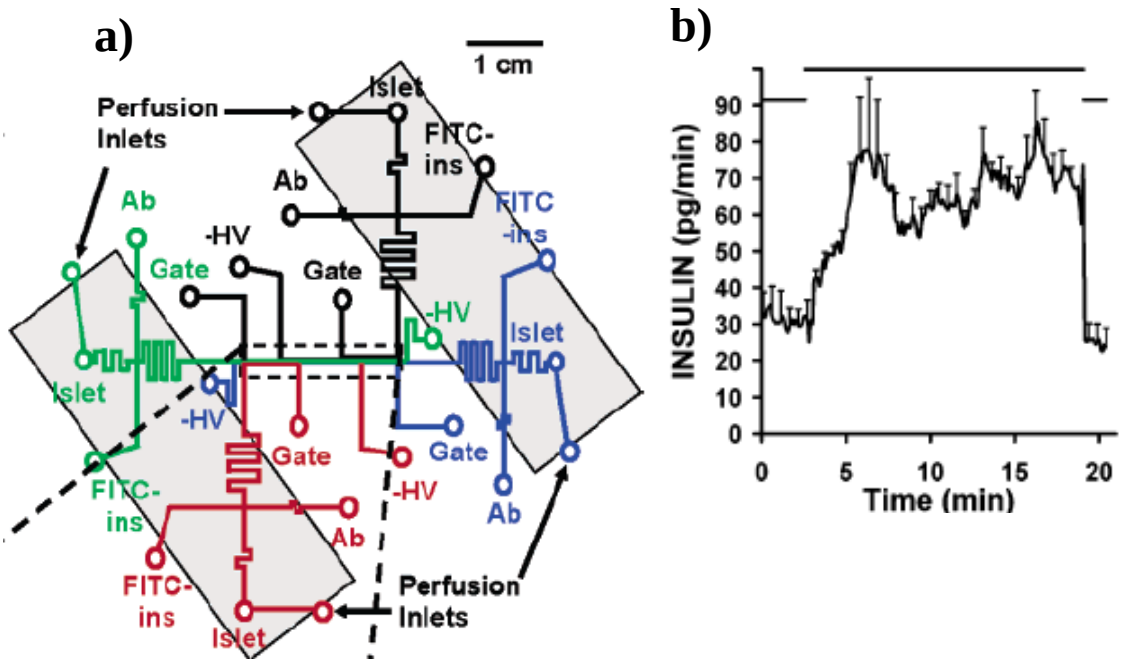

Figure 2.6: Integration of cell culture and analysis in a single microfluidic bioreactor. (Dishinger and Kennedy 2007**). a)** Channel layout of a microfluidic device for monitoring insulin secretion from four islets of Langerhans. **b)** Averaged detected insulin secretion from four islets on a single chip.

2.3.3 Three-dimensional culture

There are many cells where 3-D culture would be more physiological compared to attachment on a 2-D surface. There are many accounts of microfluidic cell culture with defined three dimensional cellular matrices (Liu et al. 2002, Leclerc et al. 2003, Kojima et al. 2003, Power et al. 2002). Some examples are discussed below.

2.3.3.1 Cells in hydrogels inside microfluidic devices

Cells have been cultured in hydrogels inside the microfluidic devices. For example, macrophages and 3T3 fibroblasts were encapsulated in poly(ethylene glycol)(PEG) hydrogel microstructures created by photolithographic polymerization inside PDMS microdevices (Koh and Pishko 2006). HepG2 cells immobilized in channels by hydrodynamic focusing of biocompatible self-assembling peptide hydrogel have been cultured with linear concentration gradients by injecting different reagents on the sides of the scaffold (Kim et al. 2007). Primary rat hepatocytes were immobilized *in situ* in a localized matrix of methylated collagen and a HEMA-MMA-MAA in a microfluidic bioreactor (Toh et al. 2005). Cells have also been grown in 3-D layers of extracellular matrix biopolymers (collagen, chitosan, fibronectin, matrigel, and fibrin) which were micropatterned in PDMS devices (Tan and Desai 2003, 2004). Anticancer drug sensitivity test was performed using PDMS microfluidic devices in which collagen gel-embedded cells were entrapped. The proliferation rate of collagen gel-embedded cells was close to that *in vivo* and their drug sensitivity was less than that of 2-D cells, suggesting that the 3-D culture conditions provide a more *in vivo*-like environment (Torisawa et al. 2005).

2.3.3.2 Cells in gel channels

Microfluidic devices were even made by molding gelatin to produce microchannels for culture of adherent epithelial cells (Paguirigan and Beebe 2006). Microfluidic bioreactors have also been fabricated from biocompatible photopolymerized poly(ethylene) glycol diacrylate (PEGDA) (Butterworth et al., 2004). Recently, Leclerc

et al. used a photosensitive biodegradable polymer (pCLLA acrylate) to create single and multistep microstructures, as well as microstructure with simple fluidic channels. These microstructures are able to support culture of mammalian cells to grow and spread on it. With Hep G2 cells, human umbilical blood vessel endothelial cells (HUVEC), 3T3-L1 mouse fibroblasts (Leclerc et al. 2004b).

2.4 Microfluidic Devices Useful for Cell Applications Other than Culture

Microfluidic devices are useful for more than cell culture. Devices have been used in cell sorting, for example, in separations of non-motile and motile cells such as sperm. (Cho et al. 2003), in separation of the contents of single cells (McClain et al. 2003), separations coupled to mass spectroscopy (Vilkner et al. 2004), high-throughput screening in drug development (Lion et al. 2003, Andersson and van den Berg 2003), bioanalyses (Sia and Whitesides 2003), and examination and manipulation of samples consisting of a single cell (Verpoorte 2002) or a single molecule (Helmke and Minerick 2006, Stavis et al. 2005).

Microfluidic devices have been used to isolate small numbers of target cells (or even single cells) from a large population of cells on the basis of physical and chemical properties such as electrical characteristics, chromatography or fluorescent markers (Brehm-Stecher and Johnson 2004, Becker et al. 1995, Hu et al. 2005, Huang et al. 2002, Fu et al. 2002, Chang et al. 2005, Revzin et al. 2005). A comprehensive review of recent developments in microfabricated flow cytometers and related microfluidic devices that can detect, analyze, and sort cells or particles is provided by Huh et al. (Huh et al. 2005).

2.5 Future Prospects for Biological Studies in Microfluidic Bioreactors

One of the useful applications of microfluidics is the culture of cells under engineered physiologic conditions. In microfluidic bioreactors, well-defined physiologically-relevant chemical and fluid mechanical microenvironments can be created for answering fundamental questions in cell biology. These *in vitro* microenvironments can be powerful tools for studying disease mechanisms, testing drug safety and efficacy, engineering microscale tissues, and developing cell-based biosensors. In these systems, one can systematically perturb cell culture conditions for specific experiments, test many different conditions on the same or different cells or even different parts of the same cell. On-chip integration of quantitative analysis and sensing greatly expands the biological applications of these devices.

Just as the electronic industry has integrated more and more components onto smaller and smaller an area, the trend in the bioMEMS community is to integrate more and more types of cells and analysis capabilities on a chip, with a possible eventual establishment of an animal-on-a-chip or a human-on-a-chip. Having all tissues growing in one single device could be a great boon to drug screening and clinical research. However, in order to achieve an organotypic culture of such complexity, we must first be able to engineer the microenvironment of each cell type with high quality and precision in terms of recapitulating physiologic conditions. This type of research requires in depth knowledge of not only microfluidic engineering and materials science but also the underlying biology. Collaborations between bioengineers and biologists or clinicians need to be

further enhanced to unleash the true potential of microfluidics for the study of cell biology and application to the clinic.

2.6 *In Vivo* Bone Marrow Biology

Bone marrow is the primary niche of HSCs in adult mammals. The features of an HSC niche include: a small number of HSCs surrounded by supporting cells, low oxygen tension, close proximity of HSCs to sinusoidal endothelial cells as well as to osteoblasts on the endosteum, and adhesive and soluble signals between HSCs and surrounding cells. Osteoblasts and other stromal supporting cells (including endothelial cells, megakaryocytes, adipocytes, and fibroblasts) play a central role in hematopoiesis, and produce many factors essential for the survival, renewal and maturation of hematopoeitic stem cells (Scadden 2006). Some of the features of *in vivo* bone marrow are represented in Figure 2.7, where a single HSC (stained in red) is in close contact with numerous supporting cells (in green and yellow), and sits very close to a sinusoidal blood vessel. These key features can be recreated in microfluidic bioreactors, as shown in Figure 2.2; however, conventional culture does not recapitulate these important features (as seen in upper panel of Figure 2.2).

The *in vivo* HSC niche is composed of an intricate blend of extracellular matrix proteins, soluble protein factors, immobilized protein factors, proteoglycans, small molecule signals, mineralized tissue, and numerous adjacent cell types, which vary in space and time. Thus, these components present the HSCs with biochemical signals, and the HSCs are continually faced with the sensing these inputs, processing the signals through signal

transduction and gene regulation networks, and executing cell behavioral or fate choices (Adams & Scadden 2006; Jang & Schaffer 2006; Shim et al. 2003). As depicted in Figure 1.1, two of the most important niche components are the *oxygen tension, niche substrate* and *3-D architecture*. We focus on these three parameters in this thesis.

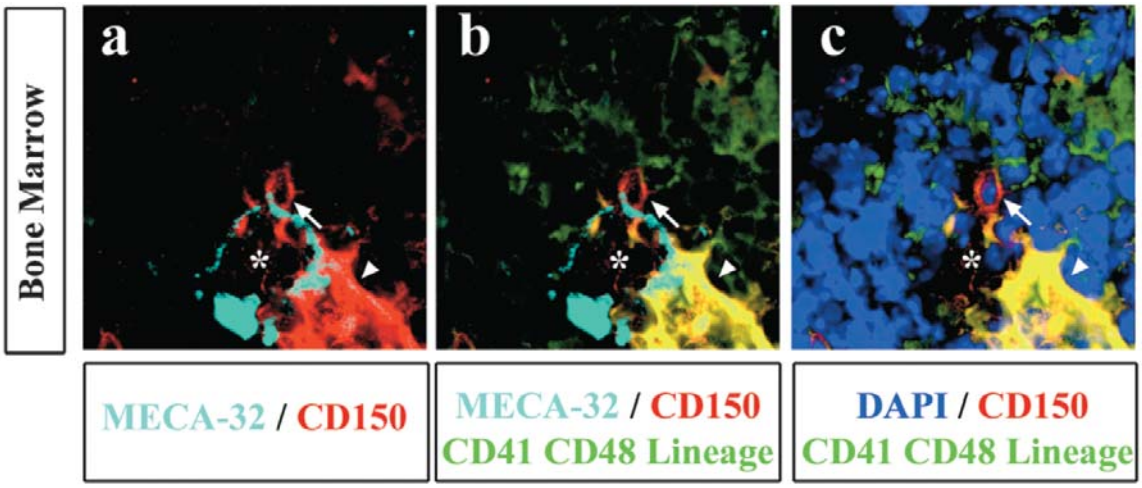

Figure 2.7: In normal bone marrow, HSCs ($CD150^{+}CD48^{-}CD41^{-}Lineage^{-}$) represent 0.0067% ± 0.0016% of cells in tissue sections shown here. Some of the HSCs are closely associated with endosteum, and most of them contact sinusoidal endothelium (C, arrow). A large megakaryocyte is also seen associated with the sinusoid (C, arrowhead). These images each represent a single optical section (Kiel et al. 2005).

Hematopoeitic stem cells (HSCs) are defined as cells that retain the capacities for both self-renewal and multilineage differentiation, and can give rise to all blood cell types (see Figure 2.8). In adult mouse BM, $CD34^{low/-}$c-$Kit^{+}Sca\text{-}1^{+}Lin^{-}$ ($CD34^{-}$KSL) cells, which constitute 0.004% of BM cells, represent HSCs with long-term repopulating (LTR) ability, whereas $CD34^{+}$KSL cells are progenitors with short-term repopulating capacity (Kiel et al. 2005a; Kiel et al. 2005b). In normal bone marrow, 0.0067% ± 0.0016% of cells in sections are $CD150^{+}CD48^{-}CD41^{-}Lineage^{-}$ (or pure HSCs). Some of these cells are closely associated with endosteum, sinusoidal endothelium and megakaryocytes.

Understanding the molecular mechanisms underlying these cell–cell interactions (mediated by cell-surface or secreted molecules) holds the key for HSC biology and is of biological and clinical interest.

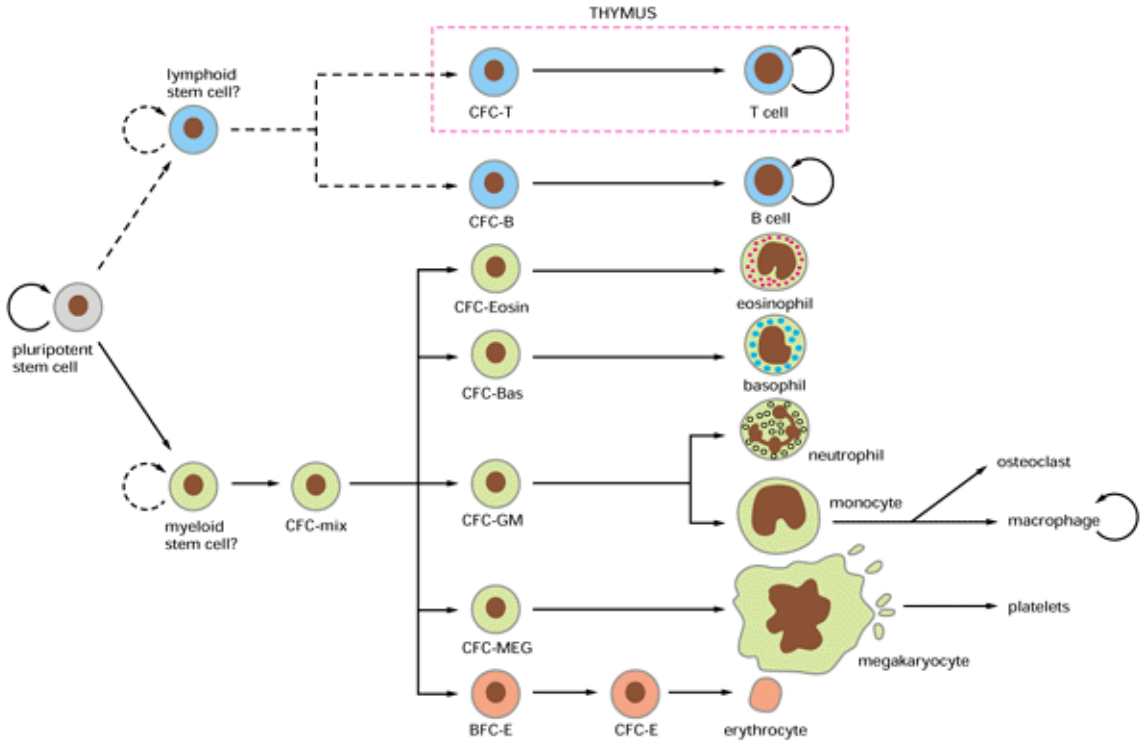

Figure 2.8: General model of hematopoiesis and hematopoietic stem cell lineages

HSCs can renew themselves, differentiate into all types of blood cells, mobilize out of bone marrow and undergo apoptosis. The bone marrow is the classic source of HSCs, along with fetal liver, umbilical cord, aorta-gonad-mesopherous region and peripheral blood. About 1 in every 100,000 cells in the marrow is a long-term, blood-forming stem cell; other cells present include stromal cells, stromal stem cells, blood progenitor cells, and mature and maturing white and red blood cells (as seen in Figure 2.9). Long-term replicating HSCs renew themselves throughout the lifespan of the organism; therefore, they are very important for developing HSC-based cell therapies. Unfortunately, to date, researchers cannot distinguish with 100% accuracy the long-term from the short-term

cells when they are removed from the bloodstream or bone marrow. A small number of stem and progenitor cells circulate in the bloodstream. HSCs that have been mobilized into peripheral circulation are mostly non-dividing cells. HSCs taken from tissues at earlier developmental stages have a greater ability to self-replicate, show different homing and surface characteristics, and are less likely to be rejected by the immune system (nih.gov).

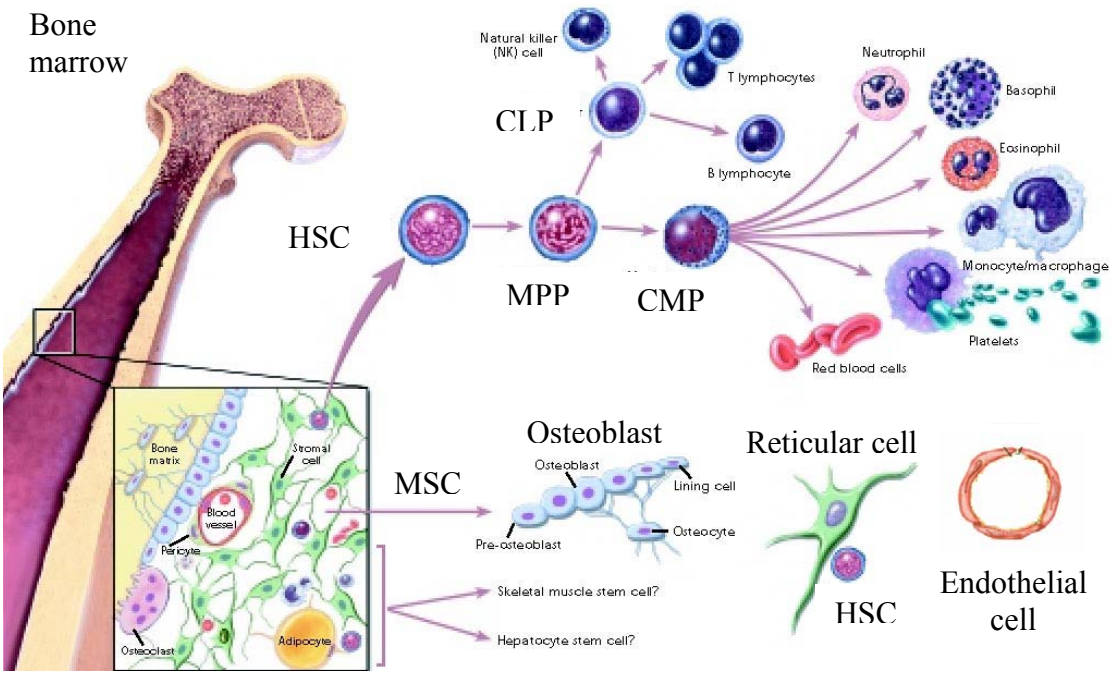

Figure 2.9: Hematopoietic and Stromal Stem Cell Differentiation (www.nih.gov)

HSCs live in intimate connection with the stroma of bone marrow in adults. Adhesion molecules in the stroma play a role in mobilization, attachment to the stroma, and in transmitting signals that regulate HSC self-renewal and progenitor differentiation. Therefore, the study of HSCs is very important for developing new cures for hematopoietic disorders.

2.6.1 Bone Marrow Stromal Cells (BMSCs)

In bone marrow, hematopoiesis occurs in close contact with the stromal microenvironment; the bone marrow stromal cells support hematopoietic stem cell growth and differentiation. As shown in Figure 2.10, the bone marrow stroma is composed of a variety of different cell types that provide structural and functional support for hematopoiesis. Stromal cells, in addition to providing the physical environment in which HSCs differentiate, generate cartilage, bone, and fat. They support hematopoiesis; differentiate towards osteogenic, chondrogenic and adipogenic lineages; and form a bone structure complete of hematopoietic marrow.

Bone marrow stromal cells (BMSCs) are isolated from the iliac crest bone marrow aspirates in humans or femurs and tibias in mice. A bone marrow sample provides a low frequency of BMSCs derived from mesoderm tissue. For gene therapies, BMSCs must be able to provide long-term proliferation. Cell therapy of bone lesions by *ex vivo* expanded osteogenic progenitor been developed to repair bone via local delivery of cells within a scaffold. The possibility of using mesenchymal progenitors in the therapy of genetic bone diseases via systemic infusion is very appealing. Experimental evidence suggests that mesenchymal progenitors delivered by this route engraft with very low efficiency and does not produce relevant and durable clinical effects.

Although BMSC multi-lineage differentiation potential is supported by substantial experimental evidence, a better understanding of the mechanisms controlling their differentiation is required to exploit them for therapy of human diseases. Furthermore, a

deeper understanding of their engraftment mechanisms will extend the field of therapeutic applications of mesenchymal progenitors. The BMSC interactions with HSCs that induce HSC commitment, differentiation, and proliferation need to be exploited to treat numerous autoimmune diseases.

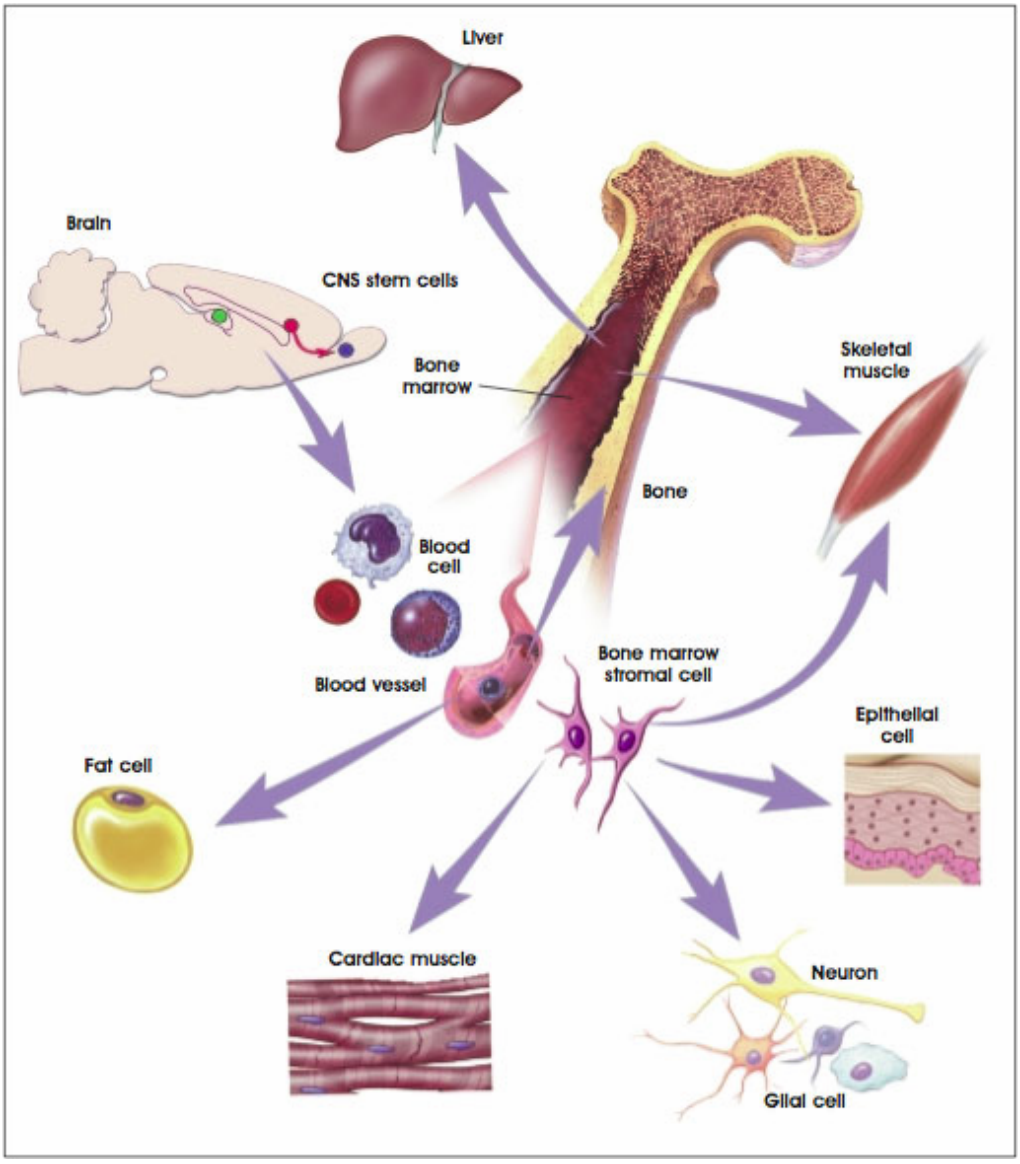

Figure 2.10: BMSC differentiation into various cell types (www.nih.gov)

2.6.2 HSC-BMSC Cell-Cell interaction in stem cell niche

Regulation of HSC fate involves multiple highly orchestrated pathways that determine the cell cycle status, and gene expression profile. HSCs do not grow as independent autonomous units; instead, they are completely surrounded by the marrow micro-environment, which is defined by cell-cell interactions, cell-ECM interactions, and exposure to variable concentrations and combinations of soluble factors including cytokines. The bone marrow microenvironment is comprised of stromal cells, a diverse population consisting of fibroblasts, smooth muscle cells, endothelial cells and others. These cells not only provide a scaffold to the developing stem cells and progenitor cells, but also produce transmembrane ligands, extracellular matrix components, and soluble proteins. HSCs are exposed in situ to many different growth factors, some soluble, some bound to ECM, and some bound to adjacent cells, some of which are outlined in Figure 2.11. Frequent cell-cell signaling occur when HSCs are in cell-cell contact with stromal cells, committed hematopoietic progenitor cells, and other HSCs. ECM of bone marrow acts in concert with cell-cell interactions and soluble factors to regulate the HSC. Adhesion of hematopoietic stem and progenitor cells to the marrow ECM inhibits cellular proliferation and prevents apoptosis, both of which leads to long term survival of quiescent hematopoietic stem cells. Numerous molecules within the HSC membranes mediate signals from the ECM including integrins, immunoglobulin-like molecules, cadherins, selectins, and mucins (Morrison et al. 2008; Taichman 2005; Taichman et al. 1998; Wilson et al. 2006; Yin et al. 2006).

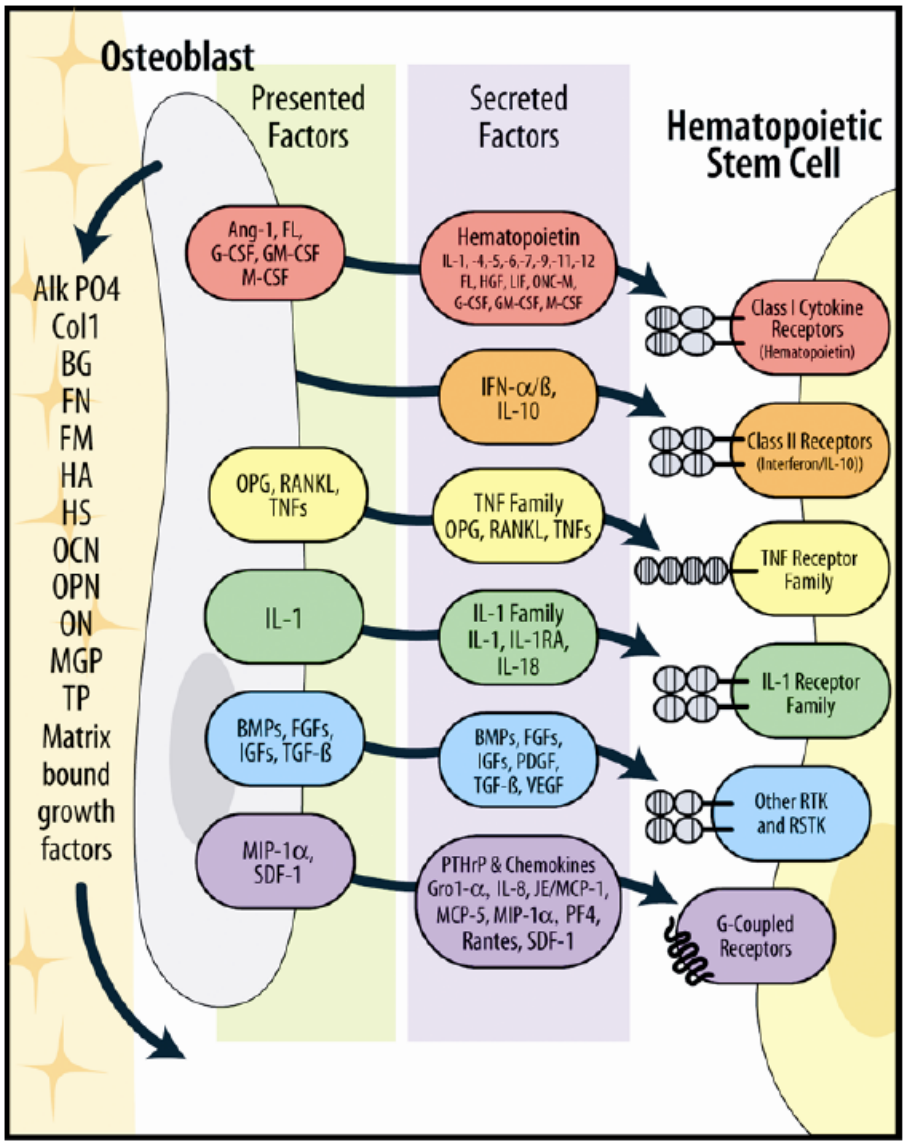

Figure 2.11: A Model of Secreted and Cell-Associated Factors Produced by Osteoblasts that Influence HSC. Stem cell fate is influenced by specialized microenvironments that remain poorly defined. Osteoblast production of soluble hematopoietic-supportive secreted and cell-associated factors work in concert so that hematopoietic stem cells derive regulatory information from bone, accounting for the localization of hematopoiesis in bone marrow. Abbreviations; alkaline phosphatase (Alk P04), bone morphogenic factors (BMPs), byglycan (BG), collagen type I (ColI), fibroblast growth factors (FGFs), Flt ligand (FL), fibronectin (FN), fibromodulin (FM), granulocyte colony stimulating factor (G-CSF), granulocyte macrophage colony stimulating factor (GM-CSF), hepatocyte Growth Factor (HGF), heparin sulfate protyoglycan (HS), insulin like growth factors (IGFs),interferon (IFN),interleukin (IL), leukemia inhibitory factor (LIF), macrophage colony stimulating factor (M-CSF), macrophage inhibitory factor (MIP), monocyte chemotactic protein (MCP)-1/JE (JE), matrix Gla protein (MGP), oncostatin-M (ONC-M), osteocalcin (OC), osteonectin (ON), osteopontin (OP) osteoprotogerin (OPG), platelet derived growth factor (PDGF), platelet

factor 4 (PF4), receptor activator of NF-kappaB ligand (RANKL), tyrosine kinase receptors (RTK), serine/threonine kinase receptors (RSTK), regulated on activation, normal T-cell expressed and secreted (RANTES), stromal derived factor -1 (SDF-1), transforming growth factor (TGF), thrombospondin (TP), tumor necrosis factor (TNF). (Taichman 2005)

HSCs are clinically useful for leukemia and lymphoma (such as acute lymphoblastic leukemia, acute myeloblastic leukemia, chronic myelogenous leukemia, Hodgkin's disease, multiple myeloma, and non-Hodgkin's lymphoma), inherited blood disorders (such as aplastic anemia, beta-thalassemia, Blackfan-Diamond syndrome, globoid cell leukodystrophy, sickle-cell anemia, severe combined immunodeficiency, X-linked lymphoproliferative syndrome, and Wiskott-Aldrich syndrome. Inborn errors of metabolism that are treated with bone marrow transplants include: Hunter's syndrome, Hurler's syndrome, Lesch Nyhan syndrome, and osteopetrosis), and as rescue in cancer chemotherapy as rapidly dividing marrow cells are often target of such treatments in addition to the cancer cells. Additionally HSCs are used in other diseases, primarily autoimmune diseases, such as diabetes, rheumatoid arthritis, and system lupus erythematosis in an effort to reconstitute or reprogram the immune system.

References

Abhyankar, V. V.; Lokuta, M. A.; Huttenlocher, A.; Beebe, D. J. Lab Chip 2006, 6, 389-393.

Adams, G. M.; Scadden, D. T. Nat. Immunol. 2006, 7, 333-337.

Allen, J. W.; Bhatia, S. N. Biotechnol. Bioeng. 2003, 82, 253-262.

Allen, J. W.; Khetani, S. R.; Bhatia, S. N. Toxicol. Sci. 2005, 84, 110-119.

Alon, R.; Hammer, D. A.; Springer, T. A. Nature 1995, 374, 539-542.

Andersson, H.; van den Berg, A. Sens. Actuators B Chem. 2003, 92, 315-325.

Ando, J.; Kamiya, A. Front. Med. Biol. Eng. 1993, 5, 245-264.

Becker, F. F.; Wang, X. B.; Huang, Y.; Pethig, R.; Vykoukal, J.; Gascoyne, P. R. Proc. Natl Acad. Sci. USA 1995, 92, 860-864.

Benninger, R. K. P.; Hofmann, O.; McGinty, J.; Requejo-Isidro, J.; Munro, I.; Neil, M. A. A.; deMello, A. J.; French, P. M. W. Opt. Express 2005, 13, 6275-6285.

Bernard, A.; Michel, B.; Delamarche, E. Anal. Chem. 2001, 73, 8-12.

Blackman, B. R.; Garcia-Cardena, G.; Gimbrone, M. A. J. Biomech. Eng. 2002, 124, 397-407.

Bock, T. A. Stem Cells 1997, 15 suppl. 1, 185-195.

Brehm-Stecher, B. F.; Johnson, E. A. Microbiol. Mol. Biol. Rev. 2004, 68, 538-559.

Breslauer, D. N.; Lee, P. J.; Lee, L. P. Mol. Biosys. 2006, 2, 97-112.

Butterworth, Amy; Lopez Garcia, Maria del Carmen; Beebe, D., Proceedings of Micro Total Analysis Systems 2004, Special Publication - Royal Society of Chemistry, 2004, 297 (Volume 2), 4-6.

Carroll, A.; Scampavia, L.; Luo, D.; Lernmark, A.; Ruzicka, J. Analyst 2003, 128, 1157-1162.

Chang, W. C.; Lee, L. P.; Liepmann, D. Lab Chip 2005, 5, 64-73.

Chang-Yen, D. A.; Gale, B. K. Lab Chip 2003, 3, 297-301.

Chao, P. G.; Tang, Z.; Anqelini, E.; West, A. C.; Costa, K. D.; Hung, C. T. J. Biomech. 2005, 38, 1273-1281.

Chiem, N.; Harrison, D. J. Anal. Chem. 1997, 69, 373-378.

Cho, B. S.; Schuster, T. G.; Zhu, X.; Chang, D.; Smith, D.; Takayama, S. Anal. Chem. 2003, 75, 1671–1675.

Choi, D.; Lee, H. –J.; Jee, S.; Jin, S.; Koo, S. K.; Paik, S. S.; Jung, S. C.; Hwang, S. –Y.; Lee, K. S.; Oh, B. Stem Cells 2005, 23, 817-827.

Chueh, B.; Huh, D.; Kyrtsos, C. R.; Houssin, T.; Futai, N.; Takayama, S. Anal. Chem. 2007, 79, 3504-3508.

Chung, B. G.; Flanagan, L. A.; Rhee, S. W.; Schwartz, P. H.; Lee. A. P.; Monuki, E. S.; Jeon, N. L. Lab Chip 2005, 5, 401-406.

Clark, S.G.; Haubert, K; Beebe, D. J.; Ferguson, C. E.; Wheeler, M. B. Lab Chip 2005, 5, 1229-1232.

Clayton, J. Nat. Methods 2005, 2, 621-627.

Cox, J. D.; Curry, M. S.; Skirboll, S. K.; Gourley, P. L.; Sasaki, D. Y. Biomaterials 2002, 23, 929-35.

Dai, G. H.; Kaazempur-Mofrad, M. R.; Natarajan, S.; Zhang, Y. Z.; Vaughn, S.; Blackman, B. R.; Kamm, R. D.; Garcia-Cardena, G.; Gimbrone, M. A. Proc. Natl. Acad. Sci. USA 2004, 101, 14871-14876.

Davidsson, R.; Boketoft, A.; Bristulf, J.; Kotarsky, K.; Olde, B.; Owman, C.; Bengtsson, M.; Laurell, T. Emneus, J. Anal. Chem. 2004, 76, 4715-4720.

Davies, P. F.; Dewey, C. F.; Bussolari, S. R.; Gordon, E. J.; Gimbrone, M. A. J. Clin. Invest. 1984, 73, 1121-1129.

Davies, P. F.; Remuzzi, A.; Gordon, E. J.; Dewey, C. F.; Gimbrone, M. A. Proc. Natl. Acad. Sci. USA 1986, 83, 2114-2117.

Desbaillets, I.; Ziegler, U.; Groscurth, P.; Gassmann, M. Exp. Physiol. 2000, 85, 645-651.

Dewey, C. F.; Bussolari, S. R.; Gimbrone, M. A.; Davies, P. F. J. Biomed. Eng. 1981, 103, 177-185.

Diamandis, E. P.; Yu, H.; Melegos, D. N. Clin. Chem. 1996, 42, 853-857.

Dishinger, J. F.; Kennedy, R. T. Anal. Chem. 2007, 79, 947-954.

Finger, E. B.; Purl, K. D.; Alon, R.; Lawrence, M. B.; von Andrian, U. H.; Spinger, T. A. Nature 1996, 379, 266-269.

Flaherty, J. T.; Ferrans, V. J.; Tucker, W. K.; Fry, D. L.; Patel, D. J.; Prierce, J. E. Circ. Res. 1972, 30, 23-33.

Forry, S. P.; Reyes, D. R.; Gaitan, M.; Locascio, L. E. Langmuir 2006, 22, 5770-5775.

Fu, A. Y.; Chou, H. P.; Spence, C.; Arnold, F. H.; Quake, S. R. Anal. Chem. 2002, 74, 2451-2457.

Fujii, S.; Uematsu, M.; Yabuki, S.; Abo, M.; Yoshimura, E.; Sato, K. Anal. Sci. 2006, 22, 87-90.

Fukuda, J.; Khademhosseini, A.; Yeo, Y.; Yang, X.; Yeh, J.; Eng, G.; Blumlimg, J.; Wang, C. –F.; Kohane, D. S.; Langer, R. Biomaterials 2006, 27, 5259-5267.

Futai, N; Gu, W.; Song, J. W.; Takayama, S. Lab Chip 2006a, 6, 149-154.

Futai, N.; Naruse, K.; Smith, G. D.; Takayama, S. Igaku no Ayumi (in Japanease) 2006b, 218, 4523-452.

Garcia-Cardena, G.; Comander, J.; Anderson, K. R.; Blackman, B. R.; Gimbrone, M. A. Proc. Natl. Acad. Sci. USA 2001, 98, 4478-4485.

German, I.; Kennedy, R. T. Anal. Chem. 2000, 72, 5365-5372.

Ghanem, A.; Shuler, M. L. Biotechnol. Prog. 2000, 16, 334-345.

Ghanem, A.; Shuler, M. L. Biotechnol. Prog. 2000, 16, 471-479.

Giaever, I.; Keese, C. R. Nature 1993, 366, 591-592.

Glasgow, I. K.; Zeringue, H. C.; Beebe, D. J.; Choi, S. J.; Lyman, J. T.; Chan, N. G.; Wheeler, M. B. IEEE Trans. Biomed. Eng. 2001, 48, 570-578.

Goto, M.; Sato, K.; Murakami, A.; Tokeshi, M.; Kitamori, T. Anal. Chem. 2005, 77, 2125-2131.

Gray, B. L.; Lieu, D. K.; Collins, S. D.; Smith, R. L.; Barakat, A. I. Biomed. Microdev. 2002, 4, 9-16.

Hatch, A.; Kamholz, A. E.; Hawkins, K. R.; Munson, M. S.; Schilling, E. A.; Weigl, B. H.; Yager, P. Nat. Biotechnol. 2001, 19, 461-465.

Hayes, M. A.; Polson, T. N.; Phayre, A. N.; Garcia, A. A. Anal. Chem. 2001, 73, 5896-5902.

Helmke, B. P.; Minerick, A. R. Proc. Natl Acad. Sci. USA 2006, 103, 6419-6424.

Heo, Y. S.; Cabrera, L. M.; Song, J. W.; Futai, N.; Tung, Y. –C.; Smith, G. D.; Takayama, S. Anal. Chem. 2007, 79, 1126-1134.

Hickman, D. L.; Beebe, D. J.; Rodriguez-Zas, S. L.; Wheeler, M. B. Comp. Med. 2002, 52, 122-126.

Hove, J. R. Pediatr. Res. 2006, 60, 6-13.

Hu, X.; Bessette, P. H.; Qian, J.; Meinhart, C. D.; Daugherty, P. S.; Soh, H. T. Proc. Natl Acad.Sci. USA 2005, 102, 15757-15761.

Huang, Y.; Joo, S.; Duhon, M.; Heller, M.; Wallace, B.; Xu, X. Anal. Chem. 2002, 74, 3362-3371.

Huh, D.; Kamotani, Y.; Grotberg, J. B.; Takayama, S., Proceedings of Micro Total Analysis Systems 2004, Special Publication - Royal Society of Chemistry, 2004, 297 (Volume 2), 282-284.

Huh, D.; Tkaczyk, A. H.; Bahng, J. H.; Chang, Y.; Wei, H. H.; Grotberg, J. B.; Kim, C. J.; Kurabayashi, K.; Takayama, S. J. Am. Chem. Soc. 2003, 125, 14678-14679.

Huh, D.; Gu, W.; Kamotani, Y.; Grotberg, J. B.; Takayama, S. Physiol. Meas. 2005, 26, R73-R98.

Huh, D.; Fujioka, H.; Tung, Y.-C.; Futai, N.; Paine, R.; Grotberg, J. B.; Takayama, S. Proc. Natl Acad. Sci. USA in revision.

Hung, P. J.; Lee, P. J.; Sabounchi, P.; Lin, R.; Lee, L. P. Biotechnol. Bioeng. 2005a, 89, 1-8.

Hung. P. J.; Lee, P. J.; Sabounchi, P.; Aghdam, N.; Lin, R.; Lee, L. P. Lab Chip 2005b, 5, 44-48.

Jang, J. H.; Schaffer, D. V. Mol. Syst. Biol. 2006, 2, 39.

Jeon, N. L.; Baskaran, H.; Dertinger, S. K. W.; Whitesides, G. M.; Water, L. V. D.; Toner, M. Nat. Biotechnol. 2002, 20, 826-830.

Jiang, X. Y.; Ng, J. M.; Stroock, A. D.; Dertinger, S. K.; Whitesides, G. M. J. Am. Chem. Soc. 2003, 125, 5294-5295.

Kane, B. J.; Zinner, M. J. Yarmush, M. L.; Toner, M. Anal. Chem. 2006, 78, 4291-4298.

Katz, M. J.; Lasek, R. J. Cell Motil. 1980, 1, 141-157.

Khademhosseini, A.; Yeh, J.; Eng, G.; Karp, J.; Kaji, H.; Borenstein, J.; Farokhzad, O. C.; Langer, R. Lab Chip 2005, 5, 1380-1386.

Khademhosseini, A.; Ferreira, L.; Blumling, J.; Yeh, J.; Karp, J. M.; Fukuda, J.; Langer, R. Biomaterials 2006, 27, 5968-5977.

Kim, L.; Vahey, M. D.; Lee, H. Y.; Voldman, J. Lab Chip 2006, 6, 394-406.

Kim, M. S.; Yeon, J. H.; Park, J. –K. Biomed. Microdev. 2007, 9, 25-34.

King, K. M.; Wang, S. Irimia, D.; Jayaraman, A.; Toner, A.; Yarmush, M. L. Lab Chip 2007, 7, 77-85.

Koh, W. G.; Pishko, M. V. Anal. Bioanal. Chem. 2006, 385, 1389-1397.

Koide, N.; Sakaguchi, K.; Koide, Y.; Asano, K.; Kawaguchi, M.; Matsushima, H.; Takenami, T.; Shinji, T.; Mori, M.; Tsuji, T. Exp. Cell Res. 1990, 186, 227-235

Kojima, K.; Moriguchi, H.; Hattori, A.; Kaneko, T.; Yasuda, K. Lab Chip 2003, 3, 292-296.

Korin, N.; Bransky, A.; Dinnar, U.; Levenberg, S., Proceedings of SPIE-The International Society for Optical Engineering, 2007, 6416 (Biomedical Applications of Micro- and Nanoengineering), 64160N/1-64160N/8.

Koutny, L. B.; Schmalzing, D. Taylor, T. A.; Fuchs, M. Anal. Chem. 1996, 68, 18-22.

Leclerc, E.; Sakai, Y.; Fujii, T. Biomed. Microdev. 2003, 5, 109-114.

Leclerc, E.; Sakai, Y.; Fujii, T. Biotechnol. Prog. 2004a, 20, 750-755.

Leclerc, E.; Furukawa, K. S.; Miyata, F.; Sakai, Y.; Ushida, T.; Fujii, T. Biomaterials 2004b, 25, 4683-4690.

Leclerc, E.; David, B.; Griscom, L.; Lepioufle, B.; Fujii, T.; Layrolle, P.; Legallaisa, C. Biomaterials 2006, 27, 586-595.

Lee, P. J.; Hung, P. J.; Rao, V. M.; Lee, L. P. Biotechnol. Bioeng. 2006, 94, 5-14.

Lin, F.; Saadi, W.; Rhee, S. W.; Wang, S. –J.; Mittal, S.; Jeon, N. L. Lab Chip 2004, 4, 164-167.

Lin, F.; Nguyen, C. M.; Wang, S. J.; Saadi, W.; Gross, S. P.; Jeon, N. L. Ann. Biomed. Eng. 2005, 33, 475-82.

Lin, F.; Butcher, E. C. Lab Chip 2006, 6, 1462-1469.

Lion, N.; Rohner, T. C.; Dayon, L.; Arnaud, I. L.; Damoc, E.; Youhnovski, N.; Wu, Z. Y.; Roussel, C.; Josserand, J.; Jensen, H.; Rossier, J. S.; Przybylski, M.; Girault, H. H. Electrophoresis 2003, 24, 3533-3562.

Liu, V. A.; Bhatia, S. N. Biomed. Microdev. 2002, 4, 257-266.

Lu, H.; Koo, L. Y.; Wang, W. M.; Lauffenburger, D. A.; Griffith, L. G.; Jensen, K. F. Anal. Chem. 2004, 76, 5257-5264.

Lucchetta, E. M.; Lee, J. H.; Fu, L. A.; Patel, N. H.; Ismagilov, R. F. Nature 2005, 434, 1134-1138.

Matsubara, Y.; Murakami, Y.; Kobayashi, M.; Morita, Y.; Tamiya, E. Biosens. Bioelectron. 2004, 19, 741-747.

McClain, M. A.; Culbertson, C. T.; Jacobson, S. C.; Allbritton, N. L.; Sims, C. E.; Ramsey, J. M. Anal. Chem. 2003, 75, 5646-5655.

Mehta, G.; Mehta, K.; Sud, D.; Song, J. W.; Bersano-Begey, T.; Futai, N.; Heo, Y. S.; Mycek, M. –A.; Linderman, J. J.; Takayama, S. Biomed. Microdev., 2007, 9, 123-134.

Mehta G.; Kiel M. J.; Lee J. W.; Kotov N.; Linderman J. J.; Takayama S.; Advanced functional Materials, 2007, 17, 2701-2709

Mitrovski, S. M.; Nuzzo, R. G. Lab Chip 2005, 5, 634-645.

Mohr, J. C.; de Pablo, J. J.; Palecek, S. P. Biomaterials 2006, 27, 6032-6042.

Ostrovidov, S.; Jiang, J.; Sakai, Y.; Fujii, T. Biomed. Microdev. 2004, 6, 279-287.

Otsuka, H,; Hirano, A.; Nagasaki, Y.; Okano, T.; Horiike, Y.; Kataoka, K. ChemBioChem 2004, 5, 850-855.

Paguirigan, A.; Beebe, D. J. Lab Chip 2006, 6, 407-413.

Park, J.; Berthiaume, F.; Toner, M.; Yarmush, M. L.; Tilles, A. W. Biotechnol. Bioeng. 2005, 90, 632-644.

Park, J.; Bansal, T.; Pinelis, M.; Maharbiz, M. M. Lab Chip 2006, 6, 611-622.

Park, T. H.; Shuler, M. L. Biotechnol. Prog. 2003, 19, 243-253.

Petronis, S.; Stangegaard, M.; Christensen, C. B. V.; Dufva, M. Biotechniques, 2006, 40, 368-376.

Power, M. J.; Domansky, K.; Kaazempur-Mofrad, M. R.; Kalezi, A.; Capitano, A.; Upadhyaya, A.; Kurzawski, P.; Wack, K. E.; Stolz, D. B.; Kamm, R.; Griffith, L. G. Biotechnol. Bioeng. 2002a, 78, 257-269

Power, M. J.; Janigian, D. M.; Wack, K. E.; Baker, C. S.; Stolz, D. B.; Griffith, L. G. Tissue. Eng. 2002b, 8, 499-513

Price A. K.; Martin, R. S.; Spence, D. M. J. Chromatogr. A 2006, 1111, 220-227.

Prokop, A.; Prokop, Z.; Schaffer, D.; Kozlov, E.; Wikswo, J.; Cliffel, D.; Baudenbacher, F. Biomed. Microdev. 2004, 6, 325-339.

Puri, K. D.; Chen, S.; Springer T. A. Nature 1998, 392, 930-933.

Raty, S.; Walters, E. M.; Davis, J.; Zeringue, H.; Beebe, D. J.; Rodriguez-Zas, S.L.; Wheeler, M. B. Lab Chip 2004, 4, 186-190.

Revzin, A.; Sekine, K.; Sin, A.; Tompkins, R. G.; Toner, M. Lab Chip 2005, 5, 30-37.

Roberts, M. A.; Durst, R. A. Anal. Chem. 1995, 67, 482-491.

Rocheleau, J. V.; Walker, G. M.; Head, W. S.; McGuinness, O. P.; Piston, D. W. Proc. Natl. Acad. Sci. USA 2004, 101, 12899-12903.

Roos, P.; Skinner, C. D. Analyst 2003, 128, 527-531.

Roper, M. G.; Shackman, J. G.; Dahlgren, G. M.; Kennedy, R. T. Anal. Chem. 2003, 75, 4711-4717.

Rossier, J.; Girault, H. H. Lab Chip 2001, 1, 153-157.

Saadi, W.; Wang, S. –J.; Lin, F.; Jeon, N. L. Biomed. Microdev. 2006, 8, 109-118.

Sanford, K. K.; Earle, W. R.; Likely, G. D. J. Natl. Cancer Inst. 1948, 9, 229-246.

Sato, M.; Ohashi, T. Biorheology 2005, 42, 421-441.

Sawano, A.; Takayama, S.; Matsuda, M.; Miyawaki, A. Dev. Cell 2002, 3, 245-257.

Schneider, T. W.; Schessler, H. M.; Shaffer, K. M.; Dumm, J. M.; Yonce, L. A. Biomed. Microdev. 2001, 3, 315-322.

Schweitzer, B.; Wiltshire, S.; Lambert, J.; O'Malley, S.; Kukanskis, K.; Zhu, Z. R.; Kingsmore, S. F.; Lizardi, P. M.; Ward, D. C. Proc. Natl. Acad. Sci. USA 2000, 97, 10113-10119.

Schweitzer, B.; Roberts, S.; Grimwade, B.; Shao, W.; Wang, M.; Fu, Q.; Shu, Q.; Laroche, I.; Zhou, Z.; Tchernev, V. T.; Christiansen, J.; Velleca, M.; Kingsmore. S. F. Nat. Biotechnol. 2002, 20, 359-365.

Shackman, J. G.; Dahlgren, G. M.; Peters, J. L.; Kennedy, R. T. Lab Chip 2005, 5, 56-63.

Shelby, J. P.; White, J.; Ganesan, K.; Rathod, P. K.; Chiu, D. T. Proc. Natl. Acad. Sci. USA 2003, 100, 14618-14622.

Shim, J.; Bersano-Begey, T. F.; Zhu, X.; Tkaczyk, A. H.; Linderman, J. J.; Takayama, S. Curr. Top. Med. Chem. 2003, 3, 687-703.

Sia, S. K.; Whitesides, G. M. Electrophoresis 2003, 24, 3563-3576.

Sin, A.; Chin, K. C.; Jamil, M. F.; Kostov, Y.; Rao, G.; Shuler, M. L. Biotechnol. Prog. 2004, 20, 338-345.

Soen, Y.; Mori, A.; Palmer, T. D.; Brown, P. O. Mol. Syst. Biol. 2006, 2, 37.

Song, J. W.; Gu, W.; Futai, N.; Warner, K. A.; Nor, J. E.; Takayama, S. Anal. Chem. 2005, 77, 3993-3999.

Stavis, S. M.; Edel, J. B.; Samiee, K. T.; Craighead, H. G. Lab Chip 2005, 5, 337-343.

Sung et al. 2006 A microfluidic cell culture analog system (CCA) for testing drugs for colon cancer. 232nd ACS National Meeting, San Francisco, CA, United States, Sept. 10-14, BIOT-393

Szita, N.; Boccazzi, P.; Zhang, Z. Y.; Boyle, P.; Sinskey, A. J.; Jensen, K. F. Lab Chip 2005, 5, 819-826.

Takayama, S.; McDonald, J. C.; Ostuni, E.; Liang, M. N.; Kenis, P. J. A.; Ismagilov, R. F.; Whitesides, G. M. Proc. Natl. Acad. Sci. USA 1999, 96, 5545-5548.

Takayama, S; Ostuni, E.; LeDuc, P.; Naruse, K.; Ingber, D. E.; Whitesides, G. M. Nature 2001a, 411, 1016.

Takayama, S.; Ostuni, E. Qian, X.; McDonald, J. C.; Jiang, X.; LeDuc, P.; Wu, M. –H.; Ingber, D. E.; Whitesides, G. M. Adv. Mater. 2001b, 13, 570-574.

Takayama, S.; Ostuni, E.; LeDuc, P.; Naruse, K.; Ingber, D. E.; Whitesides, G. M. Chem. Biol. 2003, 10, 123-130.

Tan, W.; Desai, T. A. Tissue Eng. 2003, 9, 255-267.

Tan, W.; Desai, T. A. Biomaterials 2004, 25, 1355-1364.

Taylor, A. M.; Rhee, S. W.; Tu, C. H.; Cribbs, D. H.; Cotman, C. W.; Jeon, N. L. Langmuir 2003, 19, 1551-1556.

Taylor, A. M.; Blurton-Jones, Rhee, S. W.; Cribbs, D. H.; Cotman, C. W.; Jeon, N. L. Nat. Methods 2005, 2, 599-605.

Toh, Y. C.; Ng, S.; Khong, Y. M.; Samper, V.; Yu, H. Assay Drug Dev. Technol. 2005, 3, 169-176.

Torisawa, Y.; Shiku, H.; Yasukawa, T.; Nishizawa, M.; Matsue, T. Biomaterials 2005, 26, 2165-2172.

Torisawa, Y.; Takagi, A.; Nashimoto, Y.; Yasukawa, T.; Shiku, H.; Matsue, T. Biomaterials 2007a, 28, 559-566.

Torisawa, Y.; Chueh, B.; Huh, D.; Ramamurthy, P.; Roth, T. M.; Barald, K. F.; Takayama, S. Lab Chip 2007b, 7, 770-776.

Tourovskaia, A.; Figueroa-Masot, X.; Folch, A. Lab Chip 2005, 5, 14-19.

Tourovskaia, A.; Kosar, T. F.; Folch, A. Biophys. J. 2006a, 90, 2192-2198.

Tourovskaia, A.; Figueroa-Masot, X.; Folch, A. Nat. Protocols 2006b, 1, 1092-1104.

Verpoorte, E. Electrophoresis 2002, 23, 677-712.

Vilkner, T.; Janasek, D.; Manz, A. Anal. Chem. 2004, 76, 3373-3385.

Viravaidya, K.; Shuler, M. L. Biotechnol. Prog. 2002, 18, 174-181.

Viravaidya, K.; Shuler, M. L. Biotechnol. Prog. 2004, 20, 590-597.

Vollmer, A. P.; Probstein, R. F.; Gilbert, R.; Thorsen, T. Lab Chip 2005, 5, 1059-1066.

von Heeren, F.; Verpoorte, E.; Manz, A.; Thormann, W. Anal. Chem. 1996, 68, 2044-2053.

Walker, G. M.; Zeringue, H. C.; Beebe, D. J. Lab Chip 2004, 4, 91-97.

Walters, E. M.; Clark, S. G.; Beebe, D. J.; Wheeler, M. B. Methods Mol. Biol. 2004, 254, 375-382.

Wang, N.; Miao, H.; Li, Y. S.; Zhang, P.; Haga, J. H.; Hu, Y.; Young, A.; Yuan, S.; Nguyen, P.; Wu, C. C.; Chien, S. Biochem. Biophys. Res. Commun. 2006, 341, 1244-1251.

Wei, C. –W.; Cheng, J. –Y.; Young, T. –H. Biomed. Microdev. 2006, 8, 65-71.

Weigl, B. H.; Bardell, R. L. Lab. Med. 2004, 35, 233-237.

Weinberg, E. J.; Borenstein, J. T.; Kaazempur-Mofrad, M. R.; Orrick, B.; Vacanti, J. P. Mater. Res. Soc. Sympo. Proc. 2004, 823 Biol. Bioinsp. Mater. Dev., 157-162.

Wieder, K. J.; King, K. R.; Thompson, D. M.; Zia, C.; Yarmush, M. L.; Jayaraman, A. Biomed. Microdev. 2005, 7, 213-222.

Yamamoto, K.; Sokabe, T.; Watabe, T.; Miyazono, K.; Yamashita, J. K.; Obi, S.; Ohura, N.; Matsushita, A.; Kamiya, A.; Ando, J. Am. J. Physol. Heart Circ. Physiol. 2005, 288, H1915-H1924.

Yang, M.; Yang, J.; Li, C. –W.; Zhao, J. Lab Chip, 2002, 2, 158-163.

Yu, H; Meyvantsson, I.; Shkel, I. A.; Beebe, D. J. Lab Chip 2005, 5, 1089-1095.

Zanzotto, A.; Szita, N.; Boccazzi, P.; Lessard, P.; Sinskey, A. J.; Jensen, K. F. Biotechnol. Bioeng. 2004, 20, 243-254.

Zeng, Y.; Lee, T. S.; Yu, P.; Roy, P.; Low, H. T. J. Biomech. Eng. 2006, 128, 185-93.

Zhu, X.; Chu, L. Y.; Chueh, B.; Shen, M.; Hazarika, B.; Phadke, N.; Takayama, S. Analyst 2004, 129, 1026-1031.

Adams GB, Scadden DT. The hematopoietic stem cell in its place. Nat Immunol 2006; 7 (4):333-7.

Benninger R, Hofmann O, McGinty J et al. Time-resolved fluorescence imaging of solvent interactions in microfluidic devices. Opt. Express 2005; 13:6275-85.

Chang-Yen DA, Gale BK. An integrated optical oxygen sensor fabricated using rapid-prototyping techniques. Lab on a Chip 2003; 3 (4):297-301.

Jang JH, Schaffer DV. Microarraying the cellular microenvironment. Mol Syst Biol 2006; 2:39.

Kiel MJ, Iwashita T, Yilmaz OH et al. Spatial differences in hematopoiesis but not in stem cells indicate a lack of regional patterning in definitive hematopoietic stem cells. Dev Biol 2005a; 283 (1):29-39.

Kiel MJ, Yilmaz OH, Iwashita T et al. SLAM family receptors distinguish hematopoietic stem and progenitor cells and reveal endothelial niches for stem cells. Cell 2005b; 121 (7):1109-21.

Mitrovski SM, Nuzzo RG. An electrochemically driven poly(dimethylsiloxane) microfluidic actuator: oxygen sensing and programmable flows and pH gradients. Lab Chip 2005; 5 (6):634-45.

Morrison SJ, Spradling AC. Stem cells and niches: mechanisms that promote stem cell maintenance throughout life. Cell 2008; 132 (4):598-611.

Park J, Bansal T, Pinelis M et al. A microsystem for sensing and patterning oxidative microgradients during cell culture. Lab Chip 2006; 6 (5):611-22.

Park TH, Shuler ML. Integration of cell culture and microfabrication technology. Biotechnol Prog 2003; 19 (2):243-53.

Scadden DT. The stem-cell niche as an entity of action. Nature 2006; 441 (7097):1075-9.

Shim J, Bersano-Begey TF, Zhu X et al. Micro- and nanotechnologies for studying cellular function. Curr Top Med Chem 2003; 3 (6):687-703.

Sin A, Chin KC, Jamil MF et al. The design and fabrication of three-chamber microscale cell culture analog devices with integrated dissolved oxygen sensors. Biotechnol Prog 2004; 20 (1):338-45.

Szita N, Boccazzi P, Zhang Z et al. Development of a multiplexed microbioreactor system for high-throughput bioprocessing. Lab Chip 2005; 5 (8):819-26.

Taichman RS. Blood and bone: two tissues whose fates are intertwined to create the hematopoietic stem-cell niche. Blood 2005; 105 (7):2631-9.

Taichman RS, Emerson SG. The role of osteoblasts in the hematopoietic microenvironment. Stem Cells 1998; 16 (1):7-15.

Vollmer AP, Probstein RF, Gilbert R et al. Development of an integrated microfluidic platform for dynamic oxygen sensing and delivery in a flowing medium. Lab Chip 2005; 5 (10):1059-66.

Wilson A, Trumpp A. Bone-marrow haematopoietic-stem-cell niches. Nat Rev Immunol 2006; 6 (2):93-106.

www.nih.gov

Yin T, Li L. The stem cell niches in bone. J Clin Invest 2006; 116 (5):1195-201.

CHAPTER 3

QUANTITATIVE MEASUREMENT AND CONTROL OF OXYGEN LEVELS IN MICROFLUIDIC POLY(DIMETHYLSILOXANE) BIOREACTORS DURING CELL CULTURE

3.1 Introduction

To study cells under simulated physiological microenvironments *ex vivo* (e.g. three-dimensional cell cultures and development of so-called "animals-on-a-chip") (Park et al. 2003), it is necessary to develop tools to enable quantitative real-time control of microenvironment of cell culture in microbioreactors. This approach requires three main components: (i) the ability to *actuate* the spatio-temporal distribution of nutrients, growth factors, and adhesive signals in the cellular microenvironments, (ii) the ability to *sense/measure* nutrients, metabolites, growth factors, cytokines, and other cell-secreted products, and (iii) the ability to quantitatively *model* the relationship between various

design and operating parameters to enable control and operation of the bioreactor. Our previous studies with development of highly versatile computerized microfluidic bioreactor arrays (Gu et al. 2004) are hence still incomplete in that they lack integration of chemical sensors and quantitative understanding of the bioreactions involved through modeling. This paper specifically addresses these issues for a crucial cell substrate, oxygen, by developing an optics-based method to quantify dissolved oxygen in PDMS microbioreactors and by applying a quantitative mathematical model to explain how key parameters control the spatial distribution of oxygen inside them.

Oxygen is a very important nutrient for cell culture, and its lower solubility in culture media (less than 7 mg/L at 37 ^{o}C) makes it imperative that it is constantly monitored and supplied (Fleischaker et al. 1981). One of the reasons PDMS microbioreactors are advantageous for cell-based studies is due to high diffusivity (D= 4.1 X 10^{-5} cm^2/sec) (Charati et al. 1998) and solubility (0.18 cm^3 (STP)/cm^3 atm) (Merkel et al. 2000) of oxygen in PDMS compared to other polymers and materials used for bioreactor and microfluidic device fabrication. Because of these properties of PDMS, passive permeation of oxygen through PDMS is generally assumed to be sufficient for supplying necessary amounts of oxygen for insect and mammalian cell cultures, which do not have very high oxygen uptake rates, and investigators do not typically quantify actual in-channel oxygen concentrations during microfluidic cell culture (Leclerc et al. 2006; Leclerc et al. 2003; Leclerc et al. 2004; Walker et al. 2002). Even within the range of oxygen concentrations sufficient for cell survival, the concentration of oxygen has a profound influence on cell signaling, growth factor production, growth, and

differentiation (Muschler et al. 2004). Different types of cells require different oxygen concentrations for optimal physiological function. Human embryonic stem cells benefit from low oxygen concentration (below 5%) in order to maintain their pluripotency, and transient changes in oxygen levels can change gene transcription and affect fate of stem cells in culture conditions (Ezashi et al. 2005). Hematopoeitic stem cells (HSC) self-renew and maintain pluripotency better at lower oxygen tension (lower than 5% *in vitro*), and at higher oxygen levels *in vitro*, HSCs differentiate, and undergo apoptosis (Csete 2005). Hence, there is considerable interest in the design of poly(dimethylsiloxane) (PDMS) microbioreactors conducive for culture of different types of cells, particularly cells requiring low oxygen tension.

There are various reports of measuring oxygen concentrations inside microfluidic devices using optical as well as polarographic measurements (Benninger et al. 2005; Chang-Yen et al. 2003; Mitrovski et al. 2005; Park et al. 2006; Sin et al. 2004; Szita et al. 2005; Vollmer et al. 2005). Typically, electrode or fluorescence-based sensors are used to monitor dissolved oxygen content in cell cultures (Andreescu et al. 2004; Deshpande and Heinzle 2004; Gerritsen et al. 1997a; Helmlinger et al. 2000; Hwang et al. 2004; John et al. 2003; Malda et al. 2004; Sud et al. 2006b; Sweet et al. 2002; Tolosa et al. 2002; Urayama et al. 2003; Zhong et al. 2003). Polarographic oxygen sensors based on Clark electrodes have been widely used for monitoring oxygen in cell cultures. However, they suffer from disadvantages including: consumption of oxygen; long-term instability; sterilization problems; sensor drift; difficulty of adaptation to continuous monitoring, automation, and high-throughput measurement; flow dependence; and susceptibility to

electrical interferences (Andreescu et al. 2004; Malda et al. 2004; Sweet et al. 2002). Most of these drawbacks are overcome by using optical oxygen sensors based on quenching of fluorescence by oxygen (Deshpande et al. 2004; Hwang et al. 2004; John et al. 2003; Tolosa et al. 2002). Fluorescence is attenuated in the presence of oxygen in a linearly dependent manner. Optical sensing is performed either through steady-state intensity based or lifetime based methods (Gerritsen et al. 1997a; Gerritsen et al. 1997b; Sud et al. 2006b; Urayama et al. 2003; Zhong et al. 2003).

Previous efforts on modeling oxygen transport in microchannels have shown that the spatial distribution of oxygen concentration is a function of operating velocities and the channel geometry and significant gradients in oxygen concentrations can exist in the bioreactor especially at low flow rates (Mehta et al. 2006; Roy et al. 2001). Theoretical studies of transport of oxygen have shown the possibility of axial concentration gradients in PDMS devices without any cells (Vollmer et al. 2005). Application of such mathematical models to real devices, however, requires validation with actual measurements. Some experimental studies have detected changes in oxygen concentration in a continuously perfused PDMS microbioreactor for cell culture (Park et al. 2006; Szita et al. 2005). While steep gradients (greater than 50% change in oxygen tension within 1 cm along the length of the bioreactor) have been observed in bacterial cultures in PDMS microbioreactors (Park et al. 2006; Szita et al. 2005; Zanzotto et al. 2004), no studies have reported such steep gradients in oxygen concentrations for mammalian cell culture in continuously perfused PDMS microbioreactors. Yet such steep gradients could clearly facilitate the function of those mammalian cells that need low

oxygen tension, as in the studies of tissue zonation in perfused sinusoids due to oxygen gradients. When cells are cultured in a non-gas-permeable microbioreactor, it is well known that uptake by cells can reduce oxygen levels, leading to the formation of gradients of oxygen concentration along the length of the cell culture channel (Allen et al. 2003; Allen et al. 2005). Native PDMS is highly oxygen permeable, but the permeability is subject to change when proteins are adsorbed on it or when the surface is modified by plasma oxidation as is common in construction of microbioreactors (Shiku et al. 2006). Shiku et al. (Shiku et al. 2006) demonstrated that the mass-transfer coefficient of oxygen through PDMS is reduced 1000-fold after a 5 minute plasma oxidation, and reduced by 5 times after 20 minute incubation with bovine serum albumin. Furthermore, the use of parylene C coating in the PDMS devices can add additional diffusive resistance to the oxygen transfer from the ambient air owing to the lowered permeability of the composite layer. Thus, it is crucial to confirm theoretical models with experimental measures for each type of device where the plasma oxidation conditions, protein coating methods, and other culture device fabrication and preparation methods vary, even when the devices are all made of "PDMS". Indeed, oxygen gradients in PDMS microbioreactors may be significantly steeper than expected if the oxygen permeability of device material is low.

Here, we quantitatively measure extracellular oxygen concentration in the microfluidic channels inside PDMS bioreactors containing living cells by using fluorescence intensity and lifetime studies. Fluorescence lifetime imaging microscopy (FLIM) bases image contrast on lifetime variations, which reflect local biochemistry but are oblivious of intensity based artifacts such as scattering, photobleaching and concentration variation of

fluorophore. Calibration of ruthenium tris(2,2'-dipyridyl) dichloride hexahydrate (RTDP) lifetime on a wide-field, time domain FLIM system was employed to calculate dissolved oxygen concentrations via fluorescence intensity studies (Sud et al. 2006a; Sud et al. 2006b; Urayama et al. 2003; Zhong et al. 2003). Optical sensors for oxygen estimation are beneficial since they are suited for small volumes, are minimally perturbing, and do not consume oxygen during the measurement. This technique may be used for time-lapse studies (hours or days) without disturbing the set-up, and for imaging of spatial oxygen distributions.

Using a mathematical model we have previously shown that the concentration of soluble nutrients can be manipulated by controlling operating conditions and by using channels of appropriate geometry (Mehta & Linderman 2006). We utilize this mathematical model that describes oxygen diffusion, convection, and uptake by cells within the device to draw comparisons between the model and the experimental results, and to determine the contribution of oxygen flux through PDMS to overall oxygen delivery to cells.

In this work, we show that by manipulating the operating variables, e.g. media flow rates, one can effectively achieve the desired oxygen tensions inside the bioreactor. We also see that the relative supply of oxygen via diffusion through PDMS can also be altered using the media flow, as per the model predictions. Additionally, we show that oxygen diffusion through PDMS is not always sufficient to avoid oxygen concentration gradients along the length of the bioreactor even in culture of mammalian cells that have much lower oxygen uptake rates compared to bacterial cells. The validation of the model

predictions also enables its use in controlling the oxygen levels inside the reactor. This combined capability to experimentally measure in-channel oxygen concentration gradient and to fit device-specific parameters to mathematical models ultimately propels us towards our goal of producing well-defined and controlled oxygen tensions inside PDMS microbioreactors.

3.2 Materials and Methods

3.2.1 Cell Culture

C2C12 cells (mouse myoblasts, ATCC, CRL-1772) were cultured in a media comprising Dulbecco's Modified Eagle's Medium (DMEM, 11960, Gibco), 15% Fetal bovine serum (FBS, 10082, Gibco), 1%v/v antibiotic–antimicotic (15240, Gibco) and 1%v/v GlutaMAX*2*-I Supplement (35050, Gibco). The 100 mm^2 culture dishes were placed in a humidified 5% CO2 cell culture incubator. At 70-80 % confluence, the cells were passaged by washing in PBS, and incubating with 0.25% Trypsin/EDTA (Invitrogen, Carlsbad, CA). The Trypsin solution was neutralized with 15% FBS in DMEM and spun down with a centrifuge (ThermoForma, Marietta, OH) for 2 minutes at 25 ^oC and 1000 RPM. The supernatant was removed and the pellet was resuspended in DMEM media. The pellet was reconstituted in 4 ml of DMEM media, and 1 ml of this suspension was used for creating a new plate of C2C12. The cells were passaged every third day. When the cells were to be cultured in the PDMS microbioreactor, the pellet was reconstituted in 70-100 μL of DMEM media and then injected into the seeding ports of the chip.

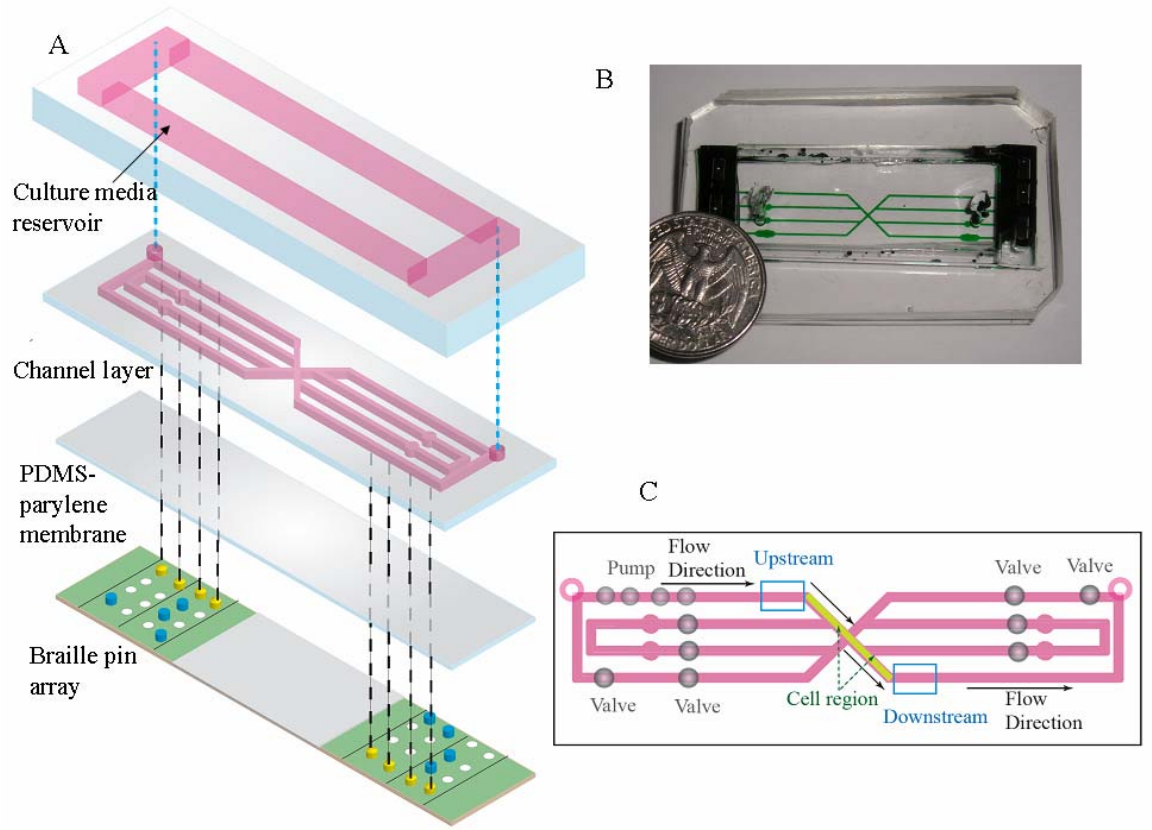

Figure 3.1: Microfluidic device design and set up. A) The top layer of the microfluidic device is a reservoir layer, connected to the channel layer with punched holes (pink holes in channel layer connected to the reservoir layer with a dashed blue line). A "horizontal" pump (yellow pins) drives cell culture media from top left to bottom right, all other channels are valved closed (blue pins are raised to close channels by deformation), and rest of the pins are in valve open position (white pins are down). The cells are attached in a part of the X-shaped channel region, between top left and bottom right. **B)** Optical photomicrograph of a complete device with green food dye to showcase channel design, placed with a quarter for scale, **C)** Top view of channel layer showing the positions of the pin driven pumps and valves when the device is used for continuous perfusion experiments. The flow direction (black arrows), areas of cell growth (green with green arrows), and, upstream and downstream positions (blue rectangles) where images were taken are shown in the figure. The flow in some of the channels is stopped by valves (grey with dark black borders), while flow is allowed in the desired channels by use of pumps (grey with no border).

3.2.2 Preparation of the microfluidic bioreactor chip

The chip consisted of three components: reservoir top layer, channel middle layer and membrane bottom layer, as seen in Figure 3.1A. The chips were formed from pre-polymer (Sylgard 184, Dow Corning) at a ratio of 1:10 base to curing agent. The top

layer contained fluid reservoirs and was cured overnight at 60 ^{o}C. The middle layer was formed using a glass wafer mold (soft lithography) (Duffy et al. 1998) to form a layer with negative relief channel features ~30 μm in height and 300 μm in width. The positive relief features of the mold were composed of SU-8 (Microchem, Newton, MA) formed on a thin glass slide (200 μm thick) using backside diffused-light photolithography (Futai et al. 2006). The glass slide was silanized with tridecafluoro-(1,1,2,2-tetrahydrooctyl)-1-trichlorosilane (United Chemical Technologies Inc., Bristol, PA). The middle layer was also cured overnight at 60 ^{o}C and holes were punched (Dermal biopsy puncher, Miltex Inc., York, PA) in the channel and reservoir layer to connect channel features to the culture media reservoir. The thickness of PDMS above the channel feature was 6±2 mm. The bottom layer was a thin sandwich of PDMS (100 μm)-parylene C (2.5 μm)-PDMS (100 μm) prepared by spin coating (Cee 100 Spin Coater, Brewer Science Inc., Rolla, MO) PDMS and vapor deposition of parylene C (PDS 2010 labcoater; Specialty Coating Systems) and curing PDMS at each step in an oven at 60 ^{o}C overnight (Heo et al. 2006). The hybrid membrane was oxidized in oxygen plasma (SPI Supplies, West Chester, PA) for 30 seconds thereby making the PDMS surfaces hydrophilic. The layers were sealed irreversibly, the flat surfaces were pressed together, and the entire chip was placed in an oven at 60 ^{o}C for 5-10 minutes. The oxygen permeability (a crucial transport property which incorporates diffusivity and solubility) of parylene C is 3.24 X 10^{-10} (cm^3 (STP) cm)/(cm^2 sec atm) (Yeh et al. 1990), while that of PDMS is 6.0800 ± 0.1519 X 10^{-6} (cm^3 (STP) cm)/(cm^2 sec atm) (Merkel et al. 2000). The bottom hybrid membrane hence, has lower oxygen permeability due to the parylene layer, despite being much thinner (~8 mm PDMS vs 0.2 mm PDMS plus 0.0025 mm parylene) than the upper all-PDMS layer. Such

low diffusivity and solubility of the parylene layer hence ensures that there is minimal diffusion of oxygen from the bottom layer of the device.

Fibronectin (100 mg/μl, F2006, Sigma) was injected (30-gauge hypodermic needles) in the cell culture channels to maintain the hydrophilic nature of the channels and to promote cell attachment (see Figure H1). This absorption was carried out for 30 minutes, following which DI water was introduced. The chips were then sterilized by placing under UV light for ~30 minutes. After sterilization, water was replaced with DMEM media in the reservoir, and the chip was placed on an array of pin actuators adapted from Braille displays for at least one hour to peristaltically pump fluid through the channels (Futai et al. 2006; Heo et al. 2006; Song et al. 2005). C2C12 cells were then seeded into the chip. We were able to manipulate the cells to attach only in the area of the bioreactor in between the upstream and downstream channel regions by use of valves (pin actuators pushing up and deforming channels closed) during cell seeding (see Figure H2). The cells were given 1-2 hours to attach under no flow (pins up and channels valved closed) condition in a dry heat incubator (Forma 310 Series Direct Heat CO2 Incubator, Thermo electron Corporation**,** Marietta, OH) maintained at 37 ^{o}C and 5% CO_2. Pumping was started after cells became adherent and the chip was perfused for 12-14 hours. 0.2 ml of the oxygen sensitive dye, ruthenium tris(2,2'-dipyridyl) dichloride hexahydrate (RTDP) (93307, Fluka) (5 mg/ml in DPBS (14190250, Invitrogen); final concentration is 1 mg/ml because of dilution) was then introduced into the reservoir of the chip, and pumping was continued for three more hours. The setup comprised of a microfluidic chip attached to the pin actuator array module was then taken to the microscope and intensity or lifetime

measurements performed at room temperature. Cell densities in the cell culture channels in the microbioreactor chips were determined by counting the number of cells present in 10 microscope brightfield images taken at different positions along the length of the cell culture channel.

3.2.3 Fluid Actuation

An array of 48 pin actuators adapted from a Braille display module (SC9, KGS, Saitama, Japan) was used for fluid actuation (Futai et al. 2006). The pin actuator module was controlled with a computer via Universal Serial Bus (USB) through a finger-sized stand alone custom controller circuit board (Olimex, Plovdiv, Bulgaria) (Futai et al. 2006; Heo et al. 2006). The microfluidic bioreactor chip interfaces with the pin actuator module by simply holding the chip in place such that the channels align with the pins which push upward closing the channel, as seen in Figure 3.1 A and C.

The pin movements for valving and pumping were controlled with a custom computer program written in C #. The software program provides effective control of the Braille hardware setup and is flexible, enabling one to define new behaviors of pumping, blocking or opening channel paths, and controlling timing and flow rates for short and long-term automated control of microfluidic devices. This software can run on PCs and control specific custom Braille hardware through a USB connection, and it acts as an interpreter enabling us to write complex sequences of actions in a shorthand text form. Multiple threads of execution within the program handle the exact timing and order of events within a main execution loop. The shorthand description form allows us to create

any number of pumps (3-4 Braille pins) and valves (1 Braille pin) on the 'grid' of braille pins (up to 16 columns and 4 rows for our setup, see Figure 3.1A). We specify the position for each of the pumps or valves (which will have a different effect on flow depending on the overlayed channel design), and in the case of pumps also their alignment (horizontal or vertical), direction of pumping flow (positive or negative), and relative speed. We also specify time intervals on an execution time axis for each of these objects, which allows us to describe more complex sequences of events, e.g. pump1 starts at 0s and stops at 30s, then valve2 closes from 30s to 50s, and pump3 and pump1 turn on from 31 to 40 seconds. Figure 3.1C shows the valves and pumps used for the continuous perfusion experiment. The software also has a user interface that allows starting, pausing, stopping, and even rewinding the execution of any loaded shorthand program of pumps and valves, and also has an independent speed control that allows running essentially the same program and sequence of actions but with different flow rates and faster or slower execution.

The average flow rate was controlled by changing the time delay between pin motions. Fluid flow was characterized by tracking 6 μm diameter fluorescent beads (Carnine, polystyrene microspheres, Molecular Probes, Eugene, OR) using a digital CCD camera (Orca-ER, Hamamatsu Photonics, Japan) and a fluorescence stereomicroscope (Nikon SMZ1500). The image sequences were acquired at ~13 frames/sec to determine the velocity of the microspheres, which are representative of the fluid velocity, and were used to determine the average fluid flow rate. An entire pumping cycle was used to measure each flow rate in order to compensate for backflow during certain steps of a

pumping cycle. The average flow rates used for these experiments were in the range of 0.0005 μl/sec to 0.22 μl/sec, and the flow rates were relatively linear with frequency. This was observed from the motion of polystyrene microspheres, and is outlined in Table 3.1.

Table 3.1: Average flow rates at different pumping time delays

Pumping Frequency (Hz)	Average Flow rate ($x10^3$ μl/sec)
0.01	0.50 ± 0.02
0.02	1.40 ± 0.40
0.04	3.00 ± 1.00
0.10	6.00 ± 2.00
0.20	12.4 ± 4.00
1.00	83.0 ± 23.0
5.00	220 ± 30.0

3.2.4 Intensity measurement

We used a Nikon TS100-F inverted microscope with Epi-Fluorescence using a 10x CFI Achromat ADL Ph1 objective (n.a. 0.25, w.d. 6.20mm), TRITC HY-Q Filter Cube, and an X-CITE 120 PC Fluor illumination system to measure intensity of the RTDP dye in the microbioreactor. The pictures were recorded using the Coolsnap CF2 12 bit Firewire Monochrome Camera with MetaVue Software. Intensity measurements were taken at upstream and downstream locations of the perfused microbioreactor at different flow rates, and at different cell densities. The fluorescent images were taken at an exposure time of 0.6 seconds for each observation, and each area was sampled three times. In total, six data-sets were created by repeating the experiments at all flow rates. The relationship between fluorescence intensity (or lifetime) and dissolved oxygen concentration is described by the Stern–Volmer equation (Gerritsen et al. 1997b; Sud et al. 2006b;

Urayama et al. 2003; Zhong et al. 2003): $I_o/ I = 1 + K_q[O_2]$ or $\tau_o/\tau=1 + K_q[O_2]$, where I_o or τ_o = uninhibited sensor dye intensity or lifetime (i.e. 0% oxygen), I or τ = sensor dye intensity or lifetime at oxygen level $[O_2]$ and K_q is the Stern-Volmer quenching constant.

For fluorescence lifetime studies, a time-domain FLIM system with a tunable, pulsed excitation source covering the UV-vis-NIR spectrum (337–960 nm) and an intensified, gated (min. 200 ps) CCD camera (Picostar, LaVision) to record images was used (Urayama et al. 2003). Lifetimes could be measured in the range of 750 ps - ∞ with a discrimination of 50 ps, and an axial resolution of 1.4 μm. RTDP fluorescence from microbioreactor compartments were collected at 600 nm via 460 nm excitation at gates of 40, 140, 240, 340, and 440 ns, with the intensifier gate width set to 100 ns. A lifetime macro implementing the rapid lifetime determination (RLD) algorithm was used to generate lifetime images on a per pixel basis from gated intensity images (Urayama et al. 2003; Zhong et al. 2003). Oxygen levels were ascertained by fitting the Stern-Volmer equation to calculated lifetimes. The data were analyzed statistically by ANOVA, Tukey's test and Student's t test at a 95 percent confidence level assuming unequal variances.

3.2.5 Mathematical Modeling

We adapted our previously published model of transport of soluble nutrient/growth factors inside a microchannel bioreactor for the current study (Mehta & Linderman 2006). Briefly, partial differential equations were written to describe the spatial distribution of oxygen inside the bioreactor in the presence of the convective transport

associated with media flow, diffusive flux through PDMS, and cellular consumption and were solved using FEMLAB®. We used a steady state model with constant cell density, as the experimental time scales are small compared to the doubling times of cells. The model assumes uniformly distributed cell density along the bioreactor, which is reasonable as the cells are seeded using a suspension, and as visualized from microscope images. We also assume that the cells are adherent to the channel walls and are preferentially located at the bottom floor of the channel. Further, the model assumes a laminar flow profile, Michaelis-Menten rate of uptake of oxygen by all cells, and a constant overall mass-transfer coefficient to describe the flux of oxygen through PDMS. We assume there is no flux of oxygen from the bottom because the thin bottom membrane contains a parylene film which has low diffusivity and permeability to oxygen relative to PDMS, as described in the preparation of the microfluidic bioreactor chip in the methods section and because we also placed a glass cover slide underneath this membrane in the cell observation region (flux from the top of the bioreactor is much more than that from bottom for modeling purposes). A brief description of model equations, geometry and the associated variables is shown in Figure 3.2.

Analysis of the model equations in dimensionless form gives us information on the three key dimensionless groups important in determining the concentration distribution of oxygen inside the bioreactor: $Pe/\alpha = \langle u \rangle H^2/(D_e L)$; $Da = V_{max}\phi H/D_e c_{in}$; $Sh = k_{la}H/D_e$. The dimensionless group Pe signifies the Peclet number ($Pe = \langle u \rangle H/D_e$), the ratio of convective transfer of species in the axial direction to the diffusive flux within the channel directed toward the lower end of the channel (i.e. toward the cell domain); α is

the geometric aspect ratio for the bioreactor, L/H. The Damkohler number (Da) is a measure of relative rates of total cellular uptake and diffusive flux from the bulk media. The magnitude of diffusive flux from PDMS is governed by the value of the Sherwood number (Sh), defined as the ratio of the diffusive transfer rate through the PDMS top surface to the diffusion rate in the media.

Key parameters of the model include the Michaelis-Menten uptake rate parameters (V_{max} and K_m) and the overall mass transfer coefficient (k_{la}). For the current study, the these parameters were estimated from a single data set from our microbioreactor (corresponding to the cell density of 5.1x 10^8 cells/m^2), with initial estimates based on physiologically relevant values, (Allen & Bhatia 2003) and then used to compare the model predictions with the remaining data. Calculations were made for several values of k_{la} for comparison with the experimental data.

3.3 Results and Discussion

3.3.1 Device Description

Figure 3.1 A, B, and C show the design and set up of the microfluidic bioreactor chip and its alignment with the pin actuator module (Futai et al. 2006). Three pin actuators act as a peristaltic pump pushing cell culture media through the microfluidic channels. The cells are seeded only in the area between the top left to bottom right of the X-shaped channel crossing region (shaded green in Figure 3.1 C). The bottom layer of the microfluidic bioreactor chip is a thin flexible membrane composed of PDMS and parylene C and has low oxygen permeability. During cell culture, the media is perfused (flow direction

shown with black arrows in Figure 3.2 C) from top left to bottom right of the microbioreactor chip by pin actuators acting as pumps (yellow pins shown in Figure 3.2 A), while all other channels are valved-off (blue raised pins). Within the parameters of the current experiments, this microfluidic bioreactor is a flow-through, rather than a recirculating, perfusion system. A part of the device (the X-shaped channel region) is viewable on an inverted microscope.

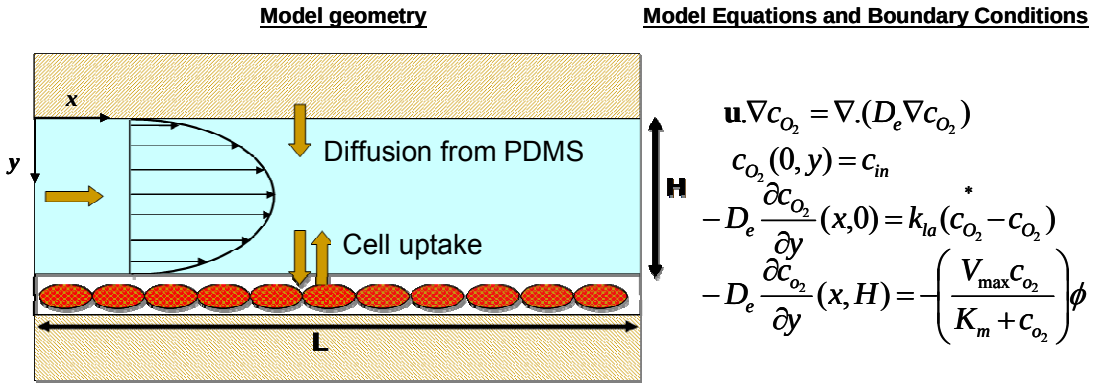

Figure 3.2: Modeling oxygen transport in the microfluidic channel bioreactor. Assuming constant cell density and idealized rectangular geometry with cells preferentially located at the channel bottom, oxygen transport can be modeled using the partial differential equations shown. The boundary conditions in the y dimension are given by diffusive flux from PDMS at the top (y = 0) and by cellular uptake at bottom (y = H). The diffusive flux from PDMS can be estimated using an overall mass transfer coefficient k_{la} based on the solubility and diffusivity of oxygen in PDMS, while the uptake of oxygen by the cells is modeled as Michaelis-Menten kinetics with parameters V_{max} and K_m. Refer to Mehta & Linderman (2006)[8] for further details on solution techniques and parameters . c_{o2} : oxygen concentration, u : velocity profile, D_e : effective diffusivity of oxygen in the media (= 2.1 x10^{-9} m^2/s), H : height of the microchannel (40 μm), L : length of the microchannel (0.01 m), ϕ : cell density, and velocity profile **u** = 6<u> (y/H- $(y/H)^2$) where <u> is the average velocity.

3.3.2 Local oxygen content measured by fluorescence intensity

We used different concentrations of the RTDP (in PBS) ranging from 0.1 mg/ ml to 1.0 mg/ml, and found that dye signal was best at 1.0 mg/ml for both intensity and lifetime-based fluorescent imaging. Thereafter, 1.0 mg/ml of RTDP in culture media was used for

all cell experiments. RTDP quenching by oxygen is a collisional process described by the Stern-Volmer equation. We employed $K_q = 2.7 \times 10^{-3}$ μM^{-1} for our measurements, as reported (Gerritsen et al. 1997b) and verified via FLIM (Sud et al. 2006b).

Our negative control comprised of microfluidic chips containing only DMEM media and RTDP and no cells. We used the intensity and lifetime observed in this control device for calculating the intensity at zero oxygen content. We observed that the average intensity of RTDP over different flow rates at upstream and downstream positions was 327 ± 7 AU, while, the average RTDP lifetime over different flow rates at upstream and downstream positions was 307 ± 7 nanoseconds. This corresponds to 8.2 mg/l of dissolved oxygen in media in the microbioreactor in the absence of any cells, while the saturation dissolved oxygen content in an aqueous solution is 8.5 mg/l at 25 ^{o}C (Fleischaker & Sinskey 1981). Thus, intensity at no oxygen was calculated using the Stern-Volmer equation, and found to be 550 AU. The Stern-Volmer equation describes the relationship between $(I/I_o - 1)$ and dissolved oxygen to be linear, as was seen in our calibration (data not shown). Thus, the intensity values obtained from the microbioreactor culture could be translated into local dissolved oxygen levels.

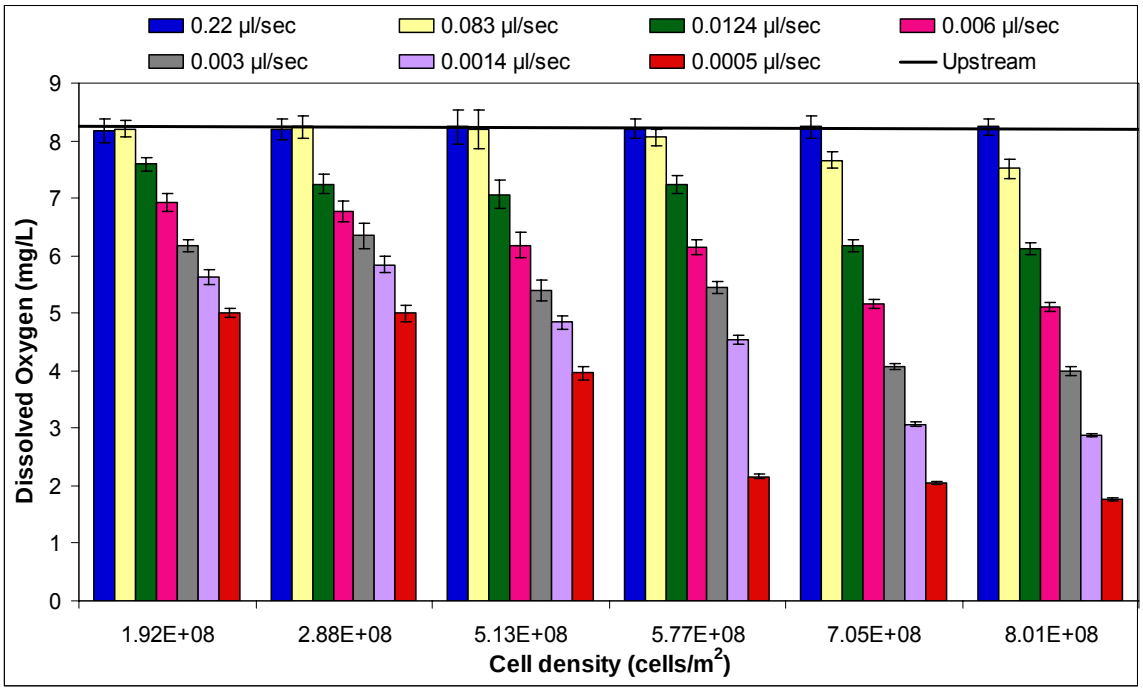

Figure 3.3: Upstream and downstream extracellular oxygen in the microbioreactor at different flow rates and cell densities. The horizontal line depicts the upstream oxygen content of 8.20 ± 0.20 mg/L. The downstream oxygen concentrations are shown as a function of six different cell densities (from 1.92 x 10^8 cells/m^2 to 8.01 x 10^8 cells/m^2) at each at seven different flow rates, from fastest flow rate (0. 22 µl/sec) to slowest (0.0005 µl/sec).

3.3.3 Observed oxygen gradients are a function of flow rate and cell density

We measured oxygen concentration at the upstream and downstream regions of the cell culture channel (see Fig. 1C) in our perfused bioreactor culturing C2C12 cells and found gradients that depend on both cell density and flow rate. The distance between each observation point and cell culture region was essentially the same. The relationship between flow rate and oxygen content at six cell densities, ranging from 1.92 x 10^8 cells/m^2 to 8.01 x 10^8 cells/m^2, is depicted in Figure 3.3. The figure shows the upstream and downstream oxygen content for all cell densities and at seven different flow rates, ranging from 0.0005 µl/sec to 0.22 µl/sec.

Upstream oxygen concentrations remained steady at 8.2 ± 0.2 mg/l (corresponding to an oxygen partial pressure of 154 mm Hg, 20.7 % oxygen in air, or 97 % saturation) for all flow rates. Downstream oxygen concentrations varied with cell density and flow rate. The lowest value of dissolved oxygen content observed was 1.76 mg/L, which corresponds to the lowest flow rate of 0.5 nL/sec and the highest cell density (8.01×10^8 cells/m^2) tested. In contrast, the downstream dissolved oxygen content observed at low cell densities and the highest flow rates was nearly identical to the upstream concentration.

As shown in Figure 3.3 and for each cell density, as the flow rate decreased the difference between upstream and downstream dissolved oxygen content increased. The concentration of oxygen decreases down the cell culture channel axis because the cells present along the axis consume oxygen. At slower flow rates the amount of oxygen-laden media coming into the culture channel is smaller, leading to a steeper concentration gradient. We also observed that for a constant flow rate, increasing cell density inside the culture channel caused oxygen content to decrease measured at the downstream region (Figure 3.3).

The downstream (see Figure 3.1C) oxygen levels at each flow rate (corresponding to a particular cell density) were statistically different from one another with a p value of less than 0.0001 (ANOVA). When comparing downstream oxygen tension data at each flow rate (at a particular cell density) with all other datasets using Tukey's test, differences were found to be statistically significant (α=0.05) for all comparisons. The downstream

oxygen levels at each cell density (corresponding to a particular flow rate) were statistically different from one another with a p value of less than 0.0001 (ANOVA). When comparing downstream oxygen tension data at each cell density (at a particular flow rate) with all other datasets using Tukey's test, differences were also found to be statistically significant at α=0.05. The oxygen concentration values observed at different flow rates as well as different cell densities were statistically significant (t-test, $p<0.01$) between the upstream and downstream regions (see Figure 3.1 C) of the cell culture channel. Comparison of the upstream oxygen tensions with those downstream for all cell densities and flow rates, using ANOVA gave p value of 0.024, which is statistically significant at α =0.05.

The oxygen tensions observed here are similar to those seen by Allen and Bhatia (Allen & Bhatia 2003) with hepatocyte culture in a perfused polycarbonate microbioreactor. They observed oxygen partial pressure differences of 23 to 133 mm Hg (1.2 to 7.1 mg/l) between the inlet and outlet of when perfusing a 55 mm long polycarbonate microbioreactor at flow rate of 0.4 ml/min to 3.0 ml/min (inlet pressure: 158 mm Hg), suggesting that there are axial gradients (0-0.107 (mg/l) mm) of oxygen within their device.

Oxygen gradients have been observed in physiological systems (Tsai et al. 2003). In microcirculation, there are radial and longitudinal gradients as oxygen exits through the vessel walls, which are related to the level of metabolic activity of the tissue. *In vivo* oxygen tensions range from 20 mm Hg to 100 mm Hg (1-8 mg/L in vessels of diameters

of 20-300 microns) in different parts of the tissues of animal models (Duling 1972; Pittman et al. 1975; Seiyama et al. 1996; Swain et al. 1989; Tsai et al. 2003). Thus, the downstream oxygen levels observed in our microbioreactor are comparable to physiological values for mammalian cells.

We used a high concentration (1 mg/ml) of RTDP to get good fluorescence signals at low exposure times. However, there are some studies suggesting that RTDP might have cytotoxic as well as phototoxic effects on mammalian cells (Dobrucki 2001). For the scope of this study we confirmed that the presence of dye in the media contributed minimally (less than 10%) to cell death within the timeframe of the oxygen concentration measurement period (up to 5 hours after dye injection) and the photoexcitation and measurements were performed in regions on the microfluidic bioreactor where cells were not present to avoid phototoxic damage to cells. We did observe that when cells were incubated with RTDP over long periods of time (24 -72 hrs) their viability decreased with time. The actual rate of oxygen consumption without added RTDP may thus be higher than what we measured since any toxicity would most likely reduce respiration.

The presence of a gradient is not necessarily indicative of insufficient oxygen transport to the cells. But it is crucial to understand and characterize the gradients generated to be able to understand and regulate cellular responses in microfluidic bioreactors. The ability to generate and regulate oxygen concentration gradients may actually be beneficial for recreating physiologic gradients as is observed, for example, in liver sinusoids (Tsai et al. 2003). We note that steep oxygen gradients of the type we describe (up to 79 % decrease

in oxygen tension within 1 cm along the length of the bioreactor) have not previously been demonstrated for mammalian cultures in continuously perfused PDMS microdevices.

Our finding of a significant oxygen gradient may provide one plausible explanation for the gradient of cell proliferation previously observed in PDMS perfusion reactors (Futai et al. 2006; Gu et al. 2004). Specifically, they observed higher cell densities of cells at the inlet of the device relative to the regions near the exit, presumably in response to a nutrient concentration gradient along the length of the channel. The range of oxygen concentrations we observed is within a range where no adverse effects on viability or marked differences in differentiation patterns is expected for C2C12 cells, as under *in vitro* culture at low oxygen tensions (5 % oxygen or 2.0 mg/L) the C2C12 cells are at similar stages of differentiation (from myoblasts to myotubes) during the hypoxic and normoxic (21% oxygen) exposure periods (Yun et al. 2005). However, the C2C12 cells may have migrated upstream or otherwise functioned differently along the length of the perfusion channel (Gu et al. 2004) because the cells were exposed to a relatively steep gradient of oxygen concentration.

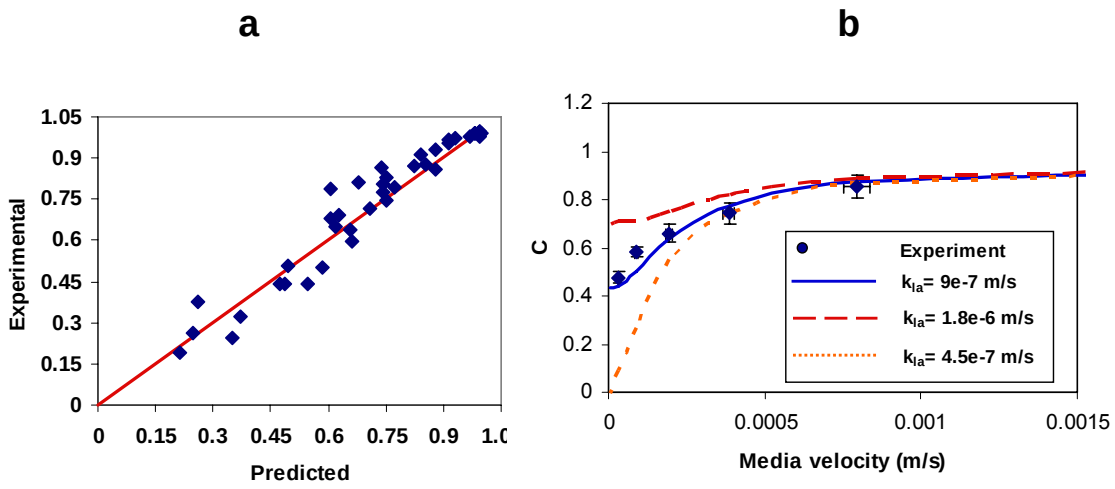

Figure 3.4: a) Model predictions vs. Experimental data. The model predictions are compared with experimental data on the oxygen concentration at the outlet. The oxygen concentration is non-dimensionalized using the inlet oxygen concentrations. The line y=x is shown as reference. The model was simulated based on the average values of cell density and operating flow rates as measured, with microbioreactor geometry parameters as described in Figure 3.2. The parameters for uptake rates and mass transfer are: V_{max} = 2.06 e -16, mol/cell/s, K_m = 0.005 mol/m^3, and k_{la} = 9e-7 m/s. **b) Effect of diffusion of oxygen through PDMS on dimensionless outlet concentration, C.** The value of mass-transfer coefficient k_{la} was varied to understand the contribution of oxygen diffusion from PDMS when ϕ = 5.12e8 cells/m^2. Solid line shows model prediction for k_{la} = 9e-7 m/s. Experimental data for the same conditions (solid circles) are shown as reference. The concentration is scaled with respect to the inlet concentration.

3.3.4 The experimental data are consistent with the mathematical model

The observed trends in the experimental data are consistent with the results of our mathematical modeling. Figure 3.4A shows the comparison of model predictions and experimental data on downstream oxygen concentrations for media flow rates and cell densities tested. The agreement between model and experiment suggests that the model captures the essential transport processes occurring in the microfluidic bioreactor. Analysis of model equations shows that when velocity is decreased relative to diffusion (low Pe/α) and for higher rates of uptake of oxygen inside the microfluidic cell cultures (high Da), the outlet concentration of oxygen decreases.

The model predicts generation of oxygen concentration gradient within PDMS channels. The relative magnitude of diffusion and convective transport are characterized by the overall mass-transfer coefficient and the media velocity in the model, and we use the model to investigate the relative contribution of diffusion through PDMS for various geometries and thicknesses of PDMS layers by varying the numerical value of the mass-transfer coefficient k_{la}.

We observed the effect of changing the overall mass-transfer co-efficient on the outlet concentration of oxygen in the microbioreactor (Figure 3.4 B). At low flow rates, higher values of k_{la} (higher Sh) lead to higher values of the oxygen concentration at the outlet. At these low flow rates, oxygen delivery to cells via diffusion through PDMS is a significant source of oxygen. It should be noted that at high flow rates, oxygen delivery occurs primarily via perfusion and is sufficient to eliminate axial gradients in the cell

culture channel, and hence the value of k_{la} (Sh) does not affect the concentration of oxygen at outlet. Our data is best fit by a $k_{la} = 9 \times 10^{-7}$ m/s. Our value of the mass-transfer coefficient is lower than that mentioned by other researchers, (e.g ~ 10^{-4} m/s, Vollmer et al. 2005). The reduced oxygen permeability of our device is likely due to various coatings and pre-treatments, i.e. plasma oxidation and protein coating.

Using the measured experimental data from oxygen concentration at the outlet, we can estimate the cellular uptake rates of oxygen. This opens up the possibility of using these microfluidic bioreactors for quantitative evaluation of cell properties. However, we note that for successful parameter inference we will require more experimental data to cover a wider range of oxygen concentrations. For example, we could not see a sensitivity of model predictions on the uptake parameter K_m for the current experimental data, as most of the experiments were performed at concentrations of oxygen well above K_m. Nevertheless, using similar experimental protocols, and careful experimentation coupled with the mathematical model, one could infer quantitative information on the cellular oxygen uptake rates for wide variety of cell types.

3.3.5 Mathematical model and microfluidic PDMS bioreactor provide tools for spatio-temporal regulation of oxygen microenvironments

The results presented here demonstrate that we can understand and predict oxygen gradients in a perfused PDMS microfluidic bioreactor as a function of media flow rate and cell density. Significant axial (along the length of the bioreactor) gradients in oxygen concentration can exist for lower flow rates (low Pe/α), even with significant diffusion of

oxygen through PDMS (high Sh). Axial concentration gradients also increase with increased cell density. These spatial gradients in oxygen concentrations could be a primary cause of spatial heterogeneity in cell density inside microfluidic bioreactors as observed in our previous experiments (Gu et al. 2004). Our modeling studies indicate that for a particular cell density the depletion in oxygen can be controlled by regulating flow velocity. Additionally, complementing perfusion with media recirculation would offer an additional means of lowering the concentration of oxygen inside the reactor to a desired level at all the stages of the cell culture. Modified channel geometries may also be used to engineer the concentration distribution of oxygen inside the reactor at desired levels (Mehta & Linderman 2006).

The combined use of models together with experimental measurements and computerized fluid actuation enable powerful experimental systems in which cell responses to various oxygen gradients can be efficiently and systematically analyzed or an optimal oxygen environment can be dialed in for better cell function. When used at relatively slow flow rates and high cell density, this microbioreactor creates oxygen limited physiology (Duling 1972; Pittman & Duling 1975; Seiyama et al. 1996; Swain & Pittman 1989; Tsai et al. 2003), which is known to be beneficial for a variety of applications, including maintaining the pluripotency of embryonic stem cells (Ezashi et al. 2005) and inducing the growth of erythroid colonies from bone marrow progenitors (Van Merris et al. 2001). Our device is capable of generating such conditions in ambient atmosphere without need of hypoxic chambers by simply taking advantage of cell respiration and the small volume of media in microfluidic systems. It has also been observed that even transient changes in

oxygen levels can change gene transcription, thus affecting the fate of stem cells in culture conditions (Pfau et al. 2004). Our system provides convenient dynamic control of the oxygen environment by computer programmed temporal changes in the perfusion rates. Our experiments and analysis do indicate that manipulating the media flow rates is not always sufficient to achieve very low oxygen tensions inside the PDMS bioreactor. In order to obtain pathologic hypoxic conditions such as 0.01% oxygen (0.004 mg/l), alternative techniques would have to be used. We envision this biomedical microdevice to be useful in conducting key biological studies pertaining to the effect of physiologic oxygen microenvironments on cell behavior. In addition to the ability to regulate oxygen microenvironments, this bioreactor reaps benefits of a typical PDMS device; including rapid prototyping, ease of fabrication, low cost, optical transparency, durability, disposability, and biological inertness.

3.4 Conclusion

We developed a method to measure dissolved oxygen content in real time in microfluidic PDMS perfusion systems using fluorescence intensity and lifetime imaging. Cell respiration created an axial oxygen gradient in the reactor along the length of a cell culture channel even though the device was mainly fabricated using highly gas-permeable PDMS. The downstream oxygen concentration decreased with increasing cell density and decreasing perfusion velocities. The measurements agree with a mathematical model which describes the spatial distribution of oxygen along the length of a microfluidic cell culture channel inside the bioreactor and enabled the estimation of oxygen transfer coefficients through the materials comprising our PDMS device.

These results are important not only for characterization of the specific device we describe in this report but also for formulating general guidelines for designing PDMS devices in regards to their oxygen microenvironment for mammalian cell culture. The relationship that describes the minimum convective flow rate that will offset specific oxygen consumption rates, as is described in this report, will be useful to the microfluidics community for designing devices and experimental conditions for microfluidic cell culture. In order to achieve oxygen gradients or hypoxic conditions in PDMS microbioreactors, researchers should plan experiments at low Sh, and low Pe/□. Our results also underscore the importance of characterizing the oxygen transfer rate of each type of PDMS device made under different conditions such as plasma oxidation and protein coating to explain cell behaviors observed as the oxygen permeability of a given device cannot always be predicted by simply using the permeability values of native bulk PDMS. The methods described here also provide an efficient method to perform such analyses.

References

Allen JW, Bhatia SN. Formation of steady-state oxygen gradients in vitro: application to liver zonation. Biotechnol Bioeng 2003; 82 (3):253-62.

Allen JW, Khetani SR, Bhatia SN. In vitro zonation and toxicity in a hepatocyte bioreactor. Toxicol Sci 2005; 84 (1):110-9.

Andreescu S, Sadik OA, McGee DW et al. Autonomous multielectrode system for monitoring the interactions of isoflavonoids with lung cancer cells. Anal Chem 2004; 76 (8):2321-30.

Benninger R, Hofmann O, McGinty J et al. Time-resolved fluorescence imaging of solvent interactions in microfluidic devices. Opt. Express 2005; 13:6275-85.

Chang-Yen DA, Gale BK. An integrated optical oxygen sensor fabricated using rapid-prototyping techniques. Lab on a Chip 2003; 3 (4):297-301.

Charati SG, Stern SA. Diffusion of gases in silicone polymers: Molecular dynamics simulations. Macromolecules 1998; 31 (16):5529-35.

Csete M. Oxygen in the cultivation of stem cells. Ann N Y Acad Sci 2005; 1049:1-8.

Deshpande RR, Heinzle E. On-line oxygen uptake rate and culture viability measurement of animal cell culture using microplates with integrated oxygen sensors. Biotechnol Lett 2004; 26 (9):763-7.

Dobrucki JW. Interaction of oxygen-sensitive luminescent probes Ru(phen)(3)(2+) and Ru(bipy)(3)(2+) with animal and plant cells in vitro. Mechanism of phototoxicity and conditions for non-invasive oxygen measurements. J Photochem Photobiol B 2001; 65 (2-3):136-44.

Duffy DC, McDonald JC, Schueller OJA et al. Rapid Prototyping of Microfluidic Systems in Poly(dimethylsiloxane). Anal. Chem. 1998; 70 (23):4974-84.

Duling BR. Microvascular responses to alterations in oxygen tension. Circ Res 1972; 31 (4):481-9.

Ezashi T, Das P, Roberts RM. Low O2 tensions and the prevention of differentiation of hES cells. Proc Natl Acad Sci U S A 2005; 102 (13):4783-8.

Fleischaker RJ, Sinskey AJ. Oxygen demand and supply in cell culture. Applied Microbiology and Biotechnology 1981; 12 (4):193.

Futai N, Gu W, Song JW et al. Handheld recirculation system and customized media for microfluidic cell culture. Lab Chip 2006; 6 (1):149-54.

Gerritsen HC, Sanders R, Draaijer A et al. Fluorescence Lifetime Imaging of Oxygen in Living Cells. JOURNAL OF FLUORESCENCE 1997a; 7 (1):11-6.

Gerritsen HC, Sanders R, Draaijer A et al. Fluorescence Lifetime Imaging of Oxygen in Living Cells. Journal of Flourescence 1997b; 7 (1):11-6.

Gu W, Zhu X, Futai N et al. Computerized microfluidic cell culture using elastomeric channels and Braille displays. Proc Natl Acad Sci U S A 2004; 101 (45):15861-6.

Heo YS, Cabrera LM, Smith GD et al. Characterization and Resolution of Evaporation-Mediated Osmolality Shifts that Constrain Microfluidic Cell Culture in Poly(dimethylsiloxane) Devices, Anal Chem, 2007; 79, 1126-1134.

Hwang EY, Pappas D, Jeevarajan AS et al. Evaluation of the paratrend multi-analyte sensor for potential utilization in long-duration automated cell culture monitoring. Biomed Microdevices 2004; 6 (3):241-9.

John GT, Klimant I, Wittmann C et al. Integrated optical sensing of dissolved oxygen in microtiter plates: a novel tool for microbial cultivation. Biotechnol Bioeng 2003; 81 (7):829-36.

Leclerc E, David B, Griscom L et al. Study of osteoblastic cells in a microfluidic environment. Biomaterials 2006; 27 (4):586-95.

Leclerc E, Sakai Y, Fujii T. Cell Culture in 3-Dimensional Microfluidic Structure of PDMS (polydimethylsiloxane). Biomedical Microdevices 2003; 5 (2):109.

Leclerc E, Sakai Y, Fujii T. Microfluidic PDMS (polydimethylsiloxane) bioreactor for large-scale culture of hepatocytes. Biotechnol Prog 2004; 20 (3):750-5.

Malda J, Rouwkema J, Martens DE et al. Oxygen gradients in tissue-engineered PEGT/PBT cartilaginous constructs: measurement and modeling. Biotechnol Bioeng 2004; 86 (1):9-18.

Mehta K, Linderman JJ. Model-based analysis and design of a microchannel reactor for tissue engineering. Biotechnol Bioeng 2006; 94 (3):596-609.

Merkel TC, Bondar VI, Nagai K et al. Gas sorption, diffusion, and permeation in poly(dimethylsiloxane). Journal Of Polymer Science Part B-Polymer Physics 2000; 38 (3):415-34.

Mitrovski SM, Nuzzo RG. An electrochemically driven poly(dimethylsiloxane) microfluidic actuator: oxygen sensing and programmable flows and pH gradients. Lab Chip 2005; 5 (6):634-45.

Muschler GF, Nakamoto C, Griffith LG. Engineering principles of clinical cell-based tissue engineering. J Bone Joint Surg Am 2004; 86-A (7):1541-58.

Park J, Bansal T, Pinelis M et al. A microsystem for sensing and patterning oxidative microgradients during cell culture. Lab Chip 2006; 6 (5):611-22.

Park TH, Shuler ML. Integration of cell culture and microfabrication technology. Biotechnol Prog 2003; 19 (2):243-53.

Pfau JC, Schneider JC, Archer AJ et al. Environmental oxygen tension affects phenotype in cultured bone marrow-derived macrophages. Am J Physiol Lung Cell Mol Physiol 2004; 286 (2):L354-62.

Pittman RN, Duling BR. Measurement of percent oxyhemoglobin in the microvasculature. J Appl Physiol 1975; 38 (2):321-7.

Roy P, Baskaran H, Tilles AW et al. Analysis of oxygen transport to hepatocytes in a flat-plate microchannel bioreactor. Ann Biomed Eng 2001; 29 (11):947-55.

Seiyama A, Tanaka S, Kosaka H et al. O2 transfer from single microvessels to acinar cells in secretin-stimulated pancreas of rat. Am J Physiol 1996; 270 (5 Pt 2):H1704-11.

Shiku H, Saito T, Wu C-C et al. Oxygen Permeability of Surface-modified Poly(dimethylsiloxane) Characterized by Scanning Electrochemical Microscopy. Chemistry Letters 2006; 35 (2):234.

Sin A, Chin KC, Jamil MF et al. The design and fabrication of three-chamber microscale cell culture analog devices with integrated dissolved oxygen sensors. Biotechnol Prog 2004; 20 (1):338-45.

Song JW, Gu W, Futai N et al. Computer-controlled microcirculatory support system for endothelial cell culture and shearing. Anal Chem 2005; 77 (13):3993-9.

Sud D, Zhong W, Beer DG et al. In., Series.; 2006a.

Sud D, Zhong W, Beer DG et al. Time-resolved optical imaging provides a molecular snapshot of altered metabolic function in living human cancer cell models. Optics Express 2006b; 14 (10):4412-26.

Swain DP, Pittman RN. Oxygen exchange in the microcirculation of hamster retractor muscle. Am J Physiol 1989; 256 (1 Pt 2):H247-55.

Sweet IR, Khalil G, Wallen AR et al. Continuous measurement of oxygen consumption by pancreatic islets. Diabetes Technol Ther 2002; 4 (5):661-72.

Szita N, Boccazzi P, Zhang Z et al. Development of a multiplexed microbioreactor system for high-throughput bioprocessing. Lab Chip 2005; 5 (8):819-26.

Tolosa L, Kostov Y, Harms P et al. Noninvasive measurement of dissolved oxygen in shake flasks. Biotechnol Bioeng 2002; 80 (5):594-7.

Tsai AG, Johnson PC, Intaglietta M. Oxygen gradients in the microcirculation. Physiol Rev 2003; 83 (3):933-63.

Urayama P, Zhong W, Beamish JA et al. A UV-Visible-NIR fluorescence lifetime imaging microscope for laser-based biological sensing with picosecond resolution. Applied Physics B: Lasers and Optics 2003; 76 (5):483.

Van Merris V, Lenjou M, Hoeben D et al. Culture of bovine bone marrow progenitor cells in vitro. Vet Q 2001; 23 (4):170-5.

Vollmer AP, Probstein RF, Gilbert R et al. Development of an integrated microfluidic platform for dynamic oxygen sensing and delivery in a flowing medium. Lab Chip 2005; 5 (10):1059-66.

Walker GM, Ozers MS, Beebe DJ. Insect Cell Culture in Microfluidic Channels. Biomedical Microdevices 2002; 4 (3):161.

Yeh YS, James WJ, Yasuda H. Polymerization Of Para-Xylylene Derivatives.6. Morphology Of Parylene-N And Parylene-C Films Investigated By Gas-Transport Characteristics. Journal Of Polymer Science Part B-Polymer Physics 1990; 28 (4):545-68.

Yun Z, Lin Q, Giaccia AJ. Adaptive myogenesis under hypoxia. Mol Cell Biol 2005; 25 (8):3040-55.

Zanzotto A, Szita N, Boccazzi P et al. Membrane-aerated microbioreactor for high-throughput bioprocessing. Biotechnol Bioeng 2004; 87 (2):243-54.

Zhong W, Urayama P, Mycek M-A. Imaging fluorescence lifetime modulation of a ruthenium-based dye in living cells: the potential for oxygen sensing. Journal of Physics D: Applied Physics 2003; 36 (14):1689.

CHAPTER 4

HOT EMBOSSED MICROFLUIDIC DEVICES FROM HYBRID BONDED MATERIALS FOR CELL CULTURE AND CHEMICAL ANALYSIS

4.1 Introduction

Microfluidic devices are useful for myriad applications, including but not limited to: biotechnology, nanotechnology, biological and chemical processing, analytical technologies (electrophoretic separation, mass spectroscopy, radionucleotide labeling), hydraulic actuation, heat transfer, and power generation (Beebe et al. 2002; Makamba et al. 2003; Weibel et al. 2006; Whitesides et al. 2001). They have been popular due to economical and efficient synthesis of chemicals, low consumption of expensive reagents, ease in performing combinatorial chemistry, ability to carry out biological and clinical analyses such as immunoassays, capacity to run a large number of analyses simultaneously, and integration of full-scale rapid analyses from sample introduction to

chemical separation and detection on single, miniaturized μTAS device (Beebe et al. 2002; Dittrich et al. 2006; El-Ali et al. 2007; Makamba et al. 2003; Weibel & Whitesides 2006; Whitesides et al. 2001).

Different materials are used for fabrication of microfluidic devices. Polymers are advantageous for microfabrication as they are available in large varieties and favorable prices; moreover, they can be prototyped rapidly using replication techniques such as hot embossing, injection molding, micromilling, wire imprinting, in situ polymerization, soft lithography and laser ablation. Poly(dimethyl siloxane) (PDMS) is one of the most popular starting materials due to its low cost, inertness, gas permeability, elastomeric nature, and rapid prototyping (Makamba et al. 2003; Shim et al. 2003). Other polymers also used for making microfluidic devices include polystyrene (PS), polycarbonate (PC), poly(methyl methacrylate) (PMMA), glycol-modified polyethylene terephthalate (PETG), poly(ethylene terephthalate) (PET), polyurethane (PU), cyclo olefin copolymer (COC) and many others. Each material has its own characteristic properties and advantages.

Due to their intrinsic characteristics, microfluidic devices fabricated using these materials can have issues such as evaporation of liquids from the channels, high permeability of oxygen leading to non-hypoxic oxygen tensions (which lead to decrease in stem cell self-renewal), or inability to integrate with popular channel deformation-based valving and pumping techniques. Such issues motivate examination and assessment of other polymers or combination of polymers to create microfluidic devices with unique advantages.

Fabrication of microfluidic devices with hybrid materials would synergize useful properties of different polymers, namely, the rigid 'hard top' (from PETG, COC, PS) which provides excellent barrier properties to the microdevice, and the 'soft bottom' (from PU or PDMS) which is deflectable. All-COC, PS, PMMA, PETG, and all- PDMS microdevices are fairly common in literature (Lin et al. 2005; Nielsen et al. 2004; Steigert et al. 2007; Tsao et al. 2007). However, there are few or no reports of PETG-PDMS, PETG-PU, PS-PDMS, PS-PU, COC-PDMS or COC-PU devices. Bonding hard top and elastomeric bottom has been shown in literature for bonding glass, quartz, SiO2 coated materials to elastomeric PDMS, PMMA and perfluoropolyethers (Osterfeld et al. 2006). PDMS and PMMA have also been bonded together to create a laminated microfluidic device for immunosensing (Ko et al. 2003). Such bonding of rigid materials with elastomeric materials has not been shown for PETG-PU, COC-PU, PS-PU or PETG-PDMS, COC-PDMS, and PS-PDMS. The bonding between the rigid polymer with channel features and elastomeric membrane, which would allow fluid actuation, although difficult to achieve, is demonstrated in this chapter.

Although our lab has established the control of fluid flow in PDMS microdevices using Braille tactile array (Futai et al. 2006; Gu et al. 2004; Heo et al. 2007; Song et al. 2005), application of the same perfusion system to devices made with thermoplastic materials has not been reported. Braille arrays are beneficial because they allow non linear and multidirectional perfusion, portability of microbioreactors, compartmentalization of channels within a single device, dynamic pumping and valving, and easy automatic

programming of fluid flow through different channels of a device. In this report, we bond thermoplastic channels with elastomeric (deflectable) membranes (either PDMS – parylene C - PDMS or PU), and demonstrate actuation, pumping and valving in a hard top-soft bottom chip using Braille array.

Evaporation of liquids through microfluidic devices is a recognized problem which arises due to high surface to volume ratios encountered at the microscale (Heo et al. 2007; Walker et al. 2004). Evaporation of water from the microchannels often leads to changes in the concentration and osmolality of the solutions, and is harmful to cells under culture as well as confounding for assays under scrutiny. Thermoplastic polymers such as PETG, COC, and PS have significantly lesser water vapor transmission rates compared to PDMS (as seen in Table 4.1), which makes the microfluidic devices fabricated using these materials less susceptible to evaporation of aqueous phases as compared to all-PDMS devices.

Table 4.1: Oxygen permeability values (in cm^3-mm/m^2-day-atm) for materials used in this report for fabricating and assembling microfluidic devices with hard tops and soft bottoms (Massey 2003).

Material	**Oxygen gas permeability (cm^3-mm/m^2-day-atm)**	**Water Vapor Transmission Rate (g-mm/m^2-day)**
PDMS	52531	125
PS	145	3.4-6
PU	78.7	0.9-3.43
COC	63.5	0.75
PETG	10.0	1.6
Parylene C	2.8	1.68

In our previous work, we have shown the modulation of oxygen tension in PDMS microbioreactors and found that dissolved oxygen can be regulated from 20% to 4.3%

level by operating the device at different cell densities and perfusion velocities (Mehta et al. 2007). However, it was difficult to get very low oxygen tensions, of the order of 1-2% in a microfluidic device made of gas permeable PDMS. Such low oxygen environments are needed for the biological studies of embryonic, adult stem cells as well as for studies of the diseases of the circulatory system and bone tissue engineering. Even though glass channels perfused with syringe pumps could be used for lowering oxygen concentration and increasing barrier to evaporation in microdevices, it would not be possible to have dynamic pumping and valving in different parts of the same microdevice, thus creating separate compartments of different flow rates and oxygen tension inside the microdevice or for performing fluid recirculation on chip. With channel deformation-based fluid actuation such as using pin actuator on refreshable Braille displays programmable deformation-based microfluidic actuation and hence control of oxygen to have different value in different parts of the same microdevice would become possible. We therefore embarked on fabricating microdevices with materials that have low oxygen permeabilities as compared to PDMS. Table 4.1 lists the permeabilities of all materials that we have used in this report. PDMS allows most oxygen transport in this comparison, followed by PS. PU and COC have similar oxygen transport properties, and PETG and Parylene C allow least oxygen diffusion through them.

Here we report microfluidic devices made using thermoplastic and elastomeric components that offer: 1) lower evaporation of aqueous solutions from the microchannels, 2) significantly lower oxygen tensions in microchannels compared to PDMS microdevices, and 3) peristaltic Braille actuation for pumping and valving in hard

top-soft bottom materials,. The new microfluidic devices are made up of two components: a rigid channel layer fabricated using PETG, COC or PS; and an elastomeric membrane of PU or PDMS to seal the channels. Bonding between dissimilar hard top and soft bottom was achieved by exposing substrates to oxygen and argon plasma. We also report the performance of the device for culture of cells and lowest oxyen tension possible in the devices with 3 different cell lines. These devices can have multiple applications in understanding fundamental biology (such as observing the effects of pliable and stiff surfaces on cellular behavior, studying cells under hypoxic environments), biochemical analysis, and analysis of cellular activities, as well as integrated devices which can perform all these functions at the same time.

4.2 Experimental Methods

4.2.1 Materials

For hot embossing, the following three polymers were obtained: Cyclic Olefin Copolymer (COC) (Zeonor 1060R and 1020 R), Zeon Chemicals L.P., Louisville, KY), Glycol-modified polyethylene terephthalate (PETG) (12" X 12" X 0.25") (McMaster Carr, Robbinsville, NJ), and Polystyrene (PS) – obtained from Fisherbrand 100 x 15 mm Fisherbrand Petri dishes (sterile) (Cat. 0875712 – 2071). For making elastomeric PU membranes, medical-grade aliphatic thermoplastic PU were used (Tecoflex®SG93A and SG80A, Thermedics Incorporated, Woburn, Massachusetts) in as a 5% solution by weight in 95% chloroform (Sigma). Epoxy molds were made using high temperature epoxy (Epoxy Cytec Industries Inc., Conapoxy FR-180, Parts A and B). PDMS was used as 10:1 base: curing agent (Dow Corning Sylgard 184). Tridecafluoro-(1,1,2,2-

tetrahydrooctyl)-1-trichlorosilane was purchased from United Chemical Technologies Inc., Bristol, PA.

4.2.2 Fabrication of the mold

Fabrication of Glass Wafer Mold

Briefly, a glass wafer mold was fabricated using backside diffused-light photolithography to form positive relief features made of SU-8 onto a thin glass wafer (200μm thick). The resulting glass wafer mold was taped to a single glass slide (75 x 50 mm) using double-sided tape and silanized with tridecafluoro-(1,1,2,2-tetrahydrooctyl)-1-trichlorosilane. This silanized glass wafer mold was then used to create a PDMS master.

Fabrication of PDMS Master (Using Soft Lithography)

The glass wafer mold supported on a glass slide was stacked on six additional glass slides (also 75 x 50 mm) using double-sided tape between each slide. The resulting 'block' was approximately 7.5 mm tall, with the channel features on the 'top' face. This block was then placed in a square Petri dish, covered with PDMS pre-polymer (10:1 base to curing agent (by mass) and degassed in a vacuum chamber), and then cured overnight at room temperature on a level surface. *It is critical that the PDMS cures on a level surface.* Any deviations from levelness will be transferred to the subsequent epoxy mold and result in uneven embossing. The levelness of the surface was easily verified using a simple, liquid/air-bubble leveling device. The resulting PDMS master had the channel features set into the bottom of a 'dish', and allowed the master to be used as a molding pattern for the subsequent epoxy mold. The final PDMS master was checked for levelness using a simple, liquid/air-bubble leveling device. Critical Dimensions used were: total height of

PDMS master: 11 mm, depth of the 'dish': 7.5 mm and PDMS height above glass wafer mold: 3.5 mm.

Fabrication of Epoxy Mold

High temperature epoxy (83:100, hardener: epoxy by mass) was poured into the PDMS master 'dish'. The PDMS master (with epoxy) was then placed onto a level surface in a 120^{o}C oven. The levelness of the surface was verified using a simple, liquid/air-bubble leveling device. As in the fabrication of the PDMS master, the levelness of the surface is critical to creating a useable mold. After about 5-10 minutes, the PDMS master was briefly removed from the oven, and a pipette tip was used to agitate the epoxy and remove all air bubbles trapped in the epoxy near the channel features (the epoxy is considerably less viscous after 5-10 minutes in oven, making removal of the air bubbles fairly easy). The PDMS master was then placed back into the oven for ten more minutes, after which it was checked again and any remaining air bubbles removed in the same way described above. The PDMS master was then placed back into the oven, and allowed to cure undisturbed for approximately 4 hours.

After the curing the epoxy and cooling it for approximately 1 hour, the hardened epoxy was carefully removed from the PDMS master. The resulting epoxy mold was checked for levelness using a simple, liquid/air-bubble leveling device.

4.2.3 Hot embossing

A 12 ton hot press with a platen size of 9 x 12" with mold area of 8 x 10" and a manual hydraulic press was used for embossing channels (model 912, maximum sustained temperature 177 C, Jackson Marking Products Co., Inc., Mt. Vernon, Illinois).

Before embossing a material, we had to find the appropriate embossing temperature that would allow imprinting of channel features on the substrates. In order to find this optimal embossing temperature (T_{emboss}), qualitative investigation with the polymers was performed by subjecting the materials to contact with epoxy mold at different temperature and same pressure. The T_{emboss} of polymers used in this report are: COC (Zeonor 1060R) T_{emboss} = 150 ^{o}C, PS T_{emboss} = 125 ^{o}C, and PETG T_{emboss} = 140 ^{o}C. The T_g of these polymers are: COC (Zeonor 1060R) T_g = 102 ^{o}C, PS T_g = 95 ^{o}C, and PETG T_g = 105 ^{o}C.

A silanized glass plate was centered on the metal tray with the silanized surface facing up, and loaded into the press. The temperature of the press to T_{emboss}, when the press temperature has stabilized at T_{emboss}, the tray was removed from the press and un-embossed material was placed in the center of the silanized glass plate. The tray was loaded back into the press and the lower platen was raised until the un-embossed material was a few millimeters away from the top platen. This insures quick and even heating of the un-embossed material. After 4-5 minutes, the tray was quickly removed from the press and the material was probed to verify that it was soft enough (or reached the glass transition temperature) for embossing (it deforms easily when gently poked with a

wooden pick). The epoxy mold was placed face-down on the softened material and the tray was load back into the press. The bottom platen of the press was raised slowly until the pressure gauze indicated the desired pressure. The pressure decreased to 0 as the material flowed around the epoxy mold. This procedure constitutes one "press." Two-four "presses" were performed to correct for any unevenness in the epoxy mold and obtain the desired thickness. When the embossed material flows up and around the edges of the epoxy mold, enough "presses" have been made. The number of "presses" will vary according to the thickness and type of material, as well as the levelness of the epoxy mold.

After embossing, the glass plate, the embossed material and the epoxy mold were removed off the tray and placed onto a cooling rack for 10-15 minutes after adding some weights on top to prevent the embossed material from warping as it cools. The embossed material was then separated from the epoxy mold, cut to rectangular shape using an electric saw. The holes for liquid inlet and outlet, as well as cell seeding ports were made on the embossed material using a drill press (Figure 4.1A).

To make PS embossed channels, a 2 mm thick PS sheet was made first from 4 layers of edge-cut petri dishes (Fisherbrand, 100 x 15 mm, sterile). The sheets were melted together at 125^{o}C using the press to make a thicker PS sheet.

4.2.4 Device assembly

In order to assemble a device, the hole punched hot embossed hot top needed to be bonded to an elastomeric soft bottom (Figure 4.1B). To make 200 um membranes from PU, 8 ml of the PU-chloroform solution (5% PU by weight) was placed in glass molds and left covered to evaporate overnight. The membranes were cut out of the glass mold next day and placed on silanized glass slides. PDMS – parylene C - PDMS membranes were fabricated as described earlier (Heo et al. 2007; Mehta et al. 2007).

The hard top and soft bottom were bonded using an Expanded Plasma Cleaner & PlasmaFlo™ (PDC-001 (115V), 200 W input, Harrick Plasma, Ithaca, NY) with argon and oxygen gases. The ratio of argon to oxygen inside the plasma chamber was 2:1. The channel piece and membrane were plasma oxidized for 1 minute at 400 mTorr. After removal from the plasma etcher, they were placed on top of each other, any remaining air bubbles were removed, and then the bonded devices were left in a 60 C oven with some weights on top until the next day.

When ready to be used, the devices were made hydrophilic again by plasma oxidation for one minute, and sterile DPBS was introduced into the channels. These devices were then sterilized by placing under a UV-C light for ~30 minutes.

4.2.5 Braille actuation

An array of 48 pin actuators adapted from a Braille display module (SC9, KGS, Saitama, Japan) was used for fluid actuation (Futai et al. 2006). The pin actuator module was controlled with a computer via Universal Serial Bus (USB) through a finger-sized stand alone custom controller circuit board (Olimex, Plovdiv, Bulgaria) (Futai et al. 2006; Heo et al. 2006). The microfluidic bioreactor chip interfaces with the pin actuator module by simply holding the chip in place such that the channels align with the pins which push upward closing the channel, as seen in Figure 4.1 C. The pin movements for valving and pumping were controlled with a custom computer program written in C sharp.

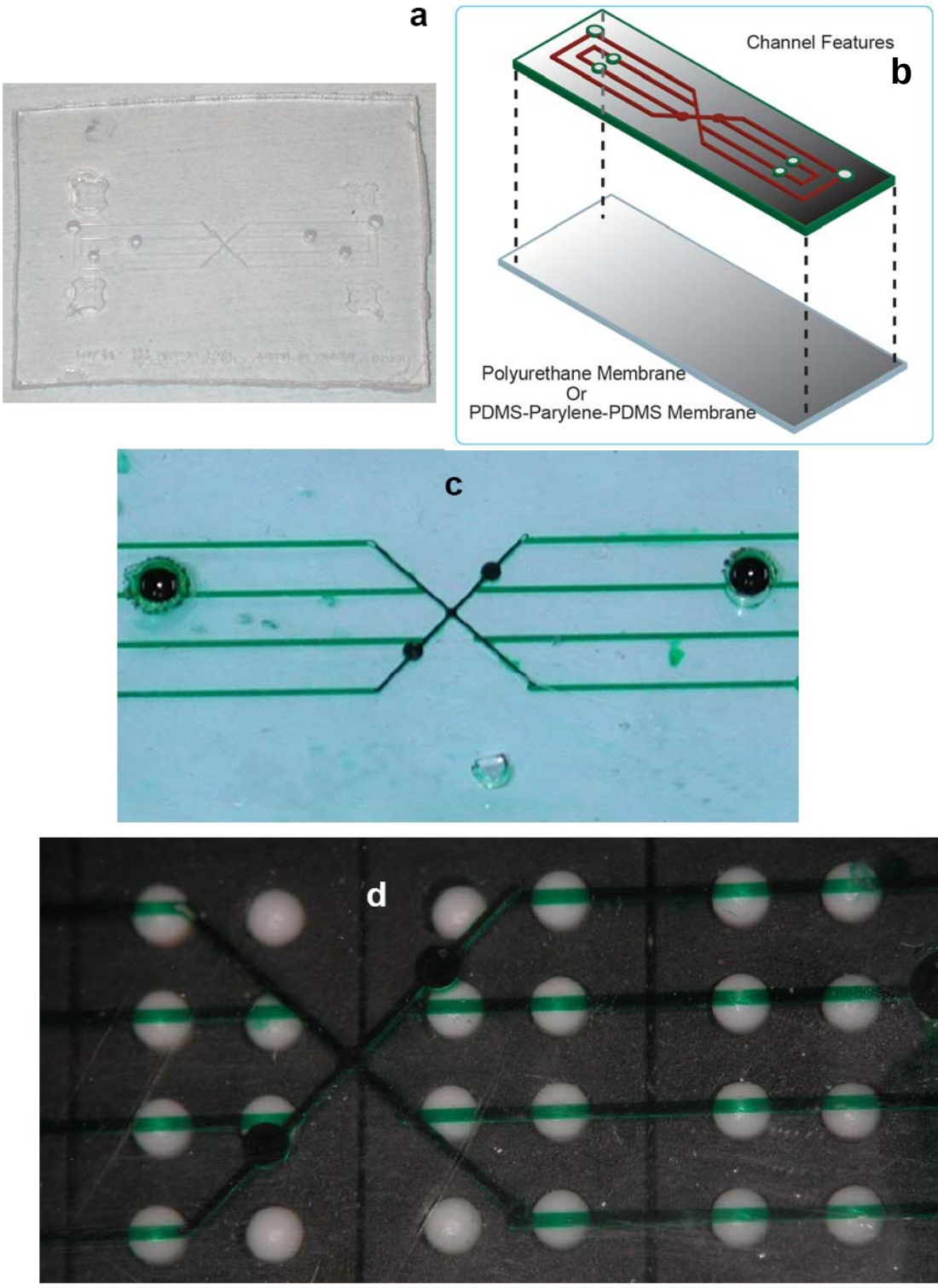

Figure 4.1: The microfluidic device used for hot embossing. a) Hot embossed COC device, **b)** overall schematic of the device showing two components: channel layer and membrane layer, **c)** an actual hard top-soft bottom device with green food dye, and d) device on the Braille array

4.2.6 Microscopy

Pictures of the devices and channel cross sections were taken using an inverted phase contrast microscope (Nikon TE 300) and a digital CCD camera (Hamamatsu) at different magnifications. Scanning electron microscope (SEM) was used for imaging the cross sections of the embossed channels. In order to prepare the samples for imaging, the channels were coated with carbon (SPI Supplies, Module Carbon Coater) for two minutes.

4.2.7 Fluid flow simulation

In order to investigate the valving behaviors of the fabricated microfluidic devices, we performed simulations using finite element analysis (FEA) software, ANSYS 10.0 (ANSYS Inc., Southpointe, PA). To reduce the computational time, a three-dimensional (3-D) model of the half of the device with a symmetric boundary condition was constructed as shown in Figure 4.2 A. Figure 4.2 B shows the cross-sectional view of the constructed model from the symmetry plane. The model was composed of a microfluidic channel with a bell-shape cross-section, which is measured experimentally, bonded with a flat membrane, and a Braille pin structure. Two sets of contact analysis were performed to simulate the interactions between the Braille pin and the membrane; the channel and the membrane respectively. The 3-D contact and target elements, CONTA173 and TARGE170, were employed in contact analysis, and the deformation of the structure was simulated using 10-node tetrahedral 3-D solid element, SOLID92. The force boundary condition was assigned to the Braille pin to simulate its actuation motion.

To simulate the large deformation of the structure, non-linear, large deformation static analysis was performed.

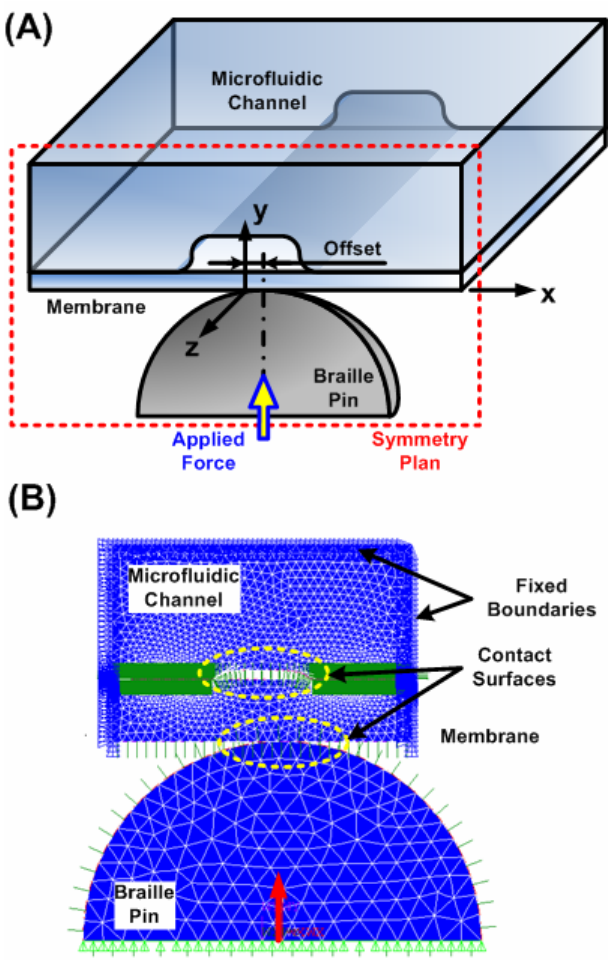

Figure 4.2: Simulation of the fluid flow inside the device with Braille actuation: a) schematic drawing of the three-dimensional (3-D) model constructed for finite element analysis (FEA) to simulate valving behaviors for various microfluidic channels using Braille display actuation, **b)** The cross-sectional view from symmetry plan of the constructed model in FEA software, ANSYS (ANSYS Inc., PA).

4.2.8 Cell culture

HepG2 cells (human hepatocellular carcinoma, ATCC, HB-8065) and C2C12 cells (mouse myoblasts, ATCC, CRL- 1772) were cultured in a media comprising Dulbecco's Modified Eagle's Medium (DMEM, 11960, Gibco), 15% Fetal bovine serum (FBS,

10082, Gibco), 1%v/v antibiotic–antimicotic (15240, Gibco) and 1%v/v GlutaMAX2-I Supplement (35050, Gibco). MC3T3-E1 cells (mouse preosteoblast, ATCC, MC3T3-E1 subclone 4, CRL-2593) were cultured in ascorbic acid free alpha-MEM media (Minimal Essential Alpha Medium, 0010083DJ, Gibco) supplemented with 10% Fetal bovine serum, 1%v/v antibiotic–antimicotic and 1%v/v GlutaMAX2-I. Primary human dermal microvascular endothelial cells (HDMECs) were cultured in EGM-2MV (EGM-2MV Microvascular Endothelial Cell Medium, CC-3202, Lonza) media supplemented with 1%v/v antibiotic–antimicotic.

The T-25 culture flasks were placed in a humidified 5% CO_2 cell culture incubator. At 70-80 % confluence, the cells were passaged by washing in PBS, and incubating with 0.25% Trypsin/EDTA (Invitrogen, Carlsbad, CA). The Trypsin solution was neutralized with 15% FBS in DMEM and spun down with a centrifuge (ThermoForma, Marietta, OH) for 2 minutes at 4 ^{o}C and 1000 RPM. The supernatant was removed and the pellet was resuspended in DMEM media. The pellet was reconstituted in 4 ml of DMEM media, and 1 ml of this suspension was used for creating a new plate of HepG2, C2C12, MC3T3-E1, and HDMECs. The cells were passaged every third day. When the cells were to be cultured in the PDMS microbioreactor, the pellet was reconstituted in 70-100 μL of DMEM media and then injected into the seeding ports of the chip.

4.2.9 Cell seeding in devices

Fibronectin (100 mg/μl, F2006, Sigma) was pipetted into the microdevices to help with cell attachment. This absorption was carried out for 30 minutes, following which media

(specific to the cells being seeded) was introduced in the device and the chip was placed on an array of pin actuators adapted from Braille displays for at least one hour to peristaltically pump fluid through the channels. Cells (HDMECs, HepG2, MC3T3E1, C2C12) were seeded into the chip through the cell seeding ports. The cells were directed into the desired location inside the microdevice by using Braille pumping and valving. The cells were given 2-4 hours to attach under no flow (pins up and channels valved closed) condition in a dry heat incubator (Forma 310 Series Direct Heat CO2 Incubator, Thermo electron Corporation**,** Marietta, OH) maintained at 37 ^{o}C and 5% CO_2. Pumping was started after cells became adherent and the chip was perfused for 12-14 hours.

4.2.10 Oxygen measurement

0.2 ml of the oxygen sensitive dye, ruthenium tris(2,2'-dipyridyl) dichloride hexahydrate (RTDP) (93307, Fluka) (5 mg/ml in DPBS (14190250, Invitrogen); final concentration is 1 mg/ml because of dilution) was introduced into the inlet of the device, and pumping was continued for three more hours. The setup comprised of a microfluidic chip attached to the pin actuator array module was then taken to the microscope where lifetime measurements performed at room temperature. Cell densities in the cell culture channels in the microbioreactor chips were determined by counting the number of cells present in brightfield images taken at different positions along the length of the cell culture channel. The oxygen measurement system consisted of Nikon TS-100F microscope with fluorescence attachment, LED light source (default is blue light with central wavelength of 470nm (LXHL-MB1D Blue Luxeon, Lumileds Lighting, LLC, CA), lock-in amplifier (SR830, Stanford Research System, Inc., CA), function generator (33220A, Agilent

Technology, Inc., CA), and silicon PIN photodiode with preamplifier (PDA36A, Thorlabs, Inc., NJ). The system is controlled by a personal computer with LabVIEW graphic user interface program for operation and data acquisition through GPIB interface (GPIB-USB-HS, National Instruments, Co., TX). Figure 4.3 shows the schematic of the Nikon TS-100F Microscope Fluorescence Intensity Detection System (FIDS). The numerical data from LabVIEW was saved in a .txt file containing values of time (in sec), intensity signal (in μV), and phase (in degree).

The relationship between fluorescence intensity (or lifetime) and dissolved oxygen concentration is described by the Stern–Volmer equation (Gerritsen et al. 1997; Sud et al. 2006; Urayama et al. 2003; Zhong et al. 2003): $I_o/ I = 1 + K_q[O_2]$ or $\tau_o/\tau=1 + K_q[O_2]$, where I_o or τ_o = uninhibited sensor dye intensity or lifetime (i.e. 0% oxygen), I or τ = sensor dye intensity or lifetime at oxygen level $[O_2]$ and K_q is the Stern-Volmer quenching constant. The system was calibrated by testing devices with just the dye and no cells and no oxygen for uninhibited sensor lifetime. The oxygen was removed by using oxygen quenching sodiumthiosuphate supersaturated solution.

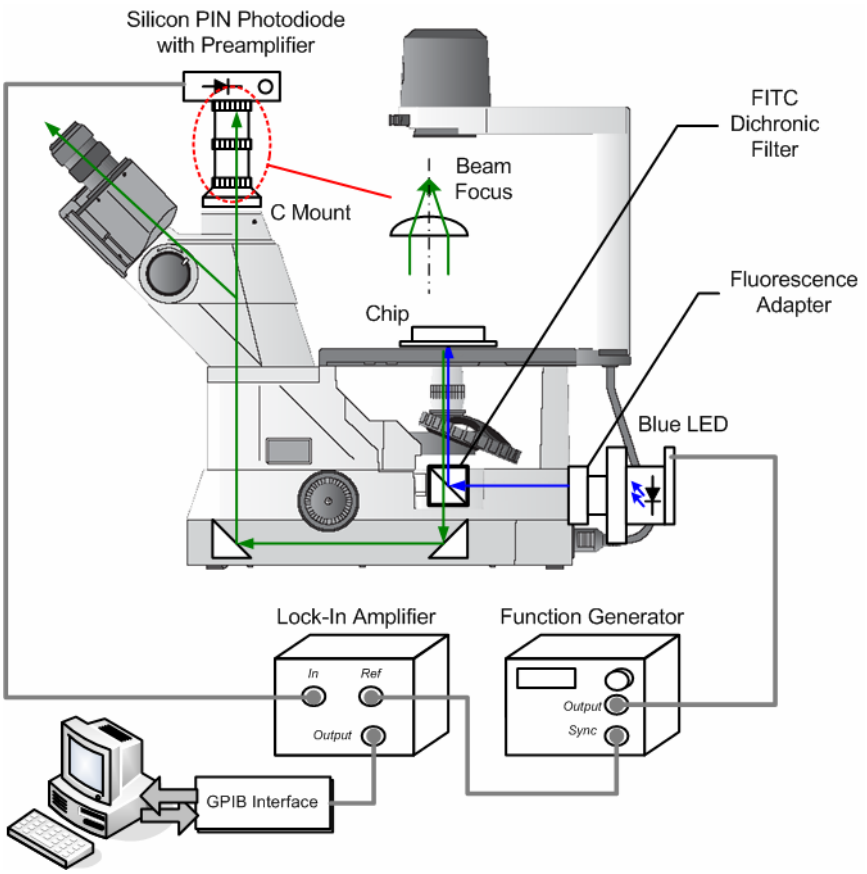

Figure 4.3: Schematic of the Nikon TS-100F Microscope Fluorescence Intensity Detection System (FIDS).

4.3 Results and Discussions

4.3.1 Hot Embossing of Hard Top Devices

Embossing temperature varies with material and is a temperature at which material flow balances with material stability. If the temperature is too low, the material will not be soft enough to flow and might result in the destruction of raised features (such as the 'X' region in our design which is 200 μm high, compared to rest of channels which are 30 μm high) on the epoxy mold as it is pressed against the relatively hard material. The destruction of these features results in an imperfect replica of the desired features. On the other hand, if the temperature is too high, the material can degrade.

In general, the optimal embossing temperature is 30-50^{o}C above the T_g (Cameron et al. 2006; Fredrickson et al. 2006; Steigert et al. 2007). For our work, we used T_{emboss} equal to 150 ^{o}C for COC, 140 ^{o}C for PETG, and 125 ^{o}C for PS. A representative image of the hot embossed COC is observed in Figure 4.1 A, which shows imprinted channel features on COC surface after de-embossing. Thus, channel features were replicated onto the PETG, COC and PS 'hard tops' with good reproducibility for channels with different heights and shapes. All channels except 'X' region were bell shaped, while the 'X' region was rectangular; likewise, all other channels except 'X' were 30 μm high while X was 200 μm high.

In order to investigate the geometry of the microfluidic channels made by various materials using soft lithography and hot embossing, we performed scanning electron microscope (SEM) imaging for the fabricated devices. Prior to imaging, the microfluidic

channels were coated with carbon (SPI Supplies, Module Carbon Coater) for two minutes. Figure 4.4 shows the SEM images of the top and cross-sectional views of the fabricated microfluidic channels. The imaging results demonstrate the excellent geometry transferring through the fabrication processes, and showcases that the surfaces of the devices are microscopically smooth. Moreover, the bell-shape cross-sectional geometries can be well transferred into the devices, which facilitate the microfluidic actuation using Braille displays.

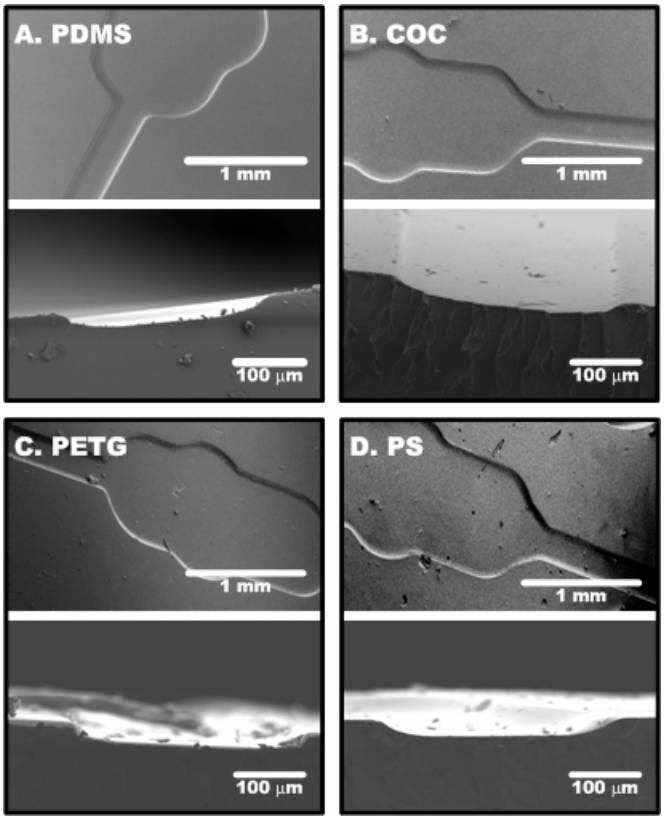

Figure 4.4: Scanning Electron Microscopy images of the cross sections of the channel features fabricated using: a) PDMS by soft lithography replica molding, and **b)** COC, **c)** PETG, and **d)** PS microfluidic channels made by hot embossing. Scale bars are 100 microns.

4.3.2 Bonding of Hard Top Devices with Soft Elastomeric Membranes

We tried various ways to bond hard tops (COC, PETG, PS) to PU or PDMS-parylene C-PDMS membranes. Methods that resulted in an unstable bond between hard top and soft bottom included oxygen plasma treatment, chemical grafting on hard top, UV polymerization between hard and soft components, and thermal sealing.

We were able to successfully bond devices by surface treatment of all components with one minute of oxygen and argon plasma, with a ratio of argon to oxygen flow rate of 2:1. After plasma treatment, the surfaces were brought together, hermetically sealed and placed in a 60 ^{o}C oven with small weights (less than 1 lb) for an overnight heat treatment. To make the devices hydrophilic, the microfluidic channels were plasma oxidized or corona treated as a complete device for 2 minutes. Devices sealed in this way had stable bond strength at room temperatures for up to several months. At high humidity (for example as in the humidified incubators), the device bonding lifetime is limited to about seven days due to delamination of the bottom elastomeric membrane from the hard top.

Bonding monolithic devices made of just COC, PETG, PS or PDMS is well established and relatively simple and long lasting (Bhattacharyya et al. 2007; Lin & Burns 2005; Mair et al. 2007; Mizuno et al. 2005; Nielsen et al. 2004; Pal et al. 2006; Tsao et al. 2007). The techniques employed in this report for bonding dissimilar materials result in devices that may have bond strength inferior to thermally bonded monolith devices because of the varied intrinsic characteristics of the materials that we bond together. The hard tops (PETG, COC and PS) all have saturated hydrocarbons in their polymeric

backbones which results in difficulty in introducing any suitable functional groups on the surface. However, in literature (Bhattacharyya & Klapperich 2007; Makamba et al. 2003; Mizuno et al. 2005), the plasma oxidation with Ar and O_2 has been reported to produce lower molecular weight polymer fragments on the surface which leads to reduction in T_g and furthermore crosslinking of activated surface groups on substrates, giving rise to a stable bond. Such explanations are often ascribed to similar surface treatments of polymers.

4.3.3 Braille Actuation and Perfusion in Hard Top Soft Bottom Devices

The analysis of fluid flow with Braille peristaltic pumping and valving was performed to confirm and validate perfusion in hard top-soft bottom devices. The bonded and hydrophilyzed devices were filled with green food dye, place on top of Braille array with channels aligned with respect to Braille pins, and the pumping and valving motion of the channels was documented (as seen in Figure 4.1 C and 4.1 D).

Figure 4.5 shows a representative picture of hard tops pumping and valving in 4.5 A and 4.5 B, while all-PDMS channels are depicted in 4.5 C and 4.5 D for comparison. As can be seen from the images, the Braille array can successfully pump and valve though a device made of a rigid top later and elastic bottom layer and there are no leaks observed with repeated pumping and valving action.

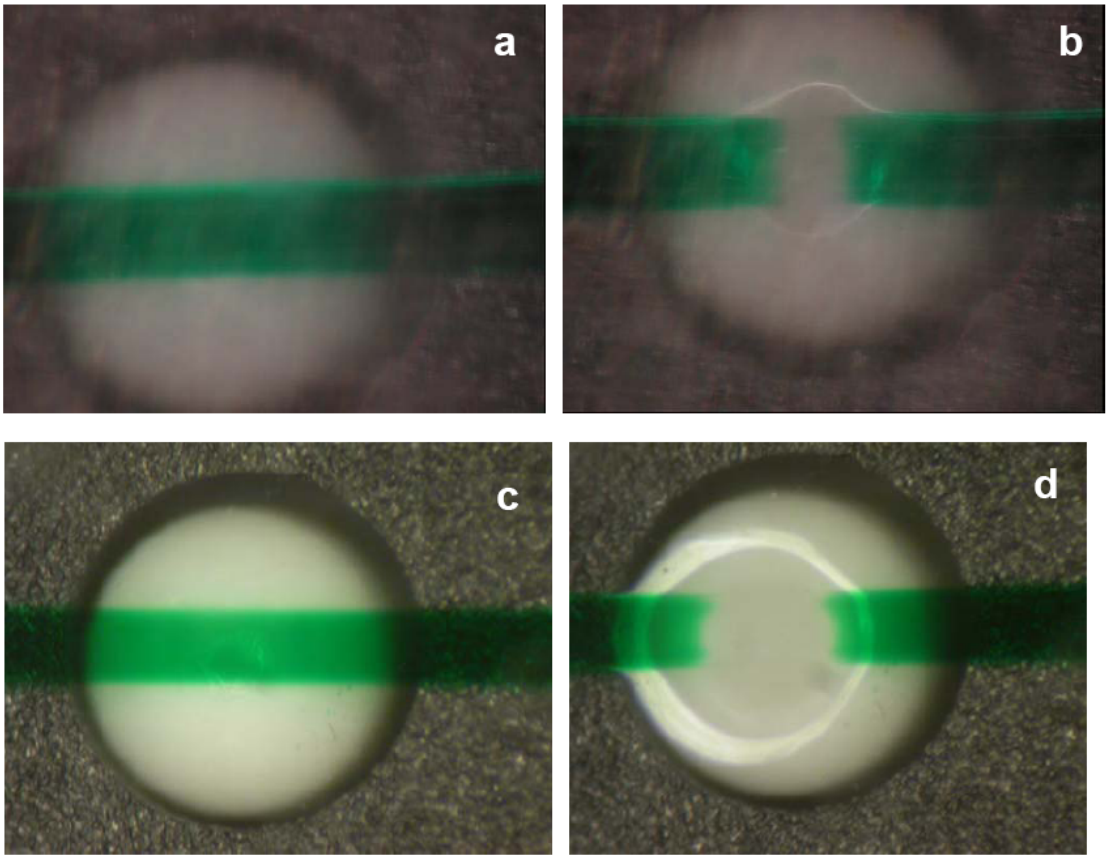

Figure 4.5: Braille actuation in hard top soft bottom devices (a and b) as compared to all PDMS device (c and d).

When comparing hard top-soft bottom channel valving to that in the all-PDMS channels, the extent of channel closure and deformation is higher in PDMS channels. This is expected because PDMS had a much higher bending strength and modulus than either PETG, COC or PS. However, it should be noted that when valving in hard top soft bottom devices, the channel does completely close under the weight of the Braille pin and there are no leaks of liquid around the bonded interface.

While PDMS is an elastomeric polymer; COC, PS, PETG are thermoplastic hard polymers, and thermoplastic PU used in this report is also flexible and elastomeric. The

control of fluid motion in hard top-soft bottom devices as compared to all-PDMS devices is also explored using a two dimensional model of pressure distribution inside the device as the Braille pin pushes up. The extent of channel closure and the strain produced is observed. The fluid flow in hard top soft bottom channels was further compared to a device made of all PDMS channels by flow simulations of Braille pumping and valving in microfluidic devices. Two dimensional finite element model of Braille pin pushing on the microfluidic channel showing the pressure and strain distribution is seen in Figure 4.2.

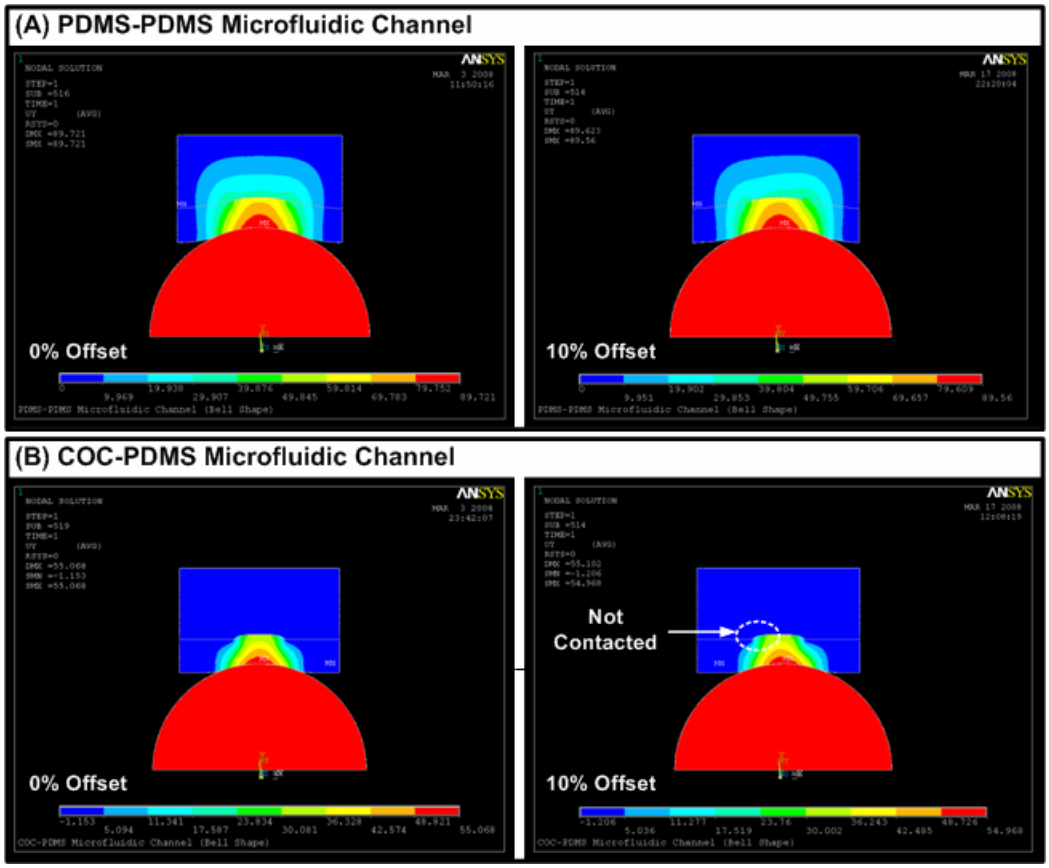

Figure 4.6: FEA simulated horizontal displacement (y-direction) results of a) PDMS-PDMS microfluidic channel, and **b)** hard top COC-PDMS microfluidic channel with the 0% and 10% channel width misalignment of the Braille pin.

Figure 4.6 shows the simulation results for PDMS-PDMS and hardtop COC-PDMS microfluidic channels. As can be seen in the figure, in the PDMS-PDMS microfluidic channel, both the channel and the membrane will be deformed to seal the channel, while in the COC-PDMS microfluidic channel, only the membrane will be deformed. Moreover, due to the higher Young's modulus of the COC, the Braille pin causes less displacement in hardtop channel (c.a. 55 μm) compared to the PDMS channel (c.a. 90 μm). The smaller displacement makes the alignment between the device and the Braille pin more critical. For instance, when the Braille pin is aligned 10% off center along the channel width, the PDMS-PDMS channel can still be sealed by Braille pin actuation for complete valving as shown in Figure 4.6 A. However, in COC-PDMS channel, the corner of the channel will not be contacted with the membrane as shown in Figure 4.6 B, which leads to a non-complete valving. For studies in which isolation of cells or analytes in particular compartments is essential, or when it is necessary to know the flow rates in microchannels with precision, accurate alignment will be essential. If the alignment is offset even by 10%, in case of hard top soft bottom devices, the microchannels will not close completely when valved, resulting in leaky valving and pumping.

4.3.4 Cell Culture in Recirculation Loop in Hard Top Soft Bottom Devices

We show culture of primary human dermal microvascular cells (HDMECs) in a very small amount of media inside a recirculation loop in the hard top-soft bottom device for 12 hours outside the incubator. This is a significant improvement over previous work from our lab where because of evaporation we could only perform the outside culture of HDMECs in PDMS devices for less than 2 hours in a device

fabricated of only PDMS. This result is also comparable to the HDMEC culture performed in a PDMS device bonded with PDMS - parylene C - PDMS membrane, where ~70% of cells were alive after 12 hours of outside incubator culture (Heo et al. 2007).

Cell survival when recirculating very small amount of media (~1 μL) in channels with reservoirs valved off for duration of 12-24 hours outside incubator is ~100% and the cell morphology after such culture is healthy, as seen in Figure 4.7. Figure 4.7 A shows HDMEC cells after seeding in the device at time = 0 or start of outside culture with continuous recirculation, and Figure 4.7 B shows the cells after 12 hours of culture outside incubator while being heated to a physiological temperature. This example indicates that the evaporation in our hard top-soft bottom devices is significantly lower than in all-PDMS devices, as can be expected from the water vapor transmission rates for these materials (Table 4.1).

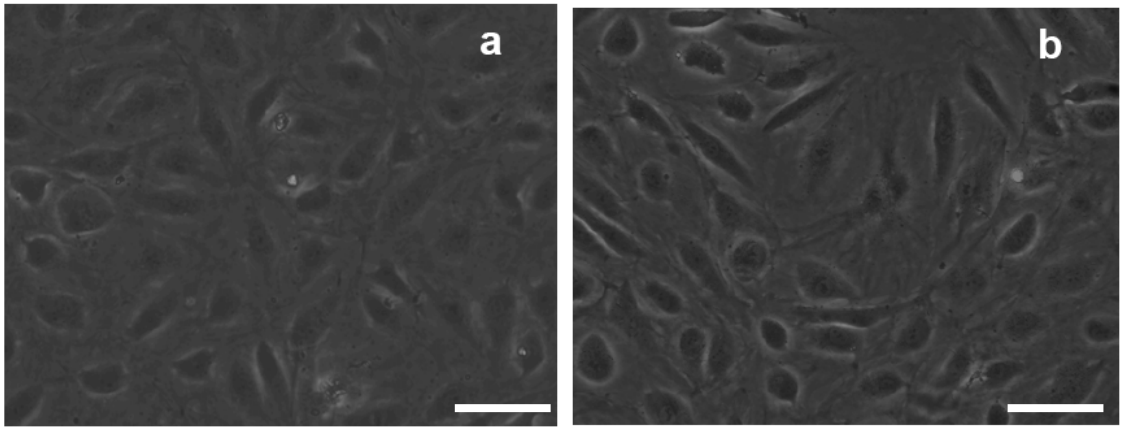

Figure 4.7: Culture of Human Dermal Microvascular Endothelial cells (HDMECs) outside incubator at room temperature humidity in the recirculation loop of the device for 12 hours. Scale bar: 100 μm.

4.3.5 Oxygen tension in Hard Top Soft Bottom Devices

We quantified oxygen tension in the hard top-soft bottom devices for three cell lines at low flow rates and high cell densities to obtain a lower bound on the dissolved oxygen concentration inside these devices. Real-time measurement of fluorescence signal intensity and phase based on Nikon TS-100F microscope with stage for Braille display systems was used for measurement of dissolved oxygen measurement in this report.

Table 4.2 shows the lowest oxygen tension recorded in the hard top-soft bottom channels with three different cell lines (HepG2, C2C12, and MC3T3-E1) at a low average velocity of 5.4 X 10^{-7} m/sec and high average cell density of 1.54 X 10^{9} cells/m^2. The average oxygen concentration at 25 ^{0}C are evaluated from the differences in the lifetime of the dye at normal room oxygen and that at downstream of cells in the devices. The standard deviations for all reported values were less than 5% of the data points. The lowest oxygen tensions in the hard top soft bottom devices are significantly different from that in a PDMS device for all cell types. Thus, we were able to achieve hypoxic conditions when culturing mammalian cells in hard top-soft bottom devices made with PETG, COC and PS, and bonded with PU membrane. Such low oxygen tensions are ideal for culture of certain embryonic and adult stem cells to control their differentiation capabilities and also for the study of ischemia injuries in specific organs (references). The hard top-soft bottom devices offer *in vitro* model for simulating physiological environments for certain cell types as compared to conventional cultures, enabling the studies of how limited oxygen can affect cell behavior not only in terms of metabolism but also in cellular signaling, gene expression and decision of cell fate.

Table 4.2: Dissolved oxygen concentrations in the microfluidic devices in mg/L

Material	Oxygen Concentration (mg/L)		
	Cell Type		
	HepG2	C2C12	MC3T3-E1
PETG	0.43	0.87	1.26
COC	0.51	0.96	1.33
PS	1.13	1.64	2.02
PDMS	1.42	2.02	2.39

4.4 Conclusions

We utilized a hot embossing technique to develop a fast, reliable method for embossing microfluidic channels into thermoplastic materials. We were able to imprint channel features reproducibly on PETG, COC and PS hard tops with great fidelity. Hot embossing enables easy fabrication of these channels, which can be scaled up to suit commercial settings. The channel features on hard tops were bonded to elastomeric soft membranes to create new microchannels which reduce evaporation problems while still taking advantages of Braille pumping. The bonding between dissimilar hard tops and soft bottoms was achieved by combination of oxygen and argon plasma. The resulting devices had lower evaporation as witnessed by outside incubator heated culture of HDMECS for 12 hours, lower oxygen tensions as measured by lifetime of oxygen sensitive dye, and ability to combine with Braille arrays to enable dynamic pumping and valving without

leakage. In conclusion, this report describes versatile hard top soft bottom devices which can be combined with Braille arrays and used for microfluidic cell culture as well as biochemical assays on the chip. These devices can have multiple applications in understanding fundamental biology (such as observing the effects of pliable and stiff surfaces on cellular behavior), hypoxic cell culture conditions, biochemical analysis, and analysis of cellular activities, as well as integrated devices which can perform all these functions at the same time. Moreover, the Braille facilitated dynamic pumping and valving is useful for creating compartments within the same device to run different experiments. Hard top soft bottom devices introduced in this report are low cost, easy to fabricate, have high quality channel features, can easily integrate analysis techniques (such as electrophoresis), are cell culture ready, can be used as chemical processing, and compatible with key detection technologies. These devices are also resistant to a large range of chemicals, organic solvents, and temperature, transparent to allow imaging related analysis, not conductive, and offer the possibility of mass-producing disposable low-cost chips.

References

Beebe DJ, Mensing GA, Walker GM. Physics and applications of microfluidics in biology. Annu. Rev. Biomed. Eng. 2002; 4:261-86.

Bhattacharyya A, Klapperich CM. Mechanical and chemical analysis of plasma and ultraviolet-ozone surface treatments for thermal bonding of polymeric microfluidic devices. Lab Chip, 2007; 7:876-82.

Cameron NS, Roberge H, Veres T et al. High fidelity, high yield production of microfluidic devices by hot embossing lithography: rheology and stiction. Lab on a Chip 2006; 6:936–41.

Dittrich PS, Manz A. Lab-on-a-chip: microfluidics in drug discovery. Nature Reviews Drug Discovery 2006; 5 (3):210-18.

El-Ali J, Sorger PK, Jensen KF. Cells on chips. Nature 2007; 442 (27):403-11.

Fredrickson CK, Xia Z, Das C et al. Effects of Fabrication Process Parameters on the Properties of Cyclic Olefin Copolymer Microfluidic Devices. Journal of Microelectromechanical Systems, 2006; 15 (5):1060-68.

Futai N, Gu W, Song JW et al. Handheld recirculation system and customized media for microfluidic cell culture. Lab Chip 2006; 6 (1):149-54.

Gerritsen HC, Sanders R, Draaijer A et al. Fluorescence Lifetime Imaging of Oxygen in Living Cells. Journal of Flourescence 1997; 7 (1):11-6.

Gu W, Zhu X, Futai N et al. Computerized microfluidic cell culture using elastomeric channels and Braille displays. Proc Natl Acad Sci U S A 2004; 101 (45):15861-6.

Heo YS, Cabrera LM, Smith GD et al. Characterization and Resolution of Evaporation-Mediated Osmolality Shifts that Constrain Microfluidic Cell Culture in Poly(dimethylsiloxane) Devices. In., Series Characterization and Resolution of Evaporation-Mediated Osmolality Shifts that Constrain Microfluidic Cell Culture in Poly(dimethylsiloxane) Devices. 2006.

Heo YS, Cabrera LM, Song JW et al. Characterization and resolution of evaporation-mediated osmolality shifts that constrain microfluidic cell culture in poly(dimethylsiloxane) devices. Analytical Chemistry 2007; 79:1126-34.

Ko JS, Yoon HC, Yang H et al. A polymer-based microfluidic device for immunosensing biochips. Lab Chip 2003; 3:106-13.

Lin R, Burns MA. Surface-modified polyolefin microfluidic devices for liquid handling. J. Micromech. Microeng. 2005; 15:2156-62.

Mair DA, Rolandi M, Snauko M et al. Room-Temperature Bonding for Plastic High-Pressure Microfluidic Chips. Anal. Chem. 2007; (79):5097-102.

Makamba H, Kim JH, Lim K et al. Surface modification of poly(dimethylsiloxane) microchannels. Electrophoresis 2003; 24 (21):3607-19.

Massey LK. Permeability and Other Film Properties of Plastics and Elastomers: A Guide to Pacakaging and Barrier Materials. 2 ed: William Andrew Inc.; 2003. (PDL Handbook Series, Plastics Design Library).

Mehta G, Mehta K, Sud D et al. Quantitative Measurements and Analysis of Cellular Oxygen Uptake in Microfluidic Poly(dimethylsiloxane) Bioreactors. *Biomedical Microdevices* 2007; 9 (2):123-34.

Mizuno J, Farrens S, Ishida H et al. Cyclo-olefin Polymer Direct Bonding Using Low Temperature Plasma Activation Bonding. In Proceedings of the 2005 International Conference on MEMS, NANO and Smart Systems (ICMENS'05): IEEE; 2005. 1-4 p.

Nielsen T, Nilsson D, Bundgaard F et al. Nanoimprint lithography in the cyclic olefin copolymer, Topas®, a highly ultraviolet-transparent and chemically resistant thermoplast. J. Vac. Sci. Technol. B - Microelectronics and Nanometer Structures 2004; 22 (4):1770-75.

Osterfeld SJ, Wang SX, Multilayer microfluidic device. United States patent US 20060210445. 2006.

Pal R, Sung KE, Burns MA. Microstencils for the Patterning of Nontraditional Materials. Langmuir 2006; 22:5392-7.

Shim J, Bersano-Begey TF, Zhu X et al. Micro- and nanotechnologies for studying cellular function. Curr Top Med Chem 2003; 3 (6):687-703.

Song JW, Gu W, Futai N et al. Computer-controlled microcirculatory support system for endothelial cell culture and shearing. Anal Chem 2005; 77 (13):3993-9.

Steigert J, Haeberle S, Brenner T et al. Rapid prototyping of microfluidic chips in COC. J. Micromech. Microeng. 2007; 17:333-41.

Sud D, Zhong W, Beer DG et al. Time-resolved optical imaging provides a molecular snapshot of altered metabolic function in living human cancer cell models. Optics Express 2006; 14 (10):4412-26.

Tsao CW, Hromada L, Liu J et al. Low temperature bonding of PMMA and COC microfluidic substrates using UV/ozone surface treatment. Lab Chip 2007; 7:499-505.

Urayama P, Zhong W, Beamish JA et al. A UV-Visible-NIR fluorescence lifetime imaging microscope for laser-based biological sensing with picosecond resolution. Applied Physics B: Lasers and Optics 2003; 76 (5):483.

Walker GM, Zeringue HC, Beebe DJ. Microenvironment design considerations for cellular scale studies. Lab Chip 2004; 4 (2):91-7.

Weibel DB, Whitesides GM. Applications of microfluidics in chemical biology. Current Opinion in Chemical Biology 2006; 10 (6):584-91.

Whitesides GM, Ostuni E, Takayama S et al. Soft lithography in biology and biochemistry. Annu Rev Biomed Eng 2001; 3:335-73.

Zhong W, Urayama P, Mycek M-A. Imaging fluorescence lifetime modulation of a ruthenium-based dye in living cells: the potential for oxygen sensing. Journal of Physics D: Applied Physics 2003; 36 (14):1689.

CHAPTER 5

CELLULAR OXYGEN UPTAKE RATES IN MAMMALIAN MIOBIOREACTOR CULTURES

5.1 Introduction

Compared to conventional culture systems, microfluidic bioreactors offer a closer approximation of the *in vivo* microenvironment for the study of cell biology. In such microbioreactors, the cellular responses are dependent on the operating conditions and physical parameters such as cell densities, perfusion rate, inlet nutrient concentrations and the device geometry. One of the key intrinsic cellular characteristics which can be different in microfluidic cultures as opposed to conventional culture is the oxygen uptake rate (OUR) of cells in culture (Balis et al. 1999; Deshpande et al. 2004; Ducommun et al. 2000; Guarino et al. 2004; Lai et al. 1982; Ruffieux et al. 1998).

We already have a well characterized experimental method to measure oxygen concentration in real time in PDMS microbioreactors as shown in Chapter 3 and 4 (Mehta et al. 2007). In this chapter, we use our oxygen concentration measurement technique of mammalian cells and an already established mathematical model (Mehta et al. 2006)

along with inference methods to accurately assess the OUR characteristics of various cells in microfluidic culture.

The OUR results obtained from these studies will specify the different metabolic states of mammalian microfluidic cell cultures over different stages of cell growth, which will be beneficial in optimizing the microbioreactors for optimal performance (Wagner et al. 1998; Worboys et al. 1997).

5.2 Experimental Methods

5.2.1 Microdevice Fabrication

The microbioreactor comprised of two compartments: channel layer and PDMS-parylene C-PDMS membrane. The device was fabricated as previously described in the experimental methods of Chapter 3. Two device designs were used for the parameter estimation experiments. The first microdevice was similar to the design as used in Chapter 3 (shown in Figure 5.1) and has a 'X' geometry at the center of the device. The cells are seeded in the X region, which is either 100 or 200 μm high, while rest of microchannels are 30 μm high and 300 μm wide. The second microdevice was the new design and can be seen in Figure 5.2 and has a single loop with a slanted channel for cell culture. The cell region is 100 μm high, while rest of microchannels are 30 μm high and 300 μm wide.

5.2.2 Cell seeding

HepG2, C2C12 and MC3T3-E1 cells were cultured, passaged, and seeded inside the device as described in experimental section of Chapter 4.

5.2.3 Oxygen measurement

Dissolved oxygen concentration in microdevices with different cell types was measured in real time using the same optics based lifetime detection technique as outlined in Chapter 4.

5.3 Results and Discussion

5.3.1 Dissolved oxygen tension profiles

The dissolved oxygen tension profiles in the 'X' microdevices (design demonstrated in Figure 5.1) with HepG2, C2C12 and MC3T3-E1 cells are shown in Figure 5.3.

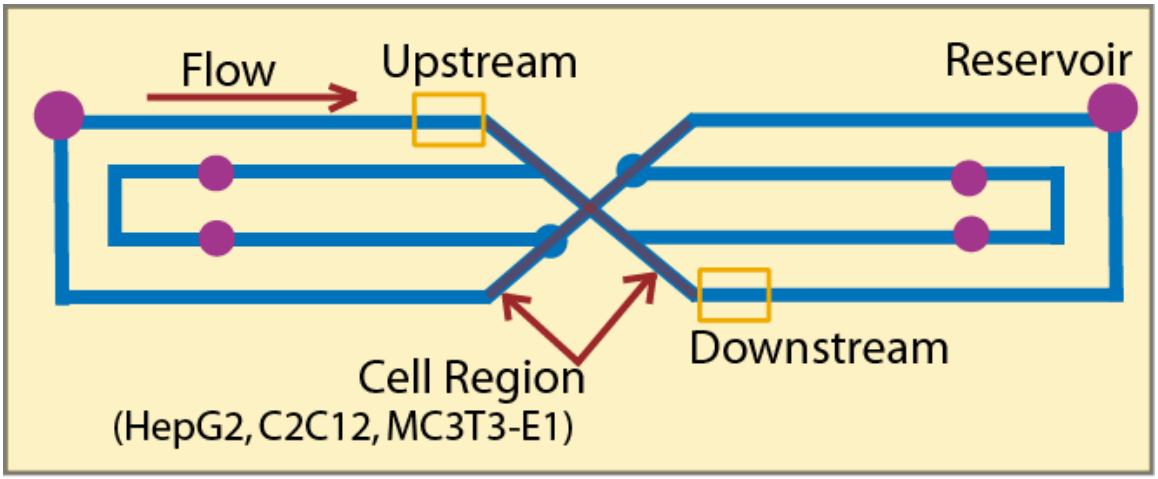

Figure 5.1: Schematic of the first microdevice design used for oxygen measurement in microfluidic cultures of HepG2, C2C12 and MC3T3-E1 cells.

The oxygen tension in the double cross 'X' PDMS design varied from 20% to 4% for MC3T3-E1 cells, from 20% to 3.7% for C2C12 cells, and 20% to 2.7% for HepG2 cells

for the cell density range of 6.7 X 10^7 to 1.6 X 10^9 cells/m^2 and velocity range of 0.5 to 28. 5 μ/sec with the cell region channel height of 100 or 200 μm.

As shown in Figure 5.3, HepG2 cells had the steepest oxygen gradients along the length of bioreactor of all three cell types, followed by C2C12 and lastly MC3T3-E1. Proliferation of HepG2 cells was very rapid compared to other cells and their culture requires frequent media changes and passaging as seen from phase contrast microscope pictures. A large and varied range of oxygen tension was observed in microfluidic cultures of these cells, moreover, from morphological data the cells seem to be healthy and growing well under these conditions. Experiments were performed at six perfusion velocities using Braille pumping to observe the effect of convection on oxygen consumption by the cells. The data also show that when cells are cultured in a microchannel with higher liquid height above the cells (300 μm compared to 200 μm), the downstream oxygen tension is lower across all flow conditions for a deeper microchannel. This might be due to a higher value of resistance to diffusion of oxygen from top of device to the cells at the bottom through the liquid column in a 300 μm microchannel compared to a 200 μm microchannel. Overall, when data from these experiments are compared with those from a similar device (discussed in Chapter 3), the lowest oxygen tension observed here for C2C12 cells (3.7%) is lower than for the culture of same cells in the previous device (4.3%), which may be due to combined effects of changes in device geometry, cell densities and perfusion velocities.

The oxygen tension axial profile in the 'single loop' microdevices (design demonstrated in Figure 5.2) with HepG2 cells are shown in Figure 5.4. Oxygen is measured at four distinct points along the length of microchannel seeded with cells: from upstream, to distance of 1 cm from upstream, to downstream and finally a distance of downstream+0.5 cm. These four oxygen tensions at the same overall device cell densities and velocities are helpful in the measurement of the gas transport through PDMS. The downstream oxygen tension in the single loop PDMS design varies from 19% to 2.4% for HepG2 cells for the cell density range of 9.8×10^7 to 1.67×10^9 cells/m^2 and velocity range of 0.09 to 31. 5 μ/sec with the cell region channel height of 100 μm.

HepG2 cells were cultures at very high densities in this microbioreactor to get an idea about the lowest oxygen tension possible in the gas permeable PDMS device. The cells were confluent inside the device at the high density (1.67×10^9 cells/m^2), and were arranged in a monolayer. The morphology of the microfluidically cultured cells suggested normal growth and nutrients were maintained by daily media change. The lowest oxygen tension observed in this system was 2.4%, which is still not low enough for the culture of certain primary cells, such as hematopoeitic stem cells, which need to be cultured below oxygen tension of 1-2% to maintain self-renewal for longer time *in vitro*. In order to further lower the downstream oxygen tension, different polymeric materials could be utilized to fabricate microbioreactors with low permeabilities to oxygen and water vapor, as discussed in Chapter 4.

The data indicated (Figure 5.4) that there is a considerable drop in the oxygen concentration as we move downstream of the cell region, which corresponded to the uptake of oxygen by cells, and this drop increases with increasing cell density. Media flow rate is also seen as an important parameter affecting oxygen tension, and increasing the flow increases the overall concentration of oxygen inside the channel as expected.

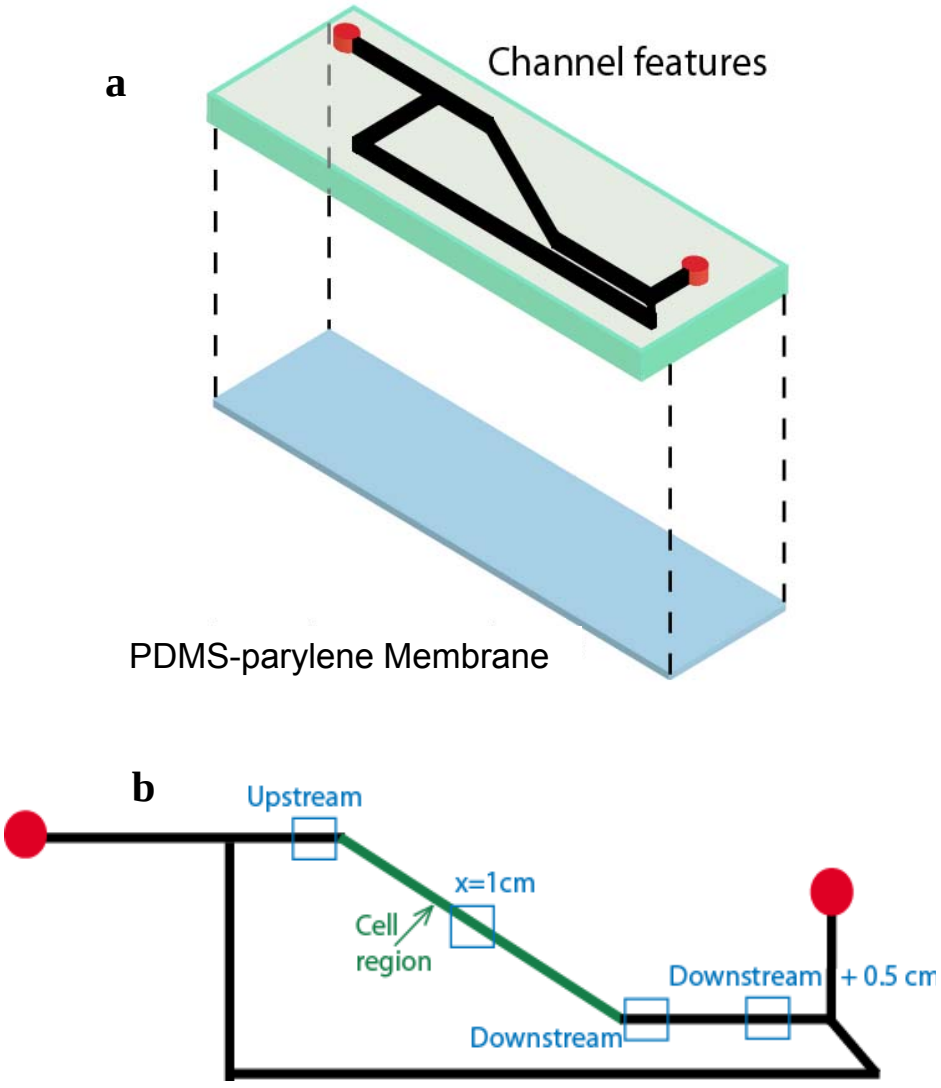

Figure 5.2: Schematic of PDMS device for measurement of axial oxygen tension profiles in a microfluidic culture of HepG2 cells.

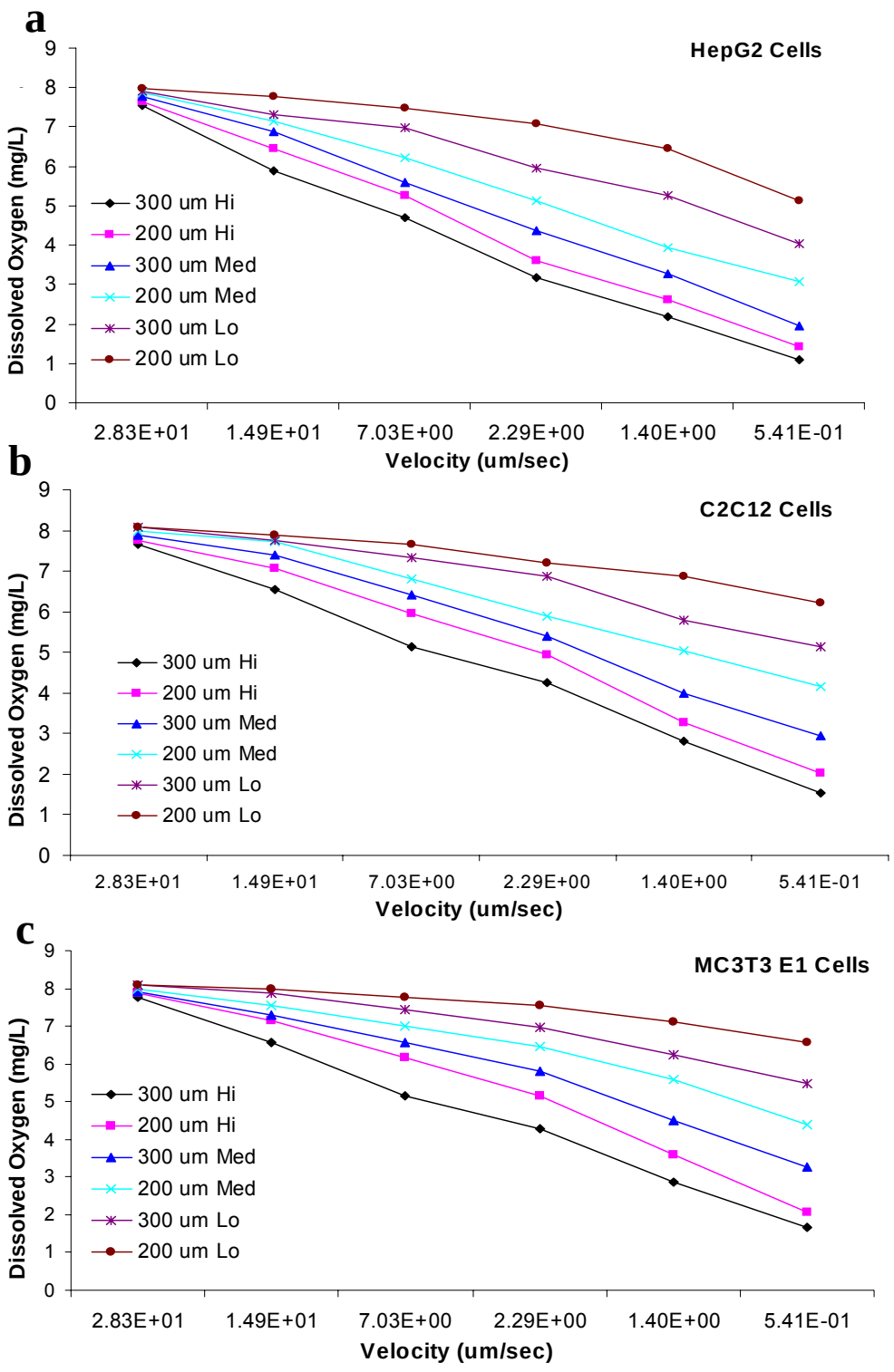

Figure 5.3: Downstream oxygen tensions for a) HepG2, b) C2C12, and c) MC3T3-E1 cells in double cross 'X' PDMS microdevice at three cell densities (high (Hi), medium (Med), low (Lo)) and two different channel heights (200 and 300μm).

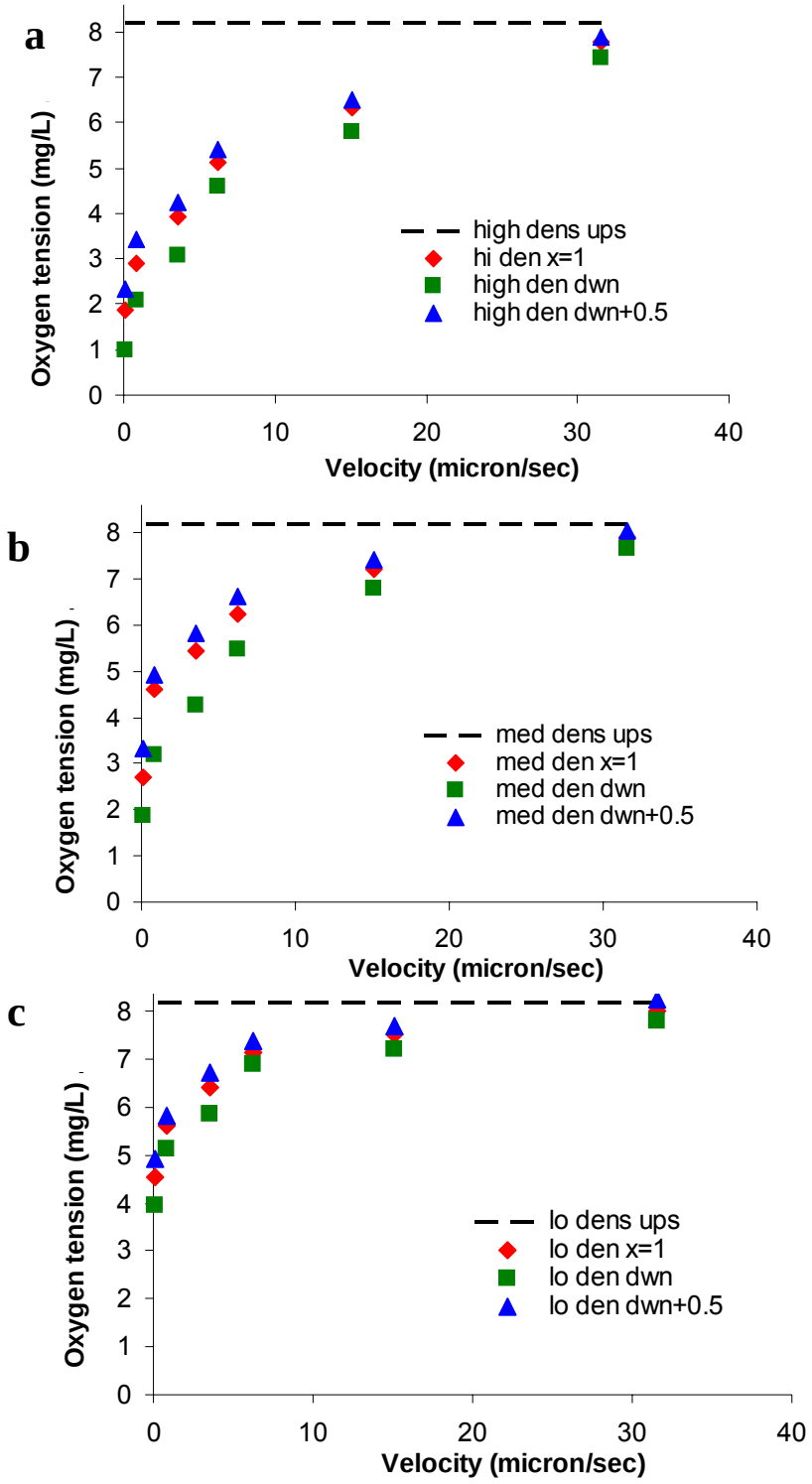

Figure 5.4: Oxygen Profile in PDMS microdevice at three different cell densities high (Hi), medium (Med), low (Lo)) of HepG2 cells at channel height of 100μm. The four points of oxygen detection in the microchannel are: upstream (ups), 1 cm from

upstream in cell laden channel (x=1), downstream (dwn), and distance of downstream + 0.5 cm (dwn+0.5).

The increase in oxygen tension at 'downstream +0.5' (where there are no cells) compared to downstream (see Figure 5.2 and 5.4) provided a direct evidence of oxygen diffusing through the PDMS microbiorector. Moreover, the diffusion of oxygen from air through the highly permeable PDMS devices, although significant, is not sufficient to avoid gradients inside the microchannel, and was demonstrated clearly by our experiments. From the experimental and modeling analysis, the overall mass transfer coefficient in the PDMS microbioreactor was found to be 1.3×10^{-8} m/s. Furthermore, the inference of cellular oxygen uptake rates and estimation of V_{max} and k_m from these experiments results was performed by Khamir Mehta and is described in detail in his thesis.

5.4 Conclusion

In this chapter we used the oxygen tension data in microfluidic culture of mammalian cells to infer OUR and to estimate cellular oxygen consumption coefficients V_{max} and K_m using a continuous partial differential mathematical model. The experimental part of the procedure and results were described in this chapter and the model estimated values of OUR, V_{max} and K_m can be found in Khamir Mehta's thesis.

References

Balis UJ, Behnia K, Dwarakanath B et al. Oxygen consumption characteristics of porcine hepatocytes. Metab Eng 1999; 1 (1):49-62.

Deshpande RR, Heinzle E. On-line oxygen uptake rate and culture viability measurement of animal cell culture using microplates with integrated oxygen sensors. Biotechnol Lett 2004; 26 (9):763-7.

Ducommun P, Ruffieux P, Furter M et al. A new method for on-line measurement of the volumetric oxygen uptake rate in membrane aerated animal cell cultures. J Biotechnol 2000; 78 (2):139-47.

Guarino RD, Dike LE, Haq TA et al. Method for determining oxygen consumption rates of static cultures from microplate measurements of pericellular dissolved oxygen concentration. Biotechnol Bioeng 2004; 86 (7):775-87.

Lai CS, Hopwood LE, Hyde JS et al. ESR studies of O2 uptake by Chinese hamster ovary cells during the cell cycle. Proc Natl Acad Sci U S A 1982; 79 (4):1166-70.

Mehta G, Mehta K, Sud D et al. Quantitative Measurements and Analysis of Cellular Oxygen Uptake in Microfluidic Poly(dimethylsiloxane) Bioreactors. *Biomedical Microdevices* 2007; 9 (2):123-34.

Mehta K, Linderman JJ. Model-based analysis and design of a microchannel reactor for tissue engineering. Biotechnol Bioeng 2006; 94 (3):596-609.

Ruffieux PA, von Stockar U, Marison IW. Measurement of volumetric (OUR) and determination of specific (qO2) oxygen uptake rates in animal cell cultures. J Biotechnol 1998; 63 (2):85-95.

Wagner KD, Geil D, Schimke I et al. Decreased susceptibility of contractile function to hypoxia/reoxygenation in chronic infarcted rat hearts. J Mol Cell Cardiol 1998; 30 (11):2341-53.

Worboys PD, Bradbury A, Houston JB. Kinetics of drug metabolism in rat liver slices. III. Relationship between metabolic clearance and slice uptake rate. Drug Metab Dispos 1997; 25 (4):460-7.

CHAPTER 6

POLYELECTROLYTE-CLAY-PROTEIN LAYER FILMS ON MICROFLUIDIC BIOREACTOR SURFACES FOR PRIMARY MURINE BONE MARROW CULTURE

6.1 Introduction

The *in vivo* cellular microenvironment is composed of an intricate blend of extracellular matrix proteins, soluble protein factors, immobilized protein factors, proteoglycans, small molecule signals, mineralized tissue, and numerous adjacent cell types, all of which may vary in space and time. These components present the cells with biochemical signals, and the cells are continually faced with sensing these inputs, processing the signals through signal transduction and gene regulation networks, and executing cell behavioral or fate choices (Jang et al. 2006; Shim et al. 2003). Two of the most important

microenvironment components are oxygen concentrations and the extracellular matrix (ECM). Recently, we demonstrated that oxygen concentrations can be regulated in microfluidic bioreactors made of poly(dimethylsiloxane) (PDMS) (Mehta et al. 2007). Here, we focus on modulating the surface chemistry of PDMS bioreactors to create advantageous adhesive microenvironments for the culture of bone marrow cells *in vitro*. Although the focus of this paper is mainly the enhancement of bone marrow cell attachment, similar ECM engineering strategies will also be useful for other cell types and for regulating more complex cellular responses such as intracellular signaling (Discher et al. 2005; McBeath et al. 2004) and adhesion-mediated increase in cellular secretions (McBeath et al. 2004; Stevens et al. 2005).

Many types of cells that attach well to surfaces such as tissue culture plastic do not attach well to an unmodified PDMS surface, even when the PDMS surface is coated with cell-adhesive proteins(Lee et al. 2004). For example, primary murine bone marrow stromal cells do not adhere well to PDMS surfaces even when coated with fibronectin or collagen (see section 6.2.5 for details). Various approaches have been used to modify PDMS surfaces for particular applications. Modification procedures include exposure to energy sources such as plasma, corona discharge, and ultraviolet light, formation of polyelectrolyte multilayers (PEMs), radiation induced graft polymerization, silanization, atom-transfer radical polymerization, chemical vapor deposition, cerium(IV) catalysis, phospholipid bilayer modification, and sol-gel modifications (Hu et al. 2003; Hu et al. 2002; Lahann et al. 2003; Wang et al. 2005a; Wang et al. 2005b). Most of these modifications do not provide long term stability, in part because hydrophobic groups in

silicones migrate up to the surface mediating hydrophobic recovery and loss of the effect of surface modification (Makamba et al. 2003). The long-term stability of biomedical devices made of PDMS is thus still questionable for applications where long-term cell attachment is required. Improved biofunctionalization methods for PDMS surfaces are needed to improve reliability.

A promising way to impart functionality to PDMS surfaces is by layer-by-layer (LBL) self assembly of polyelectrolytes and nanocomposites. LBL is a simple method that allows creation of nanoscale fuzzy assemblies or structures by alternate adsorption of macromolecular substances and most often polyanions and polycations on virtually any substrate to produce PEMs, and it has been used extensively for cell culture (Ai et al. 2003; Brynda et al. 2005; Decher et al. 1991; Haynie et al. 2005; Johansson et al. 2005; Kidambi et al. 2004; Ngankam et al. 2004; Tan et al. 2003; Thierry et al. 2003). However, most PEM coatings are known to deteriorate in performance with time (Dubas et al. 2001; Kharlampieva et al. 2003; Zhang et al. 2002). Many factors, such as the ionic strength, type of solvents, temperature, concentration of the solution, and pH of the solution (for weak polyelectrolytes) determine the multilayer structure, surface functionality, and PEM stability. Moreover, although there have been attempts to make the top surface of the PEMs biofunctional to mimic the cell-ECM interaction found in living systems and make the PEMs more versatile, more studies are needed to elucidate the interactions of the cells with the surfaces, which potentially can influence cellular processes and cell fates. Proteins are often adsorbed on PDMS to prime the surface for cell adherence; however, there are concerns that the quaternary structure of proteins,

which provides them their functionality, might not be optimal when adsorbed onto PDMS (Ratner et al. 1996). However, using only synthetic polyelectrolytes will likely not produce a biofunctional surface for cell attachment; thus, inclusion of biomolecules and inorganic compounds to avoid deterioration of the properties in the cell culture media is important. The ability of LBL assembly to produce stratified coatings (Mamedov et al. 2001; Mamedov et al. 2000) can be particularly useful in this case.

Recently, the Kotov group has shown that organic–inorganic layered composites made from montmorillonite clay platelets (clay) and poly(diallydimethylammonium) chloride (PDDA) simulate morphological and mechanical properties of nacre and other biocomposites(Tang et al. 2003) and has cultured various types of mammalian cells on different compositions of PDDA/clay PEMs or PDDA/nanoparticle PEMs, which have also been modified with proteins to create cytophilic surfaces (Lee et al. 2006; Podsiadlo et al. 2005; Sinani et al. 2003). Some groups have also created LBL coatings inside microfluidic devices for applications ranging from improvement of electrosmotic flows in PDMS microchannels (Barker et al. 2000a; Barker et al. 2000b; Barker et al. 2001) to assembling extracellular matrix (ECM) biopolymers (Tan & Desai 2003;Tan et al. 2004) and micropatterning in PDMS channels (Mohammed et al. 2004; Reyes et al. 2004; Shchukin et al. 2004). PDMS channels were also used for fast, dynamic sequential LBL deposition using PDDA/PAZO[poly(1-4-(3-carboxy-4-hydroxypheylazo)benzenesulfoamido)-1,2-ethandiyil, sodium salt)] for intended application of shear induced alignment of rod-like conjugated polymers (Kim et al. 2005).

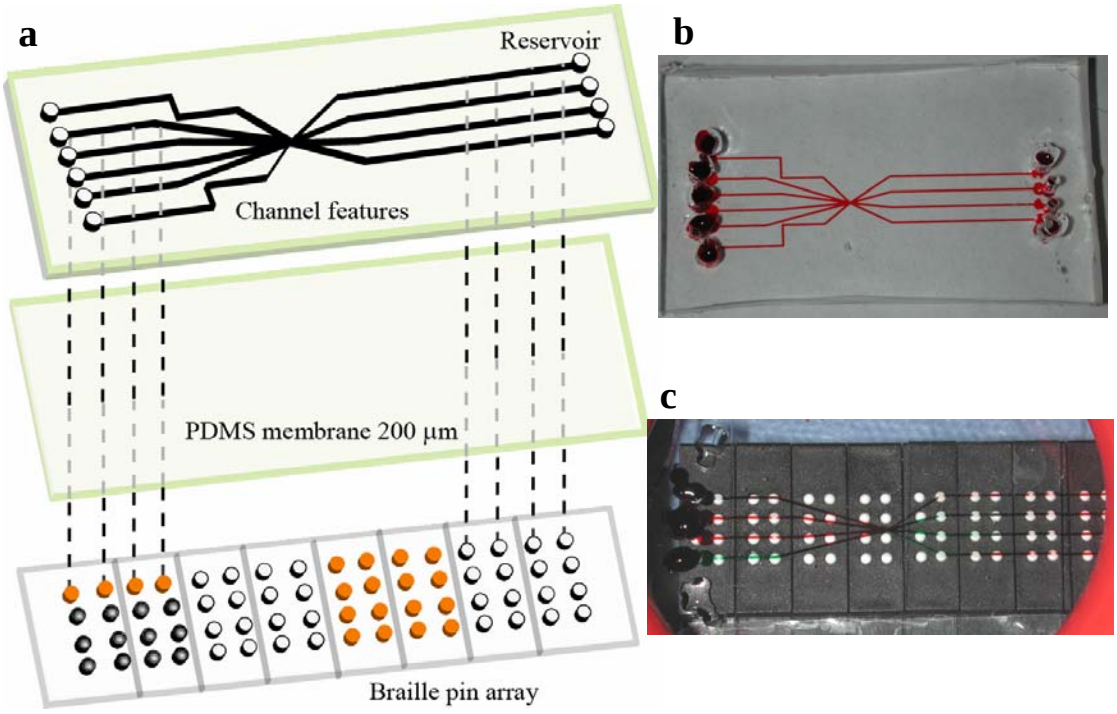

Figure 6.1: Microfluidic bioreactor chip design and set up. a) The bioreactor chip is composed of two components. The top component of the microfluidic device contains channel features and has punched holes (black circles) acting as reservoirs. The bottom component of the microbioreactor chip is a 200 µm thick spincoated PDMS membrane. A "horizontal" pump (four orange pins) drives cell culture media from left to right, all other channels are valved closed (gray pins are raised to close channels by deformation), and rest of the pins are in valve open position and allow fluid to pass (white pins are down), **b)** an actual device filled with red food dye, **c)** bioreactor chip aligned on Braille pins to facilitate pumping and valving.

In this chapter, we use Braille display-actuated microfluidic devices to automatically create multiple types of LBL films within a single run on a single bioreactor chip to screen for ideal surfaces onto which primary bone marrow stromal cells can be cultured. The LBL films tested included PDDA/Clay layers to impart chemical and mechanical stability and the two major adhesive protein components of the ECM basement membrane of the bone marrow, fibronectin (FN) and collagen (Co), to impart biofunctionality and cell adhesiveness. The coatings were tested for the ability to support

primary murine bone marrow cell adhesion, viability, and proliferation over a 15 day period. We embarked on this project because the traditional method of preparing PDMS surfaces for cell culture, i.e. adsorption of an ECM protein on the substrate, did not allow for long term culture of primary stromal cells (results and Figure J7).

6.2 Experimental Materials and Methods

6.2.1 Cell Culture

Unsorted primary bone marrow cells (hence forward called bone marrow stromal cells) from femurs and tibias of C57BL/6 mice were cultured in MyeloCult (M5300, StemCell Tech.) supplemented with 1% v/v hydrocortisone (07904, StemCell Tech.) and 1% v/v antibiotic–antimycotic (15240, Gibco). The 25 cm^2 T flasks (3815, Corning) were placed in a humidified 5% CO2 cell culture incubator at 33 ^oC. Cells were allowed to grow for two weeks in the plastic dishes in 8 ml of media before plating on PDMS substrates. Half of the media in T flasks was replaced every week.

After 2 weeks, cells were collected by washing in Hank's Balanced Salt Solution (37250, StemCell Tech) and incubated with 0.25% Trypsin/EDTA (07901, StemCell Tech). The trypsin solution was neutralized with 25% serum in MyeloCult and spun down for 5 minutes at 4 ^oC and 1000 rpm. The supernatant was removed and the pellet was resuspended in 200 μl of MyeloCult media, and this suspension was used for seeding cells onto the PDMS substrates. The cell suspension was seeded in the outlet of the channels from which it was directed into specific areas of the device.

6.2.2 Preparation of the microfluidic bioreactor chip

The chip consisted of two components: a channel top layer and membrane bottom layer, as seen in Figure 6.1A. The chips were formed from pre-polymer (Sylgard 184, Dow Corning) at a ratio of 10:1 base to curing agent. The top layer was formed using a glass wafer mold (soft lithography) (Duffy et al. 1998) to form a layer with negative relief channel features ~30 μm in height and 300 μm in width. The positive relief features of the mold were composed of SU-8 (Microchem, Newton, MA) formed on a thin glass slide (200 μm thick) using backside diffused-light photolithography (Futai et al. 2004). The glass slide was silanized with tridecafluoro-(1,1,2,2-tetrahydrooctyl)-1-trichlorosilane (United Chemical Technologies Inc., Bristol, PA). This channel layer was cured overnight at 120 ^{o}C and holes were punched (Dermal biopsy puncher, Miltex Inc., York, PA) in the channel layer to connect channel features to the bottom layer. The bottom layer was a thin membrane of PDMS (200 μm) prepared by spin coating (Cee 100 Spin Coater, Brewer Science Inc., Rolla, MO) and curing PDMS in an oven at 120 ^{o}C overnight. The PDMS pieces were bonded by plasma oxidation (Futai et al. 2006; Gu et al. 2004; Mehta et al. 2007).

6.2.3 LBL Nanocomposite Fabrication

For the coating process, the surface of cured PDMS was made reactive by placing it in oxygen plasma for 60 s at 300 mTorr. The peristaltic pumping sequences of Braille pins deposited alternate layers of 0.5 wt % poly(diallyldimethylammonium chloride) (PDDA)(+) (Mw = 200,000, Sigma, MO) and montmorillonite clay (-) (Aldrich, MO) onto the PDMS surface of the microfluidic bioreactor chip. Between each polyelectrolyte

deposition sequence, the channels were thoroughly washed with deionized water. Four to eight bilayers of PDDA/clay were deposited. To test the charge on the top exposed surface, fluorescently labeled charged dyes were used. Sulforhodamine (Sigma, MO) detected the negative charge, and 6-Carboxyfluorescein (Sigma-Aldrich, MO) detected the positive charge on the surfaces.

LBL deposition was continued by the assembly of bilayers of proteins onto the base PDDA/Clay coating. Collagen type IV (lyophilized from human placenta, Sigma, MO), positively charged at pH = 4(Sinani et al. 2003), and fibronectin (human plasma, Sigma, MO) negatively charged at pH = 7 were deposited on the PDDA/Clay bilayers. One to seven bilayers of the biomolecules were deposited on the top of PDDA/Clay bilayers. After the LBL coatings were assembled, the bioreactor chip reservoirs were rinsed multiple times with DI water, and finally sterile PBS was added to all reservoirs and the device was stored in a sealed Petri dish at 4 ^{o}C until further use. When the devices were ready for cell culture testing, they were first sterilized under UV light in a bio-safety cabinet for 30 minutes. The PBS in the reservoirs was replaced by MyeloCult, and cells were seeded from the outlet channels.

Our notation for PEM composition is as follows: $(PDDA/Clay)_5$ refers to deposition of five bilayers of PDDA and clay, and the top (exposed) surface is clay. $(PDDA/Clay)_{5.5}$ means that 5.5 bilayers of PDDA and clay were deposited, and thus the top (exposed) surface is PDDA. $(PDDA/Clay)_{5,6,7,8}$ means that a device was fabricated with composition of $(PDDA/Clay)_5$ in first outlet channel, $(PDDA/Clay)_6$ in second outlet

channel, $(PDDA/Clay)_7$ in third outlet channel, and $(PDDA/Clay)_8$ in fourth outlet channel. Likewise, Co/FN refers to a PEM built with one layer of positively charged collagen overlaid with one layer of negatively charged fibronectin. It is not a mixture of two proteins.

6.2.4 LBL Deposition on Flat PDMS Substrates

PEMs were deposited on flat PDMS substrates using LBL technique (Decher & Hong 1991; Tang et al. 2003). Six beakers were arranged in series, and PDDA was added to the first and clay to the fourth, the rest contained DI water. Two ml of PDMS was dropped in 35 mm Petri dishes and cured in a 60 C oven for two hours. After plasma oxidation, these Petri dishes were dip coated in the beakers described above to create PEMs of different compositions. The following PEM composition were created on flat PDMS substrates: $(PDDA/Clay)_5$, $(PDDA/Clay)_{5.5}$, $(PDDA/Clay)_7$, $(PDDA/Clay)_5$ $(Co/FN)_3$.

In addition, the following surfaces were also created on flat PDMS substrates: fibronectin adsorbed on a flat PDMS substrate, collagen Type IV adsorbed on flat PDMS substrate, fibronectin and collagen Type IV (1:1) adsorbed on flat PDMS substrate. A control of fibronectin adsorption was also prepared in PDMS microdevice.

6.2.5 Device Cell Seeding

After sterilization, PBS was replaced with Myelocult media in the reservoir, and the bioreactor chip was placed on an array of pin actuators adapted from Braille displays for at least one hour to peristaltically pump fluid through the channels(Futai et al. 2006).

Bone marrow stromal cells were then seeded into the chip from the outlet channels. The cells were manipulated to attach only in the area of the bioreactor chip where nanocomposite coatings were earlier formed by using a software program to block out other parts of the device. The cells were given 1-2 hours to attach under static (pins up and channels valved closed) condition in a humidified incubator (Forma 310 Series Direct Heat CO_2 Incubator, Thermo electron Corporation**,** Marietta, OH) maintained at 33 ^{o}C and 5% CO_2.

The bioreactor chips were then taken off the pumping hardware and stored in Petri dishes inside the incubator. The Petri dishes were further stored in a larger container with DI water to prevent evaporation. The cells were grown on the nanocomposite coatings for up to 15 days, with media changes every other day. The media was changed every day by simple aspiration from the inlet and outlet reservoirs. Pictures of the cells growing in different nanocomposite coatings were taken every day. Cell densities, cell spreading, cell proliferation and cell viability were recorded over 15 days.

6.2.6 Fluid Actuation

An array of 64 pin actuators adapted from a Braille display module (SC9, KGS, Saitama, Japan) was used for fluid actuation (Futai et al. 2006). The pin actuator module was controlled with a computer via Universal Serial Bus (USB) through a finger-sized stand alone custom controller circuit board (Olimex, Plovdiv, Bulgaria). The microfluidic bioreactor chip interfaced with the pin actuator module by simply holding the chip in place by using some weights such that the channels align with the pins which push

upward closing the channel, as seen in Figure 6.2. The pin movements for valving and pumping were controlled with a custom computer program written in C # (Mehta et al. 2007). The average flow rate was controlled by changing the time delay between pin motions. The flow rate was kept constant at $(8.3 \pm 2.3) \times 10^{-2}$ μL/sec for all experiments.

6.2.7 Cellular Assays for Cell Spreading, Cell Density, Cell Proliferation, and Live-Dead Assay

The microbioreactor chip was mounted on a glass slide and examined on an inverted phase contrast microscope (Nikon TE-300) with a 20X dry objective. Black and white images were captured with a CCD camera (Hamamatsu ORCA-100). Simple PCI software (Compix Inc; Cranberry Township, PA, ww.cimaging.com) was used for capturing and analyzing the images and calculating cell surface area, cell densities and cell viability. For cell viability, LIVE/DEAD Viability/Cytotoxicity Kit (Invitrogen, Carlsbad, CA) containing Calcein AM and ethidium bromide was used to quantify percentage of cells alive at day 15 of bone marrow stromal cell culture. The controls for these experiments were microbioreactor chips without any surface modifications, and the variables were chips with varying nanocomposite coatings. Cell proliferation was measured as increase in cell density at day 15 compared to day 1. Cell viability was measured as percentage of cells alive at day 15. For all the cellular assays, experiments were performed in triplicates, and fifteen images were analyzed to obtain one data point. The data were analyzed statistically by ANOVA and Tukey's test at a 95 percent confidence level assuming unequal variances. There were 14 different types of PEMs created and tested in microdevices plus 4 different types PEMS created and tested on flat

PDMS slabs. Each PEM substrate was analyzed through micrographs of ten different regions to give ten different data points each for cell viability and cell density. These ten data points were collected every day for fifteen days to give a total of fifteen data sets for each PEM tested. In addition, all experiments were performed in triplicates. ANOVA was performed to find differences between the 14 different PEMs created inside microchannels as well as between the 4 PEMs created on flat PDMS and Tukey's test was performed to find differences between specific PEMs within each set of surfaces.

6.3 Results and Discussion

We grew custom LBL nanocomposite coatings in microfluidic bioreactor chips using combinations of different building blocks. Figure 6.1 shows the design and set up of the microfluidic bioreactor chip and its alignment with the pin actuator module. The Braille peristaltic pumps and valves were used to direct flow in specific channels at different times to make LBL coatings with varying composition in four outlet channels as shown in Figures 6.2A, 6.2B and 6.2C.

6.3.1 Layered nanocomposite coatings were produced inside PDMS microfluidic bioreactor chips

The surface of cured PDMS was made reactive by exposure to oxygen plasma, which created a negative charge on the surface. The bioreactor chips with oxidized PDMS channels were aligned on the Braille pumps and the channel inlets were filled with PDDA, clay or DI water. PDDA and clay are both strong polyelectrolytes; therefore their ionic strength changes little within the pH ranges of interest. The negatively charged

PDMS surface was exposed to a PDDA stream for 10-15 minutes (Figure 6.2 A shows the process of PDDA adsorption). Subsequently, loosely attached PDDA was removed by pumping DI water to rinse the channels for 15 minutes. In the third step, the clay inlet was valved open and pumped for 10-15 minutes. Finally, clay inlet was valved off and the channels were again washed by flow of DI water. This process created one PDDA/Clay bilayers inside the microfluidic bioreactor chip, and was repeated to get the desired number of bilayers in different outlet channels. Taking advantage of the computerized microfluidic system, all four channels could be patterned at once, or alternatively, the composition of the LBL in each channel could be varied by regulating the valving and pumping sequences that determine reagent flows. Figure 6.2 B shows delivery of clay stream to only second outlet channel, while Figure 6.2 C shows the bioreactor chip with four different nanocomposite coatings in the same chip.

In order to create a stratified LBL structure with proteins on top of the PDDA/Clay bilayers, inlet reservoirs of PDDA and clay were rinsed with water and protein solutions containing fibronectin or type IV collagen were introduced. Processing procedures similar to the formation of PDDA/clay multilayers were used to get microchannels with varying number of protein patterns in the outlet regions of the bioreactor chip. It should be noted that the proteins collagen and fibronectin were added as separate layers in sequential steps and not as a mixture.

LBL assembly inside microfluidic devices has been established earlier by multiple groups using laminar flow, as discussed in the introduction (Barker et al. 2001; Reyes et al.

2004; Shchukin et al. 2004; Tan & Desai 2003). In the current study, however, with the use of Braille peristaltic actuation, it was important to not have two streams mixing with each other. When the two polyelectrolyte streams mix together due to backflow, solid debris is formed (see Appendix J, Figure J1). The backflow problem was countered by adding a small step in the software program, i.e. after a particular polyelectrolyte stream had completed its run, the water wash streams began flowing, and the polyelectrolyte stream was pumped back in the opposite direction to its reservoir for 1 - 1.5 minutes. This back-pumping ensured that no polyelectrolyte was left in the mixing region (Figure J2).

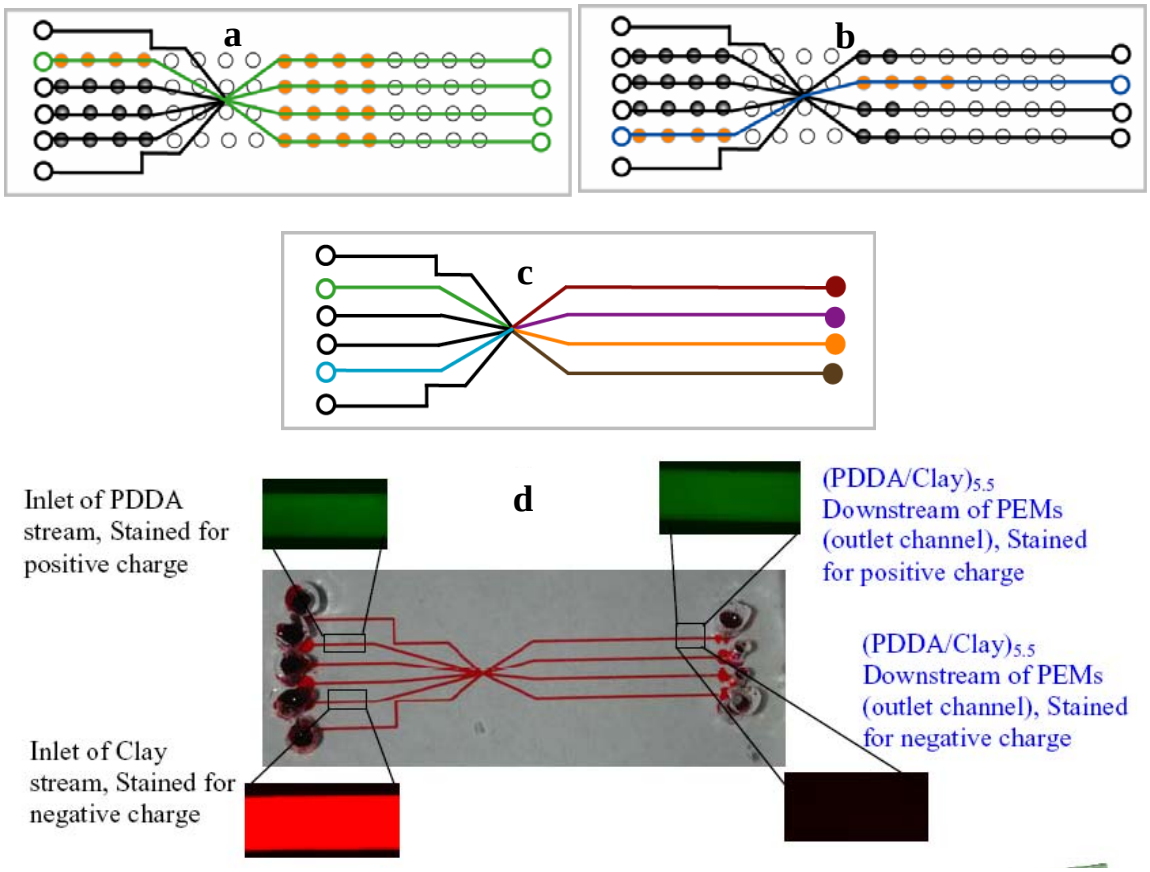

Figure 6.2: The creation of layered nanocomposite coatings. **a)** Step 1 of the process: PDDA flow and adsorption. The green channels have PDDA flowing from left to right. The black channels are valved off to avoid mingling of different streams, **b)** delivery of clay stream to only the second outlet channel. The orange Braille pins are acting as a

pump, white are in 'valve off' position and grey are 'valve on' position. **c)** Schematic representation of the completed multifunctional device with different nanocomposite coatings in the four outlet channels (four different colors in outlet channels represent different composition of coating). Cell seeding is through the outlet channels. **d)** Fluorescent micrographs of inlet and outlet regions of PDMS bioreactor (all taken with a 10X dry objective, NA=0.25). The top nanocomposite coating layer is positively charged, as shown by pictures on the right, which show a green fluorescence for negative charge but no red fluorescence for positive charge.

The resulting coatings were stable, hydrophilic, biofunctional and customizable (Figures 6.2C and 6.2D). For example, it was possible to create a device with $(PDDA/Clay)_7$ in all 4 outlet channels, $(PDDA/Clay)_3$ $(Co/FN)_4$ in all 4 outlet channels, or $(PDDA/Clay)_3$ in 1^{st} outlet channel, $(PDDA/Clay)_3$ $(Co/FN)_1$ in 2^{nd} outlet channel, $(PDDA/Clay)_3$ $(Co/FN)_2$ in 3^{rd} outlet channel, $(PDDA/Clay)_3$ $(Co/FN)_3$ in 4^{th} outlet channel. Therefore, in a multifunctional device, four different compositions of PEMs were simultaneously deposited inside one single device.

6.3.2 Microfluidic-made nanocomposite multilayers are homogenous

Fluorescent images of staining by positively and negatively charged dyes were used to verify the charges on the topmost exposed layer, stability of the layers and homogeneity of the coatings. The inlet PDDA stream is positively charged, as shown by green fluorescence of negatively charged 6-carboxyflourescein, whereas, the inlet clay stream is negatively charged as shown by the red fluorescence picture on the bottom left panel stained by the positively-charged sulphorhodamine (Figure 6.2D left inlay images). The right-side inlay images in Figure 6.2D shows green carboxyfluorescein staining of the outlet regions where a nanocomposite coatings of $(PDDA/Clay)_{5.5}$ with PDDA on the outermost layer have been formed confirming the existence of a positive charged surface.

When the same outlet is stained for negative charge, no fluorescence was observed. This study illustrates that the outlet stream has one charge on its exposed surface, and that the nanocomposite coating formed is uniform.

Figure J5 shows the fluorescence intensity of charged dyes after deposition of each layer. The fluorescence intensity is very weak in the earlier layers, and increases with layer number. At five bilayers, the intensity is very uniform, and well distributed. No change in intensity or intensity distribution was seen between five and seven layers. Thus, we conclude that five bilayers are sufficient to cover the entire area of the surface under investigation and create a homogenous surface.

The topographical similarity of the PEMs deposited ($(PDDA/Clay)_8$) on flat PDMS substrate and microfluidic PDMS device is shown in AFM images (Figure J6). The PEMs in microfluidic bioreactors were very similar to the ones deposited on flat PDMS in terms of morphology, topology and surface roughness. Thus both surfaces are structurally and morphologically similar. These surface characteristics also match well with previously reported multilayers formed from these components (Lee et al. 2006; Podsiadlo et al. 2005; Tang et al. 2003).

6.3.3 Multifunctional LBL Nanocomposite Coating

To demonstrate the efficient creation of LBL coatings with the capacity to support cells, we created four very different LBL coatings in one single bioreactor chip and compared their ability to support cell attachment and proliferation. These four layers were:

oxidized PDMS substrate without any LBL coating, a PDDA-topped LBL coating ($(PDDA/Clay)_{3.5}$), a clay-topped LBL coating ($(PDDA/Clay)_4$), and a protein-topped LBL coating ($(PDDA/Clay)_4$ $(Co/FN)_5$).

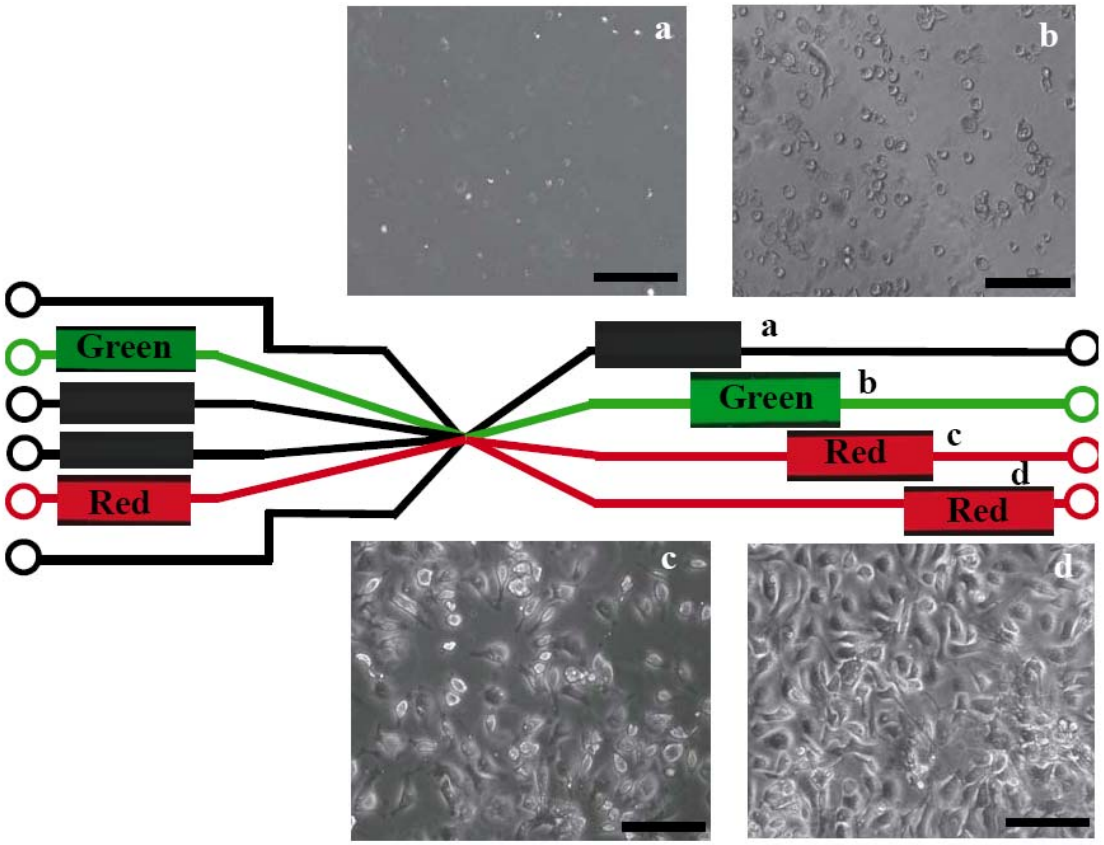

Figure 6.3: PDMS microbioreactor chip with multifunctional nanocomposite coatings. Four channels with compositions: (a) no coating, (b) $(PDDA/Clay)_{3.5}$ (PDDA topped), (c) $(PDDA/Clay)_4$ coating (clay topped), and (d) $(PDDA/Clay)_4$ $(Co/FN)_5$ were made by our process.

The fluorescent micrographs of inlet and outlet regions (all with a 10X objective, gain=2, exposure time=0.10 sec) are shown placed on specific points in the schematic of the microbioreactor chip to showcase different surface functionalities. For each region (inlet or outlet), the pictures are stained to fluoresce for positive charge (PDDA, Co) shown by green color and for negative charge (Clay, FN) shown by red color. The PDDA inlet

stream has a green fluorescent micrograph and the DI water inlet streams have no green or red fluorescence. The clay stream inlet stream has a red fluorescent micrograph. In addition, phase contrast images (20X dry objective, all scale bars= 50 μm) compare cell cultures at day 15 of culture on the four different surfaces inside the same microbioreactor chip. For composition notation, please see Experimental Materials and Methods.

Figures 6.3 shows the results from the microbioreactor chip with multifunctional LBL nanocomposite coatings. The fluorescent micrographs of the inlet and outlet regions are laid on a schematic of the bioreactor chip and show top surface charge and functionality. For each region (inlet or outlet), the pictures are stained to fluoresce green for positive charge (PDDA, Co), or red for negative charge (Clay, FN). As seen in Figure 6.2D, the fluorescent pictures for the outlet regions in Figure 6.3 also show homogenous coatings of a specific charge depending on the nanocomposite coating fabrication steps. Even in the case of protein coating, the fluorescence signal (Figure 6.3D outlet channels patterned with proteins) is strong and not mixed with the other dye, consistent with the presence of a homogenous coating.

Figure 6.3 also shows a comparison of cell spreading and attachment at day 15 of culture on the four different multifunctional nanocoated surfaces inside the same microbioreactor observed using a 20X dry objective (NA=0.45, plan fluor). The cells are clearly most spread out and covering the entire surface in the last outlet channel (Figure 6.3D), which had a nanocomposite coating of the composition $(PDDA/Clay)_4$ $(Co/FN)_5$. Cell

adherence and spreading were reasonable in the third outlet channel (Figure 6.3C) but poor on the other two surfaces. Thus by fabricating a single chip with different multifunctional nanocomposite coatings, we have compared primary bone marrow culture on four surfaces and seen distinct cellular responses. To confirm these results independently in more depth and to look at a wider range of surfaces, we performed additional experiments using multiple chips as described in the next two sections.

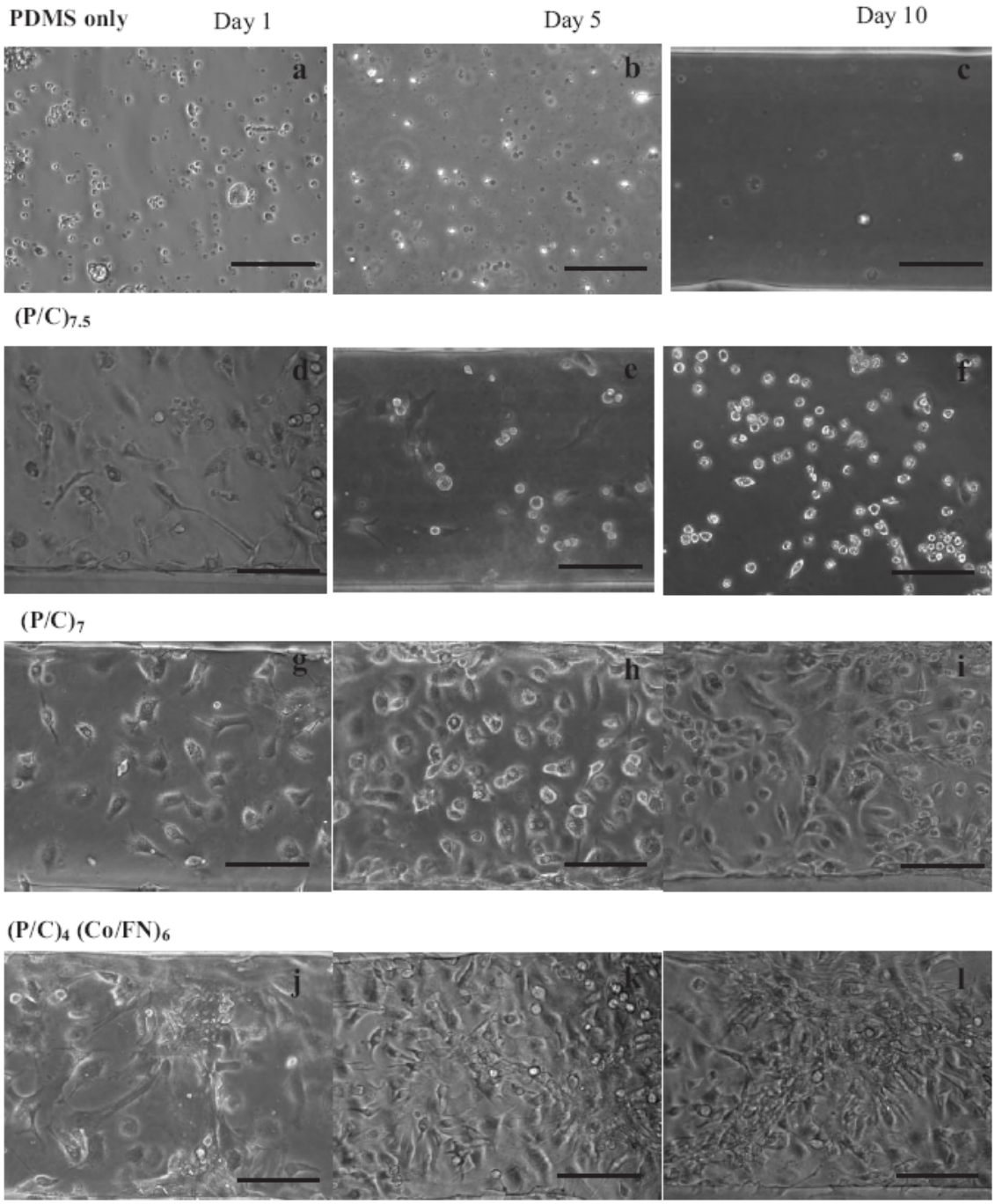

Figure 6.4: Spreading and attachment of bone marrow stromal cells on different nanocomposite coatings over 1 to 10 days (all scale bars= 50 μm). Bone marrow stromal cells from femurs and tibias of C57BL/6 mice were cultured on different surfaces. Micrographs depict the outlet regions of a microfluidic PDMS bioreactor chip where nanocomposite coatings were deposited and bone marrow stromal cells from femurs and tibias of C57BL/6 mice were seeded. The pictures are from representative samples at day 1 (left column), day 5 (middle column), and day 10 (right column). The cells do not attach on an oxidized PDMS surface on any day (a, b, and c). The cells attach first (day 1 and 5) and then lift off from a substrate with PDDA layer exposed to cells (d,

e, f, $(PDDA/Clay)_{7.5}$, PDDA on top). The cells attach well on clay topped surfaces (g, h, i, $(PDDA/Clay)_7$, Clay on top). The cells attach, spread and proliferate best on a nanocomposite coating with proteins and larger number of (PDDA/Clay)(Co/FN) bilayers (k, l, and m, $(PDDA/Clay)_4$ $(Co/FN)_6$).

6.3.4 Number of bilayers and exposed polyelectrolyte affect primary bone marrow cells culture on PEMs inside PDMS bioreactors chips

We screened a total of 30 nanocomposite coatings (different numbers of layers and combinations of components, all listed in Appendix J) of which we present data for 14 in this and the next sections (and Figures 6.4 and 6.5). The 14 different nanocomposite coatings were deposited either without protein coating (this section) or with additional protein coating (next section) and tested for bone marrow stromal cell attachment. The surfaces on which we tested cell culture were either positively or negatively charged; had no proteins or had proteins adsorbed on them; and were composed of 3 to 12 bilayers. The following are the compositions of the 14 PEMs on which whole bone marrow cell culture was tested: $(PDDA/Clay)_{7.5}$, $(PDDA/Clay)_7$, $(PDDA/Clay)_3$ $(Co/FN)_{0,1,2,3}$, $(PDDA/Clay)_4$ $(Co/FN)_{0,2,4,6}$, $(PDDA/Clay)_5$ $(Co/FN)_{0,2,4,7}$. We tested three device samples per variable, and cultured cells in these devices for more than 15 days.

We first examined the effect of increasing the number of PDDA/Clay bilayers using 4 of the 14 different nanocomposite coatings. Figure 6.4 shows bone marrow stromal cells growing on different PEMs inside microchannels at day 1, 5 and 10, and quantitative measures of spreading, proliferation, and viability are given in Figure 6.5. The cells do not attach on an oxidized PDMS surface (Figure 6.4 A, B, and C). Similarly, cells did not remain attached on PDMS surfaces with 3-4 bilayers of PDDA and clay (image data not

shown). Among surfaces that do support some degree of cell attachment, cell spreading was lowest (520 μm^2/cell on day 15, condition A in Figure 6.5 A) when cells were cultured on a $(PDDA/Clay)_3$ nanocomposite multilayer, and increased for cells on $(PDDA/Clay)_4$ (816 μm^2/cell on day 15, condition B in Figure 6.5A) and for cells on $(PDDA/Clay)_5$ (1035 μm^2/cell on day 15; condition C in Figure 6.5A). On further increasing the number of bilayers to $(PDDA/Clay)_7$, cell spreading did not change significantly (1021 μm^2/cell on day 15, condition E in Figure 6.5A). This may be an indication that at least 5 bilayers are needed to get a homogenous nanocomposite coverage, as has been illustrated previously for some LBL pairs although not in microfluidic devices (Mendelsohn et al. 2003).

There is some evidence in the literature that cells need a positively charged surface to attach well, since all vertebrate cells possess unevenly distributed negative surface charges (Freshney 1994). However, bone marrow stromal cells did not attach well to the positively charged PDDA-topped surface, initially attaching but later shrinking in size, detaching, and dying (Figure 6.4 D, E, F, $(PDDA/Clay)_{7.5}$, PDDA on top, condition D in Figure 6.5). $(PDDA/Clay)_{7.5}$ was worse for cell attachment because PDDA is exposed to cells, and PDDA has been proven to be unfavorable for primary cell attachment (Fischer et al. 2003; Kidambi et al. 2004; Mohammed et al. 2004). Therefore, even though this surface had 7.5 bilayers, the chemistry of the top exposed surface affects the cell behavior, and when polymers which are cytophobic are exposed to cells, the cells will not attach and spread for long periods of time. Other primary cells also do not attach to PDDA surfaces (Fischer et al. 2003; Kidambi et al. 2004; Mohammed et al. 2004).

In contrast, the same bone marrow stromal cells adhered to a negatively charged clay-topped surface (Figure 6.4 G, H, I, $(PDDA/Clay)_7$, Clay on top), spreading (1021 μm^2/cell on day 15, condition E in Figure 6.5A) and remaining viable (79.5% cells alive on day 15, Figure 6.5C). This might be due to the higher surface area, higher roughness, and/or composition (SiO_2, $AlO_4(OH)_4$, Na+) of the clay. This montmorillonite clay is composed of materials that the cells contact in their natural environment, and thus should be biocompatible.

As evidenced from Figure J7 as well as results from cell viability and cell density assays (data not shown), there are no apparent differences between bone marrow stromal cell responses to PEMs created on flat PDMS substrates or PEMs deposited in microfluidic devices (see Figure 6.5). However, the physiological ratio of cells to fluids found in microfluidic devices is expected to create a more physiological microenvironment, compared to conventional cells culture. Such differences will be advantageous for enhanced autocrine and paracrine effects, for example, and are expected to affect cell function (Mehta et al. 2007; Shim et al. 2003; Walker et al. 2004).

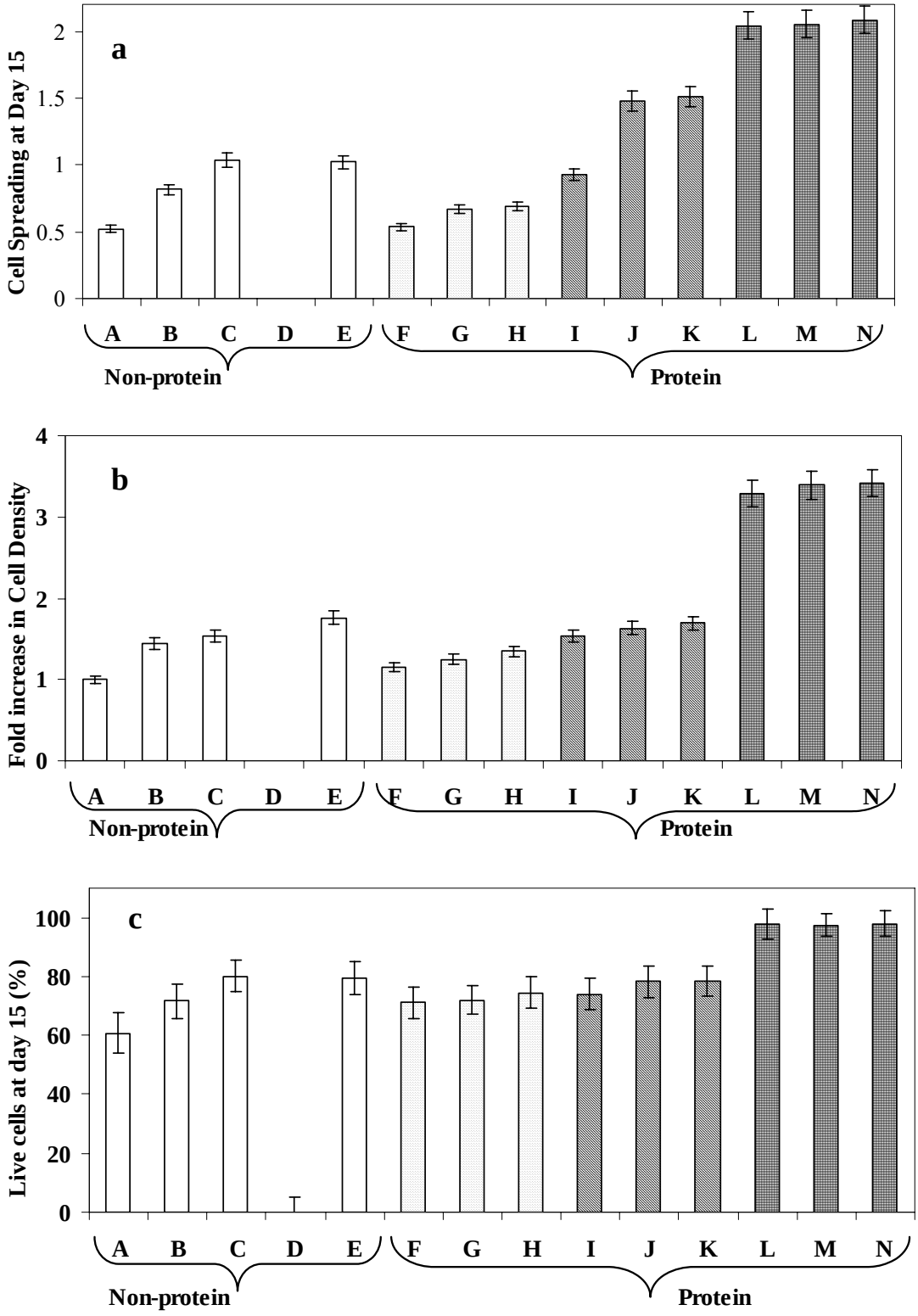

Figure 6.5: Cell spreading, proliferation and viability on 14 different nanocomposite coatings. a) cell spreading at day 15 (x 10^3 μm^2), b) fold increase in cell density at day 15 (x 10^9 cells/m^2), c) cell viability at day 15 (%). Legend: A=$(PDDA/Clay)_3$

$(Co/FN)_0$, B=$(PDDA/Clay)_4$ $(Co/FN)_0$, C=$(PDDA/Clay)_5$ $(Co/FN)_0$, D=$(PDDA/Clay)_{7.5}$ $(Co/FN)_0$, E=$(PDDA/Clay)_7$ $(Co/FN)_0$, F=$(PDDA/Clay)_3$ $(Co/FN)_1$, G=$(PDDA/Clay)_3$ $(Co/FN)_2$, H=$(PDDA/Clay)_3$ $(Co/FN)_3$, I=$(PDDA/Clay)_4$ $(Co/FN)_2$, J=$(PDDA/Clay)_4$ $(Co/FN)_4$, K=$(PDDA/Clay)_4$ $(Co/FN)_6$, L=$(PDDA/Clay)_5$ $(Co/FN)_2$, M=$(PDDA/Clay)_5$ $(Co/FN)_4$, N=$(PDDA/Clay)_5$ $(Co/FN)_7$. Surfaces topped with PDDA are not cytophilic for primary murine bone marrow cells.

3.5 Protein-topped nanocomposite coatings are better at supporting bone marrow stromal cells

The following 10 protein-topped LBL films deposited in microfluidic bioreactors were also tested for their ability to support bone marrow stromal cells: $(PDDA/Clay)_3$ $(Co/FN)_{1,2,3}$, $(PDDA/Clay)_4$ $(Co/FN)_{2,4,6}$, and $(PDDA/Clay)_5$ $(Co/FN)_{0,2,4,7}$. Figure 6.4 K, L, and M show the bone marrow stromal cells growing on PEMs with protein coating ($(PDDA/Clay)_4$ $(Co/FN)_6$) at day 1, 5 and 10. As compared to cells on $(PDDA/Clay)_{7.5}$ or $(PDDA/Clay)_7$ surfaces, the cells appear more spread.

On adding 2, 5 or 7 bilayers of Co/FN to $(PDDA/Clay)_5$, the cell spreading on day 15 increased from 1035 (no Co/FN) to 2039, 2053, and 2085 μm^2/cell respectively (Figure 6.5A, condition C, L, M, N). The cell density increased from 2.35 x 10^9 cells/m^2 (no Co/FN) to 2.61 x 10^9 cells/m^2 (Figure 6.5B, condition C, L, M, N), and the percentage of live cells increased from 80% (no Co/FN) to 98% (Figure 6.5C, condition C, L, M, N), when two to seven bilayers of Co/FN were added to five bilayers of PDDA/Clay. Differences between 2, 5, and 7 bilayers of Co/FN were not statistically significant, suggesting that two layers of Co/Fn were sufficient to coat the PDDA/Clay surface completely and provide sufficient adhesive ligands on the exposed surface. There may be a synergistic contribution of having both (PDDA/Clay) and (Co/FN) layers, as the stiff mechanical properties of (PDDA/Clay) ($E_{(P/C)1}$= 0.11 GPa (Tang et al. 2003)) compared

to the relatively soft PDMS (E_{PDMS}=2 MPa(Lee et al. 2004)) are also known to be beneficial for cellular adhesion (Lee et al. 2006; Sinani et al. 2003).

For comparison with PEMs that have PDDA/Clay coatings, bone marrow stromal cells were also cultured on flat PDMS substrates on which either Co, or FN or a 1:1 mixture of Co and FN was adsorbed for 30 minutes. On these surfaces, the stromal cells detached after only a few days of seeding. The FN adsorption control was also performed in a microfluidic device surface, and the same result was found. Lack of cell spreading on these surfaces at day 15 is shown in Figure J7.

The composition of the multilayers affects cell behavior as evidenced by cell spreading, attachment, proliferation and viability on biofunctional nanocomposite coatings. The cell sizes became larger with time on these cytophilic coatings. The bone marrow stromal cells achieved 80% confluence by day 3 of culturing in these nanocomposite coatings. These nanocomposite coatings had the most spreading, proliferation and density, and the largest number of live cells. Among the biofunctional nanocomposite coatings, the best ones for culture of bone marrow stromal cells were $(PDDA/Clay)_5(Co/FN)_{2,\ 4,\ 7}$. These results are consistent with our earlier observation about the effect of composition of nanocomposite coating on its ability to support primary bone marrow culture.

The ECM combination we used in the current study is rather unique as FN has a Co binding domain (Williams et al. 1982). In fact, FN and Co are often used together for cell culture studies(BD Biosciences BD BioCoat™ Cell Culture Inserts). Moreover,

fibronectin and type IV collagen are both important members of the extracellular matrix of the bone marrow microenvironment (Tavassoli 1989). Both positively and negatively charged proteins adsorb to some extent on multilayer surfaces regardless of the surface charge because proteins bear on their surfaces domains with both positive and negative surface excess charges. Not surprisingly, adsorbed amounts and the protein layer thicknesses are larger when the proteins and the terminating polyelectrolyte layer are oppositely charged compared to protein adsorption onto films terminating with a similarly charged polyelectrolyte layer (Ladam et al. 2001). Proteins might denature and change conformation once adsorbed on the surface (Ratner et al. 1996), which may affect biological responses and confound the data. The dominant charge of proteins depends on the pH, and pH was carefully monitored during our experiments. It is believed that other interactions, such as van der Waals and hydrophobic attraction are also likely to contribute to protein layer formation and stability (Decher & Hong 1991; Tang et al. 2003).

Our results compare well with other specific reports of culture of bone marrow cells and other primitive cells (Brynda et al. 2005; Garza et al. 2005). More broadly, PDMS substrates are widely used in medical research and in a variety of clinical devices (Makamba et al. 2005). Control of the polymer surface chemistry is a crucial aspect of such devices which rely heavily on cell-biomaterial interface. PDMS substrates are intrinsically hydrophobic due to the low surface energy backbone (Makamba et al. 2005; Makamba et al. 2003; Sia et al. 2003) and require a biofunctional hydrophilic film on the surface in order to promote cell attachment and interaction with substrate. The

biofunctional nanocomposite coating described in this report is specifically useful for making PDMS and other substrates conducive to culture of primary bone marrow cells. Our results with stratified LBL assembled films for primary murine bone marrow culture also corroborate studies with a variety of other cells types that demonstrate the broad usefulness of biofunctional LBLs on PDMS substrates (Ai et al. 2003; Forry et al. 2006; Mohammed et al. 2004; Reyes et al. 2004; Thierry et al. 2003). Thus, the computerized microfluidic LBL methods described should also be more broadly applicable to a wide range of cell types and with many complimentary advantages over traditional LBL film formation methods, such as computerized pumps and valves for greater flow control, automatic processing using programmable software, customized creation of different coating compositions in different microchannels in one experiment, and reduced use of polymer and protein solutions. Although this manuscripts describes these concepts using a relatively simple channel system with relatively low number and density of channels, the methods and devices are compatible for scale up to enable simultaneous preparation and testing of a much larger number of variables (Gu et al. 2007; Gu et al. 2004).

6.4 Conclusion

In this chapter, we have made the surface of microfluidic PDMS bioreactor chips hydrophilic, stable and cytophilic for an extended time by control of surface chemistry. This is achieved by the growth of stable biofunctional nanocomposite coatings on the PDMS surface, so that the primary murine bone marrow stromal cells can attach and spread on the substrate and mimic ECM-cell interactions *ex vivo*. The nanocomposite coatings were made utilizing computerized microfluidic perfusion systems and various

polyelectrolytes PDDA, clay, type IV collagen and fibronectin to optimize the PDMS channel surface for successful culture of primary murine bone marrow cells in ex vivo cultures. The adherent cells of marrow attached and spread on nanocoated PDMS microchannel surfaces for more than two weeks. The protein-topped nanocomposite coatings ($(PDDA/Clay)_5$ $(Co/FN)_{2,4,7}$) were best to achieve maximum cell spreading, proliferation and viability for these cells. Although this paper focused on optimizing attachment of bone marrow stromal cells, the process should be useful for creating distinctive ECM inside PDMS bioreactors for a wide variety of cell types.

References

Ai H, Meng H, Ichinose I et al. Biocompatibility of layer-by-layer self-assembled nanofilm on silicone rubber for neurons. J Neurosci Methods 2003; 128 (1-2):1-8.

Barker SL, Ross D, Tarlov MJ et al. Control of flow direction in microfluidic devices with polyelectrolyte multilayers. Anal Chem 2000a; 72 (24):5925-9.

Barker SL, Tarlov MJ, Canavan H et al. Plastic microfluidic devices modified with polyelectrolyte multilayers. Anal Chem 2000b; 72 (20):4899-903.

Barker SLR, Tarlov MJ, Ross D et al. Fabrication, derivatization, and applications of plastic microfluidic devices. In Advanced Environmental and Chemical Sensing Technology. Boston, MA, USA: SPIE; 2001. 112 p.

BD Biosciences SJ, CA. BD BioCoat™ Cell Culture Inserts. In., Series BD BioCoat™ Cell Culture Inserts. BD BioCoat™ Cell Culture Inserts.

Brynda E, Pachernik J, Houska M et al. Surface immobilized protein multilayers for cell seeding. Langmuir 2005; 21 (17):7877-83.

Decher G, Hong JD. Buildup Of Ultrathin Multilayer Films By A Self-Assembly Process.1. Consecutive Adsorption Of Anionic And Cationic Bipolar Amphiphiles On Charged Surfaces. Makromolekulare Chemie-Macromolecular Symposia 1991; 46:321-7.

Discher DE, Janmey P, Wang YL. Tissue cells feel and respond to the stiffness of their substrate. Science 2005; 310 (5751):1139-43.

Dubas ST, Schlenoff JB. Polyelectrolyte multilayers containing a weak polyacid: Construction and deconstruction. Macromolecules 2001; 34 (11):3736-40.

Duffy DC, McDonald JC, Schueller OJA et al. Rapid Prototyping of Microfluidic Systems in Poly(dimethylsiloxane). Anal. Chem. 1998; 70 (23):4974-84.

Fischer D, Li YX, Ahlemeyer B et al. In vitro cytotoxicity testing of polycations: influence of polymer structure on cell viability and hemolysis. Biomaterials 2003; 24 (7):1121-31.

Forry SP, Reyes DR, Gaitan M et al. Facilitating the culture of Mammalian nerve cells with polyelectrolyte multilayers. Langmuir 2006; 22 (13):5770-5.

Freshney RI. Culture of animal cells. A manual of basic techniques: John Wiley and Sons; 1994. 9-16. p.

Futai N, Gu W, Song JW et al. Handheld recirculation system and customized media for microfluidic cell culture. Lab Chip 2006; 6 (1):149-54.

Futai N, Gu W, Takayama S. Rapid Prototyping of Microstructures with Bell-Shaped Cross-Sections and Its Application to Deformation-Based Microfluidic Valves. Adv. Mater. 2004; 16:1320-3.

Garza JM, Jessel N, Ladam G et al. Polyelectrolyte multilayers and degradable polymer layers as multicompartment films. Langmuir 2005; 21 (26):12372-7.

Gu W, Chen H, Tung Y-C et al. Appl. Phys. Lett. 2007; 90:033505.

Gu W, Zhu X, Futai N et al. Proc. Natl. Acad. Sci. U.S.A. 2004; 45:15861-6.

Haynie DT, Zhang L, Rudra JS et al. Polypeptide multilayer films. Biomacromolecules 2005; 6 (6):2895-913.

Hu S, Ren X, Bachman M et al. Cross-linked coatings for electrophoretic separations in poly(dimethylsiloxane) microchannels. Electrophoresis 2003; 24 (21):3679-88.

Hu S, Ren X, Bachman M et al. Surface modification of poly(dimethylsiloxane) microfluidic devices by ultraviolet polymer grafting. Anal Chem 2002; 74 (16):4117-23.

Jang JH, Schaffer DV. Microarraying the cellular microenvironment. Mol Syst Biol 2006; 2:39.

Johansson JA, Halthur T, Herranen M et al. Build-up of collagen and hyaluronic acid polyelectrolyte multilayers. Biomacromolecules 2005; 6 (3):1353-9.

Kharlampieva E, Sukhishvili SA. Ionization and pH stability of multilayers formed by self-assembly of weak polyelectrolytes. Langmuir 2003; 19 (4):1235-43.

Kidambi S, Lee I, Chan C. Controlling primary hepatocyte adhesion and spreading on protein-free polyelectrolyte multilayer films. J Am Chem Soc 2004; 126 (50):16286-7.

Kim HJ, Lee K, Kumar S et al. Dynamic sequential layer-by-layer deposition method for fast and region-selective multilayer thin film fabrication. Langmuir 2005; 21 (18):8532-8.

Ladam G, Schaaf P, Cuisinier FJG et al. Protein adsorption onto auto-assembled polyelectrolyte films. Langmuir 2001; 17 (3):878-82.

Lahann J, Balcells M, Lu H et al. Reactive polymer coatings: a first step toward surface engineering of microfluidic devices. Anal Chem 2003; 75 (9):2117-22.

Lee J, Shanbhag S, Kotov NA. Inverted colloidal crystals as three-dimensional microenvironments for cellular co-cultures. Journal of Materials Chemistry 2006; 16 (35):3558-64.

Lee JN, Jiang X, Ryan D et al. Compatibility of mammalian cells on surfaces of poly(dimethylsiloxane). Langmuir 2004; 20 (26):11684-91.

Makamba H, Hsieh YY, Sung WC et al. Stable permanently hydrophilic protein-resistant thin-film coatings on poly(dimethylsiloxane) substrates by electrostatic self-assembly and chemical cross-linking. Anal Chem 2005; 77 (13):3971-8.

Makamba H, Kim JH, Lim K et al. Surface modification of poly(dimethylsiloxane) microchannels. Electrophoresis 2003; 24 (21):3607-19.

Mamedov AA, Belov A, Giersig M et al. Nanorainbows: graded semiconductor films from quantum dots. J Am Chem Soc 2001; 123 (31):7738-9.

Mamedov AA, Kotov NA. Free-Standing Layer-by-Layer Assembled Films of Magnetite Nanoparticles. Langmuir 2000; 16 (13):5530 - 3.

McBeath R, Pirone DM, Nelson CM et al. Cell shape, cytoskeletal tension, and RhoA regulate stem cell lineage commitment. Dev Cell 2004; 6 (4):483-95.

Mehta G, Mehta K, Sud D et al. Quantitative Measurement and Control of Oxygen Levels in Microfluidic Poly(dimethylsiloxane) Bioreactors during Cell Culture. In.,

Series Quantitative Measurement and Control of Oxygen Levels in Microfluidic Poly(dimethylsiloxane) Bioreactors during Cell Culture. submitted to Biomedical Microdevices; 2006.

Mehta G, Mehta K, Sud D et al. Quantitative Measurement and Control of Oxygen Levels in Microfluidic Poly(dimethylsiloxane) Bioreactors during Cell Culture. Biomedical Microdevices 2007; 9 (2):123-34.

Mendelsohn JD, Yang SY, Hiller J et al. Rational design of cytophilic and cytophobic polyelectrolyte multilayer thin films. Biomacromolecules 2003; 4 (1):96-106.

Mohammed JS, DeCoster MA, McShane MJ. Micropatterning of nanoengineered surfaces to study neuronal cell attachment in vitro. Biomacromolecules 2004; 5 (5):1745-55.

Ngankam AP, Mao G, Van Tassel PR. Fibronectin adsorption onto polyelectrolyte multilayer films. Langmuir 2004; 20 (8):3362-70.

Podsiadlo P, Paternel S, Rouillard JM et al. Layer-by-layer assembly of nacre-like nanostructured composites with antimicrobial properties. Langmuir 2005; 21 (25):11915-21.

Ratner BD, Hoffman AS, Schoen FJ et al. Biomaterials Science: An Introduction to Materials in Medicine: Academic Press; 1996. 141-7. p.

Reyes DR, Perruccio EM, Becerra SP et al. Micropatterning neuronal cells on polyelectrolyte multilayers. Langmuir 2004; 20 (20):8805-11.

Shchukin DG, Kommireddy DS, Zhao Y et al. Polyelectrolyte Micropatterning Using a Laminar-Flow Microfluidic Device. Advanced Materials 2004; 16 (5):389-93.

Shim J, Bersano-Begey TF, Zhu X et al. Micro- and nanotechnologies for studying cellular function. Curr Top Med Chem 2003; 3 (6):687-703.

Sia SK, Whitesides GM. Microfluidic devices fabricated in poly(dimethylsiloxane) for biological studies. Electrophoresis 2003; 24 (21):3563-76.

Sinani VA, Koktysh DS, Yun BG et al. Collagen Coating Promotes Biocompatibility of Semiconductor Nanoparticles in Stratified LBL Films. Nano Lett. 2003; 3 (9):1177-82.

Stevens MM, George JH. Exploring and engineering the cell surface interface. Science 2005; 310 (5751):1135-8.

Tan W, Desai TA. Layer-by-layer microfluidics for biomimetic three-dimensional structures. Biomaterials 2004; 25 (7-8):1355-64.

Tan W, Desai TA. Microfluidic patterning of cells in extracellular matrix biopolymers: effects of channel size, cell type, and matrix composition on pattern integrity. Tissue Eng 2003; 9 (2):255-67.

Tang Z, Kotov NA, Magonov S et al. Nanostructured artificial nacre. Nat Mater 2003; 2 (6):413-8.

Tavassoli Me. Handbook of the Hemopoietic Microenvironment: Humana Press; 1989. 369-433 p.

Thierry B, Winnik FM, Merhi Y et al. Nanocoatings onto arteries via layer-by-layer deposition: toward the in vivo repair of damaged blood vessels. J Am Chem Soc 2003; 125 (25):7494-5.

Walker GM, Zeringue HC, Beebe DJ. Lab on a Chip 2004; 4 (2):91-7.

Wang J, Muck Jr A, Chatrathi MP et al. Bulk modification of polymeric microfluidic devices. Lab Chip 2005a; 5 (2):226-30.

Wang Y, Lai H-H, Bachman M et al. Covalent Micropatterning of Poly(dimethylsiloxane) by Photografting through a Mask. Anal. Chem. 2005b; 77:7539-46.

Williams EC, Janmey PA, Ferry JD et al. Conformational states of fibronectin. Effects of pH, ionic strength, and collagen binding. J Biol Chem 1982; 257 (24):14973-8.

Zhang X, Wu T, Sun JQ et al. Ways for fabricating stable layer-by-layer self-assemblies: combined ionic self-assembly and post chemical reaction. Colloids And Surfaces A-Physicochemical And Engineering Aspects 2002; 198:439-42.

CHAPTER 7

THREE DIMENSIONAL CULTURES OF PRIMARY MURINE HEMATOPOEITIC CELLS IN MICROFLUIDIC BIOREACTORS FOR IMPROVING HSC *IN VITRO* SELF RENEWAL

7.1 Introduction

Hematopoeitic stem cells (HSCs) are a type of adult stem cell that give rise to all cells in the blood lineage. In adult mammals, they reside in the spongy bone marrow of the long bones. Long term HSCs (LT-HSCs), the most primitive HSCs, can both self-renew and differentiate into daughter progenies. These cells provide the constant supply of myeloid and lymphoid cells in the marrow as well as the circulatory system.

Blood is the most commonly transplanted tissue in clinical settings, which makes HSCs an important candidate in establishing better treatments for hematological malignancies.

HSCs, however, when isolated and then cultured *in vitro*, quickly lose the expression of key antigens on their cell surface (Zhang et al. 2005). They undergo differentiation as the time in culture increases. Many research groups have come up with innovative solutions to prolong the self-renewal capacity or 'stemness' of HSCs *in vitro* cultures, such as co-culturing with different support cells, exposing to a media rich in cytokines found in the bone marrow, growing HSCs in different extracellular substrates, using serum free media, changing metabolic parameters, non-contact co-cultures and changing gene expression (overexpression, deletion, forced expression of a certain gene) either in HSCs or support cells (Bellantuono 2004; Cheung et al. 2006; Kirouac et al. 2006; Madlambayan et al. 2001; Mikkola et al. 2006; Sauvageau et al. 2004; Sharma et al. 2006; Sorrentino 2004; Takagi 2005; Uher et al. 2003; Jung et al. 2005). Even with all these ways to elongate the self renewal capacity of HSCs *in vitro*, the current state-of-the-art HSCs true expansion is at 5.2 fold (initial cell number X 5.2) (Madlambayan et al. 2005). This number is much different form the *in vivo* capacity of expansion of HSCs which is 8400 fold (Sauvageau et al. 2004). We hypothesize that the *in vitro* expansion capability of true HSCs is unlikely to change significantly unless dramatic measures are taken to simulate the *in vivo* HSC niche. We aim to use microfluidic tools to create engineered niches for HSCs which will help us understand and control HSC proliferation and self renewal, and even study the biological role of HSCs in the niche using the optimized microbioreactor.

In microfluidic poly(dimethylsiloxane) (PDMS) bioreactors, a few HSCs and primary bone marrow cells (~100s of cells) can be cultured in nanoliter volumes of fluids under defined microenvironments. The nanoliter scale microfluidic bioreactors have an advantage over conventional bioreactors or other macroscopic culture systems in that the

small volume allows even one or a few HSCs to condition the culture environment significantly. An important feature of the bone marrow HSC niche or any *in vivo* HSC niche is that the cells are arranged in a three-dimensional structure. In fact, three dimensional cultures of HSCs have been reported to increase the expansion of HSCs *in vitro* (Bagley et al. 1999; Banu et al. 2001; Braccini et al. 2005; Kim et al. 2003; Li et al. 2001; Rookmaaker et al. 2005; Rosenzweig et al. 1997; Takagi 2005; Tun et al. 2000; Wang et al. 1995). Some of these studies include culturing HSCs on collagen beads, with capillaries of endothelial cells, in porous hydroxyapatite disks, on silk fiber matrices, in porous biomatrix Cellfoam, on collagen coated porous polyvinyl formal resin, on tantalum-coated porous biomaterial, porous bovine collagen microspheres, and three dimensional bone marrow spheroids.

Another salient feature of the *in vivo* HSC niches are that HSCs are surrounded by a heterogeneous population of supporting cells, which provide soluble and adhesive signals to HSCs, and typically, HSCs are very rare. For example, in the mouse bone marrow there is one HSC per 30,000 bone marrow cells. In order to export these features to our microfluidic bioreactors, we started with co-culture of hematopoeitic progenitor cells (HPCs) and different types of support cells either as cell lines or primary cells. *In vitro* co-culture of HSCs with support cells is very common in the literature (Taichman 2005). HSCs have been co-cultured with various types of cells including but not limited to: osteoblasts, brain endothelial cells, fibroblasts, bone marrow stromal cells, mesenchymal stem cells, bone marrow endothelial cells, and cell lines of stromal and osteoblastic cells such as MS-5 and OP-9.

The literature also supports the idea that primitive quiescent HSCs are located in the regions of very low oxygen tension (close to 1%) and the more differentiated progenitors are found at higher oxygen levels (Levesque et al. 2007; Parmar et al. 2007; Sipkins et al. 2005). Therefore, we conducted our experiments at two oxygen levels: 20% O_2 in a standard incubator and 1.5% O_2 in a hypoxia chamber.

The stem cell activity of hematopoeitic stem and progenitor cells co-cultures in our microfluidic system was detected by colony formation unit (CFU) assay. Among the *in vitro* assays for HSC activity, CFU is an established and popular assay. The numbers and types of colonies formed in CFU assay indicate the stage of differentiation of the HSCs or HPCs in culture. Other *in vitro* assays for HSC activity are long term culture initiation assay (LT-IC), cobblestone area formation assay (CFAC), immunostaining for surface antigens present on HSCs (sca-1, c-kit, CD150 for mouse HSCs). Apart from the *in vitro* assays, the 'gold standard' assay for quantifying HSC activity is *in vivo* competitive repopulation assay (CRU), where the 'test' cells are injected into a lethally irradiated animals and the transplantation of these cells and their repopulation of the marrow are evaluated from 4 weeks for up to 16 weeks.

For the microfluidic co-culture of hematopoeitic cells, we chose a bioreactor with gravity –driven flow as it allows culture of small number of non-adherent pure HSCs without shearing or washing away, inclusion of different supporting cell types that can provide adequate cues for HSCs, 3-D environment created by support cells in micro-compartments, gentle replacement of media from bottom channel by convection and

diffusion, and finally, easy removal of cells for CFU assays by cutting open the top microchannel containing cells. These experiments are our first step towards using microfluidically cultured HSCs for long term *in vivo* reconstitution assays.

In Chapter 8, we generated erythrocytes for 15 days in a similar semi-porous membrane based PDMS microbioreactor from unsorted bone marrow mononuclear cells. Generation of erythrocytes required differentiation of hematopoietic stem, progenitor and erythroid cells without major emphasis on stem cell self-renewal in a media formulation containing differentiation and expansion factors. In the present chapter, we focus on co-culture of hematopoietic cells with supporting cells for self-renewal, expansion and maintenance of stem and progenitor cells.

7.2 Experimental Methods

7.2.1 General Cell Culture

The cell lines used in this work were: EMLC1, K562 and Meg01; while the primary cells used were: primary murine bone marrow stromal cells (BMSC), human micro vascular endothelial cells (EC) and Lin^- $c\text{-}kit^+$ $Sca\text{-}1^+$ primary mouse marrow hematopoeitic progenitor cells (HPC).

The EMLC1 cell line was obtained from a male BDF1 mice bone marrow retrovirally infected with LRARalpha403SN. This cell line is non-adherent SCF-dependent lympho-hematopoietic progenitor cell line and can differentiate to B-lymphocyte, erythrocyte, neutrophil, macrophage, mast cell, megakaryocyte lineages. We chose this cell line as a model for HPCs and HSCs. The K-562 cell line is a non-adherent human erythroleukemia line from chronic myelogenous leukemia in terminal blast crises, highly undifferentiated

multipotential, hematopoietic malignant cells. These cells are of granulocytic series and differentiate to erythrocytic, granulocytic and monocytic lineages. The Meg-01 is a non-adherent human megakaryocyte line from megakaryoblastic crisis of chronic myelogenous lymphoma (CML). K-562 and Meg-01 cells were chosen as models for hematopoietic progenitor cells.

Cell Lines

EML C1 cells (CRL-11691, ATCC) were propagated in ATCC complete growth medium (30-2005, Iscove's modified Dulbecco's medium with 4 mM L-glutamine adjusted to contain 1.5 g/L sodium bicarbonate), supplemented with 200 ng/ml mouse stem cell factor, 20% heat-inactivated fetal bovine serum and 1% antibacterial/antimycotic at 37 C in a humidified 95% air + 5% carbon dioxide incubator.

K-562 cells (CCL-243, ATCC) were cultured in ATCC complete growth medium (30-2005) with 10% fetal bovine serum and 1% antibacterial/antimycotic at 37 C in a humidified 95% air + 5% carbon dioxide incubator.

Meg01 cells (CRL-2021, ATCC) were propagated in ATCC complete growth medium(30-2001, RPMI-1640 medium) supplemented with 10% fetal bovine serum and 1% antibacterial/antimycotic at 37 C in a humidified 95% air + 5% carbon dioxide incubator.

Primary Cells

Primary murine bone marrow stromal cells (BMSC) were isolated from adult wild type C57BL/6 mice in MyeloCult (M5300, StemCell Tech.) supplemented with 1% v/v antibiotic–antimycotic (Mehta et al. 2007a). BMSCs were the adherent cells of the bone marrow present in the culture flasks after two weeks of growth, and were propagated in MyeloCult supplemented with 1% hydrocortisone and 1% antibacterial/antimycotic.

Primary human dermal microvascular endothelial cells (EC) were cultured in EGM-2MV (EGM-2MV Microvascular Endothelial Cell Medium, CC-3202, Lonza) media supplemented with 1% v/v antibiotic–antimicotic.

Murine hematopoietic progenitor cells were isolated from adult (6- to 8-week-old) C57BL/Ka-CD45.2:Thy-1.1 mice by the following process. The bone marrow cells from femurs and tibias were flushed out and stained with Sca-1-APC (E13-161.7, BD Pharmingen; 1:400), c-kit-biotin (2B8, BD Pharmingen; 1:400), FITC-conjugated lineage antibodies (such as Ter119, CD2, Gr-1 or B220, BD Pharmingen; 1:800) as described earlier (Kiel et al. 2005). Briefly, after primary and secondary antibody incubation (StAv-APCCy7 (1:400), anti-FITC microbeads (Miltenyi Biotec Inc.; 1:10)), the cell suspension was depleted of lineage positive cells were by using the autoMACS Pro Separator (Miltenyi Biotec Inc.), and the enriched cells were sorted by flow cytometry to get c-kit$^+$ Sca-1$^+$ cells. These cells (Lin$^-$ Sca-1$^+$ c-kit$^+$) were used in devices within a few hours of cell sorting and not cultured in dishes at all.

7.2.2 Hematopoeitic Co-Culture Microfluidic Device Fabrication

The microfluidic devices consisted of two layers of microchannels separated by a polyester semi-porous membrane (0.4 micron polyester membrane (Corning 3452) (Figure 7.1) Details about fabrication of silicon molds can be found elsewhere (Torisawa et al. 2007). The upper channel was designed with a dead-end to facilitate cell capture whereas the lower channel was continuous to allow medium perfusion (Torisawa et al. 2007). Mortar made of PDMS and toluene (Chueh et al. 2007) was used to bond the two pieces of microchannels along with the membrane. The device was plasma oxidized to make it hydrophilic and fibronectin was adsorbed on it for 30 minutes. The device was then sterilized by exposure to UV for 30 minutes. Three devices were used for each set of experiments. Experiments were repeated three times.

7.2.4 Cell Seeding

The T-25 culture flasks were placed in a humidified 5% CO_2 cell culture incubator. Unless otherwise mentioned, at 70-80 % confluence, the cells were passaged by washing in PBS, and incubating with 0.25% Trypsin/EDTA (Invitrogen, Carlsbad, CA). The Trypsin solution was neutralized with 15% FBS in DMEM and spun down with a centrifuge (ThermoForma, Marietta, OH) for 2 minutes at 4 ^{o}C and 1000 RPM. The supernatant was removed and the pellet was resuspended in DMEM media. The pellet was reconstituted in 4 ml of cell specific media, and 1 ml of this suspension was used for creating a new plate of respective cells. The cells were passaged every third day.

When the cells were to be cultured in the PDMS microbioreactors, the pellet was reconstituted in 70-100 μL of respective cell specific media. The cells were counted as number of cells per ml of media, and the final cell suspension was created by aliquoting calculated volumes of cells according to the combination and ratio of cells desired for a particular co-culture (for eg. BMSC + EC + HPC (2:2:1) for one such co-culture). The co-culture combinations were: BMSC + HPC (4:1), BMSC + EC + HPC (2:2:1), EC + HPC (4:1), EC + MEG 01 + HPC (6:4:1), EC + K562 + HPC (6:4:1), and BMSC + EC + EMLC1 (2:2:1).

Cells (~5000 total per device) were seeded in the device by gravity-driven flow, by creating a height difference of 6 inches between the inlet of one channel layer, through the semi-porous membrane layer between channel layers, and the outlet reservoirs of the other channel layer. Once cells were seeded, media levels in the reservoirs were adjusted to same media volumes, and the devices were incubated at 37^{o}C and 5% CO_2 in a humidified cell culture incubator. Fresh media was pipetted into the inlet of the media transporting channel (bottom channel layer) every day and old media was removed from the outlet. Duplicate control experiments were performed in tissue culture plastic dishes.

7.2.6 Hypoxia Chamber

The co-culture of hematopoietic and support cells were performed at two oxygen tensions: 20% oxygen (in a conventional cell incubator with 5% CO_2) and 1.5% oxygen (hypoxia). A hypoxia chamber (Stem Cell Technologies) was used for keeping the microdevices containing cells at 1.5% oxygen for the duration of co-culture. The hypoxia

chamber was gassed daily with a premixed cylinder of nitrogen, carbon dioxide and oxygen with a gas composition of 93% N_2, 1% O_2 6% CO_2 (Cryogenic Gases, Metro Welding Supply Corporation, Detroit, MI) to achieve 1.5% oxygen after exchange of media in the microdevices. The oxygen tension inside the hypoxia chamber was set to 1.5% by measuring gas exiting the chamber for oxygen content using a KE-25 galvanic cell type oxygen sensor (Figaro Engineering Inc, Japan) with accuracy of ±1% within full oxygen range (0-100%). A calibration of the sensor output (mV) with respect to oxygen concentration provided by the manufacturer was used to find out the oxygen concentration.

7.2.7 Removal of Cells and CFU Assay

After seven days of co-culture, the cells were removed from microdevices to be assayed for colony forming activity. The devices were cut, washed multiple times with media to collect the removed cells. The cells were then plated in 1:9 solution of IMDM with 2% FBS and M3334 Methocult (M3434, Stem Cell Tech) in sterile non-cell culture treated 35 mm Petri dishes. The dishes were incubated for 12 days at 37°C with 5% CO2 and ≥95% humidity and the resulting colonies were identified and count colonies according to established protocol. The CFU assay was performed in the same way for the control co-cultures performed in tissue culture plastic dishes. The colonies identified and counted were: Colony-forming unit-granulocyte, erythroid, macrophage, megakaryocyte(CFU-GEMM), Colony-forming unit-granulocyte macrophage(CFU-GM), Colony-forming unit-granulocyte(CFU-G), Colony-forming unit-macrophage(CFU-M), and Burst-forming unit-erythroid(BFU-E).

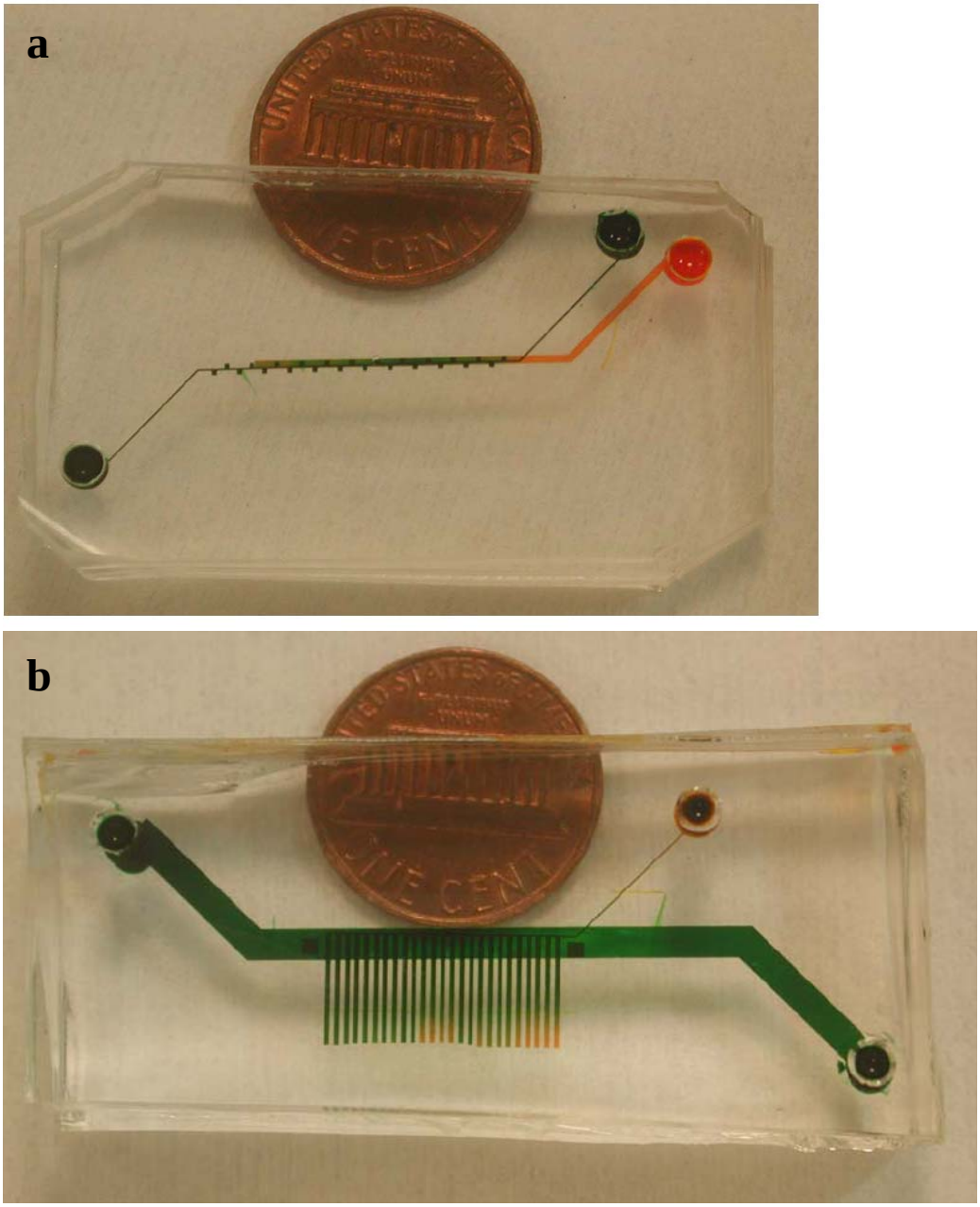

Figure 7.1: Microfluidic bioreactors used for co-culture of hematopoietic cells with support cells in different ratios.

7.3 Results and Discussion

The microfluidic devices used for co-culture of hematopoeitic cells studies are shown in Figure 7.1. In these devices, the cells were seeded in the upper channel which had only one inlet and no outlet. The bottom channel with one inlet and one outlet were used for refreshing the media and delivering it to cells through a semi-permeable membrane (pore size 400 nm) between the top and bottom channel by gravity-driven flow.

7.3.1 Three dimensional co-culture of HPCs and cell lines with different support cells

The preliminary investigation of the feasibility of hematopoeitic cell culture in microfluidic bioreactors was performed for seven days. The co-cultures performed in different ratios were: primary murine bone marrow stromal cells (BMSC) + Human micro vascular endothelial cells (EC) + EMLC1 (2:2:1), BMSC + EC + HPC (Lin^- c-kit^+ $Sca\text{-}1^+$ primary mouse marrow cells) (2:2:1), BMSC + HPC (4:1), EC + HPC (4:1), EC + MEG 01 + HPC (6:4:1), and EC + K562 + HPC (6:4:1). Pictures taken after 24 hours of co-culture at these different cellular compositions are shown in Figure 7.2 A. The co-cultures of hematopoeitic and support cells in one micro-compartment of the top channel can be seen in this figure. The cells are in close contact with each other and even seem to form three dimensional spheroid like structures reminiscent of embryoid bodies in some co-cultures (Rossi et al. 2005; Torisawa et al. 2007).

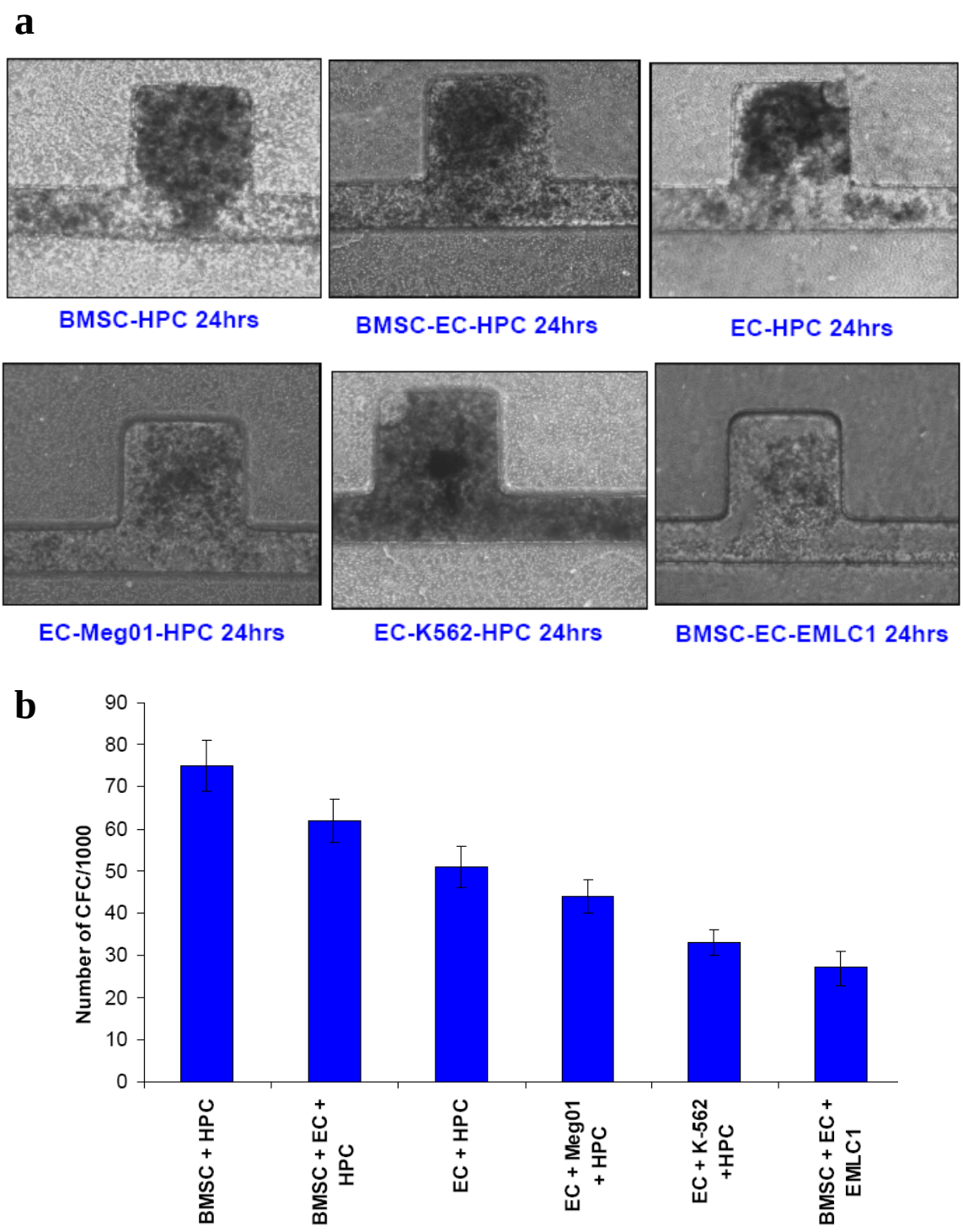

Figure 7.2: A) Pictures of microniche compartments of the top cell loaded channels after 24 hours of co-culture for all six different cell combinations tested. Each micro-compartment is 300 μm wide and long and 100 μm high. **B)** CFU data for hematopoeitic & support cell co-cultures in microfluidic bioreactors represented as number of colony forming cells per 1000 HPCs or EMLC1 for different combinations of co-cultures.

After seven days of co-culture in microbioreactors, the cells were removed from the devices and plated in methylcellulose gel supplemented with cytokines and antibacterial/mycotic. The numbers and types of colonies were quantified for each co-culture after 12 days. Figure 7.2 B shows the number of CFCs per 1000 HPCs (or EMLC1) for all six co-cultures tested. We observed a maximum number of CFCs for the co-culture of BMSCs + HPCs, followed by BMSC + EC + HPC, and others as seen in Figure 7.2 B. As expected, when using EMLC1 cell line along with EC and BMSC, we obtained minimal number of colonies. When comparing co-culture of HPCs with either BMSCs or ECs alone, more colonies were found when HPCs were with BMSCs. This may be because BMSCs consist of all heterogeneous adherent cell types in the bone marrow and can recreate the *in vivo* bone marrow microenvironment, compared to ECs which were from a completely different microenvironment (human dermal endothelium). The types of colonies observed here were CFU-G, CFU-M, CFU-E, BFU-E, CFU-GM, and a few CFU-GEMM. The types of colonies and distribution of colonies are the same for all 6 cases, and were found to be not significant statistically when tested by ANOVA. The differences in the number of CFCs between colonies formed in the six co-cultures were statistically significant at α=0.001 as tested by ANOVA.

These results indicated that it is possible to co-culture hematopoeitic cells in microfluidic bioreactors and isolate the cells to perform *in vitro* CFU assay on them. The 3-D co-culture in the devices used is especially helpful for easy removal of cells.

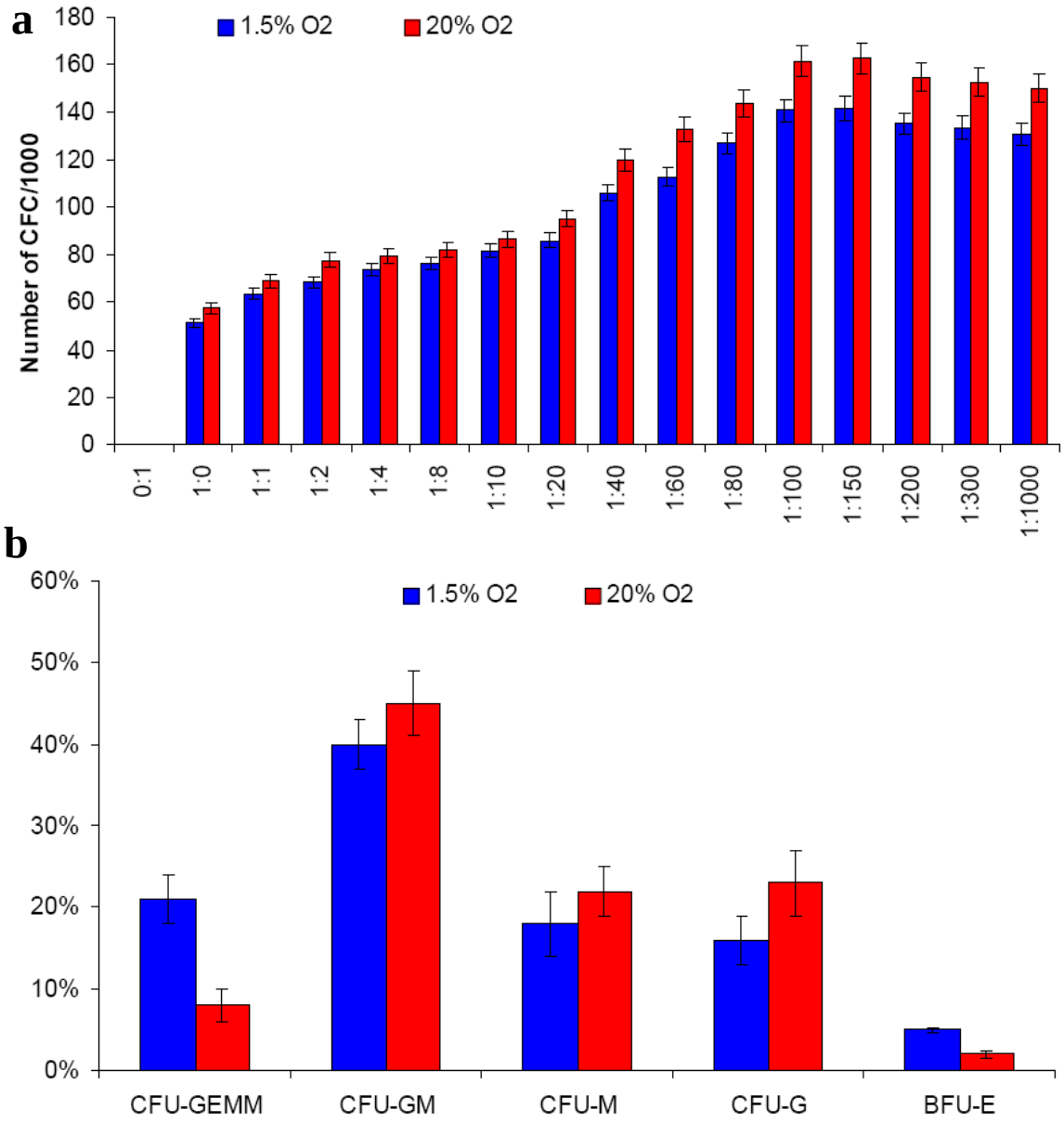

Figure 7.3: CFU data for hematopoeitic & support cell co-cultures in microfluidic bioreactors. **A)** Number of colony forming cells per 1000 HPCs for different ratios of HPCs to BMSCs ranging from 0:1 to 1:1000 for co-cultures performed at two oxygen tensions (20% and 1.5%), **B)** Distribution of colony types (as percentage of all colonies) at two different oxygen tensions for all ratios of HPCs to BMSCs.

7.3.2 Ratio of BMSCs to HPCs for maximum number of colony formation

From the Figure 7.2B we obtained maximum number of colonies when culturing BMSCs with HPCs. For our further experiments, we decided to use this co-culture to figure out

what ratios of cells needed to be cultured to get the maximum number of colonies. Figure 7.3A shows the number of CFCs per 1000 HPCs for co-cultures of HPCs and BMSCs at different ratios from 0:1, 1:0, 1:1, 1:2, 1:4, 1:8, 1:10, 1:20, 1:40, 1:60, 1:80, 1:100, 1:150, 1:200, 1:300, to 1:1000. As a negative control, when only BMSCs are cultured, there was no colony formation. However, when only HPCs were cultured in microfluidic bioreactors, there were ~55 CFCs per 1000 HPCs. This number kept increasing as more BMSCs were cultured with HPCs all the way up to the ratio of 1:100 and 1:150, when it becomes constant. After further increase in the number of BMSCs, the colony formation activity actually decreased from 1:300 all the way up to 1:1000. Thus, the optimal ratio for co-culturing HPCs and BMSCs to get the maximum number of colony formation was found to be 1:100, and this ratio was used for future co-cultures of HPCs and BMSCs. Although HSCs and HPCs have been co-cultured with different support cells or feeder layers in the past 50 years of HSC research, there was never an attempt to optimize the number of support cells needed to maintain HSCs in a self-renewing state *in vitro*. In the literature, HSCs are typically cultured over a confluent layer of feeder/support cells treated with radiation or biochemicals (such as Mitomycin C) to prevent further cell division of support cells. In such systems, the ratio of HSCs to support cells can be greater than 1:1000, which as we just saw above, is not optimal for maximal colony formation, and consequently for maintaining the stemness of HSCs *in vitro*.

Another trend emerging from this result is that fewer colonies were formed at 1.5% oxygen as compared to 20% oxygen at all ratios. This is intuitive because not all progenitors may survive and thrive at lower oxygen tension. When the same experiment

was carried out in conventional *in vitro* culture (tissue culture plastics) at the ratio of 1:100 HPCs to BMSCs, there are 80 CFCs/1000 at 1.5% oxygen and 100 CFCs/1000 at 20% oxygen. The values reported in literature for similar hematopoietic cultures at 1:100 or higher ratio of HPCs to BMSCs match those from our experiments (Fei et al. 2007; Nakayama et al. 2006).

The differences between number of colonies formed at all ratios were statistically significant at α=0.001 as tested by ANOVA. Furthermore, the colony formation (number of CFCs) at two oxygen tensions colonies were statistically significant at α=0.001 as tested by ANOVA. Additionally, when comparing microfluidic co-cultures and TCPS controls, the higher number of CFCs in microbioreactor cultures was statistically significant at both oxygen levels as evaluated by Student's t test.

7.3.3 Distribution of colonies at different oxygen levels

Figure 7.3 B shows the distribution of colony types at two different oxygen tensions for all ratios of HPCs to BMSCs. At 20% oxygen, ~10% colonies are the most primitive CFU-GEMM, while at 1.5% oxygen, double the number (~21%) colonies are the most primitive CFU-GEMM. The progenitor colonies CFU-GM, CFU-G, CFU-M are higher at 20% oxygen as compared to 1.5% oxygen. Furthermore, more BFU-E are observed at 1.5% oxygen (~5%) than at 20% oxygen (~2%), which is expected because hypoxia induces EPO production by progenitors, which enhances number of BFU-E colonies (Cipolleschi et al. 1997). For the tissue culture plastics control of the same experiment at the ratio of 1 HPCs to 100 BMSCs (1:100), 14% of colonies were CFU-GEMM at 1.5%

oxygen and 5% of colonies were CFU-GEMM at 20% oxygen tension. The values reported in literature for similar hematopoietic cultures at different oxygen levels follow a similar trend as seen in our experiments (Cipolleschi et al. 1993; Cipolleschi et al. 2000; Ivanovic et al. 2000; Ivanovic et al. 2004).

The differences between number of CFU-GEMM and BFU-E colonies at both oxygen tensions were statistically significant at α=0.001 as tested by ANOVA. Furthermore, when comparing microfluidic co-cultures and TCPS controls, the higher number of CFU-GEMM and BFU-E in microbioreactor cultures was statistically significant at both oxygen levels as evaluated by Student's t test.

Overall, we observe that microfluidic co-culture produced higher number of colonies, with more primitive colonies as compared to TCPS control, which suggests that bone marrow microenvironment, is simulated better in microfluidic bioreactors than conventional culture.

7.4 Conclusions

In this chapter, we performed 3-D co-culture of hematopoeitic cells in microbioreactors for 7 days and looked at the colony forming ability of the cells after co-culture with different support cells in various ratios. We found that of all the combinations that we tried, maximum number of colonies was observed in a co-culture of HPCs and BMSCs. Further, ratio of 1:100 for HPC to BMSC was found to be optimal for number of colonies in CFU assay in the present study. Lower oxygen tension (1.5%) better at maintaining

primitive colonies in culture compared to 20% oxygen. Future microfluidic hematopoeitic cultures will be performed using 1:100 HSCs to BMSCs in order to test the efficacy of our *in vitro* microfluidic niches.

References

Bagley J, Rosenzweig M, Marks DF et al. Extended culture of multipotent hematopoietic progenitors without cytokine augmentation in a novel three-dimensional device. Exp Hematol 1999; 27 (3):496-504.

Banu N, Rosenzweig M, Kim H et al. Cytokine-augmented culture of haematopoietic progenitor cells in a novel three-dimensional cell growth matrix. Cytokine 2001; 13 (6):349-58.

Bellantuono I. Haemopoietic stem cells. Int J Biochem Cell Biol 2004; 36 (4):607-20.

Braccini A, Wendt D, Jaquiery C et al. Three-dimensional perfusion culture of human bone marrow cells and generation of osteoinductive grafts. Stem Cells 2005; 23 (8):1066-72.

Cheung AM, Kwong YL, Liang R et al. Stem cell model of hematopoiesis. Curr Stem Cell Res Ther 2006; 1 (3):305-15.

Cipolleschi MG, D'Ippolito G, Bernabei PA et al. Severe hypoxia enhances the formation of erythroid bursts from human cord blood cells and the maintenance of BFU-E in vitro. Exp Hematol 1997; 25 (11):1187-94.

Cipolleschi MG, Dello Sbarba P, Olivotto M. The role of hypoxia in the maintenance of hematopoietic stem cells. Blood 1993; 82 (7):2031-7.

Cipolleschi MG, Rovida E, Ivanovic Z et al. The expansion of murine bone marrow cells preincubated in hypoxia as an in vitro indicator of their marrow-repopulating ability. Leukemia 2000; 14 (4):735-9.

Fei XM, Wu YJ, Chang Z et al. Co-culture of cord blood CD34(+) cells with human BM mesenchymal stromal cells enhances short-term engraftment of cord blood cells in NOD/SCID mice. Cytotherapy 2007; 9 (4):338-47.

Ivanovic Z, Bartolozzi B, Bernabei PA et al. Incubation of murine bone marrow cells in hypoxia ensures the maintenance of marrow-repopulating ability together with the expansion of committed progenitors. Br J Haematol 2000; 108 (2):424-9.

Ivanovic Z, Hermitte F, Brunet de la Grange P et al. Simultaneous maintenance of human cord blood SCID-repopulating cells and expansion of committed progenitors at low O2 concentration (3%). Stem Cells 2004; 22 (5):716-24.

Jung Y, Wang J, Havens A et al. Cell-to-cell contact is critical for the survival of hematopoietic progenitor cells on osteoblasts. Cytokine 2005; 32 (3-4):155-62.

Kiel MJ, Yilmaz OH, Iwashita T et al. SLAM family receptors distinguish hematopoietic stem and progenitor cells and reveal endothelial niches for stem cells. Cell 2005; 121 (7):1109-21.

Kim HS, Lim JB, Min YH et al. Ex vivo expansion of human umbilical cord blood CD34+ cells in a collagen bead-containing 3-dimensional culture system. Int J Hematol 2003; 78 (2):126-32.

Kirouac DC, Zandstra PW. Understanding cellular networks to improve hematopoietic stem cell expansion cultures. Curr Opin Biotechnol 2006; 17 (5):538-47.

Levesque JP, Winkler IG, Hendy J et al. Hematopoietic progenitor cell mobilization results in hypoxia with increased hypoxia-inducible transcription factor-1 alpha and vascular endothelial growth factor A in bone marrow. Stem Cells 2007; 25 (8):1954-65.

Li Y, Ma T, Kniss DA et al. Human cord cell hematopoiesis in three-dimensional nonwoven fibrous matrices: in vitro simulation of the marrow microenvironment. J Hematother Stem Cell Res 2001; 10 (3):355-68.

Madlambayan GJ, Rogers I, Casper RF et al. Controlling culture dynamics for the expansion of hematopoietic stem cells. J Hematother Stem Cell Res 2001; 10 (4):481-92.

Madlambayan GJ, Rogers I, Kirouac DC et al. Dynamic changes in cellular and microenvironmental composition can be controlled to elicit in vitro human hematopoietic stem cell expansion. Exp Hematol 2005; 33 (10):1229-39.

Mehta G, Kiel MJ, Lee JW et al. Automated Formation of Polyelectrolyte Layer Films on PDMS Bioreactor Surfaces for Primary Murine Bone Marrow Culture. Advanced Functional Materials 2007a; 17:2701-09.

Mehta G, Mehta K, Sud D et al. Quantitative Measurements and Analysis of Cellular Oxygen Uptake in Microfluidic Poly(dimethylsiloxane) Bioreactors. *Biomedical Microdevices* 2007b; 9 (2):123-34.

Mikkola HK, Orkin SH. The journey of developing hematopoietic stem cells. Development 2006; 133 (19):3733-44.

Nakayama A, Matsui H, Fukushima T et al. Murine serum obtained from bone marrow-transplanted mice promotes the proliferation of hematopoietic stem cells by co-culture with MS-5 murine stromal cells. Growth Factors 2006; 24 (1):55-65.

Parmar K, Mauch P, Vergilio JA et al. Distribution of hematopoietic stem cells in the bone marrow according to regional hypoxia. Proc Natl Acad Sci U S A 2007; 104 (13):5431-6.

Rookmaaker MB, Verhaar MC, Loomans CJ et al. CD34+ cells home, proliferate, and participate in capillary formation, and in combination with CD34- cells enhance tube formation in a 3-dimensional matrix. Arterioscler Thromb Vasc Biol 2005; 25 (9):1843-50.

Rosenzweig M, Pykett M, Marks DF et al. Enhanced maintenance and retroviral transduction of primitive hematopoietic progenitor cells using a novel three-dimensional culture system. Gene Ther 1997; 4 (9):928-36.

Rossi MI, Barros AP, Baptista LS et al. Multicellular spheroids of bone marrow stromal cells: a three-dimensional in vitro culture system for the study of hematopoietic cell migration. Braz J Med Biol Res 2005; 38 (10):1455-62.

Sauvageau G, Iscove NN, Humphries RK. In vitro and in vivo expansion of hematopoietic stem cells. Oncogene 2004; 23 (43):7223-32.

Sharma S, Gurudutta GU, Satija NK et al. Stem cell c-KIT and HOXB4 genes: critical roles and mechanisms in self-renewal, proliferation, and differentiation. Stem Cells Dev 2006; 15 (6):755-78.

Sipkins DA, Wei X, Wu JW et al. In vivo imaging of specialized bone marrow endothelial microdomains for tumour engraftment. Nature 2005; 435 (7044):969-73.

Sorrentino BP. Clinical strategies for expansion of haematopoietic stem cells. Nat Rev Immunol 2004; 4 (11):878-88.

Taichman RS. Blood and bone: two tissues whose fates are intertwined to create the hematopoietic stem-cell niche. Blood 2005; 105 (7):2631-9.

Takagi M. Cell processing engineering for ex-vivo expansion of hematopoietic cells. J Biosci Bioeng 2005; 99 (3):189-96.

Torisawa YS, Chueh BH, Huh D et al. Efficient formation of uniform-sized embryoid bodies using a compartmentalized microchannel device. Lab Chip 2007; 7 (6):770-6.

Tun T, Miyoshi H, Ema H et al. New type of matrix support for bone marrow cell cultures: in vitro culture and in vivo transplantation experiments. Asaio J 2000; 46 (5):522-6.

Uher F, Hajdu M, Vas V. Self-renewal and differentiation of hematopoietic stem cells: a molecular approach (a review). Acta Microbiol Immunol Hung 2003; 50 (1):3-21.

Wang TY, Brennan JK, Wu JH. Multilineal hematopoiesis in a three-dimensional murine long-term bone marrow culture. Exp Hematol 1995; 23 (1):26-32.

Zhang CC, Lodish HF. Murine hematopoietic stem cells change their surface phenotype during ex vivo expansion. Blood 2005; 105 (11):4314-20.

CHAPTER 8

CAPTURE AND EXPANSION OF SMALL NUMBERS OF NON-ADHERENT PRECURSOR CELLS IN MICRONICHES WITH EMBEDDED SEMI-POROUS MEMBRANES TO GENERATE ERYTHROCYTES

8.1 Introduction

Hematopoiesis is the process by which hematopoietic stem cells (HSCs) in the bone marrow, spleen and liver develop into mature blood cells. According to the monophyletic theory, a single type of stem cell gives rise to all mature blood cells in the body (Klinken 2002). Hematopoietic tissue proper includes a range of maturing hematopoietic cells originating from the proliferation, commitment, and differentiation of blood-born HSCs and progenitors, which seed the marrow (Morrison et al., 1995). Enucleated erythrocytes are one of the progenies of HSCs formed by differentiation of

erythroid progenitors, and are turned over every 21 days over the entire lifetime of humans.

There is great interest in establishing *in vitro* erythropoiesis to supply clinical blood needs and also in new research using blood as a therapeutic biodistribution vector because enucleated erythrocytes have systemic circulation and no progression of DNA into new generations of erythrocytes (Douay and Andreu, 2007, Ropars et al., 1985). In addition, small scale *in vitro* production of erythrocytes would provide a platform for physiological assays to detect toxic and mutagenic compounds (Shuga et al. 2007) as well as an assay system to identify crucial autocrine/paracrine factors.

Microfluidic devices enable greater control of the *in vitro* cell microenvironment than conventional culture systems. For example, the small ratio of fluid to cell volumes enhances autocrine and paracrine effects over what would be seen with static Petri dish culture, and active convective fluid flow in the device can regulate the chemical as well as the mechanical environment (Mehta et al. 2008, Shim et al. 2003, Walker et al. 2004). Therefore, our goal in this chapter is to use these devices to create a model of erythropoiesis-on-a-chip.

Most microfluidic devices that utilize small numbers of cells employ adherent cells because of the need to retain cells inside microchannels. However, many biologically important cells, such as hematopoietic precursor and stem cells, are non-adherent. Microfluidic devices that can mechanically capture non-adherent cells using weir-like

structures have been described but often require large numbers of cells and capture only a small percent of cells that are introduced (Lee et al. 2005 and 2006, Neville 2007). Microdevices using wells for capturing cells have also been developed (Khademhosseini et al. 2004 and 2005, Gutierrez and A. Groisman, 2007, Deutsch et al. 2006, Di Carlo et al. 2006, Sinclair and Salem 2006, Lee et al. 2006, Deutsch et al. 2006, Lee et al. 2005, Carlo, Wu and Lee 2006, Wu et al. 2007, Neville et al. 2007). There are few if any reports of performing small scale microfluidic culture of non-adherent precursor cells for extended periods of time. Trapping cells (adherent or non-adherent) within microfluidic channels is attractive for various cell studies. However, the capture efficiency of cells within microchannels (calculated as cells captured in microdevice divided by total cells input as cell suspension is not high (often below 1%) for various studies in the literature (see Table 8.1). These numbers indicate that new designs of microdevices are needed to increase cell trapping efficiency. By incorporating semiporous membrane to create small chambers for spatial confinement of cells in our microdevices, we demonstrate here a simple way to retain ~80% of non-adherent cells.

The utility of our system is demonstrated by production of erythrocytes from hematopoietic progenitor cells. In addition to the challenges of handling small numbers of non-adherent cells, small scale *in vitro* production of erythrocytes from progenitors can be difficult as multiple steps of culture, including co-culture on feeder layers and changes and replacements of media, are required. The porous membrane sandwich design allows not only efficeint capture of progenitor cells, but also gentle refreshment and exchange of media needed for expansion as well as differentiation of cells without

worry of washout. Additionally, by using a media containing both expansion and differentiation factors, we show that erythrocytes can be produced even without stepwise changes in the media composition. Overall, these experiments create first steps towards hematopoieis-on-a-chip.

Table 8.1: Cell capture efficiency of various microfluidic devices in literature

Method	Number of Cells Trapped	Arrays	Total cells	Cells in Suspension	Capture Efficiency (%) †	Reference
Straight Channel	0		0	1000000	0	_
Cell Docking* in microwell	500	10	5000	20000000	0.025	Khademhosseini et al. 2004
Cell Docking in microwell	857	7	6000	20000000	0.030	Khademhosseini et al. 2004
Cell Docking in microwell	688	8	5500	20000000	0.028	Khademhosseini et al. 2004
Cell Docking in microwell	340	25	8500	30000000	0.028	Khademhosseini et al. 2005
Dynamic Array‡	1	576	576	1000000	0.058	Carlo, Wu and Lee 2006
Dynamic Array	29	64	1856	1000000	0.186	Lee et al. 2006
Dynamic Array	10	184	1840	1000000.00	0.18	Wu et al. 2007
Dynamic Array	50000	6	300000	3020000.00	9.93	Neville et al. 2007
Side Compartments	95	21	2000	2500	80	Present work

*Cell Docking: Microchannels sealed with a substrate with microwells. Some of the cells rest in microwell grooves when cell suspension flows though the channel.
‡Dynamic Array: Mechanical structures designed to trap cells, with multiple number of repeating arrays.

†Capture efficiency calculated as: total cells captured divided by cells in suspension expressed as a percentage.

8.2. Methods

8.2.1 Microdevice Fabrication

Microfluidic devices consisted of two layers of microchannels separated by a polyester semi-porous membrane (3 micron polyester membrane (Corning 3452). Details about fabrication of silicon molds can be found elsewhere (Torisawa et al. 2007). The upper channel was designed with a dead-end to facilitate cell capture whereas the lower channel was continuous to allow medium perfusion (Torisawa et al. 2007). Mortar made of PDMS and toluene (Chueh et al. 2007) was used to bond the two pieces of microchannels along with the membrane. The device was plasma oxidized to make it hydrophilic and fibronectin was adsorbed on it for 30 minutes. The device was then sterilized by exposure to UV for 30 minutes. Three devices were used for each set of experiments. All experiments were repeated 3-4 times. A device schematic and photograph are shown in Figure 8.1.

8.2.2 Cell seeding in microdevice

Primary murine bone marrow cells were isolated from adult wild type C57BL/6 mice in MyeloCult (M5300, StemCell Tech.) supplemented with 1% v/v antibiotic–antimycotic (Mehta et al. 2007). The cell suspension was then placed on a ficoll (Stem Cell Tech) column and after 30 minutes of centrifugation the band of mature erythrocytes was removed. The resulting cell suspension was composed of bone marrow mononuclear cells (BMMNCs), which contain a small fraction of HSCs (less than 0.5%; Kiel et al.

2006). These cells were centrifuged again to form a pellet and then resuspended in 80 μl of either expansion media or the combined expansion + differentiation media.

Cells (~2000 per device) were seeded in the device by gravity-driven flow, by creating a height difference of 6 inches between the inlet of one channel layer, through the semi-porous membrane layer between channel layers, and the outlet reservoirs of the other channel layer. Once cells were seeded, media levels in the reservoirs were adjusted to similar fluid levels, and the devices were incubated at 37^{o}C and 5% CO_2 in a humidified cell culture incubator. Fresh media was added via the inlet of the media transporting channel (bottom channel layer) every day and old media was removed from the outlet.

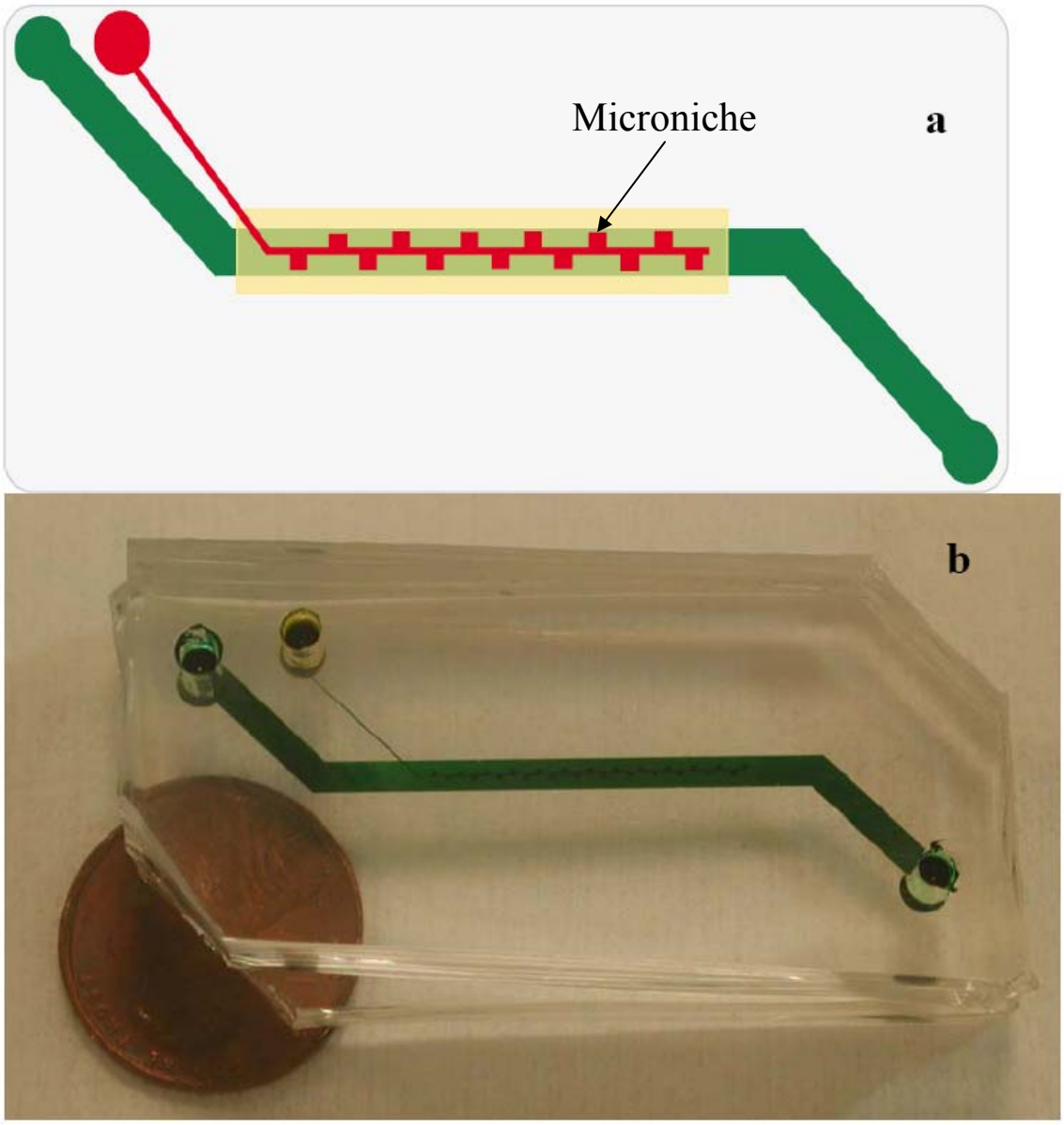

Figure 8.1: Schematic of microdevice for generation of erythrocytes. The top view of the device is shown in (a). A semi-porous membrane separates the side compartment microniches containing top channel from the straight bottom channel. An actual microdevice with a penny for scale is shown in (b). Orange colored food dye fills the top channel while a green colored food dye covers the bottom channel. Transparent semi-porous membrane is barely visible in (b).

8.2.3 Media formulation for Erythrocyte Generation

Various media compositions to support erythropoiesis have been reported (Bridell et al. 1997, Kie et al 2003, Kim et al. 2002, Neildez-Nguyen et al. 2002, Giarratana et al. 2005,

Miharada et al. 2006, Papayannopoulou et al. 1996, Wojchowski et al. 2006, Miller and Klein 1996, Rahman et al. 2000, Nagler et al. 1994, Pick et al. 2002, von Lindern et al. 1999, Szilvassy et al. 1996, Muench et al. 1993). The common ingredient in all of these cocktails is erythropoietin (Epo), a major regulator of erythropoiesis. Other cytokines which help enable differentiation of erythroid progenitors to erythrocytes are IGF-II and Tpo.

In this work, we use a medium to support erythropoiesis which contains both expansion (Zhang and Lodish, 2005) and differentiation (Neildez-Nguyen et al. 2002) factors and is well-suited to the heterogeneous starting populations of cells used. The composition of the media used for generating erythrocytes was as follows: StemSpan serum-free medium (StemCell Tech, Vancouver, CA) was supplemented with 10 μg/mL heparin (Sigma, St Louis, MO), 10 ng/mL mouse SCF, 20 ng/mL mouse Tpo, 20 ng/mL mouse IGF-2 (all from R&D Systems, Minneapolis, MN), 10 ng/mL human FGF-1 (Invitrogen, Carlsbad, CA) (Zhang and Lodish, 2005) and 1% v/v antibiotic–antimycotic (15240, Gibco); this we term the hematopoeitic 'expansion media'. Alternatively, 1% deionized BSA, 5 ng/ml mouse IL-3 (Peprotech), 10^{-6} M hydrocortisone (StemCell Tech), 6 IU/ml human Epo (Epogen), 100 μg/ml human Insulin, 90 μg/ml Ferric Nitrate, 900 μg/ml Ferric Sulfate, 150 μg/ml iron saturated Holo-Human Transferrrin (all from Sigma) were added to the serum-free media (Neildez-Nguyen et al. 2002, Giarratana et al. 2005); this we term the erythroid 'differentiation media'. Lastly, 1% v/v antibiotic–antimycotic (15240, Gibco) was also added to the (expansion, differentiation or both) media and the combined media

was sterile filtered (0.22 μm). We refer the hematopoeitic expansion media and erythroid differentiation media mixed together in 1:1 ratio as 'expansion + differentiation media'.

8.2.4 Quantification of erythrocytes

Microdevices were observed every day for 15 days from the start of cell seeding using a Nikon (TE-300) microscope. Color images were recorded with a Nikon Coolpix digital camera. The number of erythrocytes (seen as red cells) was counted over the entire length of the cell culture channel. The generation of these red cells was calculated by enumerating cell counts on a specific day (e.g. on day 0 there were no erythrocytes). May-Grunwald-Giemsa staining was performed inside devices to verify existence of erythrocytes as pink cells and nucleated cells as blue or purple. Giemsa staining was also performed on the cells after removing them from the microniches. The cells were removed from microniches by cutting the device open and washing the cells out. A smear of removed cells was created on a clean glass coverslip and observed with a microscope.

8.2.5 Mathematical model

A schematic of the pathway for progenitor cell differentiation through erythrocyte (RBC) production (hematopoiesis) is shown in Figure 8.3A and based on the literature (Aubin et al., Yoshida et al., 2004). We develop an ordinary differential equation model for the process by using a balance equation for each cell type (M, CFU-M, BFU, CFC, and RBC; denoted x_i, i=1-5 respectively) of the form:

$$\frac{dx_i}{dt} = k_{i-1}x_{i-1} - k_i x_i$$

where rate constants k_i describe the differentiation process from state i to state i+1 (k_5 = 0.) For the myeloid progenitor equation there is an additional term $k_r x_1$ to incorporate the ability of the progenitor to self-renew. This simple model ignores cell death and also the dynamics of influence of external growth factors, and is more phenomological than mechanistic. The initial values of the model were chosen based on information from previous experimental results and were equal to M = 100, CFU-M = 800, BFU = 300, CFU–E = 30 and RBC = 0. Parameters (k_r and k_1 to k_4) were estimated from our data using non-linear least square optimization and the objective function defined as

$$f(k) = \sum [x_{\exp,i} - x(k)_{pred,i}]^2$$

where $x_{exp,i}$ and $x(k)_{pred,i}$ are the measured and predicted cell numbers, respectively, and k refers collectively to the rate constants k. Rate constants were constrained to be positive. Statistics of the fit along with the correlation matrix of parameters were calculated as per the usual regression procedure (Seber and Wild, 2003) using MATLAB.

8.3 Results

8.3.1 Capture and Retention of Non-Adherent Primary Cells

Capture efficiency (cells captured/cells input) of BMMNCs in the microdevice (Figure 8.1) used in the present work is 80%, which is significantly higher than other microdevices used for trapping cells (Supplementary Table S1). Cells residing in microniches received fresh media daily by removal of old media from the outlet of the bottom channel and pipetting new media into the inlet of the bottom channel. This ensured gentle exchange of media for cells in the microniches. As quantified from microscope images, no cells were lost during the media exchange, maintaining all progenitor cells inside the microdevice for the duration of culture.

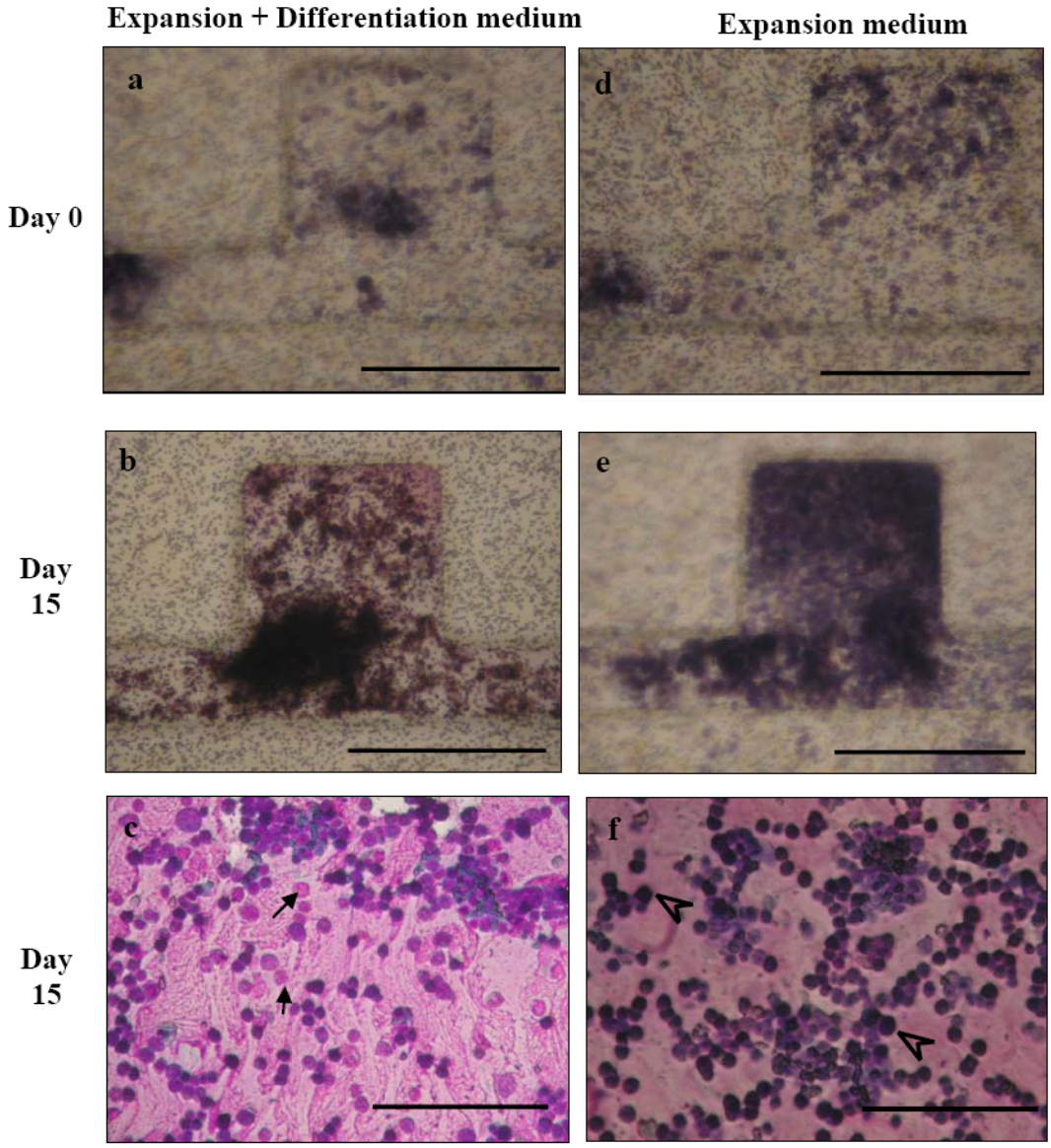

Figure 8.2: Comparison of a microfluidic side compartment microniche (See Figure 8.1 for location) on Day 0 (a and d) and Day 15 (b and e) of culture (Scale bar: 300 μm). There are no red cells on day 0 (a and d) when using either expansion media or expansion + differentiation media. However, erythrocytes can be prominently observed on day 15 (b) when the combined media is used, but there are no red cells when using just the expansion media (e). Giemsa-stained cells after removal from the microniches after 15 days (c and f, Scale bar: 100 μm). Cells in c) were cultured in combined media, while cells in f) were in expansion media. Black arrows show erythrocytes in panel c) and black arrow heads show nucleated cells in panel f).

8.3.2 Differentiation of Bone Marrow Progenitors to Produce Erythrocytes

With an initial cell seeding density of 1950 ± 78 cells (no erythrocytes) per microdevice, we produced 2048 ± 183 erythrocytes per microdevice using the expansion + differentiation media and a 15 day culture (Figure 8.2). There were no red cells on day 0 when using either expansion media or expansion + differentiation media, as seen by the purple color of cells after May-Grunwald-Giemsa staining (Figure 8.2 A and D). However, erythrocytes can be prominently observed on day 15 when the expansion + differentiation media is used as seen by the pink color after the Giemsa stain (Figure 8.2 B and C).

The phenotypic, morphological, genetic and functional analysis of erythrocytes generated *in vitro* is reported in detail in the literature (Giarratana et al. 2005, Cheung et al. 2007, von Lindern et al. 1999, Kie et al. 2003, Szilvassy et al. 1996, Muench et al. 1993). We further evaluated the cells produced in the microniches by removing cells from the devices and making smears on glass slides. The distribution of bone marrow cells in the microniches at day 15 can be seen in Figure 8.2 C and F. There are a mix of nucleated blue or purple cells (black arrowheads) and pink stained erythrocytes (black arrows). These bone marrow-derived and microdevice-cultured cells were compared with Giemsa stained cells from peripheral blood (not shown), in which more erythrocytes are observed.

If only expansion media was used, no erythrocytes were seen over a 7 day period. Once the media was replaced with the combined differentiation and expansion media, however, erythrocytes could be observed from day 8 to day 15. This result shows that change of

media can be performed efficiently and used to trigger cell differentiation on-demand. Moreover, seven days of culture in just the expansion media is enough to expand or maintain progenitor cells.

For comparison, we also cultured cells in 24 well conventional plate using the same (expansion + differentiation) media composition and an initial population of $1x10^4$ cells/well (data not shown). Both the conventional culture and our microdevice gave similar numbers of erythrocytes. However, when using a microfluidic device, we were able to get the same level of expansion (5 fold expansion) with a smaller number of starting cells. One challenge when using 24 well dishes to perform media changes is that some cells are forced out of the well by the pipette every time; however, in the microdevice, the cells are not removed during media changes.

The production of erythrocytes, computed by enumerating the number of erythrocytes on each day of the culture, is seen in Figure 8.3 B and follows the common logarithmic pattern (Neildez-Nguyen et al. 2002, Giarratana et al. 2005). The distribution of erythrocytes compared to nucleated cells was also quantified by calculating the percentage of erythrocytes of all total cells on a particular day. By the end of 15 days of microfluidic culture, there are about 30% erythrocytes in the total cell population. The generation of erythrocytes inside microdevice hints at the presence of progenitor cells in the microniches that give rise to erythrocytes. Autocrine or paracrine factors secreted within the microniches may aid in retaining progenitor cells as well as in inducing the formation of more differentiated cells.

8.3.3 Comparison between the experiments and the model

The experimental data on erythrocyte production are in agreement with the model structure (Figure 8.3B) and the parameters of the model give information on the rates of differentiation and self renewal of cells in the culture. The non-linear nature of the model and the high correlation of the parameters in the model makes it difficult to ascertain global minimum, and hence there can be multiple sets of parameter values which can minimize the objective function, and hence the absolute values of rate constants cannot be determined accurately. However, all fit sets of parameters with high R^2 demonstrate that the rate of self renewal of the progenitor cell (M) ($k_{r,}$) was slower than the rate of differentiation (k_1). This is indicative of the fact that this microfluidic culture is incapable of sustaining the self renewing cells, and hence eventually will run out of self-renewing cells resulting in the decline in production of cells, as indicated by the difficulty in sustaining such cultures over a long period of time. In this particular system, the primitive HSCs will be depleted from the culture in approximately 4 weeks, and an evidence for this is seen in Figure 8.3B where number of erythrocytes plateaus off during the later part of the microfluidic culture. However, these results compare very well with other conventional *in vitro* cultures for the generation of erythrocytes suggesting that the microbioreactors studied here are functioning much like the macro scale bioreactors in the literature. Moreover, in our microfluidic culture systems, the optimal conditions for maximizing the yield of erythrocytes can now be established using high throughput methods. Another highly efficient method to dramatically increase the number of

erythrocytes produced in these microbioreactors would be to start with a population of bone marrow cells that are highly enriched in hematopoietic stem cells.

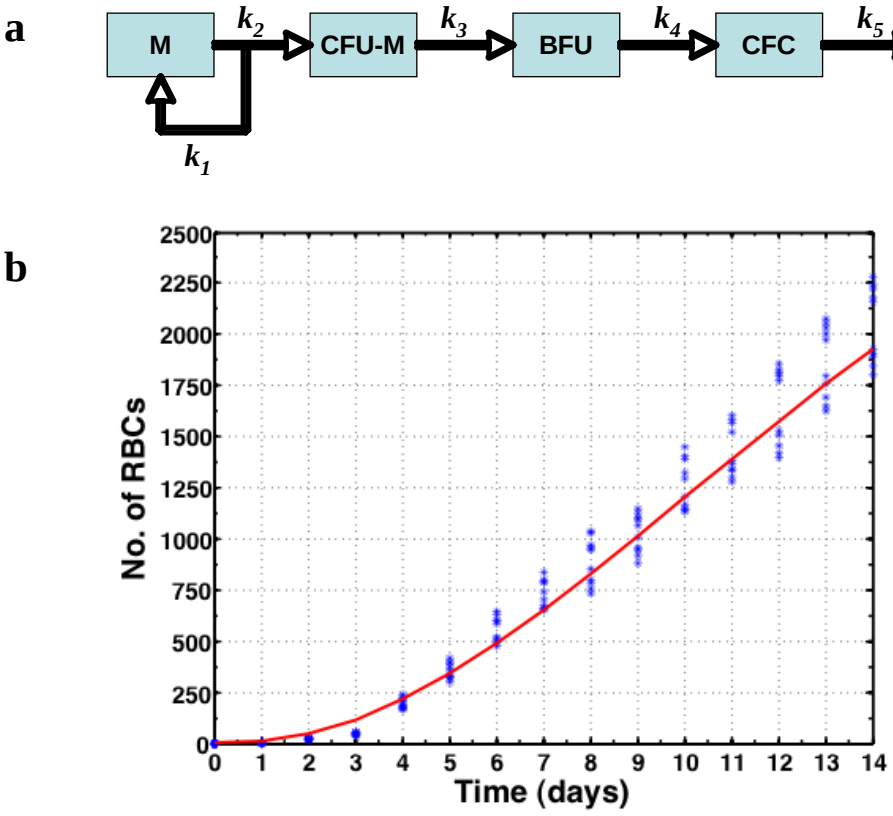

Figure 8.3: a) Schematic of the hematopoiesis pathway relevant for erythrocyte (RBC) production: M=Myleloid progenitor, CFU-M=Colony forming unit-Myeloid, BFU=Burst forming unit-erythrocytes, CFU-E=Colony forming unit-Erythroid, RBC=Erythrocytes **b**) Counts of erythrocytes from day 0 to day 15 per microdevice with 'expansion + differentiation media' (from all cell compartments) for all devices (10) are shown as points with standard deviations. Fit of the pathway model to the data from all devices is shown as a smooth curve. The five parameters were estimated to be $k_{1,sr}$ = 6.3671, k_2 = 6.5895, k_3 = 0.9185 , k_3 = 0.3783, k_4 = 0.0945. The R^2 for the fit was 99%. The highest correlation for parameters was between $k_{1,sr}$ and k_2 (= 0.99).

8.4 Conclusions

In this chapter, we describe semi-porous membrane separated PDMS microbioreactors which are highly advantageous for culture of small number of non-adherent cells. Because of the upper microchannel not having an outlet and not being open to atmosphere, the cells could not flow out anywhere, and thus important autocrine and paracrine factors were likely preserved. These results pave the way for the next wave of research with precious cells in microfluidic devices. Bone marrow mononuclear cells were moderately expanded with an expansion + differentiation media in these microbioreactors with a goal of generating erythrocytes. In the beginning of the microfluidic culture, there were no red cells visible in the microniches; however, from day 2 onwards, we started to see red cells. The red cells consistently increased in number from this point onwards until the end of experiment at day 15. Our results also confirm that we had some hematopoeitic progenitor cells in our population, which then produced the erythrocytes. Additionally, this report shows that erythrocytes can be differentiated from precursor cells in the microfluidic devices. These microbioreactors can further be optimized to ultimately maximize the yield of erythrocytes for culture of small number of any non-adherent cells using a high throughput format. Comparison with a mathematical model also shows the kinetics of generation of erythrocytes inside microdevice from precursor cells. Our next goal is to recreate entire hematopoeisis on a microfluidic device with differentiation of HSCs to all blood lineages.

References

Audet J, Zandstra PW, Eaves CJ et al. Advances in hematopoietic stem cell culture. Curr Opin Biotechnol 1998; 9 (2):146-51.

Cheung JO, Casals-Pascual C, Roberts DJ et al. A small-scale serum-free liquid cell culture model of erythropoiesis to assess the effects of exogenous factors. J Immunol Methods 2007; 319 (1-2):104-17.

Chueh BH, Huh D, Kyrtsos CR et al. Leakage-free bonding of porous membranes into layered microfluidic array systems. Anal Chem 2007; 79 (9):3504-8.

Deutsch A, Zurgil N, Hurevich I et al. Microplate cell-retaining methodology for high-content analysis of individual non-adherent unanchored cells in a population. Biomed Microdevices 2006a; 8 (4):361-74.

Deutsch M, Deutsch A, Shirihai O et al. A novel miniature cell retainer for correlative high-content analysis of individual untethered non-adherent cells. Lab Chip 2006b; 6 (8):995-1000.

Di Carlo D, Wu LY, Lee LP. Dynamic single cell culture array. Lab Chip 2006; 6 (11):1445-9.

Douay L, Andreu G. Ex vivo production of human red blood cells from hematopoietic stem cells: what is the future in transfusion? Transfus Med Rev 2007; 21 (2):91-100.

Giarratana MC, Kobari L, Lapillonne H et al. Ex vivo generation of fully mature human red blood cells from hematopoietic stem cells. Nat Biotechnol 2005; 23 (1):69-74.

Gutierrez E, Groisman A. Quantitative measurements of the strength of adhesion of human neutrophils to a substratum in a microfluidic device. Anal Chem 2007; 79 (6):2249-58.

Khademhosseini A, Yeh J, Eng G et al. Cell docking inside microwells within reversibly sealed microfluidic channels for fabricating multiphenotype cell arrays. Lab Chip 2005; 5 (12):1380-6.

Khademhosseini A, Yeh J, Jon S et al. Molded polyethylene glycol microstructures for capturing cells within microfluidic channels. Lab Chip 2004; 4 (5):425-30.

Kie JH, Jung YJ, Woo SY et al. Ultrastructural and phenotypic analysis of in vitro erythropoiesis from human cord blood CD34+ cells. Ann Hematol 2003; 82 (5):278-83.

Kiel MJ, Personal communication, 2008.

Kiel MJ, Yilmaz OH, Iwashita T et al. SLAM family receptors distinguish hematopoietic stem and progenitor cells and reveal endothelial niches for stem cells. Cell 2005; 121 (7):1109-21.

Kim SK, Koh SK, Song SU et al. Ex vivo expansion and clonality of CD34+ selected cells from bone marrow and cord blood in a serum-free media. Mol Cells 2002; 14 (3):367-73.

Klinken SP. Red blood cells. The International Journal of Biochemistry & Cell Biology 2002; 34 (12):1513.

Lee PJ, Hung PJ, Rao VM et al. Nanoliter scale microbioreactor array for quantitative cell biology. Biotechnol Bioeng 2006; 94 (1):5-14.

Lee PJ, Hung PJ, Shaw R et al. Microfluidic application-specific integrated device for monitoring direct cell-cell communication via gap junctions between individual cell pairs. Applied Physics Letters 2005; 86 (22):223902.

Mehta G, Mehta K, Sud D et al. Quantitative Measurements and Analysis of Cellular Oxygen Uptake in Microfluidic Poly(dimethylsiloxane) Bioreactors. *Biomedical Microdevices* 2007; 9 (2):123-34.

Mehta G, Torisawa Y, Takayama S. Engineering Cellular Microenvironments with Microfluidics. In: FA Gomez, editor, translator and editor Biological Applications of Microfluidics: John Wiley and Sons; 2008; p. 87-114.

Miharada K, Hiroyama T, Sudo K et al. Refinement of cytokine use in the in vitro expansion of erythroid cells. Hum Cell 2006; 19 (1):30-7.

Morrison SJ, Uchida N, Weissman IL. The biology of hematopoietic stem cells. Annu Rev Cell Dev Biol 1995; 11:35-71.

Muench MO, Firpo MT, Moore MA. Bone marrow transplantation with interleukin-1 plus kit-ligand ex vivo expanded bone marrow accelerates hematopoietic reconstitution in mice without the loss of stem cell lineage and proliferative potential. Blood 1993; 81 (12):3463-73.

Neildez-Nguyen TM, Wajcman H, Marden MC et al. Human erythroid cells produced ex vivo at large scale differentiate into red blood cells in vivo. Nat Biotechnol 2002; 20 (5):467-72.

Nevill JT, Cooper R, Dueck M et al. Integrated microfluidic cell culture and lysis on a chip. Lab Chip 2007; 7 (12):1689-95.

Nielsen LK, Papoutsakis ET, Miller WM. Modeling ex vivo hematopoiesis using chemical engineering metaphors. Chemical Engineering Science 1998; 53 (10):1913.

Peng C-A, Koller MR, Palsson BØ. Unilineage model of hematopoiesis predicts self-renewal of stem and progenitor cells based on ex vivo growth data. Biotechnology and Bioengineering 1996; 52 (1):24-33.

Ropars C, Teisseire B, Avenard G et al. Improved Oxygen Delivery to Tissues and Iron Chelator Transport through the Use of Lysed and Resealed Red Blood Cells: A New Perspective on Cooley's Anemia Therapya. Annals of the New York Academy of Sciences 1985; 445 (1):304-15.

Seber GAF, Wild CJ. Nonlinear Regression. Hoboken: John Wiley & Sons; 2003. (Wiley Series In Probability and Statistics).

Shim J, Bersano-Begey TF, Zhu X et al. Micro- and nanotechnologies for studying cellular function. Curr Top Med Chem 2003; 3 (6):687-703.

Shuga J, Zhang J, Samson LD et al. In vitro erythropoiesis from bone marrow-derived progenitors provides a physiological assay for toxic and mutagenic compounds. Proc Natl Acad Sci U S A 2007; 104 (21):8737-42.

Sinclair J, Salem AK. Rapid localized cell trapping on biodegradable polymers using cell surface derivatization and microfluidic networking. Biomaterials 2006; 27 (9):2090-4.

Szilvassy SJ, Weller KP, Chen B et al. Partially differentiated ex vivo expanded cells accelerate hematologic recovery in myeloablated mice transplanted with highly enriched long-term repopulating stem cells. Blood 1996; 88 (9):3642-53.

Torisawa YS, Chueh BH, Huh D et al. Efficient formation of uniform-sized embryoid bodies using a compartmentalized microchannel device. Lab Chip 2007; 7 (6):770-6.

von Lindern M, Zauner W, Mellitzer G et al. The glucocorticoid receptor cooperates with the erythropoietin receptor and c-Kit to enhance and sustain proliferation of erythroid progenitors in vitro. Blood 1999; 94 (2):550-9.

Walker GM, Zeringue HC, Beebe DJ. Microenvironment design considerations for cellular scale studies. Lab Chip 2004; 4 (2):91-7.

Wojchowski DM, Menon MP, Sathyanarayana P et al. Erythropoietin-dependent erythropoiesis: New insights and questions. Blood Cells Mol Dis 2006; 36 (2):232-8.

Wu LY, Di Carlo D, Lee LP. Microfluidic self-assembly of tumor spheroids for anticancer drug discovery. Biomed Microdevices 2008; 10 (2):197-202.

Yoshida T, Takagi M. Cell processing engineering for ex vivo expansion of hematopoietic cells: a review. Biochemical Engineering Journal 2004; 20 (2-3):99.

Zhang CC, Lodish HF. Murine hematopoietic stem cells change their surface phenotype during ex vivo expansion. Blood 2005; 105 (11):4314-20.

CHAPTER 9

CONCLUSIONS

The Journey

Often in our darkness
we forget to see the light:
The sun is constant,
even behind the clouds,
The river's current
washes away the debris.
Let the wind on your cheeks
help you remember
there is more -
There is more for you.

-Ruth Gilmore Langs, Ann Arbor Artist, 2006

9.1 Summary

In this thesis, we set out to create *in vitro* microfluidic niches for HSCs which simulate the features of *in vivo* bone marrow microenvironment (see Figure 9.1A). We have been able to construct develop new tools for studying biology of niches by controlling oxygen tension in microbioreactors, by enhancing optimal attachment and growth of HSC supporting stromal cells, and create three dimensional cultures of hematopoeitic and support cells.

As a part of our first aim to control oxygen tension in gas-permeable PDMS microfluidic bioreactors, we developed experimental techniques to quantify dissolved oxygen

concentrations in the microchannels in real time using fluorescence intensity and lifetime imaging of an oxygen sensitive dye, ruthenium tris(2,2'-dipyridyl) dichloride hexahydrate (RTDP). Combining such experiments with a mathematical model enabled a more quantitative understanding and better control of the physical-chemical mechanisms underlying cell biological events in such PDMS bioreactors. The data indicated that despite oxygen diffusion through PDMS, uptake of oxygen by cells inside the perfused PDMS microchannels induces an axial oxygen concentration gradient, with lower levels recorded in downstream regions ranging from 20% to 4.3%. The oxygen concentration gradient generated by a balance of cellular uptake, convective transport by media flow, and permeation through PDMS in our devices ranged from 0.0003 (mg/l)/mm to 0.7 (mg/l)/mm. The existence of such steep gradients induced by cellular uptake can have important biological consequences. Results are consistent with our mathematical model and give insight into the conditions under which flux of oxygen through PDMS into the microchannels will or will not contribute significantly to oxygen delivery to cells and also provide a design tool to manipulate and control oxygen for cell culture and device engineering. The combination of computerized microfluidics, in situ oxygen sensing, and mathematical models opened new windows for microphysiologic studies utilizing oxygen gradients and low oxygen tensions.

Many primary cells, especially adult HSCs need to be at a much lower oxygen tension (close to 1%) to remain in a self-renewing state for a longer time *in vitro*. In order to further lower the oxygen tension in microbioreactors below 4.3%, we developed new microfluidic devices made of thermoplastic and elastomeric polymers. These

microdevices offered three distinct advantages: 1) generation of low oxygen tensions with mammalian cell culture (20% to 1%), 2) lower evaporation of aqueous solutions compared to PDMS devices, and 3) perfusion using Braille actuation. Channel features were created on rigid polymers such as PETG, COC and PS by hot embossing. These 'hard tops' were bonded to elastomeric 'soft bottoms' to create devices that can be used for microfluidic cell culture as well as biochemical analysis.

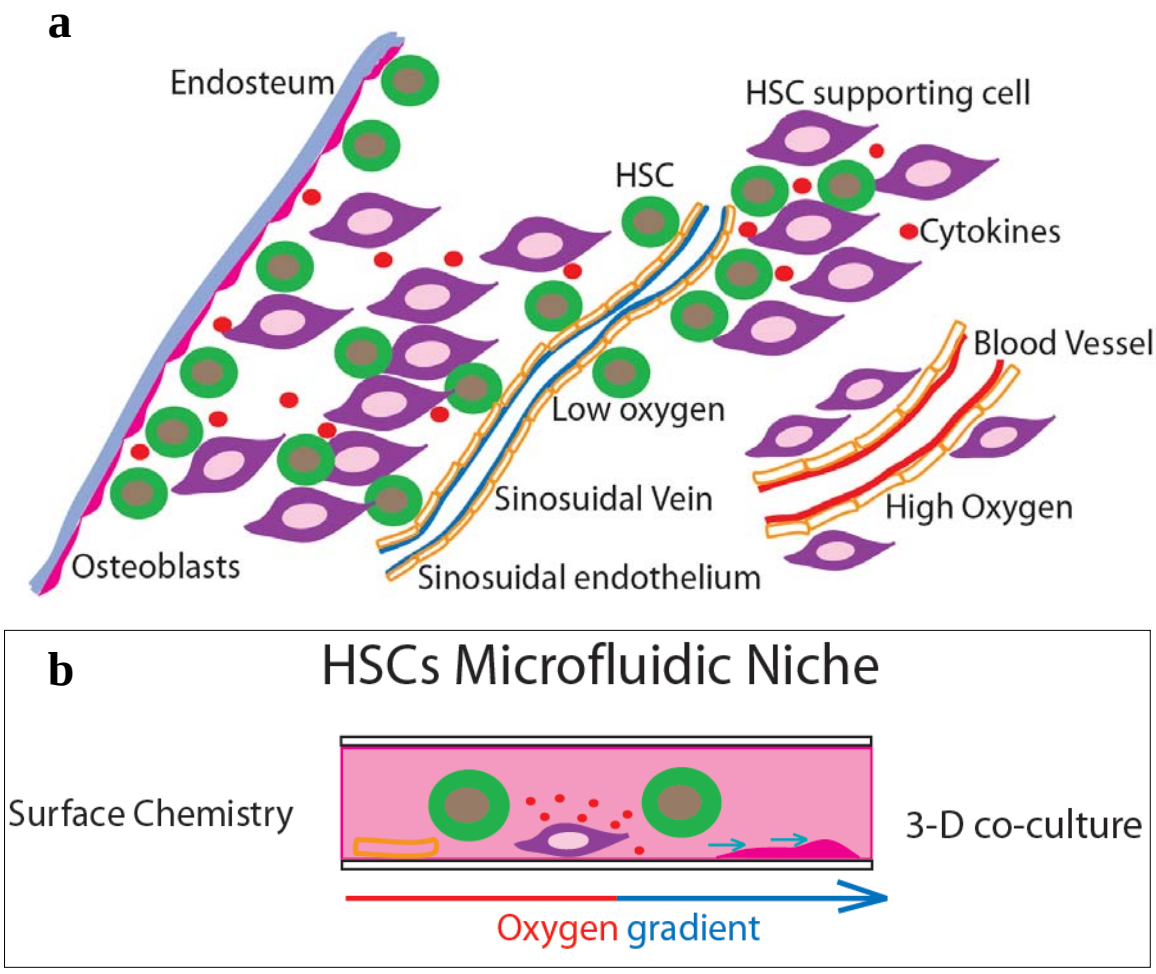

Figure 9.1: a) *In Vivo* Bone Marrow HSC Niche, and b) *in vitro* HSC microfluidic niche.

We applied our well-characterized oxygen measurement system and the mathematical model to establish cellular oxygen uptake rate parameters for different mammalian cells in PDMS microbioreactors. We estimated cell intrinsic parameters, V_{max} and K_m, for each cell type in microfluidic culture by utilizing the model and experiments together, and thereby developed a method to measure uptake rates of other nutrients / measure ligand/drug responses in microfluidic bioreactors.

HSCs need supporting cells to provide adhesive and soluble signals and to mediate cellular processes such as proliferation, differentiation, mobilization, homing and apoptosis. Primary murine bone marrow cells do not successfully grow on PDMS substrates due to the weak attachment of cells to the PDMS surface even with adsorption of cell adhesive proteins such as collagen or fibronectin. Therefore, for our second aim, we modified the surface of PDMS with biofunctional multilayer coatings to promote marrow cell attachment and spreading. We utilized an automated microfluidic perfusion system to create multiple types of polyelectrolyte nanoscale coatings simultaneously in multiple channels based on layer-by-layer deposition of PDDA (poly(diallyldimethyl ammonium chloride)), clay, type IV collagen and fibronectin. Adherent primary bone marrow cells attached and spread best on a surface with composition of $(PDDA/clay)_5$ $(Collagen/Fibronectin)_2$ with negatively charged fibronectin exposed on the top, remaining well spread and proliferating for at least two weeks. Compared to traditional more macroscopic layer-by-layer methods, this microfluidic nanocomposite process offered advantages of greater flow control, automatic processing, multiplexed fabrication, and use of lesser amounts of polymers and protein solutions. Thus, we utilized PDMS

microbioreactors with computerized perfusion controls for engineering the bone marrow microenvironment.

For our third aim, we established three dimensional *in vitro* cultures of hematopoeitic stem, progenitor and support cells for seven days in semi-porous membrane separated PDMS microfluidic bioreactors. The microdevice consists of a top channel with side compartment microniches separated from a bottom channel by a semi-porous membrane. We assayed the ability of different supporting cell combinations to maintain in vitro HSC colonies, and observed that of all combinations, the CFU activity was highest when bone marrow stromal cells were co-cultured with HPCs. Further, in the BMSC-HPC co-culture system, we optimized the ratio of hematopoeitic cell to support cells needed for maximizing the number of colony formation, and found it to be 1:100 HPCs to BMSCs. Experiments performed at two oxygen tensions (20% and 1.5%) confirmed that lower oxygen tension was better at maintaining primitive colonies in culture.

We have established erythropoiesis-on-a-chip in semi-porous membrane based PDMS microdevices using small numbers of non-adherent unsorted primary bone marrow cells to generate erythrocytes over a 15 day period. Culture of non-adherent cells in side chamber microniches of the microdevice allowed efficient change of media from the bottom microchannel as well as entrapment of cells. Primary mononuclear bone marrow cells were grown in the side compartment microniches in medium containing either expansion factors or expansion and differentiation factors. Only in the presence of differentiation factors were erythrocytes observed in microdevices. The experimental

results were also found to be consistent to mathematical model describing the growth and differentiation of the progenitor cells based on the known hematopoeisis model.

In summary, we used different microfluidic tools to recreate *ex vivo* models for HSC niches (as seen in Figure 9.1B), which can be helpful for the microenvironmental studies with other stem cell niches. Microbioreactors also allow additional functionality to control autocrine/paracrine factors, local nutrient/mitogenic gradients, continuous perfusion, micrometer control of topology and composition of substrate, and easy integration with sensing and analysis tools. Results from this thesis will contribute to development of engineered bony organs in microbioreactors (Figure 9.2) and hematopoiesis-on-a-chip. These hybrid bony organs containing mineralized tissue, marrow and microcirculatory compartments could possibly be used as biosensors and tissue replacements. Understanding the roles of the biomolecules studied in our artificial niches, and their involvement in the bone marrow-HSC continuum will catalyze further studies at the molecular level. Thus results take us closer to the goal of creating functional bony organs in microfluidic chips and to move forward in the realm of bone tissue engineering.

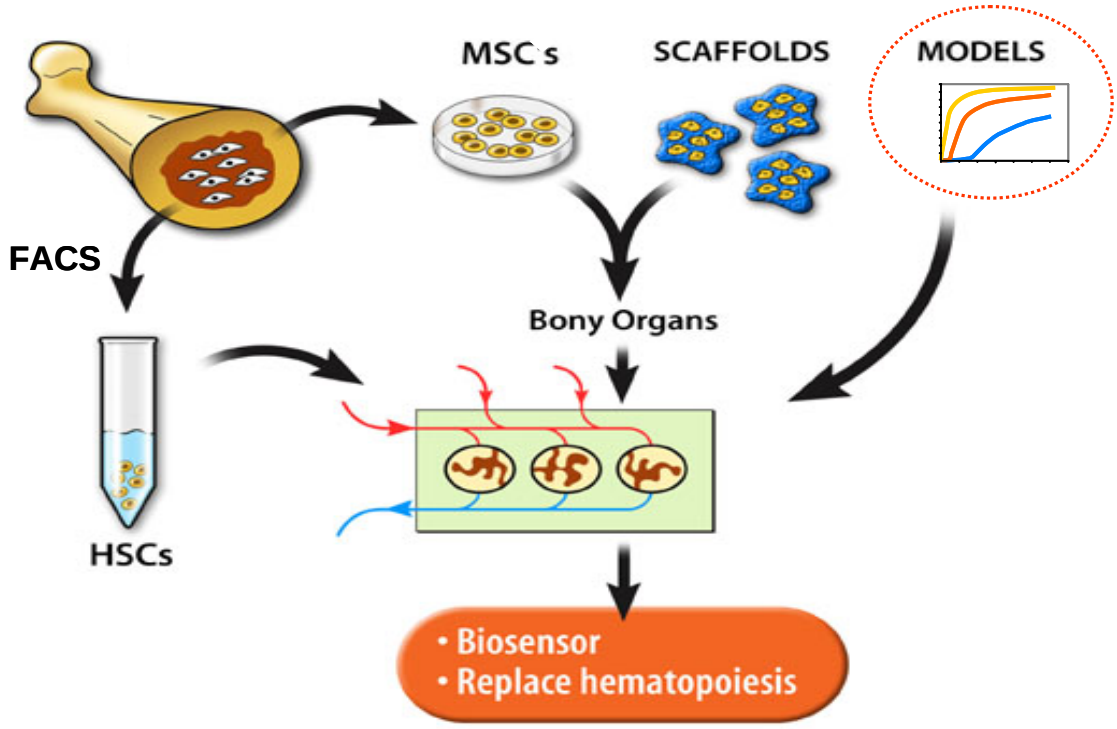

Figure 9.2: Functional bony organs on-a-chip

9.2 Future Directions

Although we have made substantial progress towards *in vitro* HSC niches that mimic features of the *in vivo* bone marrow, we are still far away from the goal of artificial bone marrow niches that are just as functional and effective as their physiological counterparts. There have been many technical and practical limitations in our work, which in retrospect may be rectified with the following measures:

High throughput screening: In the bone marrow HSC niches, a heterogeneous population of cells (support cells and HSCs) cohabitate in a hierarchical and structurally functional manner to maintain bone marrow as a complex organ. The definition of microenvironment and mimicking the *in vivo* marrow processes are not straightforward

tasks due to the highly transient processes and the largely undefined heterogeneous environment. Therefore, high throughput screening technologies are needed to test various parameters that might have an effect on *ex vivo* true long term (LT) HSC expansion.

The variables that need to be considered for such experiments include:

1) Primary murine cell types isolated from bone marrow such as mesenchymal stem cells, endothelial cells, osteoblasts, megakaryocytes, pericytes, reticulocytes, adipocytes, fibroblasts, osteoclasts, osteocytes, cells of all MSC lineage, hematopoeitic cells which are $CD48^+$ and/or $CD41^+$, heterogeneous BMSC.
2) Primary support cell types also need to combined together in various ratios and compositions to the synergistic effects of different combinations of cells
3) Genetic manipulations also need to be applied to the primary support cells to maximize the ex vivo expansion of HSCs. Some examples are overexpression of HOXB4, WNT proteins, Notch-1, Sonic hedgehog, GATA2, AML1, p18, MPL, STAT5 and p21.
4) Cytokines which are known to have any effect on the entire murine system (not just the ones expressed in the bone marrow) also need to be systematically probed at various concentrations and in different combinations to determine the effects (extent of survival, proliferation, and differentiation) they can impart on LT-HSC expansion.

5) Extracellular matrices also play a major role in how HSCs sense their environment, and also known to regulate various HSC functions. The entire range of ECM proteins found in the murine system again need to be tested alone and in all possible combinations possible to single out the particular combinations that dramatically raise LT-HSC ex vivo expansion.
6) *In vitro* physiochemical culture parameters, such as pH, osmolarity, dissolved oxygen tension, dissolved carbon dioxide tensions, and temperature, as well as metabolite concentrations (glucose, glutamine, glutamate, lactate and ammonia) also need to be monitored and optimized for the maximal HSC expansion.
7) Three dimensional cultures must be a necessary condition for in vitro culture of LT-HSCs. In addition to the 3-D cultures mentioned in this work, scaffolds of biopolymers, proteins or amino acids must be utilized to provide a conducive environment for HSCs.

When all the permutations and combinations of the above mentioned variables are added together, we get thousands of possible experiments to exhaust all possible culture conditions that may lead to high *ex vivo* LT-HSC expansion, which closely follows *in vivo* self renewal in the bone marrow. In order to narrow down the list of experiments that need to be performed, a mathematical approach is required to create a careful and intelligent design of experiments. Moreover, the high throughput experiments also need to be combined with appropriate monitoring tools to get an overall view of optimization of the *ex vivo* LT-HSC expansion.

Design of experiments (DOE): The process control of the *in vitro* HSC cultures has been difficult to achieve due to the complexity and interactions of the cells involved. The variability of cell type, transient kinetics, high sensitivity and specificity to extrinsic factors, and interaction of a multitude of these factors affecting cellular behavior pose significant challenges to process characterization. This lack of characterization and control is highly undesirable and can result in low quality, yield, and purity of the final LT-HSC produced in culture. Full factorial designs will be essential in the future studies to screen out a large number of parameters and experimental conditions which do not allow drastic increase in LT-HSC expansion. In order for such a design of experiments to be successful and insightful, the interactions between all variables must also be accounted for. Kinetic models of LT-HSC expansion might also be necessary in conjunction with DOE for predictive analysis.

Real-time process monitoring: Real time and on-line monitoring of key process parameters will provide vital information for making decisions about the optimized culture conditions. The current monitoring techniques for cell bioprocesses will have to be applied to the microfluidic LT-HSC cultures. The simultaneous monitoring of key process variables is limited to only certain parameters: a) pH, dissolved oxygen tension, carbon dioxide tension, and temperature; b) nutrients and metabolites; c) growth factors; and d) cell viability and concentration.

Measurement of paracrine secretion: The small amounts of paracrine factors secreted by support cells for use by HSCs need to be better characterized. Microfluidic HSC niches

can be integrated with in situ immunoassays to quantify the concentrations and identity of precious paracrine factors, which might also be present in a gradient in specific niches.

Mice experiments: The efficacy of the artificial microfluidic HSC niches needs to be evaluated by the '*gold standard*' bone marrow *in vivo* long term competitive reconstitution assays. We performed some preliminary studies in this context where after 7 day co-culture of HSCs and support cells in microdevices we tested the reconstitution ability of microfluidically cultured HSCs by injecting cells into lethally irradiated mice of a differing strain. The different co-culture conditions that we tried in these experiments were: HSCs control, HSCs + post-natal day1 liver endothelial cells, HSCs + osteoblasts, HSCs + megakaryocytes, HSCs + MSCs, and HSCs + megakaryocytes + endothelial cells. In these experiments, 25 to 40 HSCs were loaded into the devices with 100 times that number of support cells. When we looked at the peripheral blood of the injected mice after four weeks, we did not observe any significant myeloid, B and T cells originating from HSCs cultured in microfluidic niches. For these experiments, we had a positive control of non-cultured FACS sorted HSCs, which when immediately injected into recipient mice were able to reconstitute the bone marrow of the host. This leads us to believe that some variables that might be affecting the culture of FACS purified HSCs in our devices. There may be elements in the device itself, handling of cells, removal of cells, small numbers of pure HSCs used for culture, loading of cells, media configuration, or the *in vitro* culture that might be contributing to the lack of reconstitution using these cells.

More experiments are needed with significantly higher number of starting HSCs, for example, 5000 or more per device instead of 25-100. Furthermore, we performed positive control experiments to verify the mechanics of microfluidic cell manipulations and survivability of HSCs in our device. In these experiments, FACS purified HSCs were cultured in microfluidic bioreactors for either 5 minutes or 24 hours and then used for reconstitution assays, we found that 5 minute culture in microdevice gives rise to myeloid and lymphoid cells from the test HSCs. These experiments tell us that handling of cells in and out of device for a 5 minute culture allows reconstitution. Cells are removed from the device by pippetting, washing with a buffer, and incubating with an enzyme free dissociation media for 15 minutes. However, this protocol might be inflicting physical injury onto the fragile HSCs when they are in culture for longer than 5 minutes. These results lead us to believe that for successful *in vitro* experiments we need to use a higher number of HSCs since HSCs are either dormant, or apoptosing, or differentiating or depleting in our cultures.

Biological questions: The bone marrow niche is one of the most well known microenvironments for adult hematopoeitic stem cells. Although it has been established that osteoblasts and other stroma supporting cells (including endothelial cells, adipocytes, fibroblasts) play a central role in hematopoiesis, and produce many factors essential for the survival, renewal and maturation of hematopoeitic stem cells, it still needs to be determined whether HSCs play a role in establishing an inductive microenvironment. Bone marrow studies typically look at the effect of a particular object (cytokine, ECM protein, etc.) under evaluation on HSC proliferation, differentiation, homing, quiescence

and migration. Thus, it is important to identify the roles HSCs play in the niche and how they influence marrow cells (MSCs, osteoblasts and endothelial cells) to create an inductive microenvironment, and to study how their function is altered in abnormal or diseased marrows. It is very difficult and resource straining to perform this type of study in animal models. Therefore, *in vitro* studies can be formulated to find out the influence HSCs can have on mesenchymal stem cells (MSCs) and stromal cells of the marrow niche, including endothelial cells and osteoblasts. In such studies, different variations of abnormal HSCs in microbioreactor cultures can be configured where small populations of HSCs and stromal cells can be easily studied in simulated microenvironments.

Some of the examples of abnormal HSCs that can be explored are:

1) HSCs with reduced proliferative capacity by RNAi silencing of homeobox transcription factors, HOXB3 and HOXB4. Overexpression of HOXB4 strongly enhances hematopoeitic stem cell regeneration, and mice deficient in both Hoxb3 and Hoxb4 have defects in endogenous hematopoiesis and diminished number of hematopoeitic progenitors due to insufficient expansion of HSCs.

2) HSCs in an environment of high oxidative stress. It has been shown that elevated reactive oxygen species causes progressive bone marrow failure resulting from a defect in HSC function in mice.

3) HSCs with under-expressed and over-expressed Notch 1 and Tie 2 receptors, which are believed to be instrumental in the homing and quiescence of the HSCs respectively.

Other biological questions that remain unanswered in the context of the HSC bone marrow niche are:

- Role of osteoblasts in getting pre-HSCs and HSCs to differentiate
- Role of osteoblasts (and other BMSCs) in leukemic HSCs
- Operational structure of bone marrow microenvironment (and how it is different from leukemic bone marrow)
- Interaction between cell associated growth factors (provided by osteoblasts) and growth factor receptors (on HSCs) important for:
    - Proliferation of HSCs (eg. G-CSF, GM-CSF, etc.)
    - Niche localization or homing of HSCs (eg. ICAMs, Jagged1, CD 164 etc.)
    - Survival and quiescence of HSCs (eg. VCAM-1, N-Cadherin, Ang-1etc.)
- Important signaling mechanisms which have not yet been established for HSCs (eg. signaling by PECAM-1).

Furthermore, microfluidic culture systems described herein can be applied towards development of physiological *in vitro* drug toxicity assays, where cells on axial gradient of oxygen or any nutrient are exposed to drugs.

Overall, this work has the potential to provide major insights into bone marrow stem cell biology. Future studies in this field will lead to establishment of new protocols to

successfully expand HSCs *in vitro* without losing their multipotency. Using the *in vitro* model systems developed here, functions of HSCs in the bone marrow niche could be discerned, which will have important implications for new treatment options for hematologic and bone marrow disorders. It could lead directly to: a) improved understanding of the molecular pathways involved in hematopoiesis, b) identification of functions of other niche components, c) understanding of other adult stem cell niches, and d) targeted design of new treatment modalities for hematologic disorders.

APPENDIX A

Calculation of Oxygen Fluxes for PDMS Microbioreactor used in Oxygen Tension Experiments

This appendix shows calculation of oxygen flux through the top surface of PDMS microbioreactor for materials presented in Chapter 3.

$J = (P * \Delta p) / t$

$J = (D * \Delta C) / t$

$P = D * S$

where, J = Flux
P = permeability
Δp = pressure drop
t = thickness
D = diffusivity
ΔC = concentration gradient
S = solubility

Flux through media layer

D O2/Water = 10^{-5} cm^2/sec (Fleischer et al. 1981)
ΔC = solubility of oxygen in media at 25 C = 8.5 mg/l (Fleischer et al. 1981) = 2.67 X 10^{-7} mol/cm^3
t= 30 microns (channel height) = 30 X 10^{-4} cm

J= 10^{-9} mol/cm^3 sec

Flux through parylene C bottom layer

P O2/parylene C = 3.4 X 10^{-11} (cm^3 (STP) cm)/(cm^2 sec atm) (Yeh et al. 1990)
D O2/parylene C = 10^{-8} cm^2/sec (Yeh et al. 1990)
ΔC = solubility of oxygen in parylene C at 25 C = 10^{-3} (from P= D*S)

t = 2.5 microns (thickness of parylene layer) = 2.5 X 10^{-4} cm

J= 10^{-7} mol/cm^3 sec

Flux through PDMS top layer

P O2/PDMS = 5.88 X 10^{-6} (cm^3 (STP) cm)/(cm^2 sec atm) (Mercel et al. 2000)
D O2/PDMS = 10^{-5} cm^2/sec (Mercel et al. 2000)
ΔC = solubility of oxygen in PDMS at 25 C = 10^{-1} (from P= D*S, [0.18 cm^3 STP/ cm^3 atm] Mercel et al. 2000))

t = 1 cm (height of PDMS above channel features)
J= 10^{-5} mol/cm^3 sec

APPENDIX B

PDMS Microfluidic Cell Culture Literature

Table B1: Research work citing biological studies in microfluidic devices (Chapter 2)

Cell type	Material	Perfusion	Results	Reference
Sf 9 insect cells, Ovary cells from fall armyworm	PDMS, rectangular channels, 140 um high	Static culture	5 day culture, Cells grew slower in PDMS than in TCPS	Walker, Ozers, Beebe 2002 (Biomedical Microdevices)
Mouse embryo	PDMS	Static culture	Growth rate similar to *in vivo*	Raty et al 2001 (Theriogenology)
Mouse embryo	silicon, PDMS, borosilicate	Static culture	Faster cleavage of embryos, more blastocysts produced, lesser degenerated embryos than control microdrops	Raty et al 2004 (Lab Chip)
HepG2, human heptacarcinoma cells	PDMS, 600 um	Peristaltic pump, 5-10 uL/min	Upto 10^7 cells cultured 12 days, albumin production and glucose consumption was monitored	Leclerc, Sakai, Fujii (2004) Biotech Prog
HepG2, human heptacarcinoma cells	PDMS, 3-dimensional structure	Peristaltic pump, 5-20 uL/min	cells cultured for 10 days, albumin production and glucose consumption was monitored	Leclerc, Sakai, Fujii (2003) Biomed Microdev
GFP expressing adult hippocampal progenitor cells	Microarray Rose chamber, SU-8	Static culture	Parallel tracking of progenitor cell survival and proliferation	Chin et al (2004) Biotech Bioengg
C2C12 murine myoblasts	PDMS, 30 um high	Computerized peristaltic Braille pumps	3 day culture, differentiation of C2C12	Gu et al (2004) PNAS

		and actuators, 3-370 nl/min		
Murine osteoblasts, MC3T3-E1	PDMS, 3D, 400 um high	Static and dynamic (peristaltic pump), 5-25 uL/min	13 day culture, uniform cell growth in 3 D device, flow characterization, ALP staining for cellular activity	Leclerc et al (2005) Biomaterials
Bovine capillary endothelial (BCE) cells	PDMS	Gravity flow	PARTCELL	Takayama et al (2003) Chemistry and Biology, Takayama et al (2001) Nature
E Coli, chicken erythrocytes, BCE cells	PDMS	Gravity flow	Use of laminar flow to pattern cell culture substrate, cell deposition, and culture media	Takayama et al (1999) PNAS
C2C12	PDMS		HOMR	Zhu et al (2004) Analyst
HDMECs	PDMS	Computerized peristaltic Braille pumps and actuators, 0-0.05 uL/sec	Shearing, cell alignment, pulsitile flow	Song et al (2005) Anal Chem
HepG2	PDMS		Single cell analysis, separation of ROS and GSH by on-chip electrophoresis	Sun and Yin (2006) J chromatography A
Primary rat hepatocytes, 3T3-J2 Fibroblasts	Glass	Peristaltic pump,	Microgrooves, OURs,	Park et al (2005) Biotech and Bioengg.
C2C12	PDMS		Reconfigurable protein matrices	Zhu et al. (2005) Nature Matl
Primary rat hepatocytes	Silicon (DRIE)	Syringe pump		Powers et al (2002) Biotech Bioengg

Murine fibroblasts, Chinese hamster ovary (CHO) epithelial cells, hepatocytes	Glass, PDMS, polystyrene, silicon nitride	Syringe pump	NanoLiter BioReactor, 14 days, pH, glucose,	Prokop et al (2004) Biomed Microdev
NIH-3T3, Saos-2 osteoblasts, AML12 hepatocytes, mouse embryonic stem cells, PC-3 prostate cancer cells,	PDMS	Syringe pump	Multiphenotype cell docking	Khademhoss eini et al. (2005) Lab Chip
Human dermal fibroblasts	PDMS		Localized cell trapping	Sinclair and Salem (2006) Biomaterials

Table B2: Device technologies (Chapter 2)

Material	Technology	Results	Reference
PDMS	Backlight soft llithography	Bell shaped microstructures	Futai et al (2004) Adv Mater.
PDMS	Bending planar sheets of channels for pseudo-3D channels, "plug-in and mold" for true 3-D channels	Complex 3D microchannels	Wu et al. (2003) JACS
PDMS	UV grafting of co-mixed monomers (neutral and charged)	Tailoring surface properties	Hu et al. (2004) Langmuir
PDMS	Multilevel photolithography	Complex 3 D microchannels	Anderson et al. (2000) Anal Chem
PDMS	Applying voltage breaks the 20 um PDMS separating disconnected	Configurable microfluidic device: connections can be opened by user	McDonald et al. (2001)

	fluidic channels		Anal Chem

Table B3: PDMS based reviews (Chapter 2)

Topic	Summary	Reference
Design and fabrication of PDMS devices	Single and multilayer systems, intergrated componenets including chaotic mixer, elastomeric switch, magnet filter, embedded membranes, flouresecence detection system	Ng et al. (2002) Electrophoresis
Characterization of PDMS properties	PDMS containing different amount of crosslinker analyzed by gravimetry, contact angle, mechanical testing, XPS, SEM, FTIR, and nanoindentation	Mata et al. (2005) Biomed Microdev
Fabrication of PDMS microfluidic devices		McDonald et al. (2000) Electrophoresis

APPENDIX C

Oxygen Profiles in COC-PU and PS-PU Microbioreactors

The four points of oxygen detection in the microchannel are: upstream (ups), 1 cm from upstream in cell laden channel (x=1), downstream (dwn), and distance of downstream + 0.5 cm (dwn+0.5).

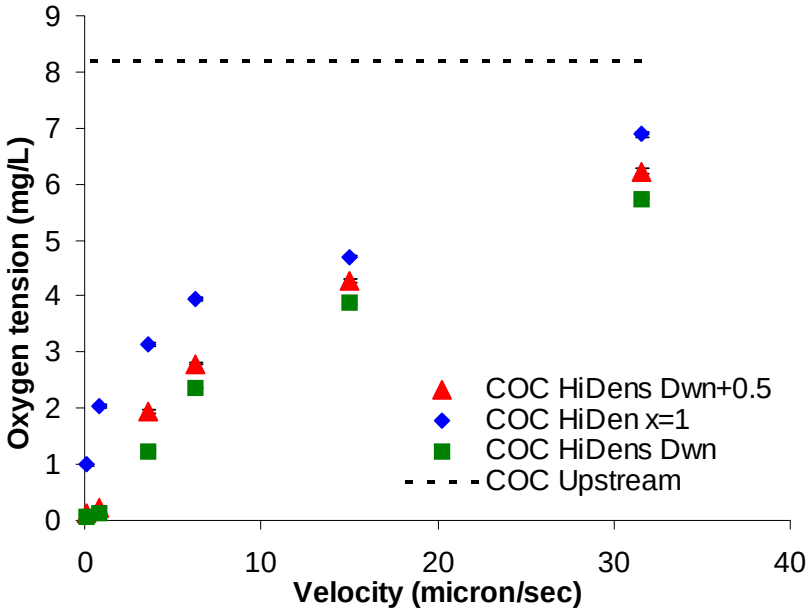

Figure C1: Oxygen profile at four distinct regions in COC-PU microdevice at high (hi dens) cell density of HepG2 cells and channel height of 100µm.

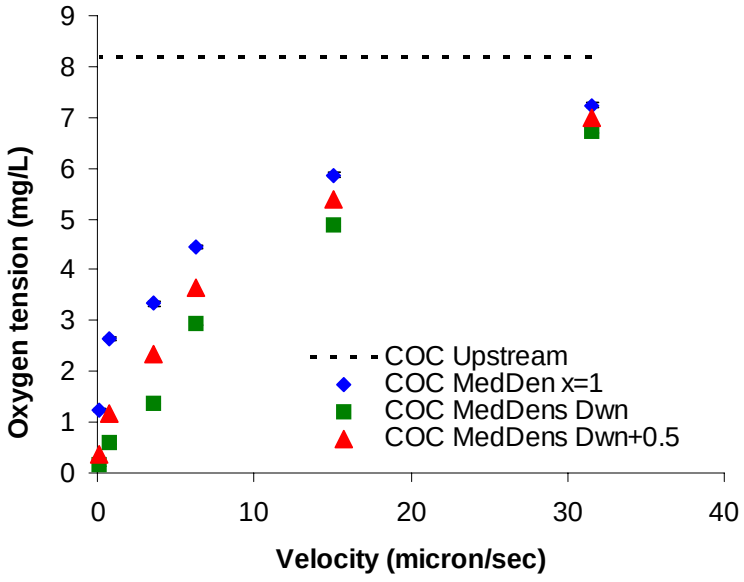

Figure C2: Oxygen profile at four distinct regions in COC-PU microdevice at medium(med dens) cell density of HepG2 cells and channel height of 100µm

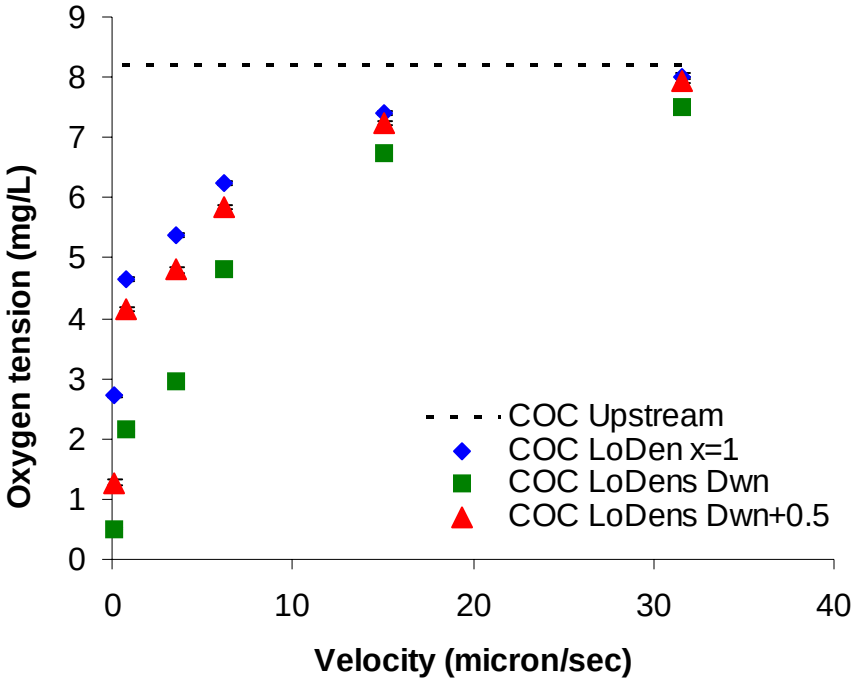

Figure C3: Oxygen profile at four distinct regions in COC-PU microdevice at low (low dens) cell densities of HepG2 cells and channel height of 100µm

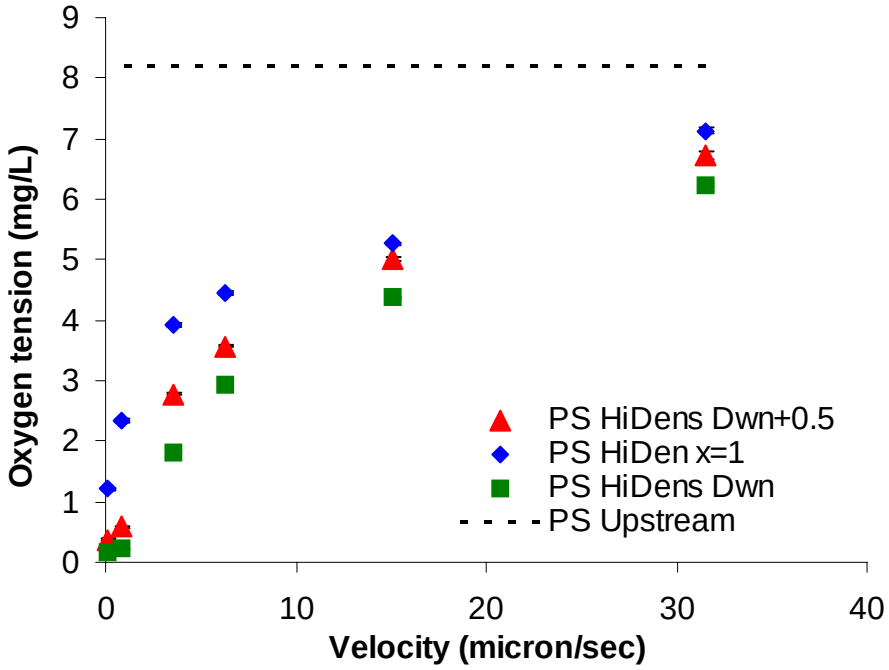

Figure C4: Oxygen profile at four distinct regions in PS-PU microdevice at high (hi dens) cell densities of HepG2 cells and channel height of 100µm

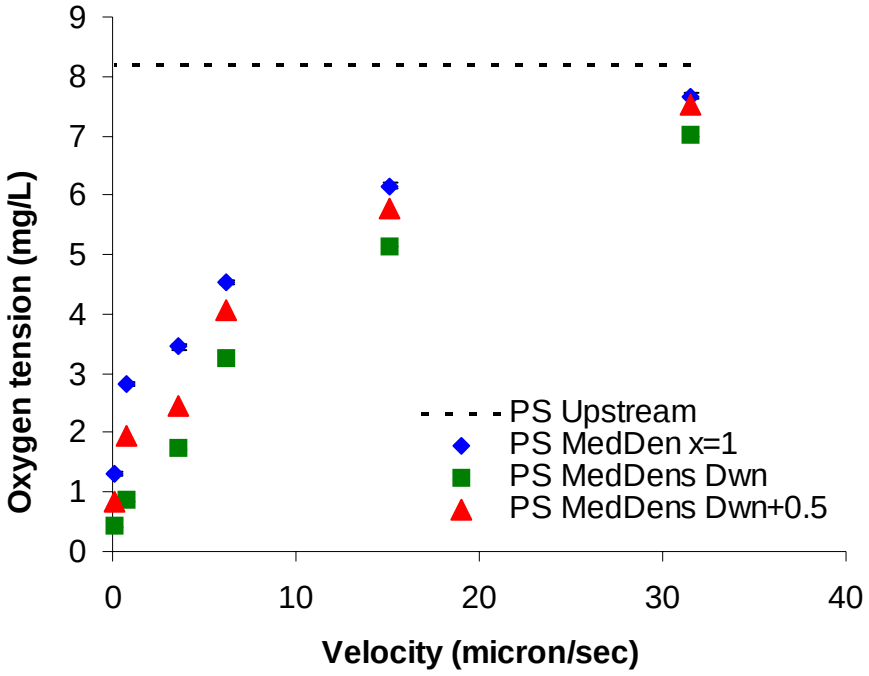

Figure C5: Oxygen profile at four distinct regions in PS-PU microdevice at medium (med dens) cell densities of HepG2 cells and channel height of 100µm

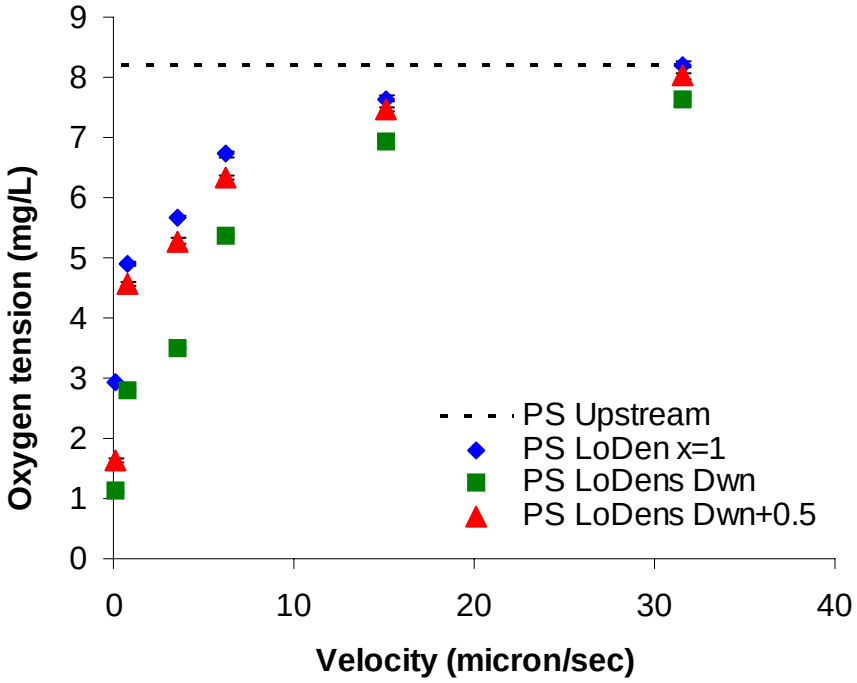

Figure C6: Oxygen profile at four distinct regions in COC-PU microdevice at low (lo dens) cell densities of HepG2 cells and channel height of 100µm

APPENDIX D

Hematopoietic Stem Cell Staining using SLAM-Family Markers

Used in Chapter 7 [From Mark Kiel (Sean J. Morrison Laboratory)]

1. Extract bone marrow from each hind limb (and humerus). Sacrifice the mice by cervical dislocation and then extract bone marrow from each according to the following procedure.

2. Fix the animal to the surgery pad by inserting needles through each paw. Wet pelt with 70% EtOH.

3. Cut the skin at the ankle and up along the side to expose the muscles of the hindlimb. Cut away as much muscle and fascia from the femur and tibia as possible.

4. Using forceps and scissors, pinch the femur and gently pull laterally to dislocate the hip; cut attached muscle and ligament using scissors.

5. Cut the bone at the ankle and remove from animal. Repeat this procedure for each hindlimb.

6. Clean both femur and tibia of muscle by passing through a Kimwipe. Separate femur and tibia by hyperextension at the knee joint. Place the clean bones into a petri dish containing 2 ml of ice-cold staining medium.

7. Cut away both ends of all bones to gain access to the marrow cavity.

8. Using a 3 ml syringe containing ice-cold staining media (2% heat-inactivated calf serum in Hank's Buffered Salt Solution) and 25G needle, separate the contents of the marrow from the bone by flushing the marrow cavity with staining medium. This may be repeated several times for each bone to ensure all marrow has been removed.

9. After flushing all the marrow from the bones, dissociate the marrow by gently pipetting up and down.

10. Filter marrow through nylon mesh into a clean 15ml centrifuge or 5ml FACS tube.

11. Allocate the cell sample into appropriately labeled tubes for subsequent staining.

12. Centrifuge cell suspension for 5 min at 500g. While sample/s is/are being centrifuged, begin to prepare the antibody solutions for subsequent staining steps as below.

13. Aspirate supernatant using a vacuum flask and resuspend the cell pellet in 400 μl of staining media (for 1-2 mice, 800 μl for 3 mice) containing the following antibodies at the specified dilutions:

CD150-PE (TCF15-12F12.2, Biolegend; 1:100),
CD48-FITC (HM48-1, BD Pharmingen; 1:100),
CD41-FITC (MWReg30, BD Pharmingen; 1:100),
Sca-1-APC (E13-161.7, BD Pharmingen; 1:400),
c-kit-biotin (2B8, BD Pharmingen; 1:400),
Ter119- FITC-conjugated lineage antibody (BD Pharmingen; 1:800),
CD2- FITC-conjugated lineage antibody (BD Pharmingen; 1:800),
Gr-1- FITC-conjugated lineage antibody (BD Pharmingen; 1:800),
B220- FITC-conjugated lineage antibody (BD Pharmingen; 1:800),

Inclusion of lineage antibodies in this staining step to enhance the discrimination of true $CD150^{+}CD48^{-}CD41^{-}$ HSCs from background levels of florescence.

14. Incubate cells in antibody solution for 20 min on ice, resuspending the suspension every 5-10 minutes. After 20 min, dilute cell suspension in 15 ml of staining media and centrifuge as above.

15. Aspirate the supernatant and resuspend cell pellet in 400ul of staining media containing the following second step reagents at the specified dilutions: StAv-APCCy7 (1:400). To enrich HSCs, pre-select using MACS, include in this staining step anti-biotin microbeads (Miltenyi Biotec Inc.; 1:10) and select according to manufacturer's instructions after completing step 17 below.

16. Incubate cells in antibody solution for 20 min on ice, resuspending the suspension every 5-10 minutes. After 20 min, dilute cell suspension in 15 ml of staining media and centrifuge as above.

17. Aspirate the supernatant and resuspend pellet in 1 ml of staining media containing 7-AAD (1:500 of 1mg/ml stock). Filter through nylon mesh into a clean 5 ml FACS tube.

18. HSCs are identified as $CD150^{+}CD48^{-}CD41^{-}(lineage^{-})$ in addition to being 7- AAD^{-} $FSC^{mid}SSC^{mid}$. Gating on this population of cells should reveal a 90-95% $Sca\text{-}1^{+}c\text{-}kit^{+}$ double-positive population. The representative FACS plots of first and second sort are shown in Figure D1 and D2.

19. For color compensation, create the following FACS tubes with bone marrow cells: blank (no color), PE (CD48), FITC (CD48), APC (Sca-1), Biotin-Streptavidin or PHAR (c-kit biotin developed with StAv-APC-Cy7), and 7-AAD.

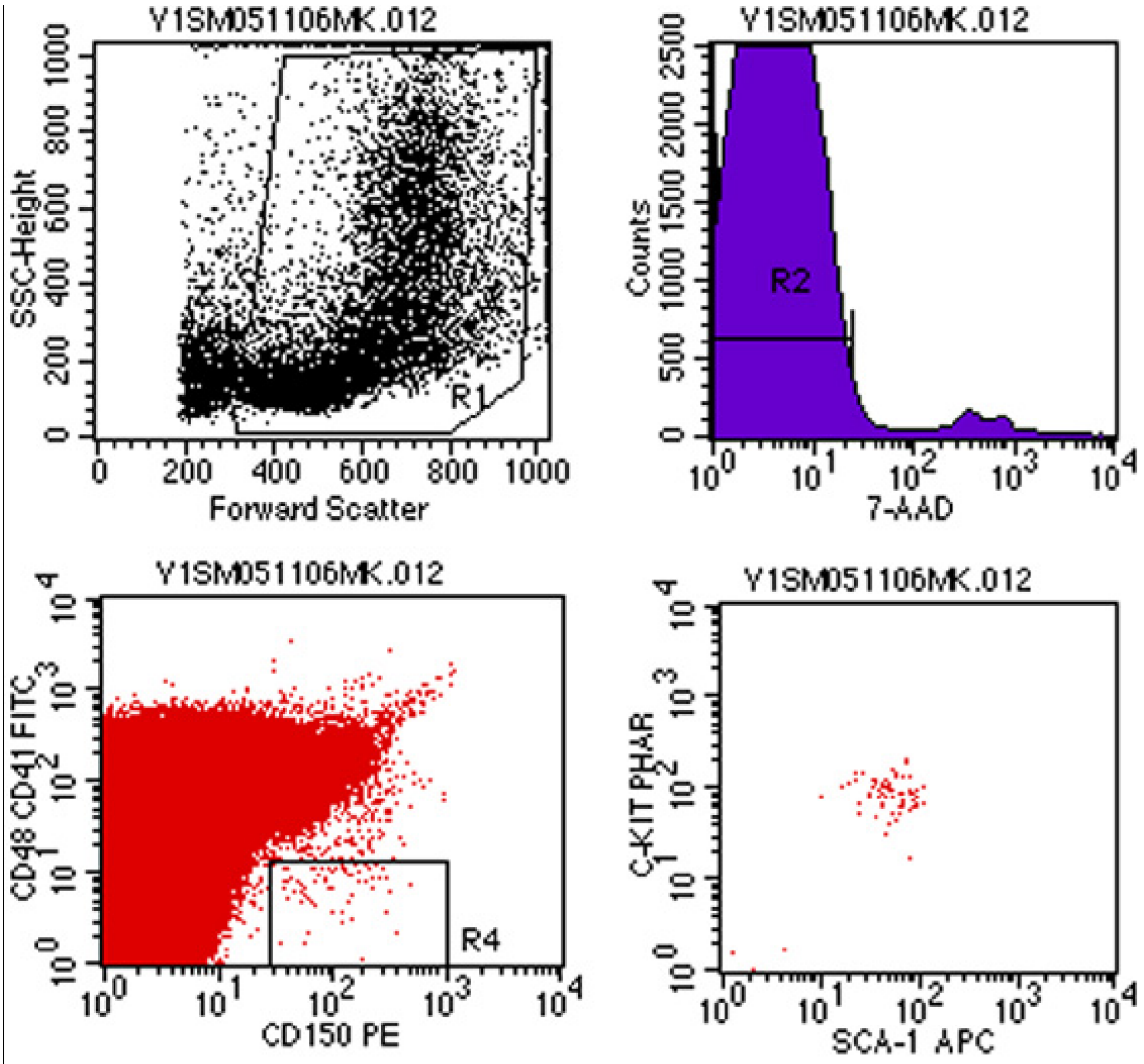

File: Y1SM051106MK.012
Sample ID: 5/11 BA BM
Gate: .R1.R2.R3

Region	Events	% Gated
R1	792299	100.00
R2	792299	100.00
R3	792299	100.00
R4	73	0.01

File: Y1SM051106MK.012
Sample ID: 5/11 BA BM
Gate: .R1.R2.R3.R4

Region	Events	% Gated
R1	73	100.00
R2	73	100.00
R3	73	100.00
R4	73	100.00

Figure D1: Representative first FACS sort from bone marrow cells enriched in HSCs.

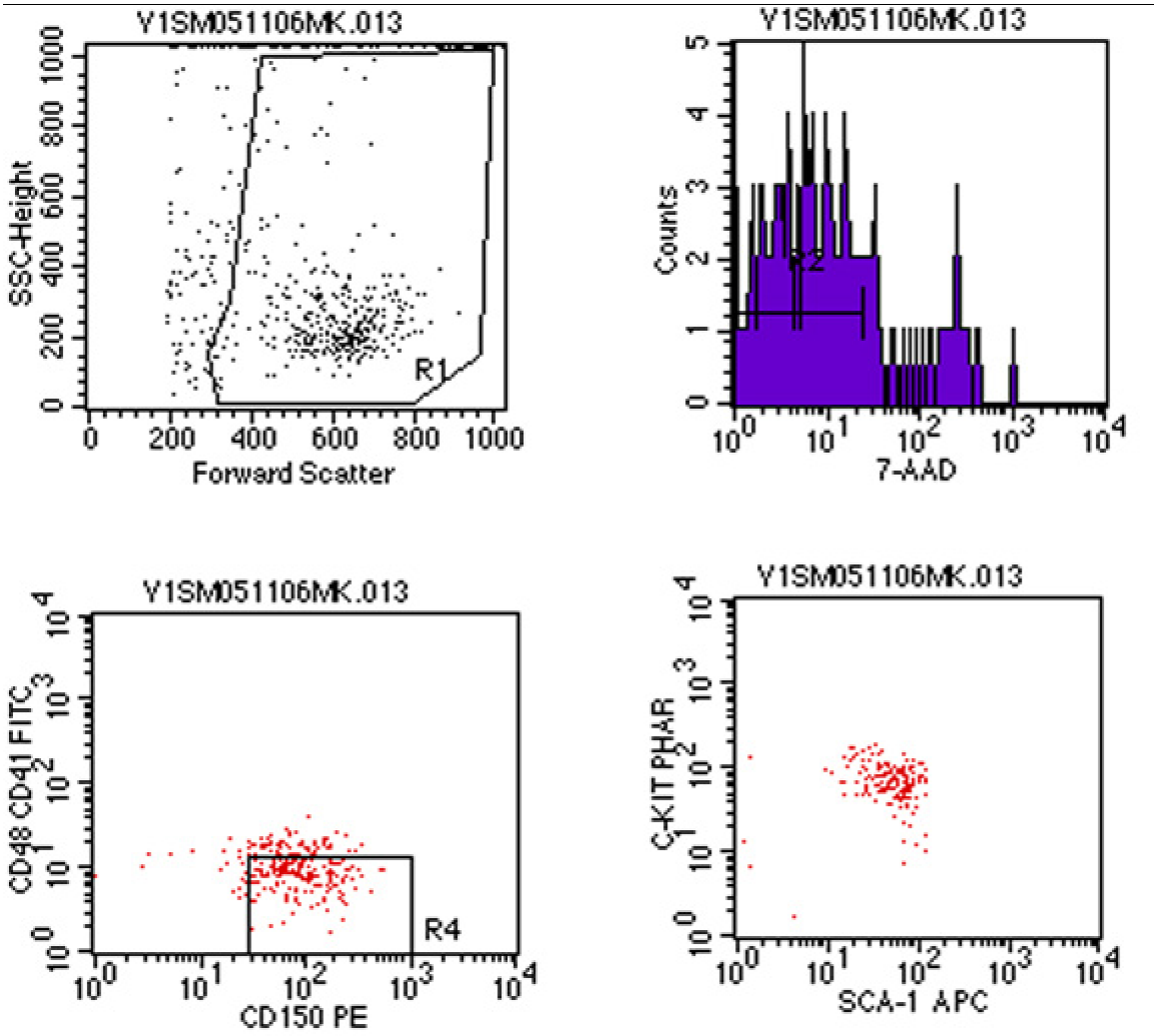

File: Y1SM051106MK.013
Sample ID: 5/11 BA BMresort
Gate: .R1.R2.R3

Region	Events	% Gated
R1	272	100.00
R2	272	100.00
R3	272	100.00
R4	176	64.71

File: Y1SM051106MK.013
Sample ID: 5/11 BA BMresort
Gate: .R1.R2.R3.R4

Region	Events	% Gated
R1	176	100.00
R2	176	100.00
R3	176	100.00
R4	176	100.00

Figure D1: Representative double FACS sort from bone marrow cells enriched in HSCs.

APPENDIX E

Stem Cell Tech EasySep Lineage$^-$ and Sca-1$^+$ / c-kit$^+$ Selection from Mouse Bone Marrow Cells

Used in Chapter 7 for removing Lin$^-$ cells from bone marrow and selecting c-kit$^+$ cells.

For Lineage$^-$ Selection:

1. Prepare single nucleated cell suspension at a concentration of **1 x 10^8 cells/mL** in recommended mediumcontaining 5% Normal Rat Serum and 2 mM EDTA. Cells must be placed in a 5 mL (12 x 75 mm) polystyrene tube to properly fit into the purple EasySep® Magnet. **Do not exceed a volume of 2.0 mL (i.e. 2 x 10^8 cells) per 5 mL tube** or 8.5 mL (i.e. 8.5 x 10^8 cells) per 14 mL tube.
Falcon™ 5 mL (Becton Dickinson Catalog #352058) or 14 mL (Catalog #352057) Polystyrene Round-Bottom Tubes are recommended.

2. Centrifuge the tube of EasySep® Mouse Hematopoietic Progenitor Enrichment Cocktail before use to ensure recovery of entire contents. Add cocktail at **50 µL/mL of cells** (e.g. for 2 mL of cells, add 100 µL of cocktail). Mix well and incubate in refrigerator (4-8°C) for 15 minutes.

3. Wash cells and resuspend at 1 x 10^8 cells/mL in recommended medium. Centrifuge cells.

4. Add EasySep®Biotin Selection Cocktail at **100 µL/mL of cells** (e.g. for 2 mL of cells, add 200 µL of selection cocktail). Mix well and incubate in refrigerator (4-8°C) for 15 minutes.

5. **Vortex** EasySep® Mouse Progenitor (M Prog) Magnetic Microparticles to ensure that they are in a uniform suspension. Add the microparticles at **100 µL/mL of cells** (e.g. for 2 mL of cells, add 200 µL of microparticles). Mix well and incubate in refrigerator (4-8°C) for 10 minutes.

6. Bring the cell suspension to a **total volume** of 2.5 mL by adding recommended medium (Normal Rat Serum is not required at this stage). Mix the cells in the tube by gently pipetting up and down 2 - 3 times. Place the tube (without cap) into the magnet. Set aside for three minutes.

7. Pick up the EasySep® Magnet, and in one continuous motion invert the magnet and tube, pouring off the desired fraction into a new polystyrene tube. The magnetically labeled unwanted cells will remain bound inside the original tube, held by the magnetic field of the magnet. Leave the magnet and the tube in inverted position for 2-3 seconds, then return to upright position. *Do not shake or blot off any drops that may remain hanging from the mouth of the tube.*
The enriched cells in the new tube are now ready for use.

8. After this step place the new tube with the desired fraction back in the magnet and incubate for ten minutes.

9. Then perform another pour of as per the instructions in step 7. Once again your desired cells are in the pour off.

10. It will then be necessary to spin down your cells and proceed to step one in the 18757 protocol.

For Sca-1$^+$ or c-kit$^+$ Selection:

1. This procedure is used for processing up to 2 x 10^8 cells per preparation. Prepare a single cell suspension at a concentration of 1 x 10^8 cells/mL in recommended medium. For samples containing 10^7 cells or fewer, resuspend in 100 µL. At this point, cell suspension must be in a 12 x 75 mm polystyrene tube to properly fit into the EasySep® Magnet.
Falcon™ 5 mL Polystyrene Round-Bottom Tubes (Becton Dickinson, Catalog #352058) are recommended.

2. Add CD117 (cKit) PE Labeling Reagent at 50 µL/mL of cells (e.g. for 2 mL of cells, add 100 µL of labeling reagent). Mix well and incubate at room temperature for 15 minutes.

3. Add EasySep® PE Selection Cocktail at 70 µL/mL cells (e.g. for 2 mL of cells, add 140 µL of cocktail). Mix well and incubate at room temperature for 15 minutes. *Note: PE Selection Cocktail is supplied in excess and may be discarded when CD117 (cKit) PE Labeling Reagent vial is empty.*

4. Mix EasySep® Magnetic Nanoparticles to ensure that they are in a uniform suspension by pipetting vigorously up and down 5 times. Add the nanoparticles at 50 µL/mL of cells (e.g. for 2 mL of cells, add 100 µL of nanoparticles). Mix well and incubate at room temperature for 10 minutes.

5. Bring the cell suspension to a total volume of 2.5 mL by adding recommended medium. Mix the cells in the tube by gently pipetting up and down 2-3 times. Place the tube (without cap) into the magnet. Set aside for five minutes.

6. Pick up the magnet, and in one continuous motion invert the magnet and tube, pouring off the supernatant fraction. The magnetically labeled cells will remain inside the tube, held by the magnetic field of the EasySep® Magnet. Hold the magnet and tube in inverted position for 2-3 seconds, then return to upright position. *Do not shake or blot off any drops that may remain hanging from the mouth of the tube.*

7. Remove the tube from the magnet and add 2.5 mL of recommended medium. Mix the cell suspension by gently pipetting up and down 2-3 times. Place the tube back in the magnet and set aside for five minutes.

8. Repeat Steps 6 and 7 two times, and then Step 6 once more, for a total of four 5-minute separations in the magnet. Remove tube from magnet and resuspend cells in an appropriate amount of desired medium. These positively selected cells are now ready for use.

CFC assay using MethoCult

Summary of % recovery and fold enrichment of CFC from mouse bone marrow enriched for CD117+(c-kit) or Sca-1+ cells using EasySep™ positive selection

Positive selection only

target cell	n	number of CFC/1000 cells	total CFC % recovery	Fold enrichment	n	number of CFC/ 1000 cells	total CFC % recovery	fold enrichment
Unseparated	12	3.4 ± 1.0	-		12	3.4 ± 1.0	-	
		2x separated*				***4x separated****		
c-kit+	6	32 ± 15	77 ± 15	9 ± 4	11	70 ± 18	57 ± 17	26 ± 12
Sca-1+	6	23 ± 7	54 ± 18	6 ± 3	11	29 ± 9	35 ± 14	10 ± 6

Values are means ± 1 sd; n= no. of expt´s.

* 2 or 4 rounds of separation

Positive selection followed by lineage depletion with SpinSep™

target cell	n	number of CFC/1000 cells	total CFC % recovery	Fold enrichment
c-kit+ -> lin depletion	3	95 ± 4	26 ± 11	59 ± 28
Sca-1+ -> lin depletion	3	57 ± 22	8 ± 4	33 ± 16

Values are means ± 1 sd

APPENDIX F

Blood and Bone Marrow Cells

Background information for Chapter 8

PERIPHERAL BLOOD SMEARS:
- only contains mature cells (no precursors)
- cell types:
  - erythrocytes (RBCs)
  - platelets
  - leukocytes (WBCs)
    - granulocytes: neutrophils, basophils, eosinophils
    - agranulocytes: lymphocytes, monocytes (macrophages)

PERIPHERAL BLOOD SMEARS

1. **erythrocyte**
   - largest proportion of cells in the blood
   - biconcave discs (7-8 μm)
   - lack nucleus and cellular organelles
   - cotains hemoglobin (carries O_2 and CO_2)
2. **neutrophil (polymorphonuclear leukocyte, PMN)**
   - 50-70% of WBCs in peripheral blood
   - diameter = 10-12 μm (larger than RBC)
   - **3-5 lobed nucleus stains deep purple**
   - pale cytoplasm
   - small, light purple granules
     - few azurophilic (1°) granules (myeloperoxidase, lysosomal enzymes)
     - many specific (2°) granules (lysozyme, collagenase)
   - function: acute inflammation (exit circulation to site of injury, phagocytose pathogen, granules fuse with phagosome to destroy pathogen)
3. **basophil**
   - rare, hard to find (less than 1% of WBCs)
   - diameter = 8-14 μm
   - lobulated nucleus, obscured by granules
   - **dark blue specific granules of varying sizes**
     - contain hydrolytic enzymes, heparin sulfate, histamine, slow reacting substance, SRS
   - act like tissue mast cells, bind antigen specific IgE, exposure to antigen releases vasoactive substances from granules, leads to inflammation
4. **eosinophil**
   - 2-4% of WBCs
   - diameter 10-14 μm
   - **bilobed nucleus**
   - **bright pink eosinophilic granules of uniform sizes**

    - contain arginine rich major basic protein, peroxidase, histaminase, arylr-sulfatase
- important in allergic reactions, parasitic infections, and phagocytosis of antibody-antigen complexes

5. monocytes
- 3-8% of WBCs
- diameter 9-18 μm (usually larger than PMN's)
- **kidney shaped nucleus, less compact nucleus than PMN**
- pale, basophilic cytoplasm without specific granules, but do contain azurophilic lysosomes
- exit circulation to tissues, differentiate into phagocytes (macrophage, osteoclast, alveolar macrophage, etc)
- differentiated monocytes function in phagocytosis & antigen presentation to lymphocytes

6. lymphocytes
- 20-40% of WBCs
- diameter = 6-12 μm
- **intensely staining, round to oval nucleus; may be slightly indented**
- **thin, pale blue rim of cytoplasm WITHOUT granules**
- B cells & T cells are indistinguishable
    - B cells: function in antibody production, carry Ig on plasma membrane which recognize antigen
    - T cells: function in cell mediated immunity, destroy virally infected cells, provide help to B cells

ERYTHROID SERIES

PROERYTHROBLAST
- relatively large cell 12-15μm in diameter
- large, central, spherical nucleus with one or two nucleoli
- cytoplasm: moderately basophilic (blue) due to ribosomes
- look for an unstained region of cytoplasm=Golgi ghost

BASOPHILIC ERYTHROBLAST
- smaller than proerythroblast
- checkerboard nucleus (heterochromatic and smaller)
- intense basophilia (blue) due to lots of free ribosomes

POLYCHROMATOPHILIC ERYTHROBLAST
- smaller than basophilic erythroblast
- smaller intensely heterochromatic nucleus
- purple/lilac cytoplasm due to combo of basophilia from ribosomes and eosinophilia from increasing amount of hemoglobin
- LAST MITOTIC STAGE

NORMOBLAST
- smaller than polychromatophilic erythroblast
- small, compact, intensely staining nucleus; getting ready to extrude the nucleus
- eosinophilic cytoplasm (abundant hemoglobin); NOTE: the color of a normoblast is close to the normal pinkish color of the mature erythrocyte

RETICULOCYTE
- immature erythrocyte that still retains some basophilia due to the presence of RNA
- only seen with a special (supravital) stain on the peripheral smear
- increased # seen with anemia

ERYTHROCYTE
- smallest (7-8 μm)
- NO NUCLEUS
- Acidophilic (pink)

TRENDS
Immature → Mature
Basophilic → Eosinophilic
Large euchromatic nuclei → heterochromatic → pyknotic → no nucleus

GRANULOCYTE SERIES

MYELOBLAST
- 15-20 μm
- large, euchromatic, spherical nucleus (>3nucleoli)
- basophilic cytoplasm with no granules
- prominent nucleoli
- can be seen in peripheral blood with certain leukemias

PROMYELOCYTE
- 18-24 μm
- Large nucleus
- **Golgi ghost**
- **azurophilic granules (purple) **
- CANNOT tell which type of granulocyte it will develop into

MYELOCYTE (Neutrophilic, Basophilic, or Eosinophilic)
- smaller
- eccentric, spherical nucleus
- ** granules specific to N,B,E appear**

- LAST MITOSIS

METAMYELOCYTE
- **indented, heart-shaped nucleus**
- many cell-specific granules

BAND CELL
- immature granulocyte
- U-shaped nucleus just prior to segmentation
- increased # seen with acute infections (a left shift)

MATURE GRANULOCYTE
- Neutrophil, Eosinophil, or Basophil
- Segmented nucleus

TRENDS:
Immature → Mature
Large cell → Small cell
No granules → Azurophilic (non-specific) granules → Cell-specific granules
Round nucleus → indented nucleus → U-shaped → multilobed (specific for cell type)

PLATELET PRECURSOR

MEGAKARYOCYTE
- HUGE compared to other cells
- Contain multi-lobed nucleus (as opposed to osteoclasts which are multinucleated)
- Platelets are formed by invaginations of the plasma membrane that fuse to form clefts that eventually break off

APPENDIX G

Efficacy of Microfluidic *In Vitro* HSC Niches tested by *In Vivo* Experiments

Device preparation for HSC Co-culture

- Device assembly: PDMS mortar 3:2 Toulene: PDMS
- Desiccated to remove all air + O2 for 24 - 48 hours
- Put in hypoxia chamber at 1% N2 for 24 - 48 hours
- Plasma oxidized for 2-3 minutes
- FN (0.4 mg/ml) coating for 30 minutes
- UV sterilization for 30 minutes
- Myelocult media (containing 25% serum, horse + bovine 1:1) in devices
- Hypoxia chamber compartments: UV for 30 minutes

Experimental Groups

- Donor HSCs: adult (6- to 8-week-old) C57BL/Ka-CD45.2:Thy-1.1 mice
- Donor supporting cells: adult C57BL/Ka-CD45.1:Thy-1.2 mice
- Recipient mice in reconstitution assays: adult C57BL/Ka-CD45.1:Thy-1.2 mice

- Microfluidic culture groups:
  - HSC control (1:0)
  - HSC - osteoblast co-culture (1:100)
  - HSC - mesenchymal stem cell co-culture (1:100)
  - HSC - megakaryocytes co-culture (1:100)
  - HSC - endothelial cells co-culture (1:100)
  - HSC - megakaryocytes- endothelial cells co-culture (1:50:50)
  - HSC - megakaryocytes- endothelial cells- mesenchymal stem cell co-culture (1:34:33:33)
  - HSC - mixed culture with all above supporting cells (1:25:25:25:25)
  - HSCs (5 minute culture)
  - HSCs (24 hour culture)

- 3-9 devices for each condition (total 85)
- Devices seeded with support cells 24-48 hours before adding HSCs
- 7 day culture experiments in microdevices at 1 % O2
- 42 - 50 HSCs in each device
- HSCs: CD 150^{+} CD 48^{-} $CD41^{-}$ Lin^{-} Sca-1^{+} c-kit $^{+}$ FACS double sorted
- Devices in hypoxia chamber filled with 1% O2 + 6% CO2 + 93% N2 for 2-3 minutes
- Control experiments: All experimental groups in 96 well plates
- Megakaryocyte progenitors (FACS double sorted)
- Megakaryocyte progenitors and HSCs also placed in Methylcellulose gel for CFU
- Media replaced daily in devices for 7 days

    - Time for devices to equilibrate to 1 % oxygen after going back into incubator
- Removal of cells from devices- efficiency of removal
    - Cells removed using enzyme free cell dissociation buffer
- Cells from one microdevice injected into one mouse via retro orbital sinus

Media Formulations

- Primary mouse osteoblasts
    - Alpha-MEM (without AA) + 10% FBS + 1% antibacterial/mycotic
    - Bone specific media: Alpha-MEM (without AA) + 10% FBS + 10-8 M DMSO + 10 mM β-glycerophosphate + 50 mg/L L- ascorbic acid- 2-phosphate + 1% antibacterial/mycotic

- Primary mouse mesenchymal stem cells
    - Alpha-MEM (without AA) + 10% FBS + 1% antibacterial-antimycotic

- Primary mouse endothelial cells
    - EGM-2MV (Lonza) media supplemented with endothelial growth factors

- Primary mouse megakaryocytes (megakaryocyte progenitors FACS isolated, to be expanded in culture)
    - Media: IMDM + 10% FBS + 1% antibacterial-antimycotic + 2 mM GlutaMax-1 + 0.1mM non-essential amino acid + 1 mM sodiumpyruvate + 50 mM 2-mercaptoethanol + SCF (25 ng/ml) + Flt3 ligand (25 ng/ml) + IL-11 (25 ng/ml) + IL-3 (10 ng/ml) + Tpo (25 ng/ml) + Epo (2.5 U/ml) +GM-CSF (10 ng/ml)

- HSC expansion media: StemSpam (StemCell Tech) + 10 micro g/mL heparin + 10 ng/mL mouse SCF + 20 ng/mL mouse TPO + 20 ng/mL mouse IGF-2 + 10 ng/mL human FGF-1 + 5 ng/ml IL-3 + 6 U/ml human EPO +100 ugm/ml human insulin + 1 % deionized BSA

Mouse Mature Megakaryocytes Isolation

- Isolate marrow as usual (2 mice)
- Have one of the centrifuges left open to warm to RT (leave a note to others that it should be left open)
- Stain the cells with CD41-FITC (1:200) for 20 min on ice
- Dilute and centrifuge as usual
- Resuspend in anti-FITC MACS beads (1:10) for 20 min on ice
- Dilute and centrifuge as usual
- Resuspend pellet in 6 ml of staining media
- Aliquot 3 ml of FICOLL medium into two 15 ml tubes

- Carefully pipet 3 ml of cells onto each FICOLL tube ensuring that the separation between layers is preserved
- Centifuge at 800 RCF for 15 min at RT
- A leukocyte band should appear in the middle of the liquid column- the megs (and erythroid cells) are in the pellet
- Resuspend the pellets in 3 ml total and select once (for recovery) or twice (for purity) using the autoMACS
- Examine the end result under the inverted microscope to document purity- Megakaryocytes are substantially larger than other leukocytes

Mouse Pups Liver and Spleen Endothelial Cells Isolation

Livers and spleens from BA pups (less than 5 days old)

Need:
2% FBS + HBSS (Ca, Mg free)
Collagenase IV
37 C shaking water bath

- 3 pups
- 3 days old
- Isoflurane in mouse room
- Anaesthized
- Brought up to lab and chopped heads off
- Opened the body cavity (working media: 2% FBS + HBSS free)

- Took off viscera
- Below diaphragm
- Red tissues are liver and spleen
- Three-four lobes of liver
- Spleen just behind the stomach (like a red cylinder)
- Stomachs white-filled with milk
- Pinch off livers like a bud from behind don't chop off from front or will lose tissue
- 5 min 1500 rpm
- Remove the supernatant
- Sterile filter 10% FBS+ HBSS+ 1% Collagenase IV
- 18 gage needle
- Triturate 5-6 times
- 37 C shaking water bath 1.5 hours
- After 20 minutes, each 20 minutes, triturate with a 25 gauge needle

- ***FACS (Flow Cytometry)***

- Working media: RPMI 1640
- Isotype control (CD 31 only, CD 105 only, Sca-1 only)
- Live dead stain (7AAD or DAPI)
- All staining on ice
- CD 31 (PE) 1:100
- CD 105 (biotin) 1:100
- Sca-1 (FITC) 1:400
- Streptavidin (APC Cy5) 1:400 (for biotin)

Microfluidic Device Design for Co-culture of HSCs and Support Cells

- Small number of cells
- Different supporting cells
- Gentle replacement of media from bottom channel by convective diffusion

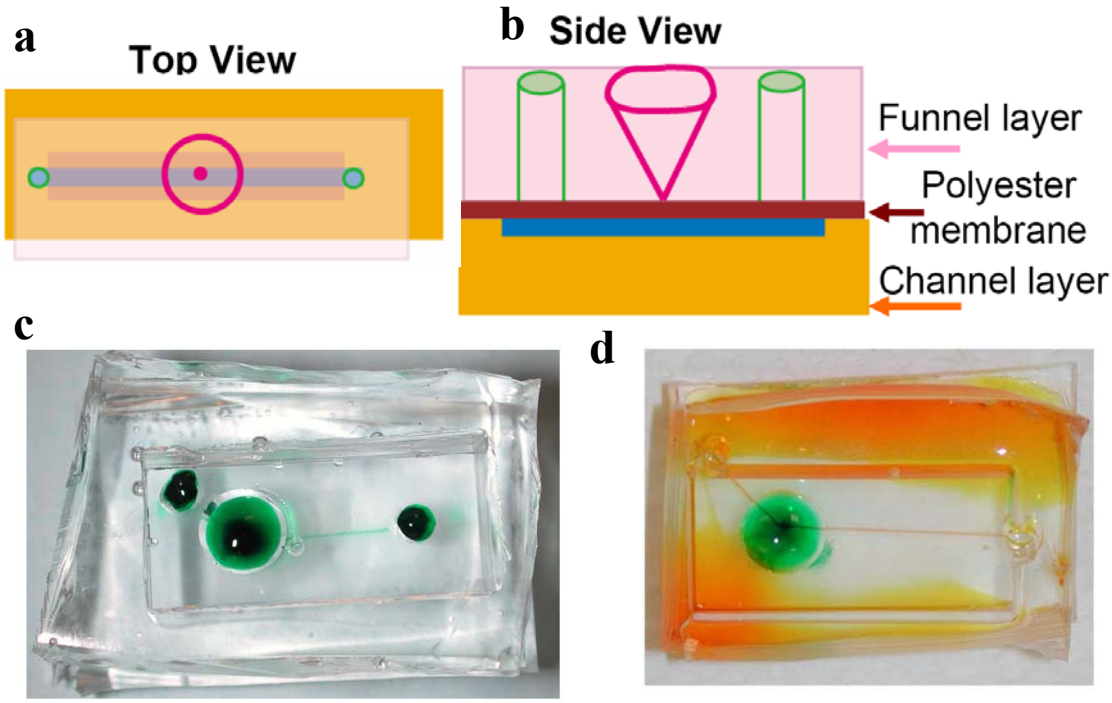

Figure G1: Semi porous membrane based microfluidic device for co-culture of FACS sorted HSCs and support cells

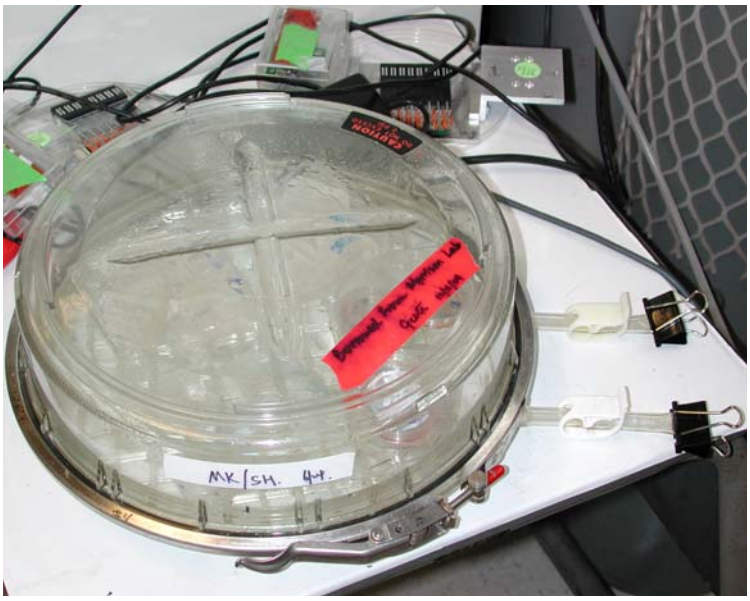

Figure G2: Hypoxia chamber for maintaining 1% oxygen in microfluidic cultures of HSCs and support cells

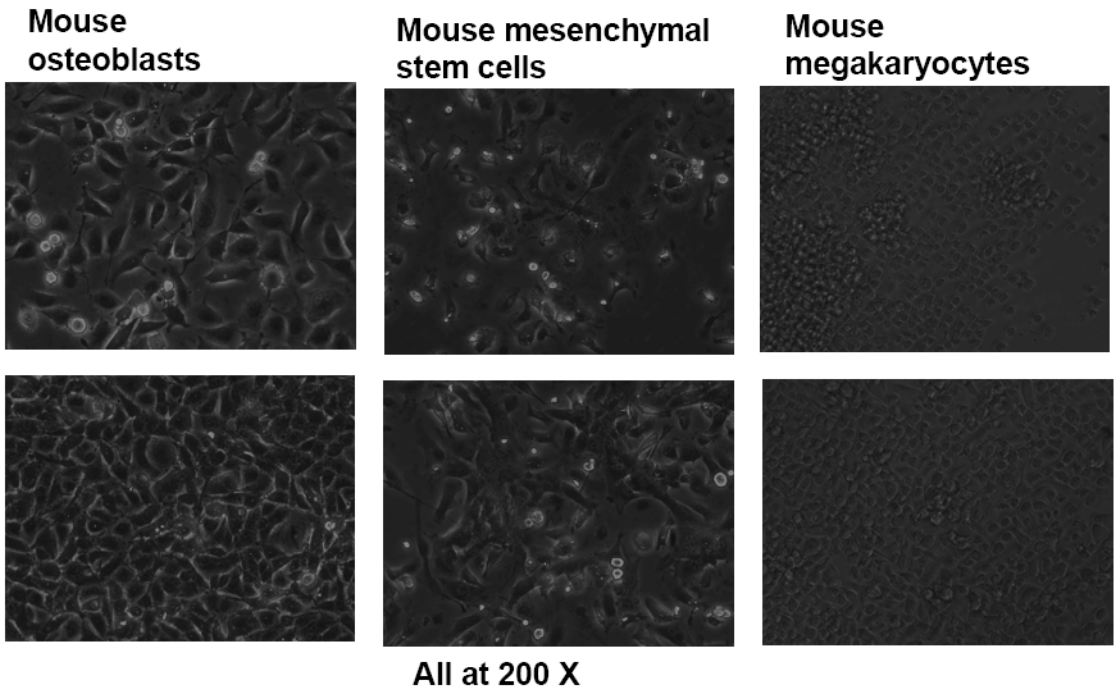

Figure G3: Osteoblasts, mesenchymal stem cells and megakaryocytes used as supporting cells for HSC microfluidic culture

Figure G4: C57BL/6 mouse for isolation of bone marrow cells

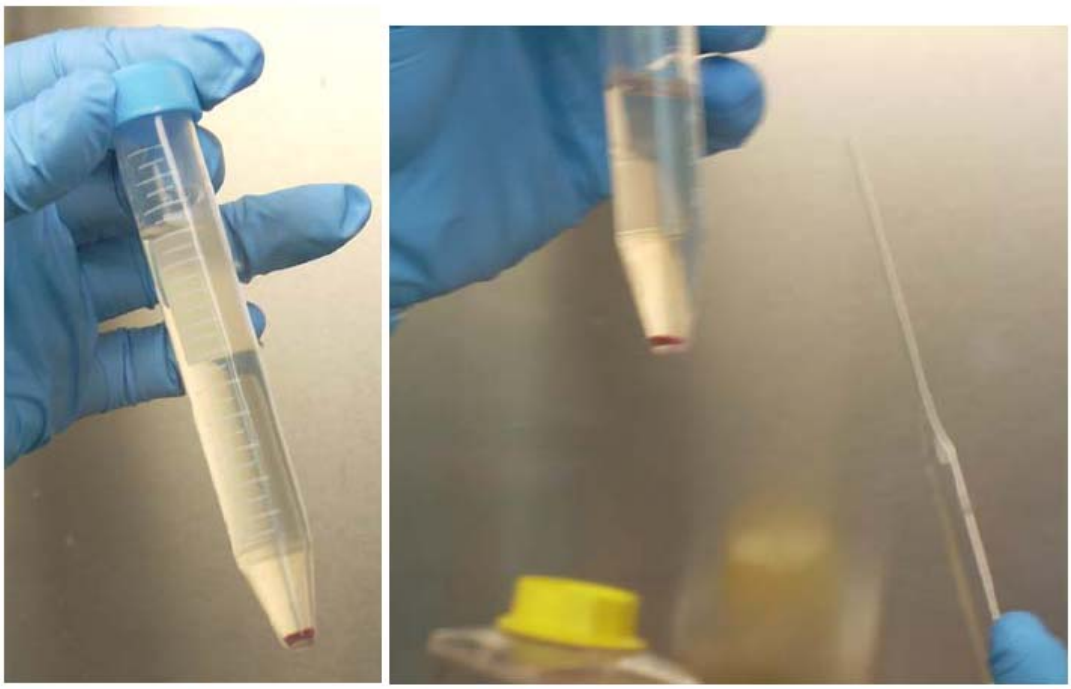

Figure G5: Bone marrow cells from femurs, tibias and humeruses of two mice

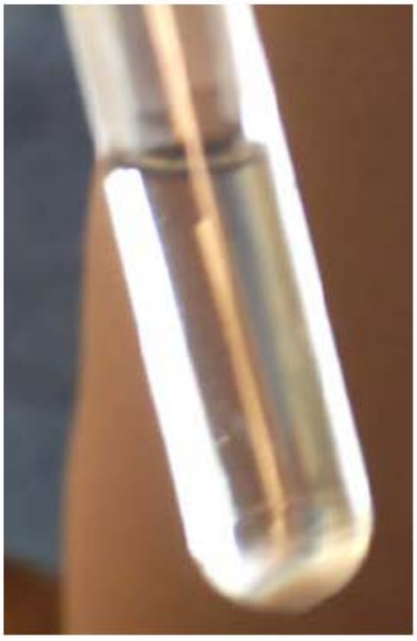

Figure G6: Cell suspension containing bone marrow cells from two mice enriched in Lin^{-} $c\text{-}kit^{+}$ cells using aMACS

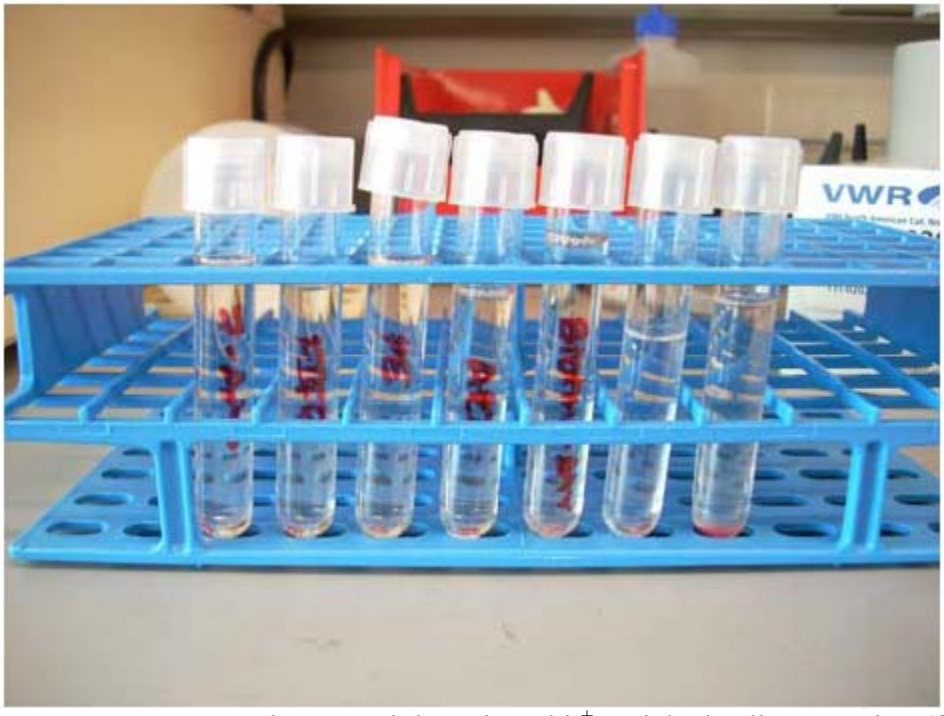

Figure G7: FACS tubes containing Lin^{-} $c\text{-}kit^{+}$ enriched cell suspension (far right) and color compensation cell samples for FACS

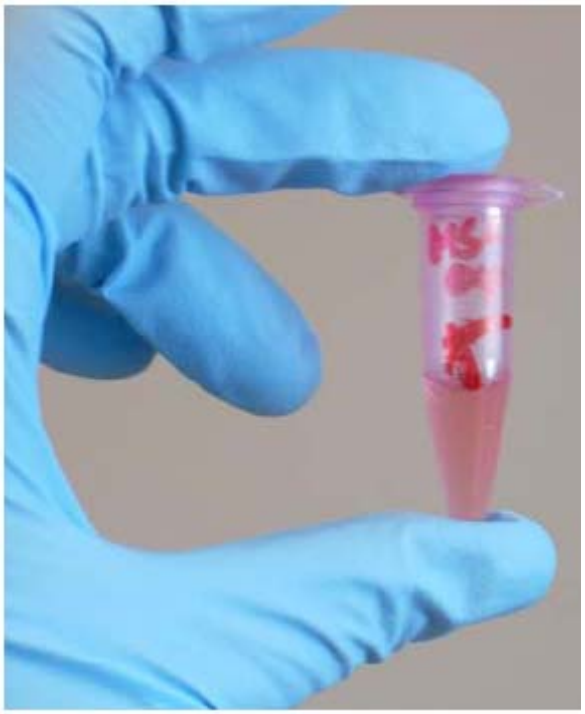

Figure G8: Aliquoted 400 µl of HSC expansion media for collecting FACS sorted HSCs

Efficacy of *In Vitro* HSC Niche

- After removal from microfluidic devices, 'test' cells prepared for *in vivo* injection in lethally irradiated Ly 5.2 mice (500 cGy for 5 minutes)
- 300,000 radio protective bone marrow cells (RPD) from BA mice
- Injection of RPD + test cells through retro orbital sinus after anaesthetizing mice with isoflurane
- Mice given antibiotic water for first 3 days after injection
- Four weeks after injection, peripheral blood of host mice analyzed for cells from donor mice
- Subsequent peripheral blood analysis at 8, 12, and 16 weeks

Peripheral Blood Analysis

- Peripheral blood from mice tail
- Cells from donor CD 45.2 mice
- FITC-conjugated anti-CD45.2 antibody (clone A20)
- B220: B Cells
- Mac-1: Myeloid cells
- Gr-1: Granulocytes
- CD 3: T cells
- FACS: Look at myeloid, B and T cells originating from HSCs cultured in microfluidic devices

FACS Plot

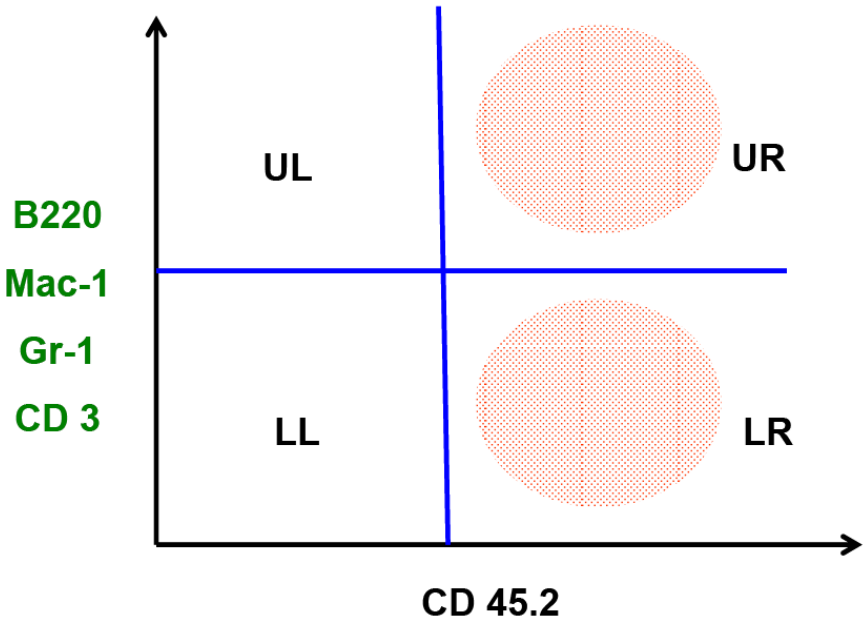

Figure G9: Representative FACS plot of myeloid, B and T cells against CD45.2 antibody

B220 and MAC-1

Gate: ALL CELLS

Quad	Events	% Gated
UL	2959	60.11
UR	2	0.04
LL	1960	39.81
LR	2	0.04

Negative Control

Gate: ALL CELLS

Quad	Events	% Gated
UL	1505	30.57
UR	6	0.12
LL	3410	69.27
LR	2	0.04

Gate: ALL CELLS

Quad	Events	% Gated
UL	0	0.00
UR	1170	34.65
LL	14	0.41
LR	2193	64.94

Positive Control

Gate: ALL CELLS

Quad	Events	% Gated
UL	3	0.09
UR	1229	36.39
LL	10	0.30
LR	2135	63.22

Gr-1 and CD3

Gate: ALL CELLS

Quad	Events	% Gated
UL	8355	63.03
UR	9	0.07
LL	4891	36.90
LR	1	0.01

NEGATIVE Control

Gate: ALL CELLS

Quad	Events	% Gated
UL	3748	28.27
UR	7	0.05
LL	9495	71.63
LR	6	0.05

Gate: ALL CELLS

Quad	Events	% Gated
UL	22	0.53
UR	892	21.47
LL	18	0.43
LR	3222	77.56

POSITIVE Control

Gate: ALL CELLS

Quad	Events	% Gated
UL	1	0.02
UR	646	15.55
LL	17	0.41
LR	3490	84.02

CFU colonies

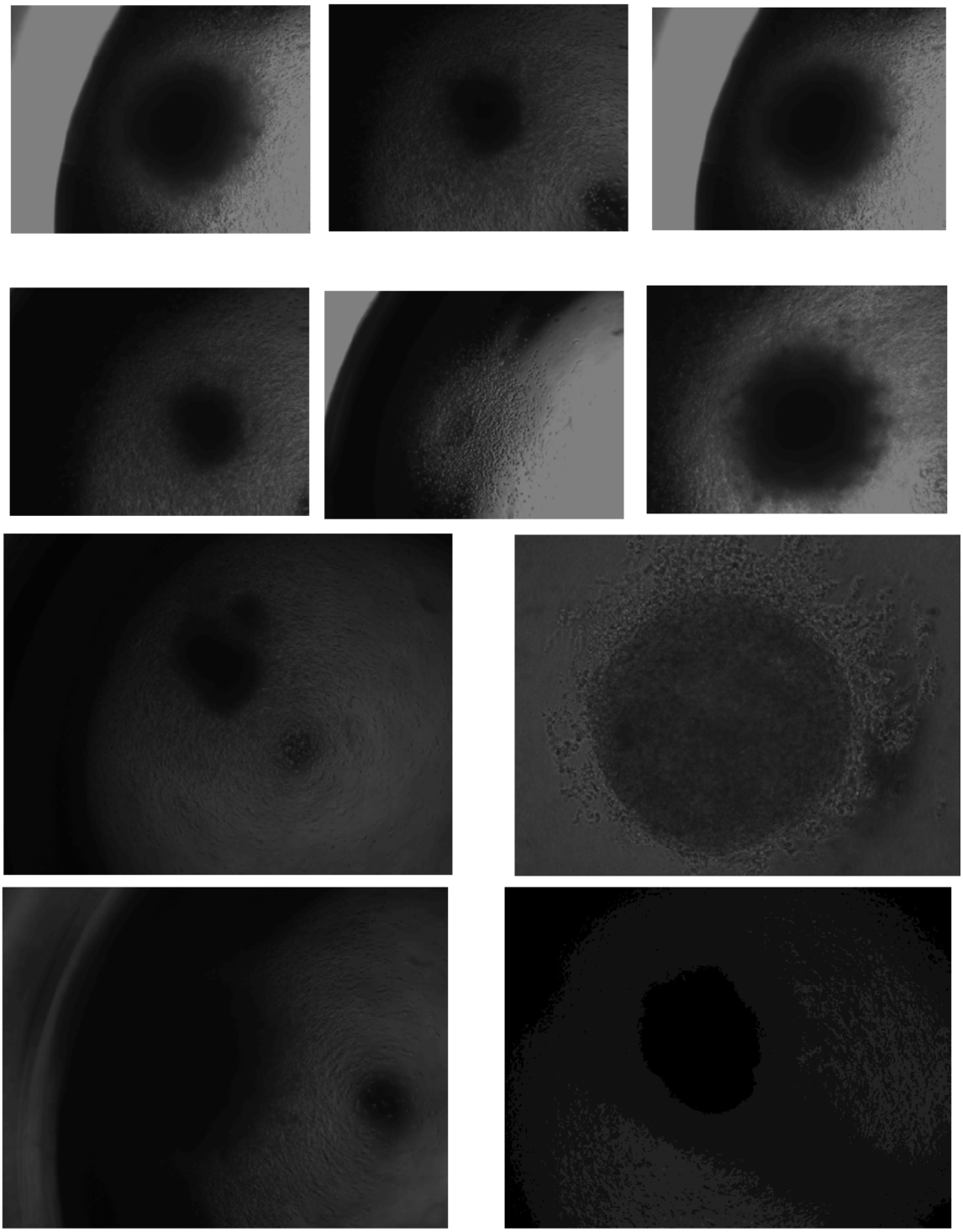

Figure G10: Representative colonies obtained from CFU assays

Reasons for No *In Vivo* Engraftment

- Ineffective cell removal
- Cell death
- Not enough HSCs in microdevices

Adding/Removing Small Number of Cells from Microdevices

- Counted number of cells in microbioreactor
- Kept for 2 hours in incubator
- Removed cells by triturating and washing
- Cell viability after removal (Trypan Blue)

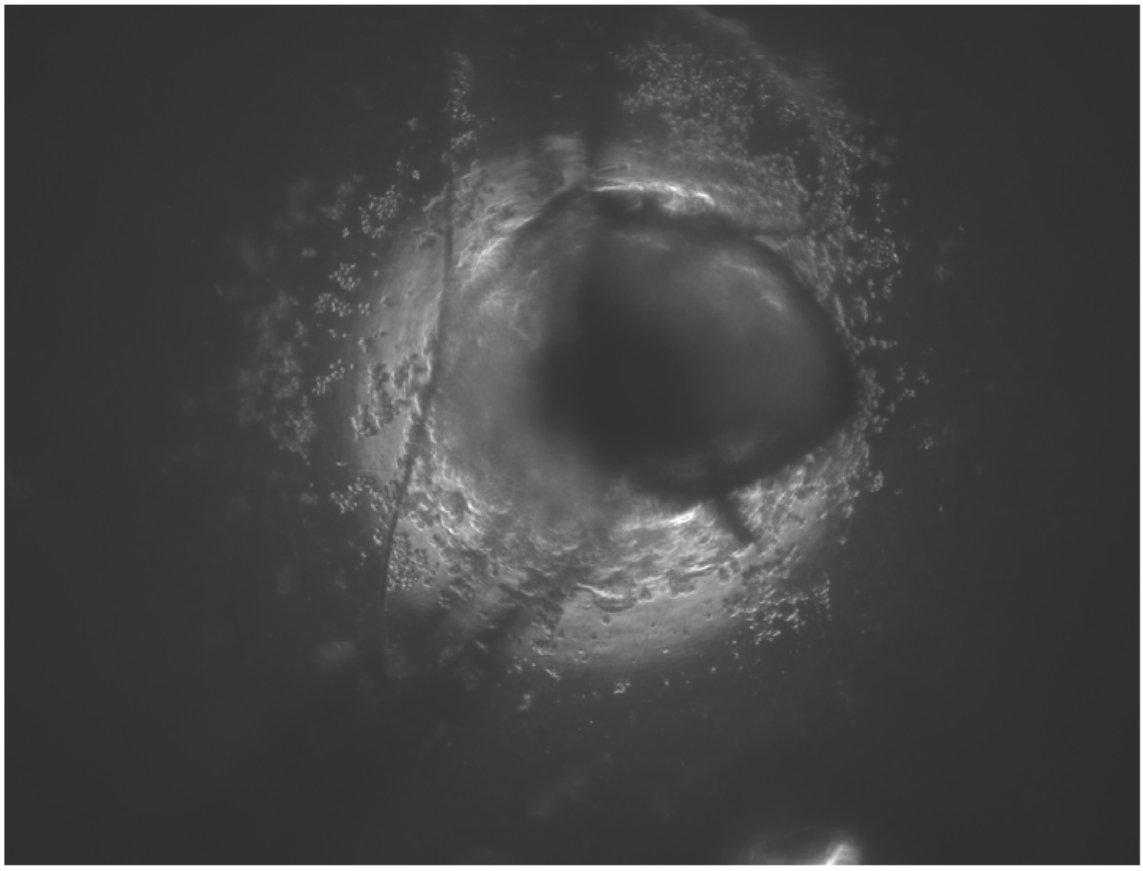

Figure G11: Cells in microdevice funnel region at 4X magnification

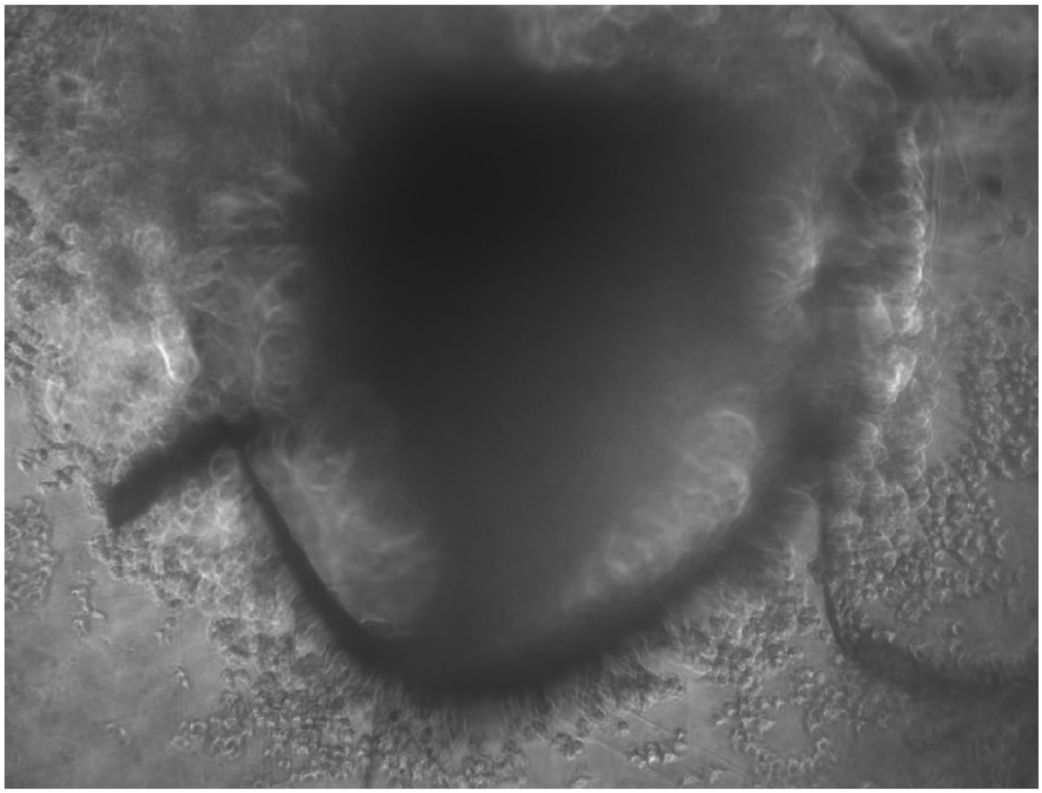

Figure G12: Cells in microdevice funnel region at 10X magnification

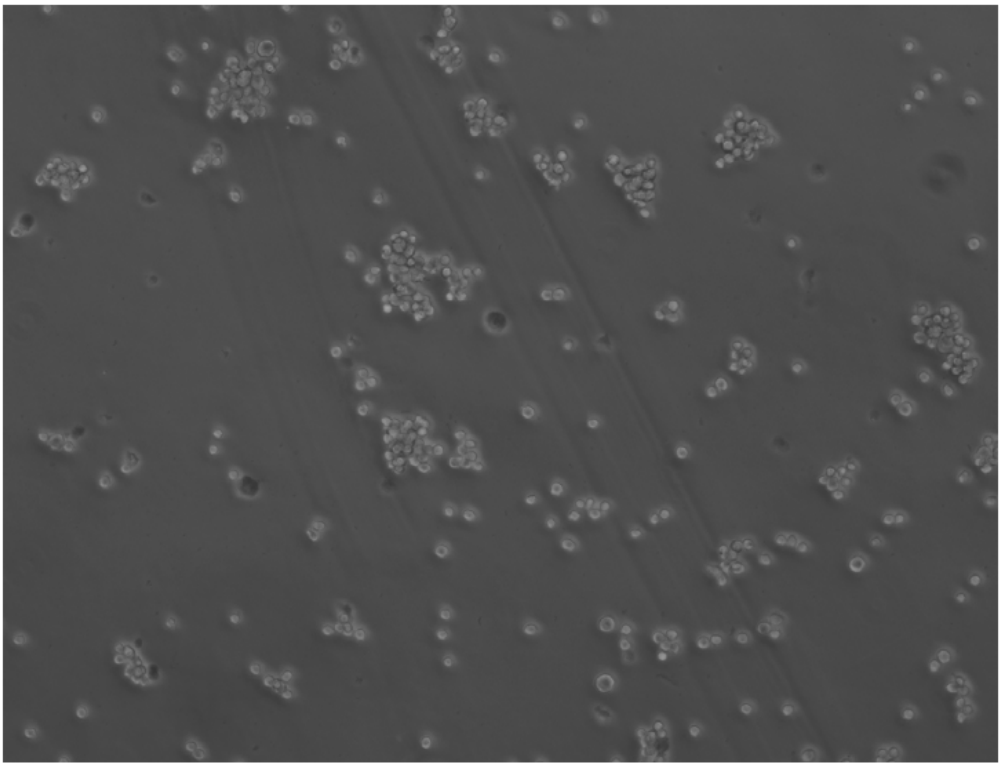

Figure G13: Trypan blue staining after removal of cells from the microdevice funnel

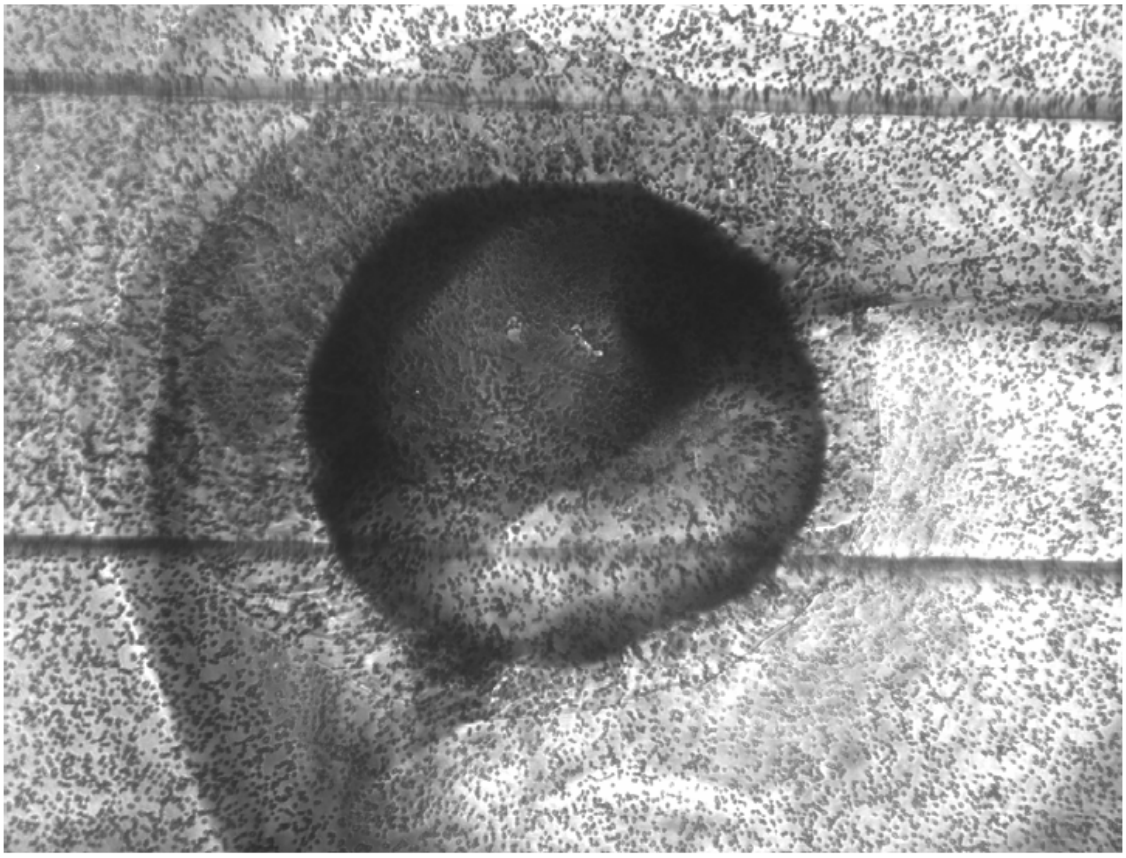

Figure G14: Microdevice after removal of cells at 10X magnification (Note: the grainy structures seen in the figure are pores of the polyester membrane)

APPENDIX H

Cell Seeding in PDMS Microbioreactor for Real Time Oxygen Measurements

(Supplementary for Chapter 3)

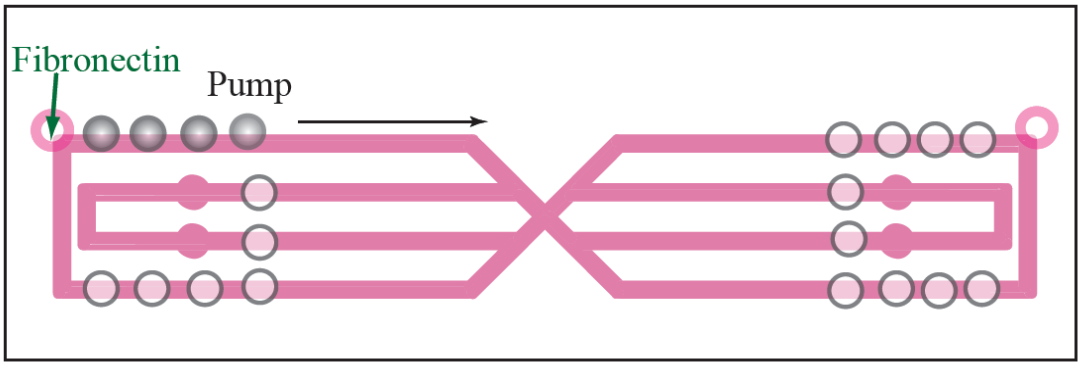

Figure H1: Braille pump (gray) and valve (valves down, white) positions during fibronectin adsorption

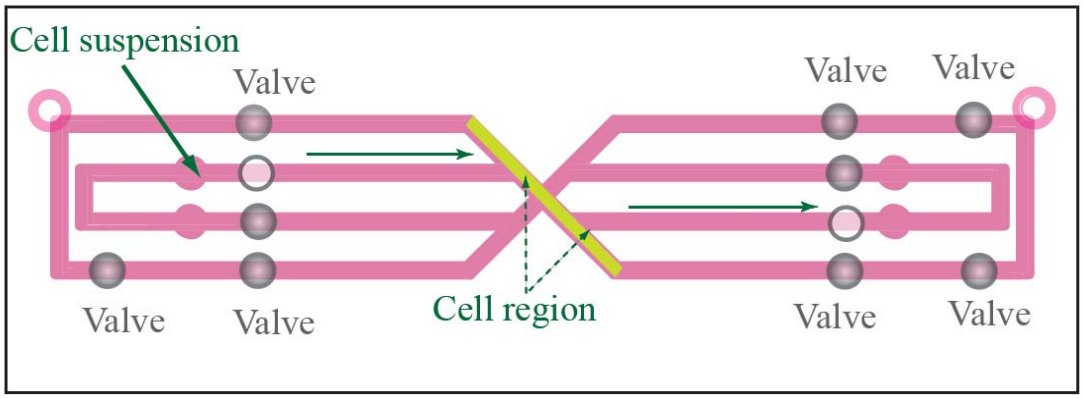

Figure H2: Flow direction (solid green arrows) and valve (valve-up: gray with black border, valve-down: white) positions during cell seeding

APPENDIX I

LabVIEW Graphic User Interface for Measurement of Changes in Florescent Lifetime of Ruthenium based Oxygen sensitive Dye

(Supplementary for Chapter 4)

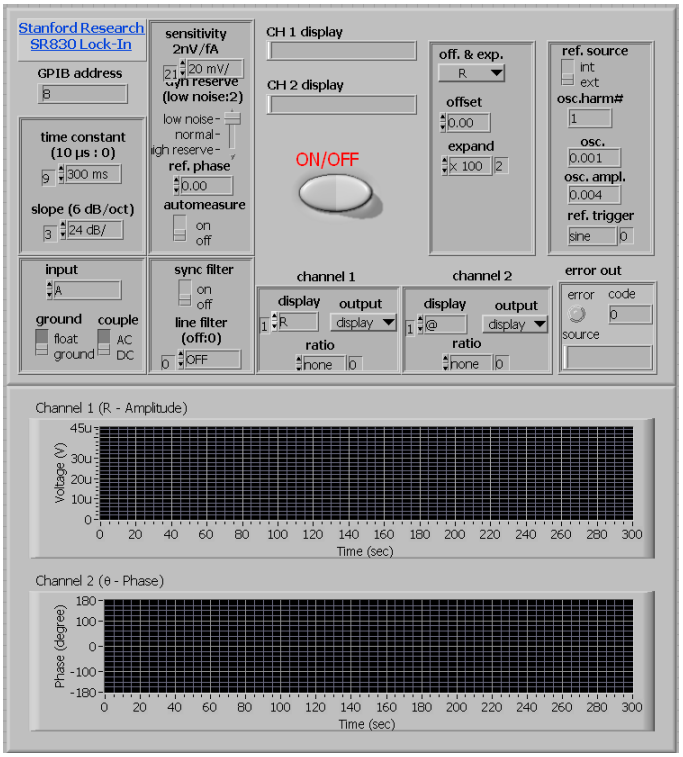

Figure I: FIDS LabVIEW graphic user interface

APPENDIX J

Polyelectrolyte Multilayers inside Microfluidic Bioreactors

(Supplementary for Chapter 6)

Description of 30 PEMs created inside PDMS microfluidic bioreactors:

PEMs (14 out of total 30) which are discussed in the manuscript: $(PDDA/Clay)_3(Co/FN)_0$, $(PDDA/Clay)_4(Co/FN)_0$, $(PDDA/Clay)_5(Co/FN)_0$, $(PDDA/Clay)_{7.5}(Co/FN)_0$, $(PDDA/Clay)_7(Co/FN)_0$, $(PDDA/Clay)_3(Co/FN)_1$, $(PDDA/Clay)_3(Co/FN)_2$, $(PDDA/Clay)_3(Co/FN)_3$, $(PDDA/Clay)_4(Co/FN)_2$, $(PDDA/Clay)_4(Co/FN)_4$, $(PDDA/Clay)_4(Co/FN)_6$, $(PDDA/Clay)_5(Co/FN)_2$, $(PDDA/Clay)_5(Co/FN)_4$ and $(PDDA/Clay)_5(Co/FN)_7$.

The rest of 16 PEMs which are not discussed in the manuscript: $(PDDA/Clay)_{4.5}(Co/FN)_0$, $(PDDA/Clay)_{5.5}(Co/FN)_0$, $(PDDA/Clay)_6(Co/FN)_0$, $(PDDA/Clay)_{6.5}(Co/FN)_0$, $(PDDA/Clay)_8(Co/FN)_0$, $(PDDA/Clay)_{10}(Co/FN)_0$, $(PDDA/Clay)_{12}(Co/FN)_0$, $(PDDA/Clay)_{15}(Co/FN)_0$, $(PDDA/Clay)_5(Co/FN)_8$, $(PDDA/Clay)_5(Co/FN)_9$, $(PDDA/Clay)_7(Co/FN)_1$, $(PDDA/Clay)_7(Co/FN)_2$, $(PDDA/Clay)_7(Co/FN)_3$, $(PDDA/Clay)_7(Co/FN)_4$, $(PDDA/Clay)_7(Co/FN)_5$ and $(PDDA/Clay)_7(FN/Co)_6$.

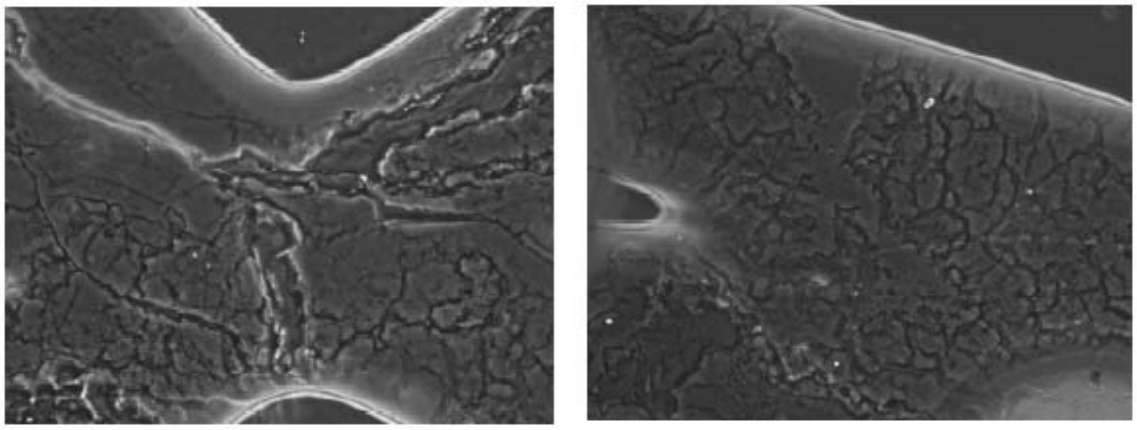

Figure J1: Mixing of clay and PDDA streams together in the middle of the microfluidic device.

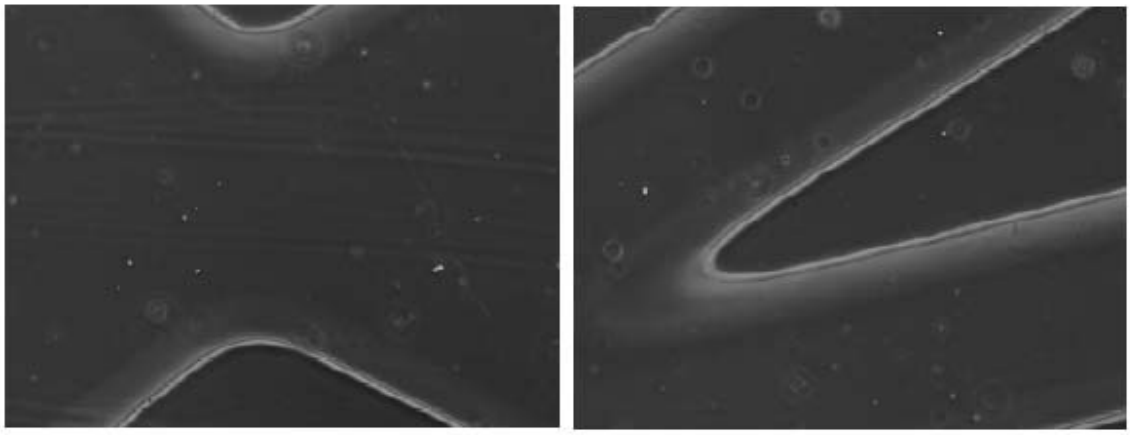

Figure J2: Mixing of clay and PDDA is avoided by returning the polyelectrolyte back to its reservoir at the start of water rinse. The white spots in the pictures are dust particles.

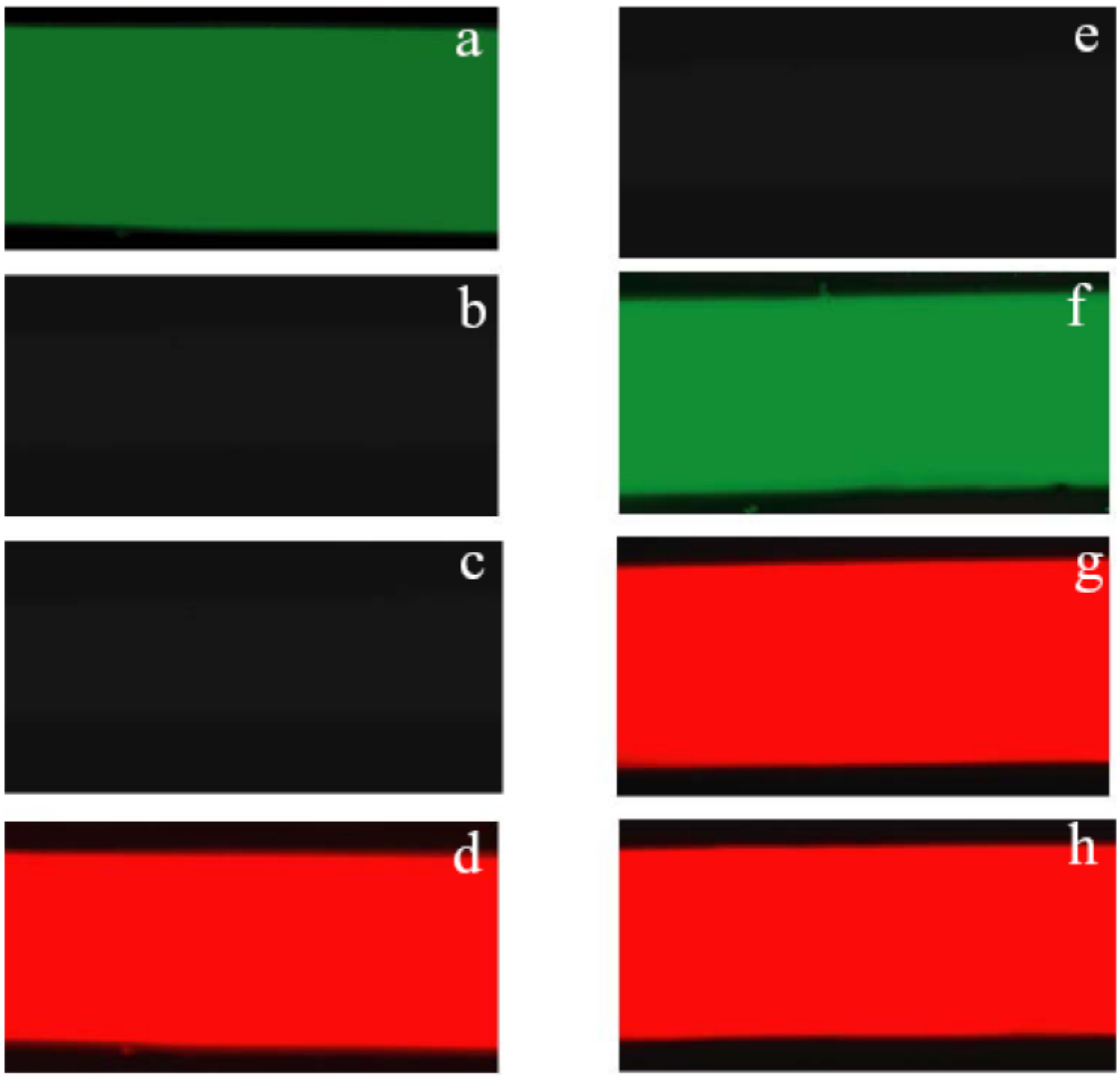

Figure J3: Fluorescent micrographs of inlet streams and multifunctional nanocomposite coatings created in outlet channels inside PDMS microbioreactor chips (images taken with a 10X objective). The pictured from (a) to (d) represent the inlet streams, while those from (e) to (h) represent the outlet streams. For each region (inlet or outlet), the green pictures are stained to fluoresce for positive charge (PDDA, Co), while red are stained for negative charge (Clay, FN). The picture (a) shows the PDDA inlet stream; (b) and (c) illustrate the DI water streams; and (d) shows the clay stream. The picture (d) represents the first outlet channel which has no nanocomposite coating on PDMS surface; (e) shows the second channel with the composition $(PDDA/Clay)_{3.5}$ coating (PDDA topped); (f) illustrates the third outlet channel with $(PDDA/Clay)_4$ coating (clay topped), DI water stream; and (g) shows the last outlet channel with $(PDDA/Clay)_4$ $(Co/FN)_5$ coating.

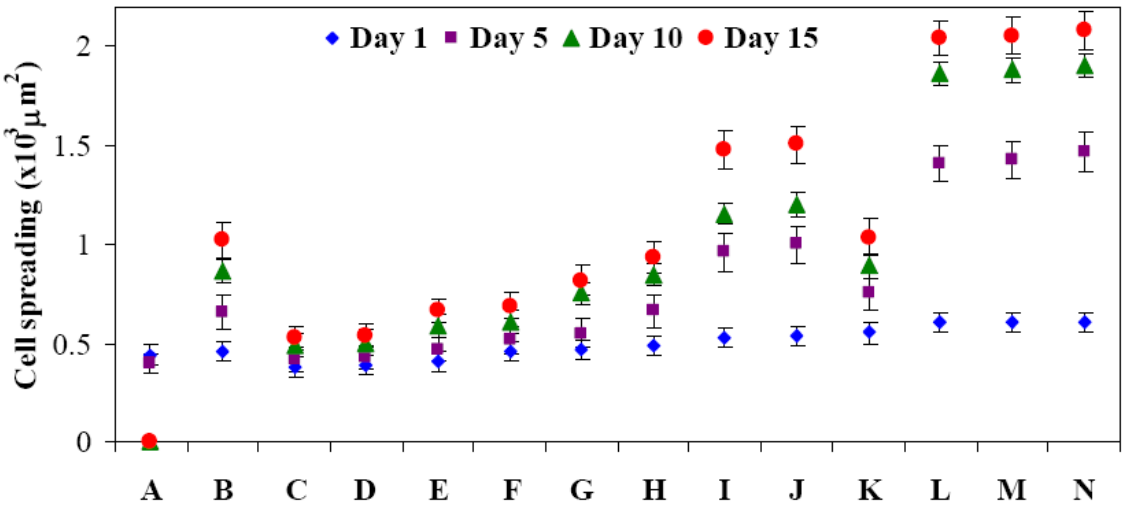

Figure J4: Cell spreading on nanocomposite coatings microfluidic bioreactors at day 1, 5, 10 and 15 (x 10^3 µm^2). Legend: A=$(PDDA/Clay)_{7.5}(Co/FN)_0$, B=$(PDDA/Clay)_7(Co/FN)_0$, C=$(PDDA/Clay)_3$ $(Co/FN)_0$, D=$(PDDA/Clay)_3$ $(Co/FN)_1$, E=$(PDDA/Clay)_3$ $(Co/FN)_2$, F=$(PDDA/Clay)_3$ $(Co/FN)_3$, G=$(PDDA/Clay)_4$ $(Co/FN)_0$, H=$(PDDA/Clay)_4$ $(Co/FN)_2$, I=$(PDDA/Clay)_4$ $(Co/FN)_4$, J=$(PDDA/Clay)_4$ $(Co/FN)_6$, K=$(PDDA/Clay)_5$ $(Co/FN)_0$, L=$(PDDA/Clay)_5$ $(Co/FN)_2$, M=$(PDDA/Clay)_5$ $(Co/FN)_4$, N=$(PDDA/Clay)_5$ $(Co/FN)_7$.

a

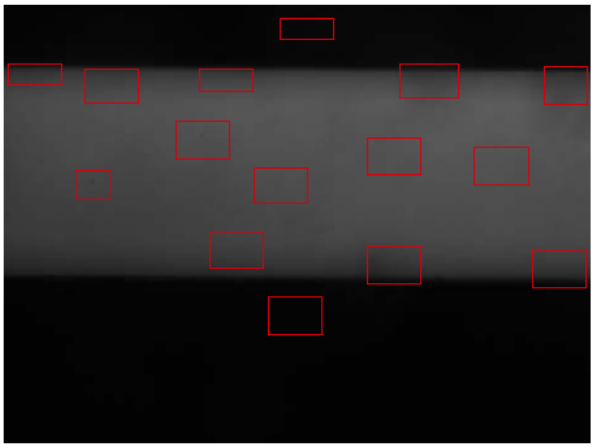

b

Number of bilayers	Fluorescent intensity (mean ± standard deviation) (A.U.)
0	10.3 ± 5.7
1	63.8 ± 24.4
2	91.7 ± 29.2
3	126.8 ± 37.5
4	177.9 ± 33.1
5	232.4 ± 21.6
6	237.1 ± 19.8

Figure J5: Comparison of fluorescence intensity of charged dyes after deposition of each bilayer. The fluorescence of a PEM with 3 bilayers is shown in a), and b) shows the change in intensity with increasing number of bilayers. The fluorescent intensities were analyzed using SimplePCI on a Nikon TE-300 microscope with a Hamamatsu-ORCA 100 camera. The bin size of 2 was used for all images, with a gain of 2 and exposure time of 1 second. The fluorescent image shows uneven intensity inside the channel after coating 3 bilayers.

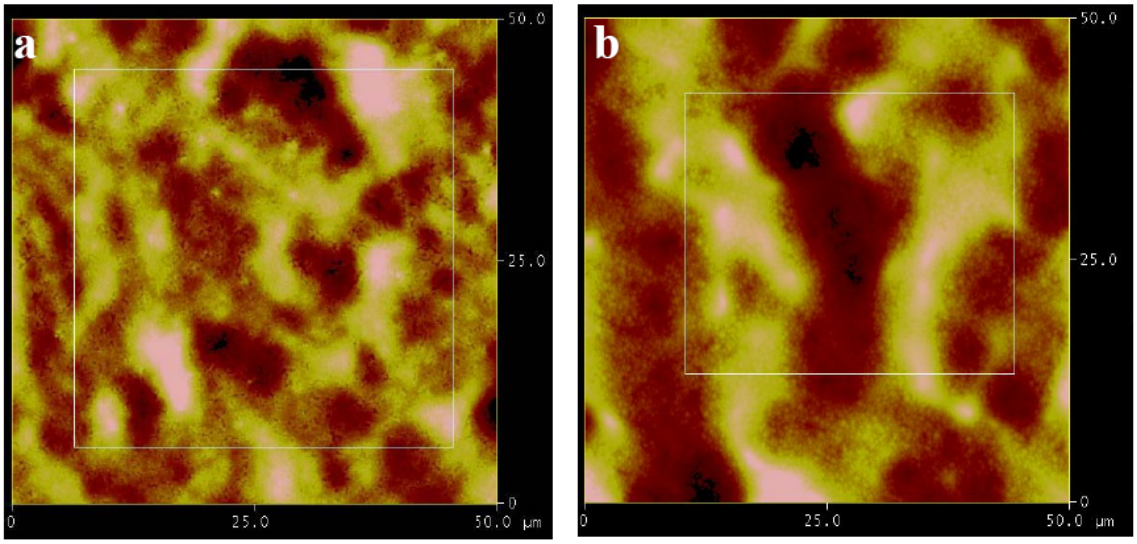

Figure J6: AFM images of PEMs deposited on flat PDMS substrate and microfluidic device. PEMs of composition $(PDDA/Clay)_8$ were scanned with AFM in the tapping mode. The images are 50 µm in both dimensions, a) is an AFM scan for PEM on flat PDMS substrate, and b) is the counterpart inside PDMS microfluidic bioreactors. The mean roughness (R_{ms}) of both images is similar (~70 nm).

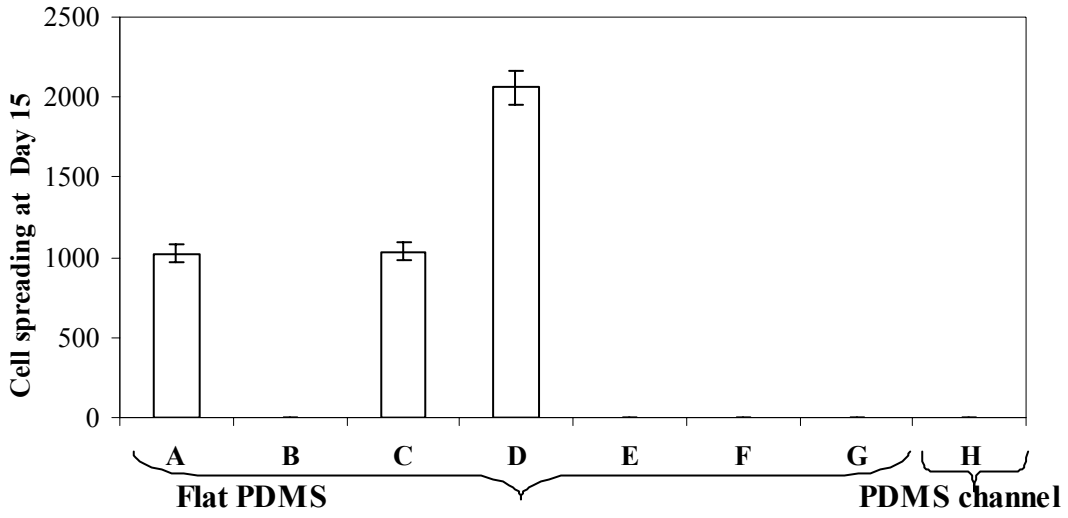

Figure J7: **Cell spreading at Day 15 on surface modified flat PDMS substrate (µm^2).** Legend: A=$(PDDA/Clay)_5$ on flat PDMS substrate, B=$(PDDA/Clay)_{5.5}$ on flat PDMS substrate, C=$(PDDA/Clay)_7$ on flat PDMS substrate, D=$(PDDA/Clay)_5$ $(Co/Fn)_3$ on flat PDMS substrate, E=Fibronectin adsorption on flat PDMS substrate, F=Collagen Type IV adsorption on flat PDMS substrate, G=Fibronectin and Collagen Type IV (1:1) adsorption on flat PDMS substrate, H=FN adsorption only in PDMS microdevice